SYNTHETIC GENETIC CIRCUITS TO MONITOR NANOMATERIAL TRIGGERED TOXICITY

A DISSERTATION SUBMITTED TO

THE GRADUATE SCHOOL OF ENGINEERING AND SCIENCE

OF BILKENT UNIVERSITY

IN PARTIAL FULFILLMENT OF THE REQUIREMENTS FOR

THE DEGREE OF

DOCTOR OF PHILOSOPHY

IN

MATERIALS SCIENCE AND NANOTECHNOLOGY

By

BEHIDE SALTEPE

JULY 2020

SYNTHETIC GENETIC CIRCUITS TO MONITOR NANOMATERIAL TRIGGERED TOXICITY

By Behide Saltepe

July 2020

We certify that we have read this dissertation and that in our opinion it is fully adequate, in scope and in quality, as a thesis for the degree of Doctor of Philosophy.

_____

Urartu Özgür Şafak Şeker (Advisor)

_____

İhsan Gürsel

_____

Eda Çelik Akdur

_____

Fatih İnci

_____

Açelya Yılmazer Aktuna

Approved for the Graduate School of Engineering and Science:

_____

Ezhan Karaşan
Director of the Graduate School

ABSTRACT

SYNTHETIC GENETIC CIRCUITS TO MONITOR NANOMATERIAL TRIGGERED TOXICITY

Behide Saltepe

PhD in Materials Science and Nanotechnology

Advisor: Urartu Özgür Şafak Şeker

July, 2020

In the past decades, nanomaterial (NM) usage in various fields has been of great interest because of their unique properties that show tuneable optical and physical properties depending on their size. Yet, safety concerns of NMs on human or environment arise with increased NM usage. Thanks to their small size, NMs can easily penetrate through cellular barriers and their high surface-to-volume ratio makes them catalytically active creating stress on cells such as protein unfolding, DNA damage, ROS generation etc. Hence, biocompatibility assessment of NMs has been analyzed before their field application such as drug delivery and imaging which requiring human exposure. Yet, conventional biocompatibility tests fall short of providing a fast toxicity report.

One aspect of the present thesis is to develop a living biosensor to report biocompatibility of NMs with the aim of providing fast feedback to engineer them with lower toxicity levels before applying on humans. For this purpose, heat shock response (HSR), which is the general stress indicator, was engineered utilizing synthetic biology approaches. Firstly, four highly expressed heat shock protein (HSP) promoters were selected among HSPs. In each construct, a reporter

gene was placed under the control of these HSP promoters to track signal change upon stress (i.e., heat or NMs) exposure. However, initial results indicated that native HSPs are already active in cells to maintain cellular homeostasis. Moreover, they need to be engineered to create a proper stress sensor. Thus, these native HSP promoters were engineered with riboregulators and results indicated that these new designs eliminated unwanted background signals almost entirely. Yet, this approach also led to a decrease in expected sensor signal upon stress treatment. To increase the sensor signal, a positive feedback loop using bacterial communication, quorum sensing, method was constructed. HSR was integrated with QS circuit showed that signal level increased drastically. Yet, background signal also increased. Moreover, instead of using activation based HSR system as in *Escherichia coli*, repression based system was hypothesized to solve the problem. Thus, a repression based genetic circuit, inspired by the HSR mechanism of *Mycobacterium tuberculosis*, was constructed. These circuits could report the toxicity of quantum dots (QDs) in 1 hour. As a result, these NM toxicity sensors can provide quick reports, which can lower the demand for additional experiments with more complex organisms.

As part of this study, a source detection circuit coupling HSR mechanism with metal induced transcription factors (TFs) has been constructed to report the source of the toxic compound. For this purpose, gold and cadmium were selected as model ions. In the engineered circuits, stress caused by metal ions activates expression of regulatory elements such as TFs of specific ions (GolS for gold and CadR and MerR(mut) for cadmium) and a site-specific recombinase. In the system, the recombinase inverts the promoter induced by TF-metal ion complex,

and a reporter has been expressed based on the inducer showing the source of the stress as either gold or cadmium.

Finally, a mammalian cellular toxicity sensor has been developed using similar approaches used in bacterial sensors. To begin with, two HSP families have been selected: HSP70 and α-Bcrystallin. Initial circuits were designed using promoter regions of both protein families to control the expression of a reporter, *gfp*. Both circuits were tested with heat and cadmium ions with varying concentrations and results showed that HSP70-based sensor had high background signal because of its active role in cellular homeostasis and protein folding in cells. Additionally, a slight increase was observed after heat treatment. Similar results were observed for α-Bcrystallin-based sensor; yet, these outcomes were not suitable for a desirable sensor requiring tight control. Thus, we decided to transfer the bacterial repression based toxicity sensor into mammalian cells. At the beginning, expression of the repressor, HspR, from *M. tuberculosis* was checked in HEK293T cell line and modified with nuclear localization signal (NLS) to localize the repressor in the nucleus. Further, a minimal promoter (SV40) controlling the expression of a reporter was engineered with single and double inverted repeats (IRs) for HspR binding. Then, HspR and engineered reporter circuits were co-trasfected to track signals at normal growth conditions and upon stress. Each circuit was tested with heat and cadmium treatment and results were showed repression of GFP expression by HspR at normal conditions, but no significant signal increase was observed upon stress. Hence, constructed mammalian circuits require more optimization to find optimum working conditions of sensors.

To sum up, in this study, a powerful candidate to manufacture ordered gene circuits to detect nanomaterial-triggered toxicity has been demonstrated. Unlike previous studies utilizing HSR mechanism as stress biosensors, we re-purposed the HSR mechanism of both bacteria and mammalian cells with different engineering approaches (i.e., riboregulators, quorum sensing mechanism, promoter engineering). As a result, an easy-to-use, cheap and fast acting nanomaterial-triggered toxicity assessment tool has been developed. Also, initial principles of mammalian whole cell biosensor design for the same purpose have been indicated to expand the limited toxicity detection strategies utilizing mammalian cells. This study contributed for the detection of toxic NMs providing a feedback about the fate of these NMs so that one can engineer them to make biocompatible before field application.

Keywords: Nanomaterials, Nanomaterial-triggered Toxicity, Nanotoxicity, Whole-cell Biosensors, Heat Shock Protein Response

ÖZET

NANOMALZEME KAYNAKLI TOKSİSİTENİN GÖZLEMLENMESİ İÇİN TASARLANAN SENTETİK GEN DEVRELERİ

Behide Saltepe

Malzeme Bilimi ve Nanoteknoloji, Doktora

Tez Danışmanı: Urartu Özgür Şafak Şeker

Temmuz, 2020

Son bir kaç onyıl içerisinde çeşitli alanlarda nanomalzeme kullanımı artmıştır. Bunun temel sebeplerinden biri, nanomalzemelerin sahip olduğu eşsiz özelliklerdir. Bu özelliklerden başlıcaları, boyuta bağlı olarak değişen ve ayarlanabilen optik ve fiziksel özelliklere sahip olmalarıdır. Artan nanomalzeme kullanımı ile bu malzemelerin insan ve çevre üzerindeki etkilerine dair endişeler de artmaktadır. Küçük boyutları sayesinde nanomalzemeler, hücre duvarlarından kolayca geçebilmektedir. Aynı zamanda, yüksek yüzey alanı-hacim oranı sayesinde bu malzemeler katalitik olarak oldukça aktif olabilmektedirler. Bunun sonucunda da hücre içerisinde stres yaratma potansiyeline sahiptirler. Bu stres belirtilerinin başlıcaları protein katlanmalarında hatalar, reaktif oksijen türlerinin (ROS) oluşması ve DNA hasarıdır. Bu yüzden, nanomalzemelerin insan üzerinde kullanımından önce (kontrollü ilaç salınımı ya da manyetik görüntüleme gibi) bir takım biyouyumluluk testinden geçmesi gerekmektedir. Yine de, günümüzde kullanılan biyouyumluluk testleri oldukça komplike olmakla birlikte geç sonuç vermektedir.

Bu tezin amaçlarından biri, hızlı cevap verebilen yaşayan bir biyouyumluluk testi oluşturmaktır. Bu sayede, toksik olan nanomalzemelerin modifikasyonları daha erken yapılabilecek, böylelikle toksik olmayan nanomalzemelerin kullanıma girmesi daha hızlı olabilecektir. Bu doğrultuda genel bir stres göstergesi olan ısıl-şok protein mekanizması (HSR) seçilmiştir. Bu mekanizma, sentetik biyoloji yaklaşımları kullanılarak yeniden düzenlenmiş ve sentetik gen devreleri oluşturulmuştur. Öncelikle, stres durumunda en çok aktif rol alan dört farklı proteinin promotör bölgeleri seçilmiştir. Bu promotörlerin her biri ile ayrı ayrı gen devresi oluşturulmuştur. Bu gen devrelerinde, her bir promoter, bir raportör gen ifadesini kontrol etmektedir. Yapılan ilk denemeler sonucunda elde edilen bulgulara göre, ısıl-şok proteinleri hücre savunma mekanizması için rol aldığından oldukça aktif olup, stres olmadığı zamanlarda da yüksek raportör sinyali verdiği gözlemlenmiştir. Bu yüzden, tek başlarına bu promotörlerin kullanılamayacağına karar verilmiştir. Stres kaynağı olmayan durumdaki gürültü sinyalini düşürmek amacıyla, literatürde daha önce geliştirilmiş olan riboregülatör sekanslarının kullanılmasına karar verilmiştir. Böylece her bir promotör riboregülatörler ile yeniden düzenlenmiş, yeni gen devreleri oluşturulmuştur. Elde edilen bulgular, oluşturulan bu yeni sensörlerin, gürültü sinyalini hemen hemen tamamen yok ettiğini göstermiştir. Ancak, stres uygulamasından sonra beklendiği şekilde yüksek sinyal elde edilememiş, riboregülatörler toksisite sinyalini de düşürmüştür. Sensör sinyalini arttırmak amacıyla, sensör içerisinde bir pozitif geribesleme döngüsü eklenmiştir. Bunun için bakteriyel iletişim (QS) mekanizması ile ısıl-şok mekanizması birleştirilmiştir. Bu sayede ortamda var olan stres durumundan bütün bakterilerin haberdar olup birbirini uyarması amaçlanmıştır. Beklendiği

üzere sensörün sinyal seviyesi oldukça artmıştır. Ancak bununla birlikte, gürültü sinyalinde de aynı oranda artış gözlemlenmiştir. Bu yüzden, *Escherichia coli* içerisindeki gibi aktivasyona dayalı ve yüksek gürültü veren sistem kullanmak yerine, baskılamaya dayalı yeni bir sisteme geçilmesi kararlaştırılmıştır. Bu yüzden, *Mycobacterium tuberculosis* ısıl-şok mekanizması örnek olarak alınmıştır. Oluşturulan gen devreleri, model nanomalzeme olarak kullanılan kuantum noktacıklara (QD) 1 saat içerisinde oldukça yüksek tepki vermiştir. Oluşturulan bu sensörler ile de nanomalzeme toksisitesi oldukça hızlı tespit edilebilecek, karmaşık deneylere (hayvan deneyleri gibi) gerek duyulmadan, toksik olan nanomalzemelerin yeniden gözden geçirilerek modifikasyonlar yapılmasına olanak sağlayacaktır.

Bu çalışmasının ikinci kısmı da oluşturulan toksisite sensörlerini kaynak gösterecek şekilde tasarlamak, bu sayede ortamda toksisite yaratan malzemenin ne olduğuna dair rapor elde etmektir. Bunun için de ısıl-şok yolağı ile ağır metal spesifik transkripsiyon faktörleri (altın için GolS, kadmiyum için ise MerR(mut) ve CadR) birleştirilmiştir. Bunun için altın ve kadmiyum iyonları model olarak seçilmiştir. Bu sistemler rekombinaz ile birleştirilerek yeni gen devreleri tasarlanmıştır. Bu gen devrelerinde, rekombinaz, stres ile aktive olarak ters halde duran metal spesifik promotörü düzleştirmekte, bu sayede de ilgili metal varlığında raportör gen ifadesi başlamaktadır. Bu sayede stres faktörünün kaynağının altın ya da kadmiyum olarak belirlenmesi mümkündür.

Son olarak, memeli hücresi kullanılarak toksisite sensörü yapılması amaçlanmıştır. Öncelikle, bakteriler ile yapılan yaklaşımlara benzer şekilde, stres

durumunda aktif rol oynayan iki farklı ısıl-şok protein ailesi seçilmiştir. Bunlardan birincisi, hücrelerin genel savunma mekanizması olan HSP70 ailesi iken, diğeri de küçük ısıl-şok protein ailesine ait α-Bcrystallin proteinidir. Her iki proteinin promotör bölgesi raportör gen ifadesini kontrol edecek şekilde tasarlanmıştır. Oluşturulan her iki devre de ısı ve kadmiyum iyonları ile test edilmiştir. HSP70 ailesi hücre içerisinde oldukça aktif olduğundan, stres uygulanmayan durumlarda da yüksek sinyale sebep olmuştur. α-Bcrystallin ile oluşturulan sensörde ise, ısıl-şokun ardından bir miktar artış gözlense de, sensör çalışmaları için yeterli değiltir. Bu sebeple, bakteriyel sensörlerde yapıldığı gibi baskılayıcı gen devresi tasarımına karar verilmiştir. Öncelikle, ısıl-şok promotörlerini baskılayıcı genin (HspR) memeli hücrelerde de ifade edilebildiği gösterilmiştir. Daha sonrasında minimal promotör bölgesine (SV40) HspR bağlanma dizileri tekli ve çiftli tekrarlar halinde eklenerek raportör gen ifadesindeki azalış ve artışlar takip edilmiştir. Oluşturulan devreler ısıl-şok ve kadmiyum iyonları ile test edilmiştir. Elde edilen sonuçlara gore, HspR varlığında raportör gen ifadesinde azalış olduğu gözlemlenmiştir. Ancak, stres uygulamasının ardından belirgin bir sinyal artışı elde edilememiştir. Bu yüzden, oluşturulan gen devrelerinin optimizasyonunun yapılması ve sensörün optimum çalışma koşullarının tespit edilmesi gerektiği sonucuna varılmıştır.

Sonuç olarak, bu çalışma ile bakteriyel ve memeli bütün hücre sensörü tasarlanma prensipleri ele alınmıştır. Oluşturulan bakteriyel sensörler, nanomalzemelerin toksisite tayini için güçlü bir adaydır. Şimdiye kadar yapılan çalışmaların aksine, bu çalışmada, hücreleri toksisite tayini için programlarken çeşitli mühendislik yaklaşımları kullanılmıştır (riboregülatörler, bakteriyel iletişim mekanisması,

promotör üzerinde yapılan çeşitli değişiklikler v.b.). Sonuç olarak, kullanımı kolay, hızlı cevap veren ve ucuz bir toksisite testi elde edilmiştir. Ayrıca, memeli hücresi kullanılarak yapılan biyosensör çalışmasının optimizasyon gerektirmesine rağmen, tüm hücre sensörü alanı için nitelikli bir tasarım örneğidir. Literatürde memeli hücrelerinin toksisite tayini için programlanmasına nadiren rastlanmaktadır. Bu sebeple, buradaki çalışma da Alana önemli bir katkı sağlayacak türden olmuştur. Genel anlamda bu çalışma nanomalzeme toksisitesi tayinini hızlı bir şekilde sağlayarak, toksik olan nanomalzemelerin yeniden yapılandırılarak alana daha hızlı şekilde uygulanabilmesini sağlayacaktır.

Anahtar kelimeler: Nanomalzemeler, Nanomalzeme Kaynaklı Toksisite, Nanotoksisite, Tüm Hücre Biyosensörleri, Isıl Şok Protein Tepkisi

Acknowledgements

Life is a journey and the tough part of this journey is to learn how to survive under pressure. Almost six years of Ph.D. life has taught me things not only scientifically but also about life. I had to face with many challenges. Time to time I got used to them, but sometimes I had to accept things even if I did not want to. I would like to thank all of the people who supported me during this period.

I would like to start to show my gratitude to my advisor and mentor, Dr. Urartu Özgür Şafak Şeker. He always showed the uttermost support. He was always very kind, and he tried to provide all possible options to motivate all group members all the time. I learnt a lot from his research experience and I believe that I have improved my professional skills as a scientist thanks to his mentorship. I am very grateful to complete my Ph.D. with him. Next, I would like to thank to my thesis tracking committee members Dr. İhsan Gürsel and Dr. Eda Çelik Akdur for helpful discussions and advices through our biannual progress meetings. Also, I would like to thank to Dr. Fatih İnci and Dr. Açelya Yılmazer Aktuna for being jury members of my thesis defense. Lastly, I would like to express my gratitutes to all UNAM members, especially to Duygu Kazancı and Ayşegül Torun.

Coming up with the right lab mates is a chance. Fortunately, I was very lucky and I worked with hard working people. I have to express my sincere thanks to both former and recent SBL lab members for their friendship. Especially I want to express my gratitude to Dr. Esra Yuca for her support and kindness. Next, I thank to Nedim Hacıosmanoğlu and Eray Ulaş Bozkurt for their contribution to this project, hard work, and friendship. Also I thank to Ebru Şahin Kehribar and Recep

Erdem Ahan for their intellectual conversation and coffee breaks. It was always my pleasure to work with such knowledgeable people. Finally, I thank to the rest of the lab members (Anooshay Khan, Büşra Merve Kırpat, Cemile Elif Özçelik, Gökçe Özkul, İlkay Çisil Köksaldı, Julian Ostaku, Merve Erden Tüçer, Merve Yavuz, Murat Alp Güngen, Sıla Köse, and Volkan Aslan). I have worked in such warm environment with them.

One of the most precious things that I gained during these years is the lifelong friendship. I experienced many delightful and memorable moments. I thank to my best friend Recep Erdem Ahan for 10 years of cheerful friendship. He supported me a lot when I went down. Also, I am very happy to be roommate with Çağla Eren Çimenci during her master's period in Ankara. We shared a lot and she became my sister. Next, I would like to thank to Onur Apaydın for his weird advices and funny stories during breaks. Also, I thank to Özlem Arslan for being my after work drinking buddy. Additionally, I thank to Cemile Elif Özçelik, Büşra Merve Kırpat, and Eray Ulaş Bozkurt for gaming nigths, top-secret gossiping times and tea breaks which always cheer me up. Especially, I am glad to have Eray nearby all the time. He enlightened me whenever I stucked with some issues. I am very lucky to spend time with him and share happiness and misery.

Lastly, my deepest gratitude goes to my family for their unrequited love and support. Without their support I could not achieve such things in my life. I would like to thank my father Dilaver, my mother Gülten, my brother Berkant and his wife Gülay and their little angel Elçin, my older brother Feyzi and his wife Filiz.

This study was supported by TÜBİTAK Project Number 114Z653 and 118S398.

Table of Contents

List of Figures

List of Tables

CHAPTER 1

Introduction

1.1. General Understanding of Cellular Stress

Deviations from the optimal growth conditions (i.e. temperature, pH and osmolarity changes, increased reactive oxygen species (ROS), decrease in nutrient availability, chemical exposure, mechanical forces etc.) might trigger stress on cells. Exposure to exogenous toxicants causes cellular toxicity which can cause cellular impairments such as DNA damage, protein unfolding, mitochondrial dysfunction, oxidative stress and even cell death. In the presence of any stress inducing stimuli, cells either re-establish homeostasis to the former state or they adapt themselves to the new environment. In general, cells may follow four different paths against stressors: (i) activation of repair mechanisms, (ii) temporary adaptation to stressor, (iii) autophagy, and cell death (iv) [1].

1.1.1. Cell Repair Mechanisms upon Stress

Stressors may damage intracellular components of cells such as DNA, RNA, proteins and lipids. Such kinds of effects trigger some gene expression alterations in cells to activate chaperones [2] so that cells can clear damaged macromolecules and set cellular homeostasis. Certain stress conditions such as heat shock, nutrient stress, hypoxia, and DNA damage change gene expression patterns in cells via recruitment of ribosomes on selected mRNAs [3]. Not only environmental factors

cause stress on cells. Also, incomplete protein translation, misfolded intermediates, and unassembled protein subunits exposing hydrophobic regions may trigger aggregation; hence, cellular stress. In any conditions, cells cope with these stress mechanisms either by increasing chaperone expression to repair them or degrading the unfolded proteins [2].

Chaperones are accessory proteins that facilitate folding or unfolding of proteins to re-fold them in their correct structures. Although there are different classes of chaperones serving variable functions (i.e. folding of newly synthesized proteins, re-folding of misfolded proteins, assisting protein degradation, membrane transport etc.), many of them identified after elevated heat exposure of cells. Thus, a huge chaperone family has named as heat shock proteins (HSPs).

1.1.2. Temporary Adaptation to Stress

Organisms should adapt themselves to changes in environment to increase their survival. It has been proved that cells can adapt themselves to mild stress conditions and revert to their normal growth conditions in a few days after stress exposure. This adaptation provides resilience to cells [4, 5]. In some cases, adaptation to sublethal stress was also observed resulting in higher stress tolerance [6-8]. For instance, hydrostatic pressure increased survival of mouse blastocysts after freezing [7]. From very simple to more complex organisms, cells have to adapt themselves to sublethal stressors and tolerate larger changes. As an example, papillas of mammalian kidney need to adapt themselves with the changing hyperosmolarity since the state of hyperostomic stress is dynamic and changes based on the hydration status of the organism [1].

1.1.3. Autophagy

An intracellular lysosomal degradation action is called as autophagy. Autophagy is conducted by autophagosomes, double-membrane vesicles, sequestering the cytoplasm. Various processes involve autophagy such as macroautophagy, microautophagy, and chaperone-mediated autophagy [9]. In the first one, the cytoplasmic target is engulfed by autophagosome and further fused with lysosome directly to be degraded immediately. In the second one, only a portion of the cytosol is engulfed by lysosome. In the last one, selected proteins (i.e. ubiquinated proteins) are degraded. Autophagy is conserved among all domains of life aiming to eliminate aggregation of proteins and to save resources in cells. For instance, under starvation, autophagy recycles amino acids in cells for protein synthesis to rescue the cell from stressed condition. Besides, autophagy is the last chance of cell to survive at stress conditions before it dies [1].

1.1.4. Cell Death

Cells try to survive until stressor has gone. Yet, at very high ratio of stress factors trigger apoptosis, the cell death. Apoptosis is the process that cells shrink, bleb, and condensate [10]. It has been shown that different stress factors such as irradiation, chemotherapeutic agents, endoplasmic reticulum (ER) stress, and oxidative stress trigger apoptosis. A family of cysteine proteases, caspases, has a critical role in apoptosis which is inactive at normal conditions while gets activated upon stress cleaving various substrate in cells [11].

Cell death has been defined by various forms one of which is necrosis. Necrotic cell death is characterized by swelling of cells and organelles, membrane rupture,

and intracellular component loss because of the ruptured membrane. Various studies showed that some stress conditions such as ischemia [12], glutamate excitotoxicity [13], and alkylating DNA damaging agents [14] cause necrotic cell death.

1.2. Cellular Stress Responses

To maintain cellular homeostasis, cells have developed different mechanisms to protect themselves under severe stress conditions. Based on the stress stimuli, cells activate related mechanisms to recover themselves to the initial healthy positions. However, in the case of very harsh conditions, stress overcomes the protective responses and cells have to activate cell death mechanisms [1].

1.2.1. Oxidative Stress Response

Cells need an appropriate amount of molecular oxygen and antioxidants for survival. Reactive oxygen species (ROS) such as singlet oxygen, superoxide anion ($O_2•^-$), hydrogen peroxide (H_2O_2), hydroxyl radical (OH•), peroxy radicals, and nitric oxide (NO•) which forms peroxynitrite ($ONOO^-$) via reacting with $O_2•^-$. At normal growth conditions, pro-oxidant species and antioxidant mechanisms (i.e. antioxidant proteins as glutathione (GSH) and ROS-metabolizing enzymes as glutathione peroxidase, superoxidase dismutase (SOD) and catalase) are in balance. Besides, ones this balance has been broken, oxidative stress arise in cells [15]. ROS in cells damages macromolecules in cells such as DNA, RNA, proteins, lipids, and carbohydrates. ROS level can increase in cells via various factors including intracellular and extracellular stimuli. These species can be eliminated

through SOD enzymes at the first stage. Also, GSH plays role in neutralization of auto-oxidized species in cells to prevent ROS formation [16]. When ROS overwhelms the defense mechanism of cells, it triggers cell death mechanism eventually [15, 17].

Oxidative stress not only stimulates its own machinery, it also activates other stress pathways: heat shock response (HSR) and unfolded protein response (UPR). The former one protects cells from various stress sources (radiation, oxidants, chemicals, heavy metals etc.) besides heat [18-20], and the latter one upregulates antioxidant genes [21].

1.2.2. DNA Damage Response

Chemotherapeutic agents, some therapeutics, irradiation, genotoxic agents and ultra violet (UV) light create damages such as single or double strand breaks on DNA. Under these circumstances, the repair mechanism ensures survival of cells otherwise to trigger cell death at very severe damaged conditions [22]. DNA repair is controlled with two main mechanisms; non-homologous end joining (NHEJ) and homologous recombination (HR) [23]. In NHEJ, either DNA repair proteins change the damaged base or incorrectly paired bases is excised [24]. The whole process could be error-free in ideal case, or error-prone in some cases. Several proteins play role in the machinery to make the process error-free, because some of the mutations in DNA may trigger cell death pathways [25].

1.2.3. Unfolded Protein Response (UPR) Mechanism

In eukaryotes, proteins fold and undergo posttranslational modifications (i.e. glycosylation and disulfide bond formation) in ER. Thus, ER environment plays critical role in efficient folding and secretion of proteins. Stressful conditions such as glucose starvation, oxygen deprivation, disturbance of Ca^{2+} homeostasis, and inhibition of protein glycosylation lead unfolded protein accumulation in ER; hence, ER stress. Accumulation of unfolded proteins in ER triggers sets of pathways known as unfolded protein response (UPR) targeting chaperones in ER, subunits of translocation machinery, folding catalysts, degradation molecules, and anti-oxidants [26]. Glucose-regulated proteins (GRPs) are one of the UPR targets induced by ER stress, especially in glucose starvation. These proteins provide cell survival upon ER stress caused by hypoxia-ischemia [27, 28], neurodegeneration [29-31], and glutamate excitotoxicity [32].

The UPR ensures cell survival providing the balance between the protein load and the folding and secretion capacity in ER. Nevertheless, if this balance is disturbed in the favor of increased protein load, and UPR mechanism could not achieve homeostasis back, cells tend to die [33].

1.2.4. Heat Shock Response (HSR) Mechanism

On the contrary to its name, heat shock response (HSR) is a universal and well-conserved stress response mechanism to different stressors including elevated heat, anticancer drugs, osmotic shock, toxic chemicals, and heavy metals. At stress exposure, general gene expression of cells is halted, and a subset of

protective proteins; heat shock proteins (HSPs), is expressed. HSPs are a protein family which is evolutionary conserved in all domains and named according to their molecular weights generally (i.e. Hsp40, Hsp60, Hsp70, Hsp90, and small Hsp (sHsp) etc.). Some of the HSPs are constitutively expressed in cells (i.e. Hsp90) to prevent premature folding while the others are expressed in cells at basal levels and increased upon stress exposure (i.e. Hsp70). All of these proteins play role in maintaining cellular survival upon stress and prevention of cell death caused by stressor [34].

1.2.4.1. Heat Shock Response in Bacteria

Although general HSR is conserved among domains, some certain differences are still observed. The HSR mechanism of bacteria is well-characterized in *Escherichia coli*. Expression of HSPs is controlled by a stress-specific subunit (σ^{32}) of RNA polymerase, encoded by *rpoH* gene. At normal conditions, σ^{32} is kept at low levels because of its rapid turnover. Upon stress, σ^{32} level increases with increased stability as well as enhanced synthesis. As a result, σ^{32}-dependent transcription starts to express HSPs such as DnaK (Hsp70), DnaJ (Hsp40), GrpE, GroEL (Hsp60), and GroES (Hsp10) [35]. A negative feedback mechanism controls the σ^{32}-dependent transcription. DnaK-DnaJ-GrpE chaperones recognize σ^{32} and block its activity. Further, inactivated σ^{32} is degraded by a specific protease, FtsH (Figure 1.1).

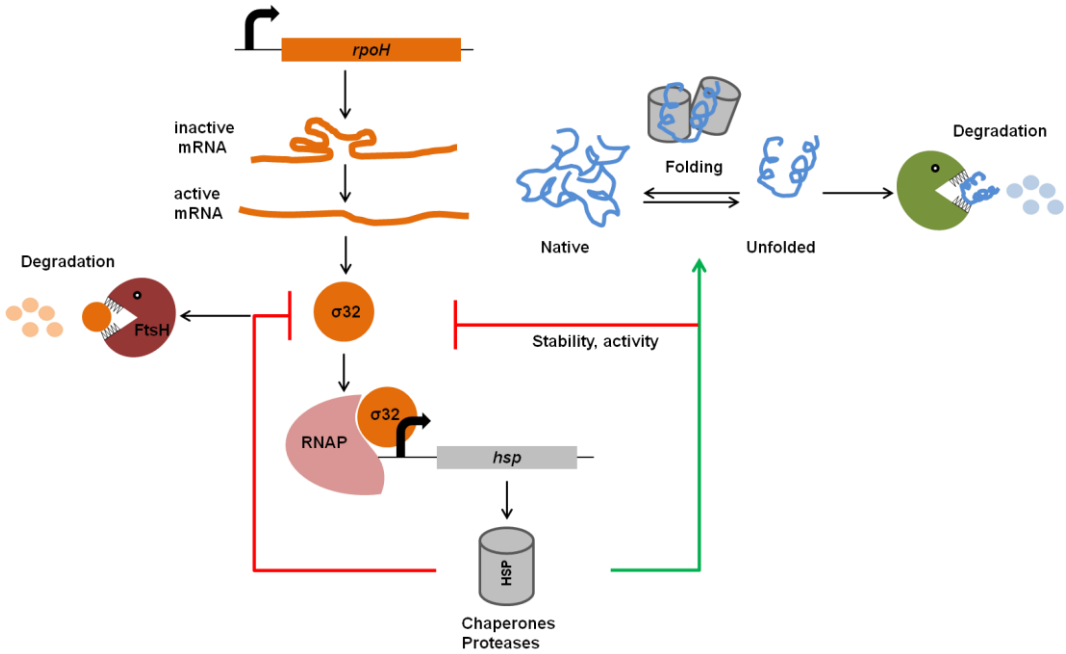

Figure 1.1: Representative heat shock response mechanism in *E. coli*. Upon stress, σ^{32} level increases and σ^{32}-dependent transcription starts to express HSPs. A negative feedback mechanism controls the σ^{32}-dependent transcription. Chaperones recognize and block σ^{32} activity and inactivated σ^{32} is degraded by FtsH protease. Reprinted with permission from ref [36]. Copyright 1999 Elsevier.

Although the σ^{32}-dependent regulation is well-conserved among Gram negative bacteria, some distinctive mechanisms also have been discovered. For instance, *Bacillus subtilis*, Gram positive bacteria, regulates HSR mechanism with a repressor, HrcA, which recognizes specific elements (CIRCE elements) on HSP promoter (Figure 1.2) [36, 37].

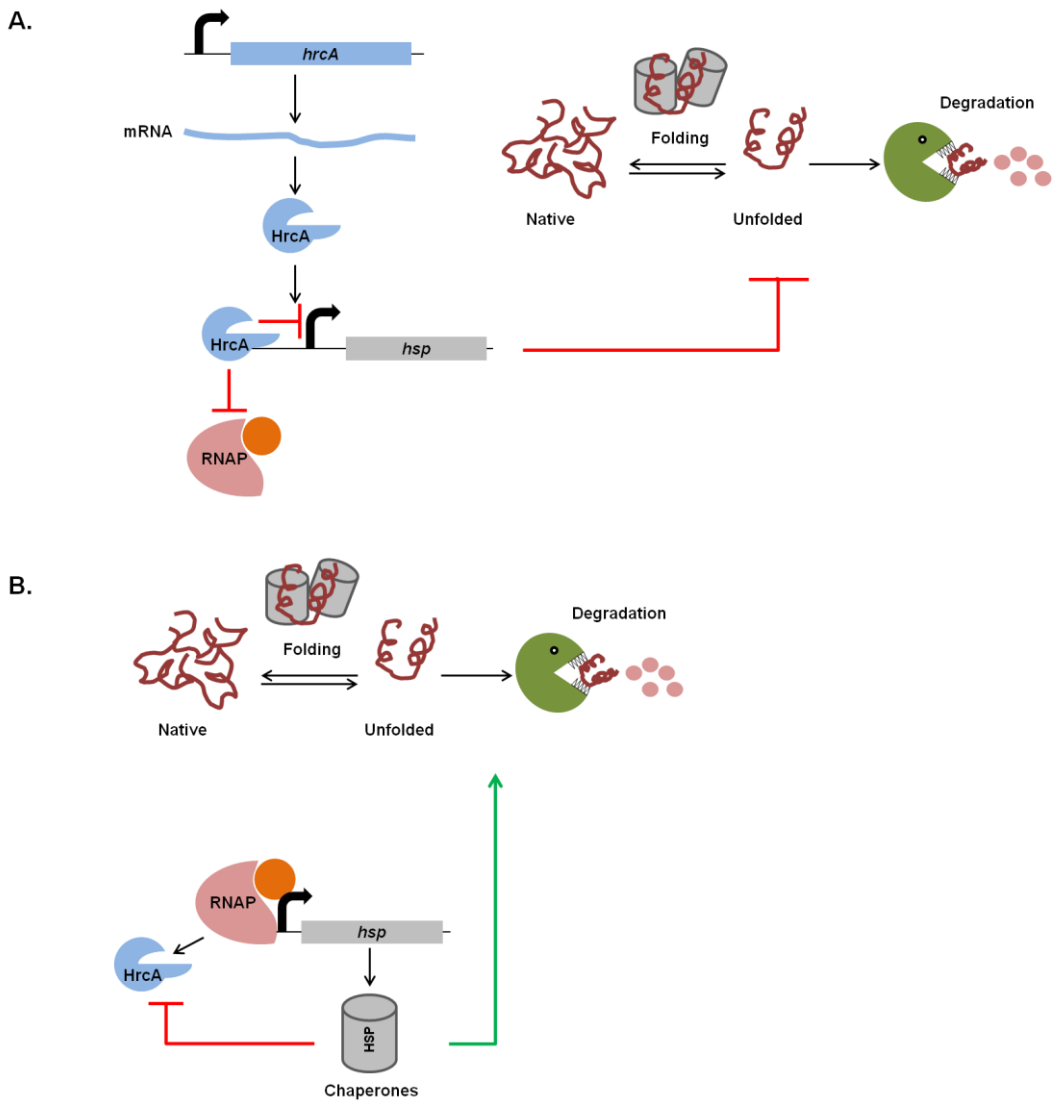

Figure 1.2: Representative heat shock response mechanism in *B. subtilis*. A. At normal conditions HrcA blocks the HSP machinery. B. Upon stress, HrcA dissociates from the promoter initiating HSP expression. Reprinted with permission from ref [37]. Copyright 2017 Oxford University Press.

1.2.4.2. Heat Shock Response in Eukaryotes

Expression of HSPs is controlled by a set of heat shock transcription factors; HSFs. Mammalian cells utilize four different HSFs (HSF1-4) while others such as

yeast, *Caenorhabditis elegans*, and *Drosophila* have only HSF1 [38]. Each HSF has unique as well as common functions. HSFs might be tissue specific and processed by various post-translational modifications. HSF1 is the master regulator among the others. It is inactivated by HSP chaperones in cytoplasm as its monomeric form. To be activated, HSF1 is released, trimerized, and transported to nucleus. Afterwards, HSF1 trimer complex is hyperphosphorylated by kinases. Following the sumoylation, HSF1 is activated via recognition of heat shock elements (HSEs), and other components of transcription machinery are recruited (Figure 1.3) [39].

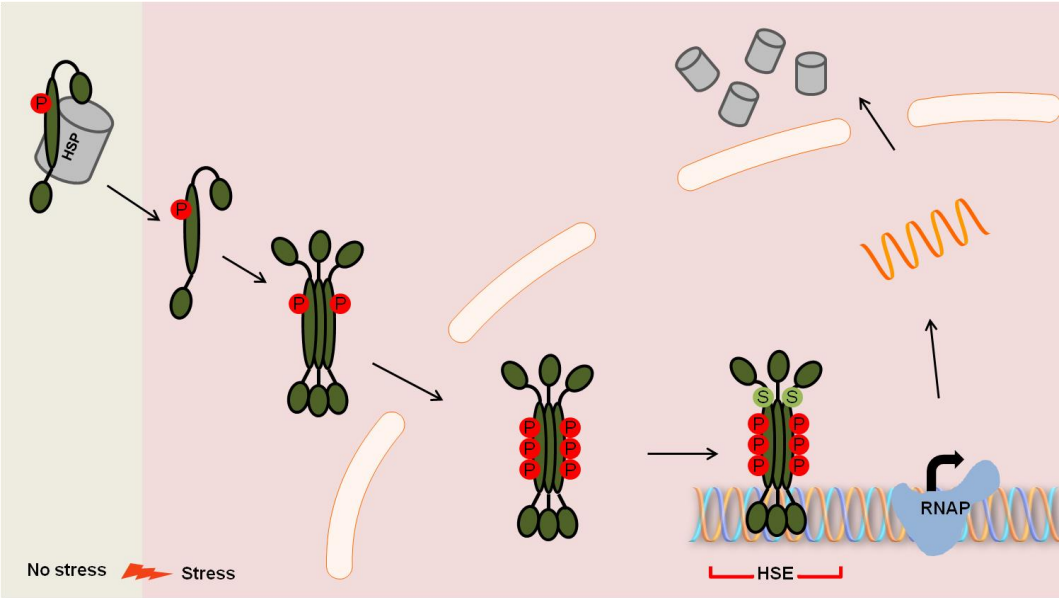

Figure 1.3: Illustration of eukaryotic HSR mechanism. Monomeric HSF1 is inactivated by HSPs in cytoplasm at normal growth conditions. Upon stress, HSF1 is released, trimerized, and transported to nucleus where it is hyperphosphorylated and sumoylatied. Following activation, HSF1 recognizes heat shock elements (HSEs), and other components of transcription machinery are recruited. HSPs expressed and transported through the cytoplasm to maintain

cellular survival against misfolded and unfolded proteins. Reprinted with permission from ref [39]. Copyright 2010 Elsevier.

1.3. Nanotechnology and Nanomaterial Applications

Nanotechnology concept by miniaturizing materials was firstly introduced by famous physicist Richard Feynman with a lecture entitled “There’s plenty of room at the bottom” in 1959 [40]. Further developments in physics, biology and chemistry have been established the roots of nanotechnology. Since then, nanotechnology has been applied by many fields in numerous applications such as electronics and communication, medical and environmental applications, or food and cosmetics industry. In this manner, nanomaterials have played a crucial role in these applications. Specifically, many nanoparticles have been developed in cosmetics, food technology, paintings and coatings [41].

Nanotechnology, as a term, refers combinations of “nano” and “technology” dealing with materials whose size ranges from 1-to-100 nm. One of the most fundamental members of nanomaterials is called nanoparticles (NPs) [42]. Unlike their bulk form, NPs exhibit a wide range of tunable properties based on their sizes. NPs have considerably high surface-to-volume ratio due to their small size making them different in terms of physical, chemical, optical, biological, and electronic properties [41]. For instance, chemical reactivity of NPs increases with decreasing size since there is an increase of the fraction of surface atoms. Based on the application of interest, NPs can be synthesized in different sizes, shapes (spherical, cubical, rode), and dimensions (one-dimensional, two-dimensional,

and three-dimensional). Variable potentially applicable fields give raise NPs to be synthesized and categorized in different ways.

Engineered nanomaterial usage in various fields such as electronics, transportation, imaging, biomedicine, remediation, cosmetics, coatings, and textile has been increased in the past decades. To begin with, in electronics, transistors with very small sizes have been achieved thanks to developments in carbon nano tube (CNT) technology [43]. In transportation, NPs of carbon black has been used many years in car tires. In imaging technology, atomic force microscopy (AFM) tips from SWCNTs have been used to image small molecules such as DNA or antibodies providing high resolution [44]. NPs have various application areas in biomedicine. Because of antimicrobial properties of silver and titanium dioxide NPs, they are used as coatings for surgical masks [45]. Also, dextran coated superparamagnetic magnetite particles have been used in medical imaging application for long time [46]. In remediation, Paints with titanium dioxide NPs have been developed to absorb noxious gases coming from exhausts [43]. Also, iron NPs have been used in water remediation removing many carcinogens [47]. Many personal care and cosmetic products such as toothpaste, cream, shampoo, lipstic, sunscreen, parfume, etc. contain nanomaterials such as fullerenes, lipid-based NPs, titanium dioxide NPs, silicon, etc. Nanomaterials as coatings have been used for decades in a range of areas. For instance, self-cleaning windows coated with titanium dioxide NPs have been demonstrated that they can break the dirt and contaminants in the presence of water and sunlight. Also, NPs in textile for antimicrobial characteristics have been used for many years [43]. Besides their current usage, nanomaterials are very promising for future applications. Still there

are ongoing researches to develop nanoscaffolds for regenerative medicine applications [48], nanospheres for targeted and controlled drug delivery [49], nasal vaccines [50], and biosensing [51].

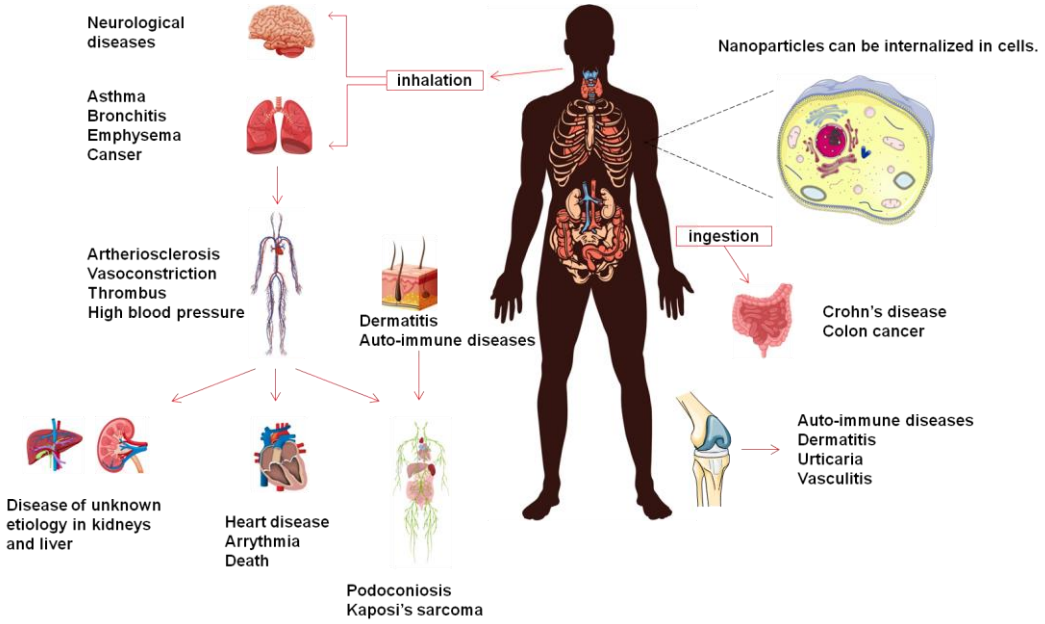

Figure 1.4: Nanoparticle exposure related diseases of human body with exposure pathways and affected organs. Reprinted with permission from ref [43]. Copyright 2007 American Vacuum Society.

1.3.1. Nanomaterial-triggered Toxicity

Human can contact with nanomaterials through skin contact, inhalation, or ingestion. Because of their small size, nanomaterials can easily pass cellular barriers. Further, nanomaterials can distribute and localize through the body by using circulation or lymphatic system. Nanomaterials might show some unexpected effects on living organisms. At cellular level, nanomaterials may interact with macromolecules in cells (i.e. proteins, lipids, nucleic acids) causing cellular dysfunction and stress [43]. On the other hand, based on the size, shape,

charge, concentration, route of administration, surface coating and composition, adverse effects of NPs might show variability [52].

Toxicity of nanomaterials depends on various factors such as size, shape, aggregation, surface functionalization, chemical composition, etc. Thus, not all nanomaterials illustrate the same adverse effects as others. Yet, in general, nanomaterials (i.e., carbon nanotubes, fullerenes, quantum dots, etc.) cause certain common toxicity features on cells such as ROS generation [53]. Because of ROS in cells, proteins, lipids, and nucleic acids are damaged [54]. ROS generation can be caused by several sources in cells such as from surface particles, transition metals in NPs, damaged mitochondria, and activated inflammatory cells. Another adverse effect of NPs is inflammation which is the normal response against any injury. Oxidative stress caused by NPs triggers inflammation by triggering proinflamatory mediators or cytokines [55, 56]. Also, oxidative stress triggers production of antioxidant proteins to neutralize the oxidative stress in cells [57]. Yet, ROS may overwhelm the antioxidants and lead DNA damage and heritable mutations in cells [57, 58]. Besides ROS-mediated toxicity, NPs may cause toxicity via direct contant with cell surface. Especially positively charged NPs are adsorbed easily by negatively charged cell membrane. This charge-charge interaction is able to disturb the structure of lipid bilayer changing the membrane permeability [59].

Similar to any stress conditions, cells try to adapt themselves to changes caused by nanomaterial exposure. Several studies have reported that cells mainly activate ROS scavenger genes to eliminate over produced ROS and their damages in cells. Other than ROS scavengers, cells initiate expression of genes related with

membrane structure, electron transfer machinery, DNA repair, cellular transport, heat shock response, protein efflux machinery, etc [60].

NP uptake mechanism by cells is still unclear; yet, some proposed mechanisms exist. One way of NP uptake is passive diffusion necessitating no accessory mechanisms but only transfer of particles though forces (i.e. van der Waals, electrostatic charges, etc.). Also, released ions from NPs may enter the cells by using divalent metal transporters [61]. Finally, in some cases NPs can be internalized with phagosytosis. After NPs are internalized, they can locate anywhere in cells such as cytoplasm [62], outer-cell membrane [62], mitochondria [63], nucleus [62, 63], nuclear membrane, or lipid vesicles [62, 64] interacting macromolecules in cells.

1.4. Principles of Whole-cell Biosensors

Whole-cell biosensors are a type of biosensors which utilize the whole organism, generally microorganisms, as sensor. Similar to conventional sensing system, whole-cell biosensors are composed of three major subunits: a receiver, a transducer, and an actuator. The receiver element senses the analyte of interest. Further, the transducer element processes the upcoming signal and converts it into a measureable output [65]. Whole-cell biosensors have been used in biomedical as well as environmental applications for many years to detect disease biomarkers, chemicals, heavy metals antigens, amino acids, viruses, toxins, etc. Besides, reporter choice in whole-cell biosensors is crucial since the output should be distinguishable from any background signal [66]. Various output genes have been utilized so far during whole-cell biosensor construction those are enzymes

(luciferase, β-galactosidase, chloramphenicol acetyltransferase, etc.), fluorescent proteins (green fluorescent protein and its analogous) or pigments [67].

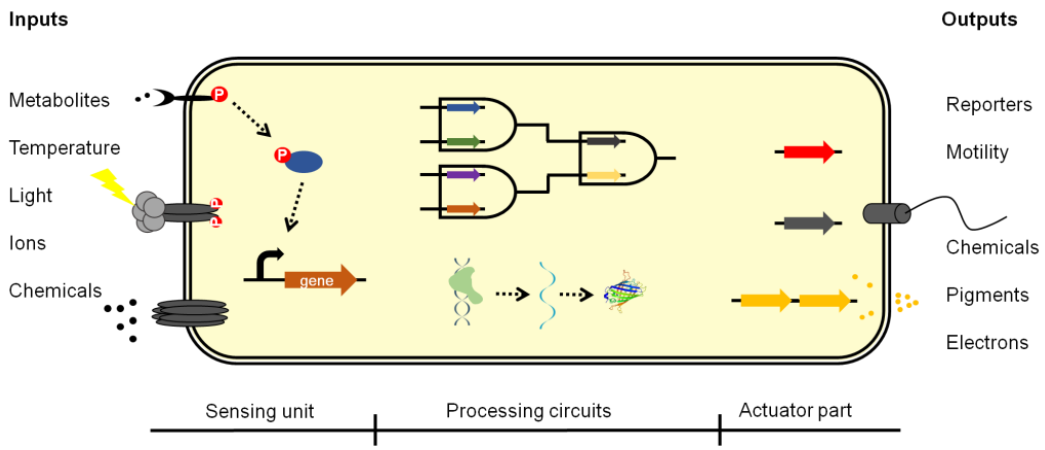

Figure 1.5: Working principle of a whole-cell biosensor. The sensor cell receives environmental signals (i.e., small metabolites, chemicals, ions, temperature shift, or light) activating processing units. Signal processing could be conducted via different mechanisms (i.e., transcriptional regulation, or logic operation). After processing the incoming signal, the sensor cell responds through reporter expression, motility changes, or chemical secretion. Reprinted with permission from ref [67]. Copyright 2018 American Chemical Society.

1.4.1. Whole-cell Biosensor Approach for Toxicity Assessment

Current cytotoxicity and biocompatibility assessments of nanomaterials such as analytical methods, *in vitro* and *in vivo* models are expensive, time consuming, or expert-oriented [68]. Among those tests, a fast-acting whole-cell biosensor designs have become more favorable. In the earliest toxicity determination approaches, non-specific whole-cell sensors have been used. The most famous

one is the luminescent bacterial toxicity assay (LBTA) which measures the reduction of the signal caused by toxicants. Yet, this system is highly open to false positive results [69]. Next, semi-specific whole-cell biosensors utilizing stress regulators have been developed. Among them, HSP promoters controlling the expression of a reporter have been utilized commonly. However, their native forms show high leakage which makes the system inadequate [70-73]. The most precise way to detect analyte of interest is to create specific whole-cell biosensors utilizing certain promoter-transcription factor pairs. Many heavy metal detecting regulatory proteins have been identified in various organisms so far. For instance, CadC and its cognate promoter are used to detect cadmium or ZntR and its cognate promoter are used for zinc detection. This mechanism is either activation or repression-based which is activated or repressed only in the presence of analyte of interest [67]. Thus, this system provides precision to the whole-cell biosensor approach. Yet, making a general stress indicator to screen toxicity of nanomaterials is limited to its source.

CHAPTER 2

Synthetic Genetic Circuit Design to Monitor Nanomaterial-triggered Toxicity

This work is partially described in the following publication [74]:

Behide Saltepe,[†,‡] Eray Ulaş Bozkurt,[†,‡] Nedim Hacıosmanoğlu,[†,‡] Urartu Özgür Şafak Şeker*[†,‡]

† UNAM−Institute of Materials Science and Nanotechnology, National Nanotechnology Research Center, Bilkent University, 06800 Ankara, Turkey

‡ Institute of Materials Science and Nanotechnology, Bilkent University, 06800 Ankara, Turkey

* Corresponding author

E-mail address: urartu@bilkent.edu.tr

Reprinted (adapted) with permission from *ACS Synth. Biol*. 2019, 8, 10, 2404-2417. Copyright 2019 American Chemical Society.

2.1. Objective of the Study

Biocompatibility assessment of nanomaterials has been of great interest due to their potential toxicity. However, conventional biocompatibility tests fall short of providing a fast toxicity report. We developed a whole cell based biosensor to track biocompatibility of nanomaterials with the aim of providing fast feedback to engineer them with lower toxicity levels. We engineered promoters of four heat shock response (HSR) proteins utilizing synthetic biology approaches. As an initial design, a reporter coding gene was cloned downstream of the selected promoter regions. Initial results indicated that native heat shock protein (HSP) promoter regions were not very promising to generate signals with low background signals. Introducing riboregulators to native promoters eliminated unwanted background signals almost entirely. Yet, this approach also led to a decrease in expected sensor signal upon stress treatment. Further, coupling of HSR mechanism with bacterial communication systems (namely quorum sensing (QS) mechanism), increased the overall output causing high level of background noise. Thus, it has been observed that activation based circuits are not suitable to construct such tightly controlled sensors, since they indicate higher basal signal, and require more engineering approaches to fine tune the system.

2.2. Introduction

Cytotoxicity and biocompatibility assessment are the crucial steps during the development of new biomaterials. For any clinical use, such evaluation is required in order to have a better understanding and prevention of possible complications

may be caused by newly developed materials in patients. In order to perform such assessments, many methods have been developed. There are mainly three approaches to assess toxicity: (i) analytical methods, (ii) *in vitro*, and (iii) *in vivo* models. Among them, analytical methods such as flow cytometry, mass spectrometry, and other spectroscopic and microscopic techniques are efficient and reliable. Yet, they are expensive and require high degree of expertise [68]. Thus, *in vitro* and *in vivo* models are mostly preferred. However, there is an ongoing need for a cytotoxicity test with high degree of speed and reliability. International Organization for Standardization (ISO) defines three types of *in vitro* cytotoxicity test in ISO 10993-5 [75]. MTT assay is the most widely used and a colorimetric assay based on reduction of yellow MTT to purple formazan by mitochondrial dehydrogenase activity. Thus, the color change indicates cell's activity instead of cytotoxicity causing several false-positive results in many cases [75-77]. Furthermore, it requires specific equipment and chemicals to test toxicity making it relatively expensive and time consuming (3-5 days for cell culture period and 4-6 hours for toxicity assessment) [78]. Agar overlay method can also be used to evaluate toxicity to visualize the destruction of cells caused by toxicant via electron microscopy. This method is easier to apply; however, requires expensive tools (i.e. special facility equipped with a proper electron microscopy) and considerably longer times [75]. Direct contact method is used to track morphological changes of cells upon toxicant treatment which requires specific equipment and higher expertise [75, 79]. However, toxicity testing of nanoparticles (NPs) has specific challenges. Their small size results in greater surface-to-volume ratio, therefore higher biological reactivity causing stress

response [80-82], reactive oxygen species (ROS) generation [80, 81], and DNA damage response [80]. Furthermore, other unique properties such as high adsorption, hydrophobicity, surface charge and catalytic activities can interfere with conventional methods. Guadagnini *et al.* used six NPs with different properties and tested with conventional *in vitro* assessment methods, inflammatory response and oxidative stress methods and showed that NPs interfere with many of the tests used (WST-1, MTT, lactate dehydrogenase, neutral red, propidium iodide, 3H-thymidine incorporation, ELISA for inflammatory response, monobromobimane, dichlorofluorescein and NO assays for oxidative stress) [83]. As an alternative, many model organisms including daphnia [84], algae [85], zebrafish [86-88], mice [89, 90] and monkey [90] are also employed to test NPs. To develop a fast-acting toxicity assessment method, choice of appropriate model organism is vital and using microorganisms, either prokaryote or eukaryote, has significant advantages over higher eukaryotes. Due to their higher growth rate, microorganisms can ensure sufficient biomass which will lead to considerable amount of reporter signal in shorter times. Moreover, microorganisms are easier to handle and manipulate. Most importantly, the motivation behind utilizing microorganisms is to assess possible toxicity prior to more complex, expensive and time-consuming experiments and trials including higher eukaryotes such as mice, monkey and humans [91]. On the other hand, in general, *in vivo* studies require special model organisms (daphnia [84], algae [85], zebrafish [86-88], mice [89, 90] or monkey [90]) and utilize indirect measure of toxicity (i.e., mortality rate, swimming speed, and body length measurements are examined in zebrafish.) [85-88]. In addition, they need longer periods of time to

report toxicity.[84, 87] Development of biosensor-based assays became a promising solution to overcome most of the above mentioned problems since they are relatively fast, cheap, and easy-to-use. In early stages, Luminescent Bacterial Toxicity Assays (LBTAs), such as Microtox®, have been utilized to assess mostly environmental toxicity. Later, these systems were criticized due to hormesis effect, stimulation of luminescence from tested chemicals and false positive results. Therefore, these systems were lack in precision and specificity, and problematic in application [69]. Later, semi-specific biosensors utilizing stress regulators have been developed to detect toxicity; heat shock protein (HSP) promoters were the most commonly used elements in these studies [70-73]. Although they brought a new perspective to the field, a gap remains to be fulfilled by a quantitative assay with high degree of speed and low leakage. Thus, synthetic biology approaches can compensate the need for more developed biosensors by employing Heat Shock Response (HSR) elements to detect toxicity.

Heat shock mechanism is a universal process exhibited by cells to any kind of stress such as heat, osmotic stress, chemicals, ions, or nanomaterials (NMs) [92]. Several transcriptomic analyses indicate that exposure to any stress agent, especially to toxic compounds, prompts changes in gene expression profile, specifically genes related to stress response [80-82], reactive oxygen species (ROS) metabolic processes [80, 81], DNA damage response [80], and cell redox homeostasis [80]. In order to maintain cellular integrity and survival, nanomaterial exposure (i.e., silver nanoparticles (NPs) [93], silica NPs [94], quantum dots (QDs) [95], or carbon nanotubes [96]) triggers the production of a set of HSPs [97]. The HSPs are a sub-group of molecular chaperones; accessory proteins that

manage mechanisms crucial for the cell survival and maintenance including protein folding and assembly mechanisms [35]. Some chaperones such as Hsp60, Hsp70 and Hsp90 cope with misfolded proteins to refold them properly [98], while others, such as ClpB (or its eukaryotic homolog Hsp104), Lon and HtrA degrade protein aggregates in cells [99, 100]. Although HSR is controlled differently in many organisms, some of the chaperones play a common role in different organisms like Hsp70 which is the major stress related chaperone protein in bacteria as well as in eukaryotes.

In *Escherichia coli*, main HSR is conducted by DnaK (Hsp70)-DnaJ (Hsp40)-GrpE machinery. Unlike many transcription mechanisms in *E. coli*, HSPs are not regulated by σ^{70} factor; a universal subunit of RNA polymerase. Instead, HSPs are controlled by a special stress-inducible subunit, namely σ^{32} factor, encoded by *rpoH* gene [35, 101]. Under normal growth conditions, σ^{32} level is maintained at constant levels due to its unstable nature; however, after exposure to any stress, σ^{32} level is dramatically elevated via improved stability as well as increased synthesis [35, 36, 102]. σ^{32} is regulated by a negative feedback loop controlled by DnaK-DnaJ-GrpE mechanism [103]. Accumulation of chaperones in this mechanism holds σ^{32} and blocks its activity [104, 105], leading to degradation of σ^{32} by FtsH; a special σ^{32} degrading protease [106]. Therefore, monitoring of HSP levels in cells can be used as a promising stress indicator of heavy metals and newly developed nanomaterials.

Detection of heavy metal toxicity [107-109] and other toxic compounds [110] through HSR mechanism is a quick and more straightforward way to evaluate negative effects caused by different stress agents [70]. Many HSP promoters [71,

82, 111] such as dnaK, grpE, clpB, or fxsA have been studied in the literature with different reporter genes such as *gfp* [70, 72, 112, 113], *lacZ*, or *lux* [107, 110, 112, 114, 115] to detect the stress response caused by pollutants and many chemicals. Cha *et al.* designed GFP-based biosensors by fusing promoter elements of σ^{32}, clpB and dnaK to the upstream of the reporter to detect cellular stress caused by heat and ethanol. They observed the maximum response at 8th hour after stress exposure [70]. Similarly, Seo *et al.* utilized two hours of heat shock treatment for HSR induction with the same approach (σ^{32}, clpB and dnaK promoters fused with reporter) and similar results were observed [71]. In another study, grpE promoter was fused to fluorescence reporter and ethanol was used as inducer. The study concluded that fluorescence signal was not significant in short period of time (90th min), and 10th hour of fluorescence signal was significant enough due to reporter accumulation to make an assessment [112]. Martinez *et al.* utilized four stress promoters (katG for oxidative stress, dnaK for protein damage, fabA for membrane damage, and recA for DNA damage) and treated these sensors with specific stressors (H_2O_2, ethanol, SDS and mitomycin, respectively). Stress sensor with dnaK showed less than 2-fold response in two hours [116]. Although these biosensors eliminated high cost and provided easy usage, they were inadequate in shortening the response time and preventing false positive signal. After the development of advanced synthetic biology tools, many opportunities arose to redesign and optimize existing mechanisms. Thus, applying synthetic biology approaches allows construction of different biosensors with complex genetic circuits [67] to detect analyte of interest [117, 118] (i.e., heavy metal exposure). In this manner, a biosensor circuit coupled with HSP promoters and a

reporter is one of our objectives to detect stress response of cells caused by NM-triggered toxicity.

Nanomaterials and nanoparticles are of great interest for their wide range of applicability across many areas from medicine to optoelectronics. They have size-dependent tunable optical and physical properties; which are not usual for bulk materials [119-121]. NMs are widely used in innovative applications such as in medical diagnostics, drug delivery and targeted photo-thermal therapy which necessitates patient interaction with NMs [122]. Also, utilization of NMs in consumer goods may contaminate environment, food and textiles [123]. NMs have high surface-to-volume ratio which makes them desirable elements for many chemical reactions, or self-assembly applications. Despite their success in many applications, small size of NMs makes them able to penetrate through cellular barriers easily; besides, their high surface-to-volume ratio opens a room for causing cellular stress. Furthermore, stress caused by NMs in cells might provoke protein unfolding [124], DNA damage [125, 126], ROS generation [127-129], and disruption of gene expression [125, 126, 130] leading potential health problems. The relation between toxicity and surface-to-volume ratio has also a critical effect on membrane passage. As size of the NMs decreases, the ratio of NMs passing the membrane increases, eventually causing many stress related problems summarized above. Additionally, defects on NMs increase surface area of NMs which facilitates protein corona formation through adsorption of molecules in the cellular environment (i.e., proteins like serum albumin, immunoglobulin, fibrinogen etc.) on NMs via several forces such as hydrogen bonds or Van der Waals interactions [124]. This process may cause blocking of membrane pores,

leading starvation and cell death [131]. At the system level, NMs can trigger inflammation and alter immune system response [132-134].

Recently, a few efforts have been made in order to assess toxicity of QDs by employing different organisms such as daphnids [84], algae [85] and zebrafish, which is the most common model organism in QD toxicity studies [86-88]. In these experiments, indirect quantitative methods, such as mortality rate for dapnids [84] and swimming speed, heartbeat, or body length for zebrafish [88] have been used. Also, such methods require days to make a comment on toxicity of particular QDs and the measurements may not reflect a dose-responsive analysis. On the other hand, although QD toxicity has been analyzed with viability assays, microscopy, microcalorimetry, growth inhibition, membrane damage assessments and transcriptomic analysis in bacteria, there is no HSR sensor-based toxicity evaluation of NM-triggered toxicity [61, 128, 135, 136]. Thus, development of a quick, dose-responsive and cheap sensor system that reports NM-triggered toxicity is very critical to monitor biocompatibility of NMs prior to field application.

2.3. Materials and Methods

2.3.1. Media and Strains

E. coli DH5α (New England Biolabs, Inc.) was grown in LB medium (1% (w/v) tryptone, 0.5% (w/v) yeast extract, 0.5% (w/v) NaCl) with proper antibiotics at 37°C and 180 rpm shake in Erlenmeyer flasks. Overnight cultures were prepared from frozen glycerol stocks and incubated for 16 h with the same culturing conditions mentioned previously. 1% of inoculums from overnight cultures were

used to start experimental cultures and monitored via spectrophotometer (GENESYS 10 Bio, Thermo Scientific) until OD_{600} reached 0.4-to-0.6 before induction steps were applied.

2.3.2.Plasmid Construction

E. coli heat shock promoters were amplified from *E. coli* DH5α genomic DNA by primers shown in Table B.1. Engineered riboregulators with PclpB promoter part and PibpA-taRNA part were synthesized by GENEWIZ Company. Q5 Hot Start High-Fidelity DNA Polymerase (New England Biolabs, Inc.) was used for all PCR reactions (Reaction conditions were described in Appendix E). To construct the stress sensor plasmid backbone, pZa-tetO-eGFP vector was digested with XhoI-KpnI restriction enzymes (New England Biolabs, Inc.) (Reaction conditions were described in Appendix E). NucleoSpin Gel and PCR Clean-up kit (Macherey-Nagel) was used according to the manufacturer's instructors to purify digested DNA samples or PCR products from 1 to 1.8% Agarose gels stained with SYBR Safe DNA Gel Stain (Thermo Fisher Scientific). Plasmid construction was made via ligation with DNA T4 ligase (New England Biolabs, Inc.) or via Gibson Assembly method described by Gibson *et al.* [137], and for quorum sensing plasmid cloning, Golden Gate Assembly, Gibson Assembly [138], and T4 ligation methods were used. (All reaction conditions were described in Appendix E). After all assembly methods, mixes were directly transformed into chemical competent *E. coli* DH5α cells. Constructed genetic circuits were sequence verified by Sanger Sequencing (GENEWIZ). All genetic part sequences used this chapter was

introduced in Table A1, and all constructed vector maps were indicated in Appendix C with their sequencing verification results in Appendix D.

2.3.3. Chemical Competent Cell Preparation and Transformation of DNA in Cells

Overnight cultures of *E. coli* DH5α were prepared from frozen glycerol stocks and incubated for 16 h with the same culturing conditions mentioned previously. 1% of inoculums from overnight cultures were used to start fresh culture for competent cell preparation. Culture was incubated at 37°C and 180 rpm shake in Erlenmeyer flasks until OD_{600} reached 0.2-to-0.5. Following, culture was cooled in ice for 10 min and cells were collected by centrifugation at 1000 ×g for 10 min at +4°C. After centrifugation, supernatant was discarded and cell pellet was resuspended in 10% (v/v) of TSS Buffer (10% (w/v) PEG-8000, 5% (v/v) DMSO, 50 mM $MgCl_2$ pH 6.5 in LB). For each aliquot, 100 µl of cultures were placed in each microcentrifuge tubes and stored at -80°C.

Chemical competent cells were thawed on ice for 30 min before transformation. For transformation, whole ligation product, Gibson Assembly reaction product, or 100 ng of intact plasmid DNA was introduced to thawed cells and incubated on ice for 20-30 min. Following, cells were shocked by heat treatment at 42°C for 30 sec. After the heat shock, cells were cold shocked for 2 min on ice. Then, 250-1000 µl of LB was added onto the cells and incubated at 37°C and 180 rpm shake for 45-60 min. At the end of the incubation, cells were collected at 1000 ×g for 10 min and the supernatant was discarded. The collected cells were resuspended in 50 µl of LB and spread onto LB-agar supplemented with proper antibiotics.

2.3.4.Sequencing Alignments with Geneious Software

All plasmid maps were constructed on an online vector tool; Benchling. Following, all plasmid maps were exported as .gb files and imported in Geneious software together with the sequencing results of plasmid maps as .abi files. In order to align plasmid map and its sequencing data, both sequences were selected and pairwise alignment performed. The sequencing results for all vectors were indicated in Appendix D.

2.3.5.Heat Shock Experiments and Toxicity Assay

After OD_{600} of experimental cultures reached 0.4-to-0.6, Erlenmeyer flasks corresponding to heat shock treatment were immersed in 55°C water bath for 30 min as describe by Rodrigues *et al.* [82], while Erlenmeyer flasks corresponding to toxicity assay were treated with water-soluble thiol-capped CdTe QDs with varying concentrations. QDs were prepared using the method as explained in a previous work by Seker *et al.* [139].

2.3.6.Fluorescence Measurement and Data Analysis

All fluorescence measurement studies were conducted via microplate reader (SpectraMax M5, Molecular Devices). Excitation and emission wavelengths for eGFP were set as 485 and 538 nm, respectively. Each measurement was conducted in Corning 96-well clear flat bottom polystyrene plates with 250 µL of culture sample resuspended in 1×PBS (137 mM NaCl, 2.7 mM KCl, 4.3 mM Na_2HPO_4, 1.47 mM KH_2PO_4, pH 7.4). For signal normalization, raw fluorescence

intensity was divided by OD_{600} values of each sample. For each treatment (corresponding temperature or concentration), its control group (cells with mock vector) was subtracted from sensor data. The data for the initial expression level was recorded as the 15th min to eliminate errors caused by delays in early protein expression.

2.3.7.RNA Purification and cDNA Synthesis

NucleoSpin RNA kit (New England Biolabs, Inc.) was used according to the manufacturer's instructors to isolate total RNA from each sample. Three independent biological replicas were prepared for each group. RNA concentration was quantified with NanoDrop 2000 spectrophotometer (Thermo Fisher Scientific). Samples were stored at −80°C until cDNA synthesis. Reverse transcribed RNA concentration were set to 500 ng in 20 µLof reaction volume for each sample. iScript cDNA Synthesis Kits (Bio-Rad) were used to convert RNAs into cDNAs according to the manufacturer's instructions (Reaction conditions were described in Appendix E).

2.3.8.qPCR and Data Analysis

After cDNA preparation, qPCR experiment was performed with 1 µL of cDNA for each sample via SsoAdvanced Universal SYBR Green Supermix (Bio-Rad) for *egfp* and a housekeeping gene (*hcaT*) according to the manufacturer's instructions. Primers were specified in Table B1. Three technical replicas were prepared for each independent biological replica. PCR cycles were proceeded as follows: initial denaturation for 3 min at 95°C, denaturation for 10 sec at 95°C,

annealing for 15 sec at 60°C, extension for 10 sec at 72°C for 39 cycles, 10 sec at 95°C (Reaction conditions were described in Appendix E). Product specificity was confirmed by a melting curve analysis (65−95 °C). Comparative Ct method (ΔΔCt) was used to analyze the results.

2.3.9.Time Resolved Fluorescence Spectroscopy

Experiments were performed using a PicoQuant Fluo Time 200 timecorrelated single photon counting system. A laser diode operating at 375 nm had a repetition rate of 80 MHz with 200 ps width. 300 nM 500 μL of QDs were added to quartz cuvette, and cell number was kept around 4×10^{8}. To prevent the aggregation of the QDs upon addition of the cells, the mixture was mixed rigorously. The measurements were taken by adjusting the emission maxima of the GFP. The results were provided in Appendix F.

2.3.10. Microscopy

Samples were prepared together with each fluorescence measurement assays with specified time points in each figure. All imaging was conducted with LSM 510 Confocal Microscope (Zeiss). Samples were excited with Argon 488 nm for reporter imaging and emission was collected with LP 505 filter for eGFP, while QD samples were excited with HeNe 543 nm laser, and emission was collected with LP 585 filter. For dose−response curve analysis, bright field imagings of samples were also conducted, which were merged with corresponding fluorescence images afterward. All microscopy images of the sensors were provided in Appendix F.

2.3.11. Statistical Analysis

All data were expressed as mean ± standard error mean. Depending on the groups of interest, either one-way analysis of variance (ANOVA) or two-way ANOVA with Dunnett's/Tukey's/Sidak's multiple comparison tests (GraphPad Prism v6) were used to compare groups.

2.4. Results

2.4.1.Cloning of Initial HSR Circuits

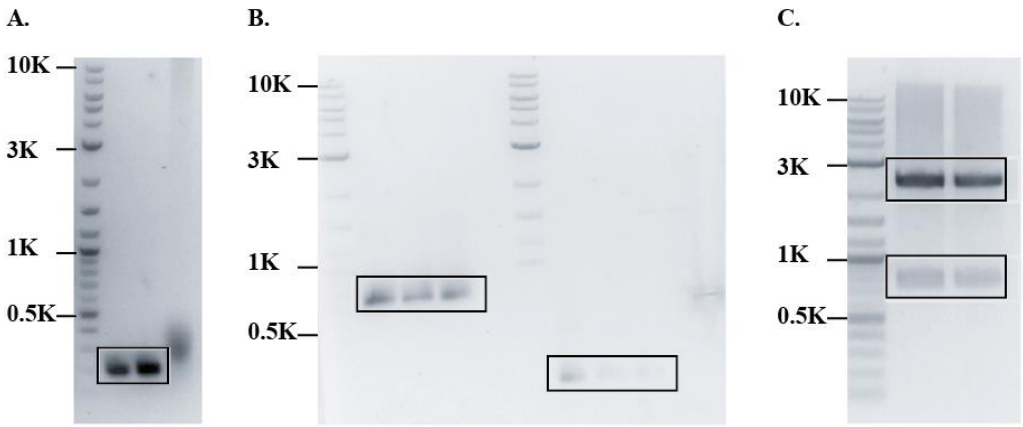

Figure 2.1: Construction of PdnaK-GFP-pZa-tet vector. A. PdnaK were isolated from *E. coli* genome and observed at 200 bp on the gel. B. eGFP (left) and PdnaK (right) PCR products with Gibson Assembly primers. Bands were observed at 750 bp and 250 bp, respectively. C. Digested tet-GFP-R5-pZa vector with HindIII-pnI enzyme pairs. Linear vector and GFP-R5 piece were observed at 2100 bp and 800 bp, respectively. 1 kb+ DNA Ladder (NEB) was used as DNA marker.

For cloning of PdnaK-GFP-pZa vector, DnaK promoter (PdnaK) was isolated from *E. coli* genome via PCR using primers in Table B.1. PCR products were run on 1% Agarose gel (Figure 2.1A) and isolated using MN-gel extraction kit according to manufacturer's instructions. Further, eGFP and isolated PdnaK promoter were amplified with Gibson Assembly primers (Table B.1), and PCR products were run on on 1% Agarose gel (Figure 2.1B left and Figure 2.1B right, respectively) and isolated to be assembled with Gibson Assembly reaction. For backbone, tet-GFP-R5-pZa vector, constructed by Dr. Tolga Tarkan Ölmez in our lab previously, were digested with HindIII-KpnI enzyme pairs and linearized. Digested backbone products were run on 1% Agarose gel (Figure 2.1C) and isolated. Obtained pieces were assembled with Gibson Assembly reaction. After Gibson Assembly, selected colonies were verified with restriction digestion (Figure 2.2A) and sequencing (Appendix D).

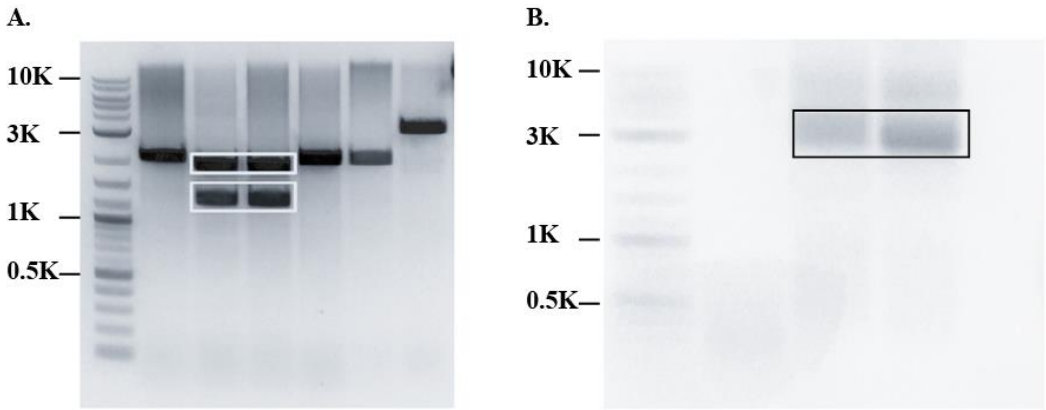

Figure 2.2: Verification of PdnaK-GFP-pZa-tet vector with restriction digestion (A), and backbone linearization for PdnaK-GFP-pZa (B). A. After restriction digestion, expected bands (1200 bp for tet-PdnaK-GFP piece and 2200 bp for pZa backbone) were observed only for colony 3 and 4. B. PCR product of linear

PdnaK-GFP-pZa vector was observed at 2800 bp. 1 kb+ DNA Ladder (NEB) was used as DNA marker.

To construct PdnaK-GFP-pZa, verified PdnaK-GFP-pZa-tet vector was linearized with PCR to exclude tet operon from the vector utilizing primers in Table B1. PCR products were run on 1% Agarose gel (Figure 2.2B) and isolated. Isolated linear vector was assembled with Gibson Assembly reaction. After Gibson Assembly, selected colonies were verified with sequencing (Appendix D).

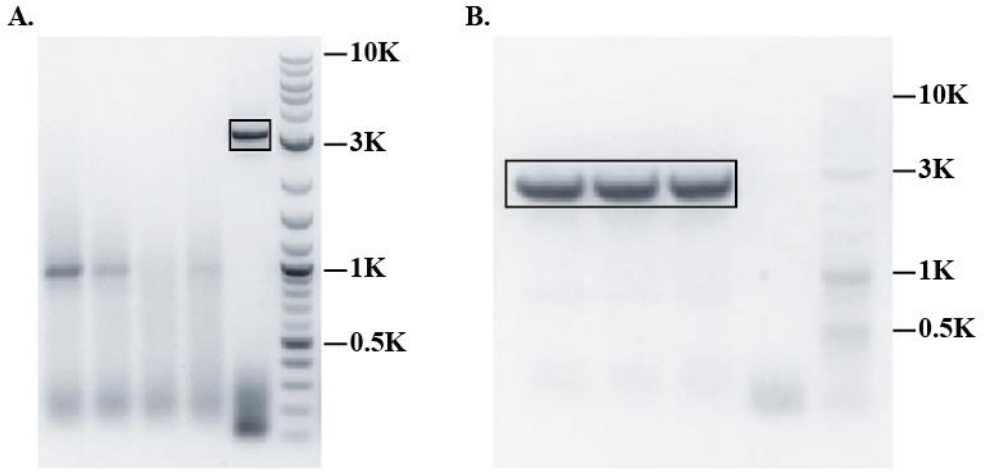

Figure 2.3: Construction of PclpB-GFP-pZa vector. A. PCR product of linear PclpB-GFP-pZa-tet vector was observed at 3000 bp. B. PCR product of linear PclpB-GFP-pZa vector was observed at 2600 bp. 1 kb+ DNA Ladder (NEB) was used as DNA marker.

To construct PclpB-GFP-pZa vector, first PdnaK-GFP-pZa-tet vector was amplified with PclpB overhang primers (Table B1.) to exclude PdnaK region. The

PCR products were run on 1% Agarose gel (Figure 2.3A) and isolated. Isolated linear vector was assembled with Gibson Assembly reaction. After Gibson Assembly, selected colonies were verified with sequencing (Appendix D). Further, to exclude tet operon from the vector, PclpB-GFP-pZa-tet vector was linearized with PCR to exclude tet operon from the vector utilizing primers in Table B1. PCR products were run on 1% Agarose gel (Figure 2.3B) and isolated. Isolated linear vector was assembled with Gibson Assembly reaction. After Gibson Assembly, selected colonies were verified with sequencing (Appendix D).

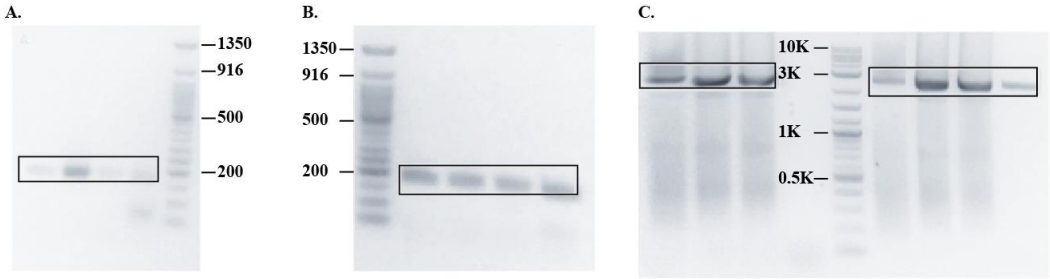

Figure 2.4: Construction of PfxsA-GFP-pZa and PibpA-GFP-pZa vectors. A. PCR product of PfxsA was observed at 190 bp. B. PCR product of linear PibpA was observed at 180 bp. C. PCR product of linear backbone was observed at 2700 bp. 50 bp DNA Ladder (NEB) and 1 kb+ DNA Ladder (NEB) were used as DNA markers for promoters and backbone, respectively.

For cloning of PfxsA-GFP-pZa and PibpA-GFP-pZa vectors, FxsA and IbpA promoters (PfxsA and PibpA, respectively) were isolated from *E. coli* genome via PCR using primers in Table B.1. Small PCR products were run on 1.8% Agarose gel while large PCR products were run on 1% Agarose gel (Figure 2.4A for PfxsA and Figure 2.4B for PibpA) and isolated using MN-gel extraction kit according to

manufacturer's instructions. Further PdnaK-GFP-pZa backbone was amplified to exclude PdnaK with primers in Table B.1 and run on 1% Agarose gel (Figure 2.4C) and isolated. Obtained pieces were assembled with Gibson Assembly reaction. After Gibson Assembly, selected colonies were verified with sequencing (Appendix D).

2.4.2.Cloning of Circuits with Engineered Riboregulators

For cloning of PdnaK-riboswitch-GFP-pZa vector, four independent PCR reactions for PdnaK-taRNA, taRNA-terminator, PdnaK-crRNA, and crRNA-GFP DNA pieces were performed with primers in Table B.1 to be assembled via Gibson Assembly method (Appendix E). All PCR products were run on 1% Agarose gel (Figure 2.5) and isolated using MN-gel extraction kit according to manufacturer's instructions. For backbone, formerly constructed PdnaK-GFP-pZa-tet vector were digested with HindIII-AatII enzyme pairs and linearized. All pieces were assembled with Gibson Assembly reaction. After Gibson Assembly, selected colonies were verified with sequencing (Appendix D).

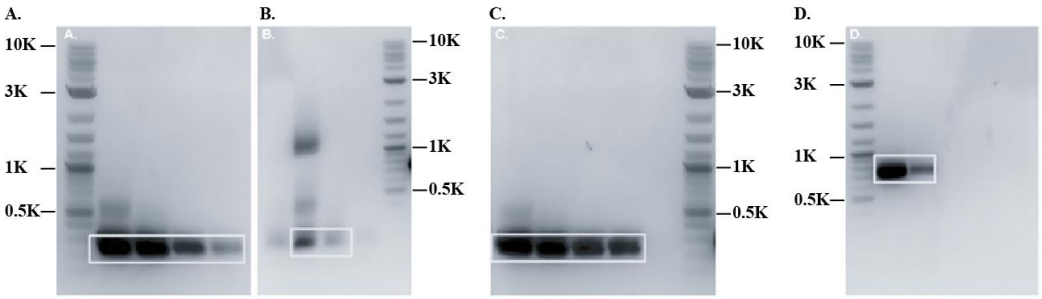

Figure 2.5: Construction of PdnaK-riboswitch-GFP-pZa vector. A. PCR product of PdnaK-taRNA was observed at 250 bp. B. PCR product of taRNA-terminator was observed at 184 bp. C. PCR product of PdnaK-crRNA was observed at 247

bp. D. PCR product of crRNA-GFP was observed at 787 bp. 1 kb+ DNA Ladder (NEB) was used as DNA marker.

For cloning of PclpB-riboswitch-GFP-pZa vector, PclpB-taRNA-rrnBT1-PclpB-crRNA DNA piece including all riboregulator mechanism was synthesized from GenScript and received in pUC57 vector. To obtain the whole piece, the pUC57 vector was digested with KpnI-AatII enzyme pairs. The digestion products were run on 1% Agarose gel (Figure 2.6) and isolated using MN-gel extraction kit according to manufacturer's instructions. For backbone, formerly constructed PdnaK-GFP-pZa vector were digested with the same enzyme pairs and linearized. All pieces were assembled with T4 ligation reaction (Appendix E). After ligation, selected colonies were verified with sequencing (Appendix D).

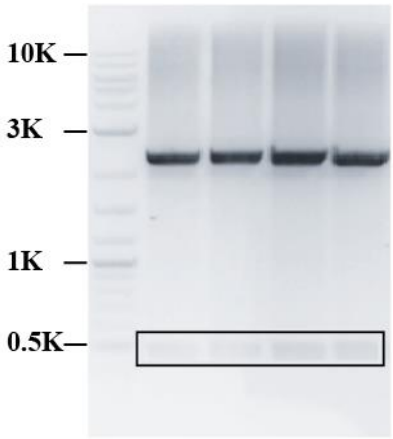

Figure 2.6: Construction of PclpB-riboswitch-GFP-pZa vector. Digested riboregulator region in pUC57 vector was observed at 500 bp. 1 kb+ DNA Ladder (NEB) was used as DNA marker.

For cloning of PfxsA-riboswitch-GFP-pZa vector, two independent PCR reactions for PfxsA-taRNA and PfxsA-crRNA DNA pieces were performed with primers in Table B.1 to be assembled via Gibson Assembly method (Figure 2.7C). Also, for taRNA-terminator, formerly synthesized PclpB-riboregulator piece was digested with SalI-XhoI enzyme pairs (Figure 2.7A), and for the linear backbone PdnaK-riboswitch-GFP-pZa vector was digested with PstI-BamHI enzyme pairs (Figure 2.7B). Both PCR and digestion products were run on Agarose gel (1.8% Agarose gel for small fragments and 1% Agarose gel for large fragments were used.) and isolated using MN-gel extraction kit according to manufacturer's instructions (Figure 2.7). All pieces were assembled with Gibson Assembly reaction. After Gibson Assembly, selected colonies were verified with sequencing (Appendix D).

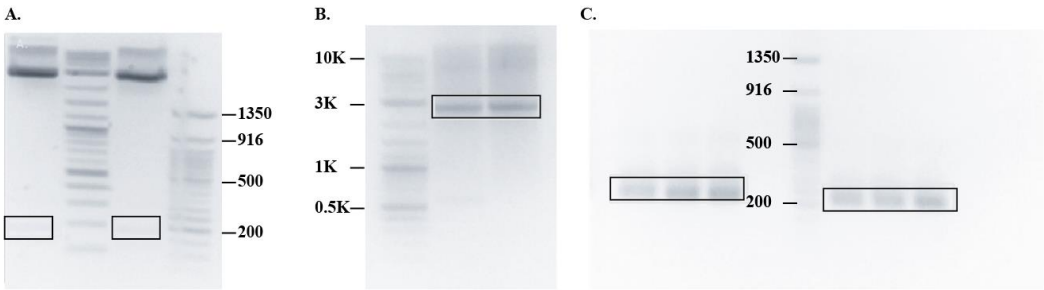

Figure 2.7: Construction of PfxsA-riboswitch-GFP-pZa vector. A. Digestion product of taRNA-terminator was observed at 180 bp. B. Digestion product of linear backbone was observed at 2600 bp. C. PCR products of PfxsA-taRNA (left) and PfxsA-crRNA (right) were observed at 230 bp. 50 bp DNA Ladder (NEB) and 1 kb+ DNA Ladder (NEB) were used as DNA markers for small and large DNA pieces, respectively.

For cloning of PibpA-riboswitch-GFP-pZa vector, two independent PCR reactions for PibpA-taRNA and PibpA-crRNA DNA pieces were performed with primers in Table B.1 to be assembled via Gibson Assembly method (Figure 2.8). Also, for taRNA-terminator, formerly synthesized PclpB-riboregulator piece was digested with SalI-XhoI enzyme pairs (Figure 2.7A), and for the linear backbone PdnaK-riboswitch-GFP-pZa vector was digested with PstI-BamHI enzyme pairs (Figure 2.7B). All pieces were assembled with Gibson Assembly reaction. After Gibson Assembly, selected colonies were verified with sequencing (Appendix D).

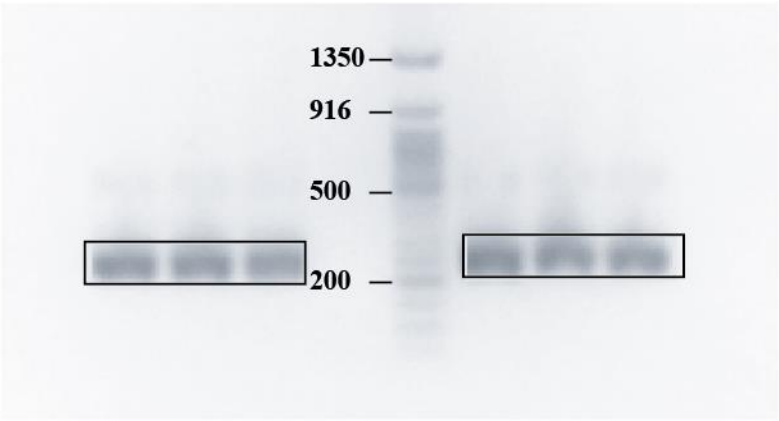

Figure 2.8: Construction of PibpA-riboswitch-GFP-pZa vector. PCR products of PibpA-taRNA (left) and PibpA-crRNA (right) were observed at 230 bp. 50 bp DNA Ladder (NEB) was used as DNA marker.

2.4.3.Cloning of Engineered Quorum Sensing Circuit

Cloning of the engineered quorum sensing vector was designed based on Golden Gate Assembly method. To add a BsaI restriction enzyme recognition site to all parts, each DNA piece was amplified by PCR primers in Table B.1. All PCR products were run on 1% or 1.8% Agarose gels (for large and small fragments,

respectively) and isolated using MN-gel extraction kit according to manufacturer's instructions (Figure 2.9). All pieces were assembled with Golden Gate Assembly reaction (Appendix E). After assembly, selected colonies were sent for sequencing analysis. However, sequencing results showed that some pieces (PdnaK, luxI, and a terminator) did not inserted in the backbone, and these pieces were assembled with Gibson Assembly method. First, these pieces were amplified by PCR primers (Table B.1) to add homology regions. All PCR products were run on 1% Agarose gel and isolated using MN-gel extraction kit according to manufacturer's instructions (Figure 2.10). For backbone, product of Golden Gate Assembly was used and digested with SalI enzyme to linearize the vector. PCR products were assembled with linear backbone with Gibson Assembly, and selected colonies were sent for sequencing. After verification, colonies and the eGFP were digested with KpnI-MluI restriction enzyme pair. Both products were ligated with T4 ligation method and selected colonies were verified by sequencing (Appendix D).

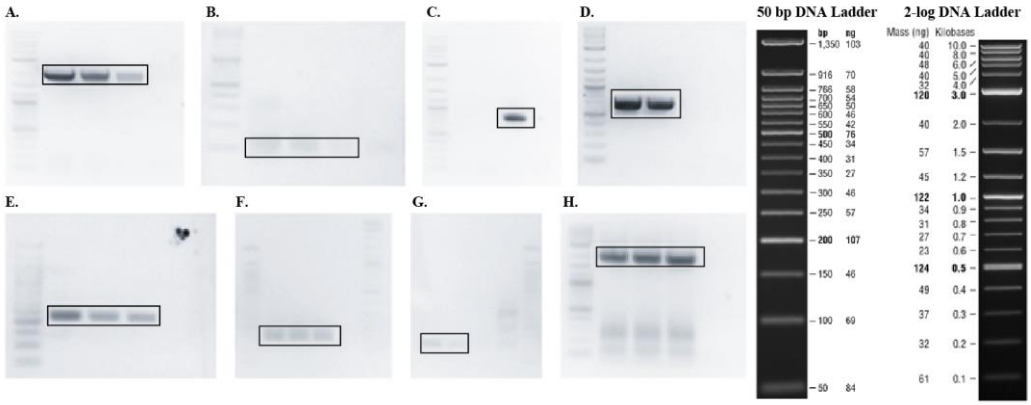

Figure 2.9: Construction of engineered quorum sensing vector with Golden Gate Assembly. A. Plux-pZa vector was observed at 1900 bp. B. Plux-terminator was observed at 130 bp. C. BsaI site added luxR was observed at 800 bp. D. BsaI site

added luxI was observed at 650 bp. E. BsaI site added PdnaK was observed at 230 bp. F. BsaI site added terminator was observed at 130 bp. G. BsaI site added Plux-terminator was observed at 160 bp. H. BsaI site added Plux-pZa vector was observed at 2000 bp. 50 bp DNA Ladder (NEB) and 2-log DNA Ladder (NEB) were used as DNA markers for small and large DNA pieces, respectively.

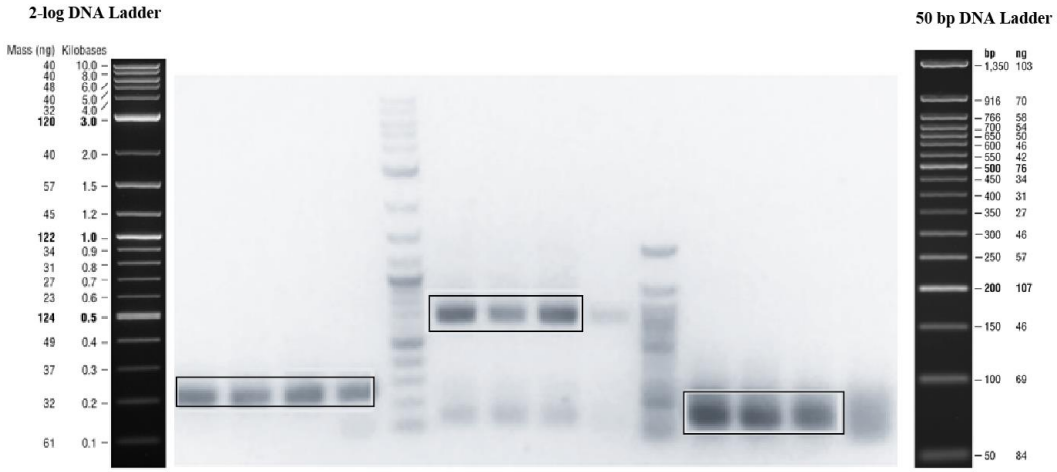

Figure 2.10: PCR products of engineered quorum sensing vector for Gibson Assembly. PCR product of PdnaK (left), luxI (middle), and terminator (right) were observed at 250 bp, 675 bp, and 150 bp, respectively. 50 bp DNA Ladder (NEB) and 2-log DNA Ladder (NEB) were used as DNA markers for small and large DNA pieces, respectively.

2.4.4.Characterization of Native HSR and Riboregulator-mediated Stress Circuits with Heat

For heat shock experiments, each group was subjected to either 37°C or 55°C heat treatment for 30 min. HSR circuits with native HSP promoters (PdnaK, PclpB, PfxsA, and PibpA) showed no significant difference upon exposure to elevated

heat (Figure 2.11). Additionally, their initial background signal was high. On the other hand, riboregulator-mediated circuits decreased the background signal, but signal coming from the stressor also decreased. Among the characterized circuits, PibpA with riboregulators showed significant signal increase upon elevated heat treatment (Figure 2.11D).

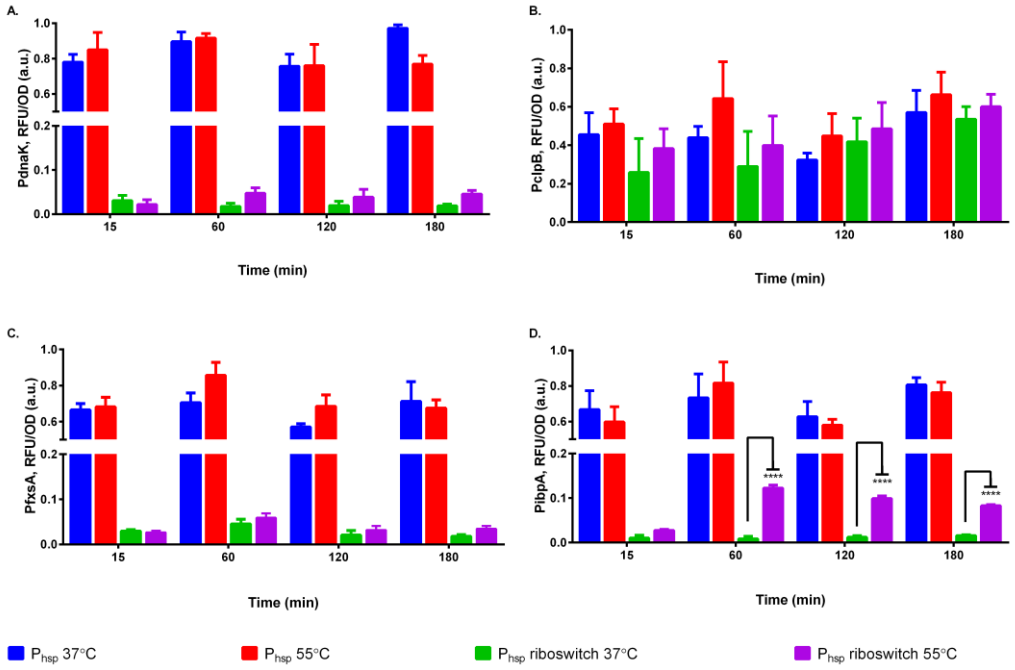

Figure 2.11: Fluorescent signal results of heat treated toxicity sensors with native HSP promoters and their riboregulator-mediated constructs for PdnaK (A.), PclpB (B.), PfxsA (C.), and PibpA (D.) circuits. Experiments were performed as three biological replicates in different days. Heat shock was applied at 55°C water bath for 30 min, and control samples were kept at 37°C. Sensors with native HSP promoters and sensors with riboregulators in each group were normalized between each other based on formula stated in Materials and Methods section. $p \leq 0.0001$ was represented with four stars while statistically non-significant results had no stars.

2.4.5.Sensing the Nanomaterial-triggered Toxicity Using Riboregulator-mediated Stress Circuits

For toxic stressor, CdTe QD was selected as model nanomaterial. Each riboregulator-mediated sensor group was either subjected to 300 nM of QD treatment or kept as uninduced. Upon stress, circuits, except riboregulator-mediated PibpA sensor, showed a significant response upon immediately after QD exposure (Figure 2.12).

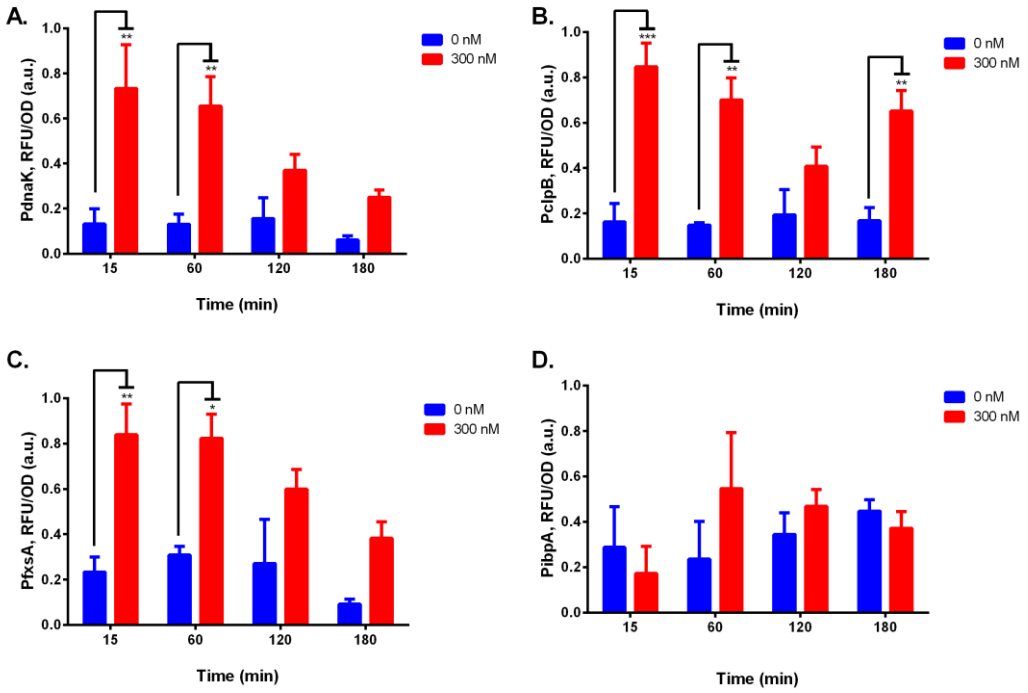

Figure 2.12: Fluorescence signal results of CdTe QD treated riboregulator-mediated stress sensors with PdnaK (A.), PclpB (B.), PfxsA (C.), and PibpA (D.). Experiments were performed as three biological replicates in different days. 300 nM QD was applied as stress factor. All data were normalized according to formula stated in Materials and Methods section. $p \leq 0.05$, $p \leq 0.01$, and $p \leq 0.001$

were represented with one, two, and three stars, respectively. Statistically non-significant results had no stars.

2.4.6.RT-qPCR of Riboregulator-mediated Stress Circuits

For expression analysis at mRNA level, riboregulator-mediated PibpA circuit was selected as model sensor. Both heat at 55°C and 300 nM CdTe QD treatment were performed on sensor. After 60 min of stress treatment, cells were collected and RNAs were isolated. After RT-qPCR analysis, the riboregulator-mediated PibpA sensor showed a significant response upon heat shock while there was no significant response to QD treatment (Figure 2.13).

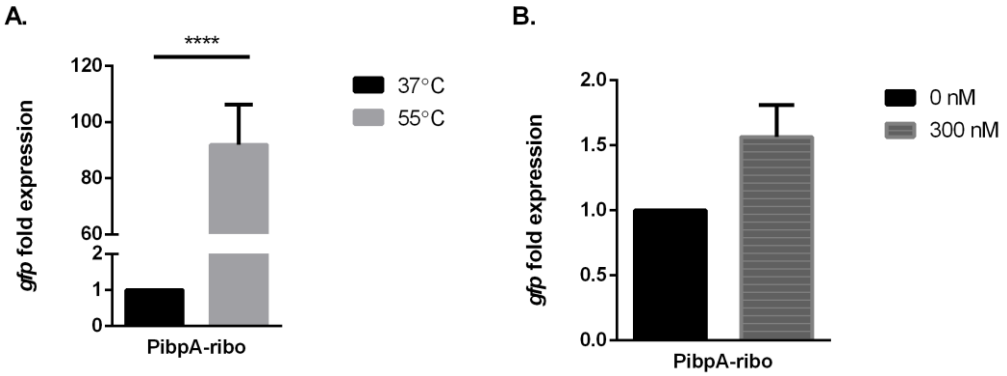

Figure 2.13: RT-qPCR analysis of riboregulator-mediated PibpA sensor induced with heat (A.) and CdTe QDs (B.). Experiments were performed as three biological replicates in different days. Samples were collected for RNA isolation at 60th min after stress treatment. All data was normalized to un-treated control sample. $p \leq 0.0001$ was represented with four stars. Statistically non-significant results had no stars.

2.4.7. Characterization of Engineered Quorum Sensing Circuit with HSR

Similar to other stress sensors, engineered QS circuit was either subjected to 300 nM of QD treatment or kept as uninduced. Results showed a significant response upon immediately after QD exposure and high background signal was observed (Figure 2.14).

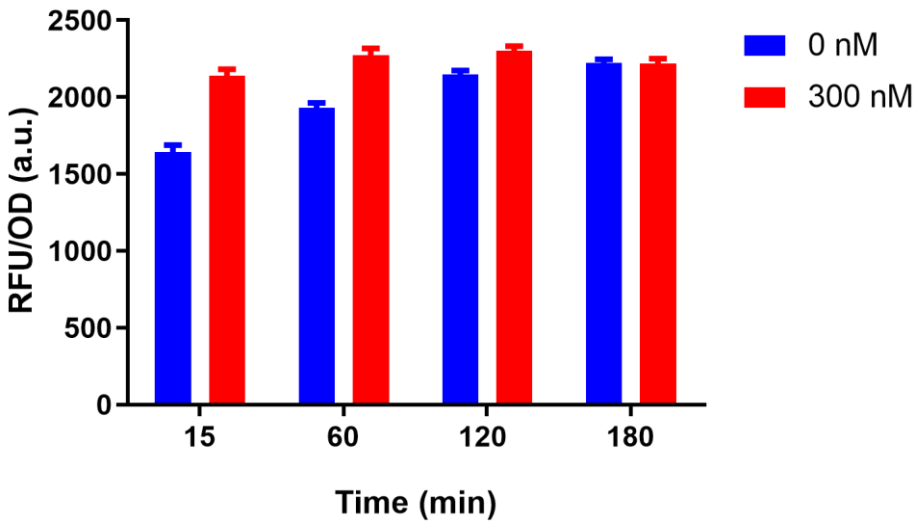

Figure 2.14: Fluorescence signal results of CdTe QD treated engineered quorum sensing stress sensors with PdnaK. Experiments were performed as three biological replicates in different days. 300 nM QD was applied as stress factor.

2.5. Discussion

Selection of a proper promoter is crucial in whole cell biosensor studies since reporter expression rate highly depends on promoter strength. HSR pathway offers many promoter options with varying strengths from very low to high

expression level. We chose HSP promoters which show moderate or high expression levels in response to heat induction [82]. Among them, we considered following HSP promoters which were characterized in previous studies namely: dnaK [70, 71, 82, 111], clpB [70, 71, 111], fxsA [82] and ibpA [82]. Initial stress sensor circuits were constructed with these highly stress-inducible HSP promoters controlling the expression of a reporter (*gfp*). Before toxicity assessment, we characterized all constructed circuits with elevated heat stress; main stressor of HSR mechanism. Also, we aimed at finding the best performing promoter between the selected ones so that we could fully characterize the most promising stress sensor candidate afterwards.

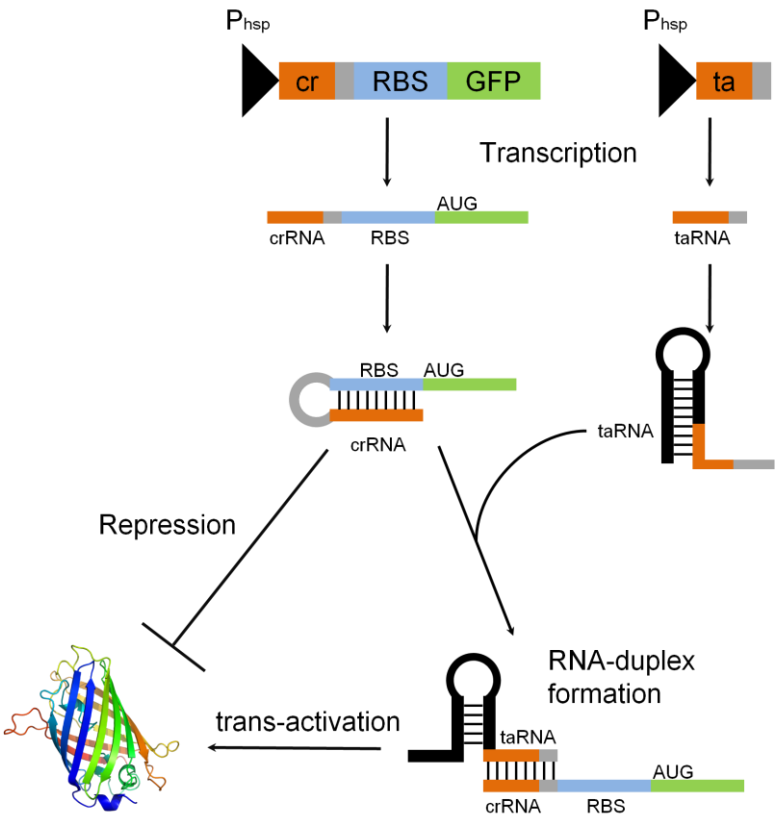

Figure 2.15: Working mechanism of engineered riboregulators. In the absence of taRNA, reporter expression is blocked by crRNA with a loop formation.

However, taRNA favorably forms a complex with crRNA which makes RBS free so that gene expression starts. Reprinted with permission from ref [140]. Copyright 2004 Springer Nature.

The native HSP promoters are active in cells while the cells are growing. To be able to make a significant comparison, 15th min following heat induction was used as the starting point. This allows us to eliminate any errors due to the delay in sampling and measurements. In general, reporter expression reaches its maxima at one hour after heat induction at 55°C for 30 min and the signal decreases afterwards (Figure 2.11). Previous studies have reported that cells start adapting themselves to the environment and decreasing σ^{32}-dependent gene expression. Besides transcription, decrease in translation efficiency might cause a decline in signal accumulation [82]. Thus, not only promoters but also RBS strength might be engineered to overcome insufficient signal output.

Among the four initial circuits, the one harboring the clpB promoter region (originally active in the synthesis of the ClpB heat shock protein) did not give a useful signal. However, the rest of the initial circuits gave high signals both in the presence and the absence of the stress condition, which was the elevated temperature. Although ClpB shows similar function with DnaK machinery (preventing aggregation of denatured proteins), its expression is lower at elevated heat conditions [141-143]. Thus, clpB promoter might not be activated significantly upon heat treatment. Therefore, the increase in the signal upon heat treatment was not significant. Based on the high background signal, it was

suspected that initial circuits with HSP promoters were leaky. By taking this point into consideration, we engineered them with riboregulators adapted from Isaacs *et al.* [140] to prevent any background signal in initial circuits. We modified our initial toxicity sensor circuits with riboregulators to eliminate any leakage may be caused by HSP promoters. Isaacs *et al.* characterized a library of artificial riboregulators to tightly control the gene expression. Working principle of riboregulators has been summarized in Figure 2.15: This system employs small non-coding RNAs (sncRNAs) found in cells. At normal growth conditions, one of the sncRNAs, namely cis-repressing RNA (crRNA), blocks the gene expression with a loop formation on ribosome-binding site (RBS). Upon induction, trans-activating RNA (taRNA) has been expressed to form a complex with crRNA. As a result of crRNA-taRNA complex formation, RBS becomes accessible to ribosome which initiates the gene expression. The riboregulators constructed by Isaacs *et al.* were coupled with HSP promoters at transcription initiation sites of toxicity sensors. The test results of the initial circuits with increased heat stress were presented in Figure 2.11A, 2.11B, 2.11C, 2.11D, riboregulator-modified and non-modified initial sensor circuits were compared and representative fluorescent microscopy images were shown in Appendix F. Riboregulator-mediated toxicity sensors showed a dramatic decrease in background signal, except for clpB promoter as discussed above. Although riboregulators decreased the background signal almost entirely, a significant fold-expression was not observed upon heat treatment. Nevertheless, riboregulator-mediated ibpA promoter showed the best performance compared to the dnaK promoter, clpB promoter, and fxsA promoter upon heat treatment. IbpA protein, in cooperation with IbpB protein, is

responsible for inclusion body prevention in cells. It has been shown that IbpA expression increases with elevated heat and in some cases with chemical exposure that causing inclusion body formation under stress [144]. Elevated heat treatment (55°C, 30 min) might induce inclusion body formation in cells driving expression from ibpA promoter. Yet, further engineering strategies to increase the sensor signal was required.

QDs are used for many applications such as fluorescent labeling or drug delivery since they exhibit high photostability, and are easy to functionalize [145]. Due to the high demand for the utilization of QDs we aimed to use them as potential test materials for their toxicity. Testing NMs for their cytotoxicity is a common approach in every synthesis work for biomedicine related applications [146]. Yet, there is no specific and rapid biosensor to assess toxicity of QDs. Here we are proposing a fast feedback about the NM-triggered toxicity that can be obtained from the whole cell sensor system. Such information can help one to engineer NPs and save significant amount of time without carrying out complex tests at every step. QDs show toxicity on bacteria through photogeneration and ROS formation. Light induced release of heavy metals from QD surface might increase heavy metal ion uptake by cells which cause DNA damage, loosen membrane integrity, interrupted electron transfer chain or oxidation of proteins and lipids in cells [128, 145].

After characterization of constructed circuits with heat, riboregulator-mediated stress sensors were screened by employing red emitting CdTe QDs to analyze NM-triggered toxicity as the main motivation was to detect toxicity of NMs. CdTe QDs were selected as representative NMs used for many applications (i.e.,

fluorescent labeling or drug delivery) in medicine. The riboregulator-mediated sensors were treated with CdTe QDs and showed a quick stress response right after QD treatment, except for PibpA-mediated sensor (Figure 2.12). Stress could activate different pathways such as SOS, ROS, and HSR. Yet, not all of the elements in these pathways could be activated by each stress conditions. For instance, elevated temperatures fully activate HSR, but not the oxyR dependent ROS response, or vice versa for H_2O_2 exposure [147]. IbpA, referring inclusion body binding protein A, is one of the sHSPs playing roles in protein aggregate prevention. It was shown that IbpA expression increases at elevated temperatures which might lead to aggregation. However, although IbpA responds immediately to heat treatment, it does not respond with the same fashion to all chemicals [148, 149]. Our result indicated that CdTe QD exposure did not initiate gene expression from PibpA (Figure 2.12D), but from others (Figure 2.12A, 2.12B, 2.12C), and a quick and high response was observed in each case independent from the promoter type. The data was supported by representative fluorescent microscopy images in Appendix F.

Moreover, to demonstrate QDs do not interfere with the GFP signal, we treated and evaluated constitutively expressed GFP as positive control (Appendix F). These results showed that GFP signal continued increasing even in the presence of higher concentrations of QDs. Also, time resolved fluorescence spectroscopy (TRF) measurement indicated that QDs had no effect on GFP quenching. Additionally, reporter of the sensor (GFP) is interchangeable so that one can use different reporter genes in the case of interference of GFP with NM of interest to eliminate possible quenching of the signal.

Following, we aimed at analyzing the IbpA-mediated sensor working principle at transcription level so that we measured its response to heat as well as to QDs. Using RT-qPCR, a representative set of experiment was carried out. Results showed that gene expression was increased up to 90-fold upon heat treatment (Figure 2.13A) while QD treatment had no dramatic effect compared with untreated control group (Figure 2.13B). The data support that elevated heat treatment has adverse effect on cells perhaps causing inclusion body formation.

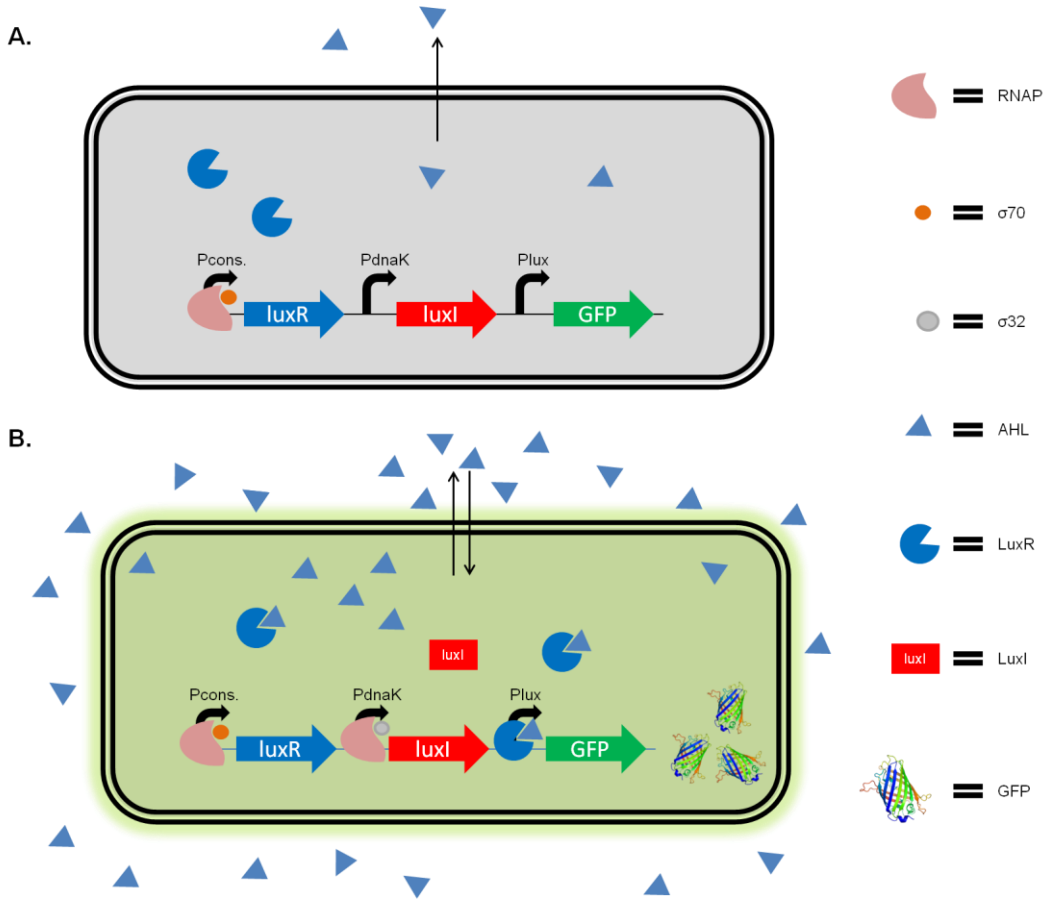

Figure 2.16: Working mechanism of engineered QS mechanism with HSR. A. At normal growth conditions, constitutively expressed LuxR is degraded in cells and AHL level is kept at basal level. B. Upon stress, σ^{32}-dependent transcription is activated in cells and LuxI transcription through PdnaK promoter starts. The LuxI

converts more AHL which are freely diffusible within cells to stimulate other cells in the environment. Cells trigger reporter expression with LuxR-AHL complex and increased signal is observed.

We also tested growth kinetics of cells upon both heat and QD treatment and observed that both stressors slowed down cell growth compared with the untreated control group (Appendix F). However, no detrimental cell death was observed upon QD treatment at the applied concentration, 300 nM. The same observation was also valid for heat treatment at 55°C.

Because of decreased stressor signal, quorum sensing (QS), bacterial communication, mechanism was introduced to HSR as a feedback mechanism to increase the signal upon stress exposure. QS is the mechanism of bacterial communication through mediator signaling molecules, autoinducers (AIs). As bacteria population increases, AIs in environment also increases to facilitate altering the gene expression collectively. Such collective behavior includes bioluminescence, biofilm formation, sporulation, antibiotic production, or virulence factor production [150]. In a typical Gram negative bacterium, QS mechanism is based on LuxI-LuxR system which discovered in a bioluminescent bacterium, *Vibrio fischeri* [151]. In this system, the LuxI is the AI synthase which synthesizes a freely diffusible acyl homoserine lactone (AHL); the AI molecule. The LuxR is the transcription factor which is recognized by AHL and activates QS operon forming a feed-forward loop by producing more LuxI in cells. The LuxR is unstable in cells in the unbound form while AHL binding stabilizes it

[150]. Here we engineered the LuxI-LuxR-based QS mechanism to make a toxicity sensor. In the circuit, constitutively expressed LuxR is expected to be degraded when it is not bound to AHL (Figure 2.16A). Upon stress, LuxI production increases from PdnaK promoter which synthesizes AHL in cells. Further, LuxR-AHL complex recognizes Plux promoter, controlling the reporter expression (Figure 2.16B). The stress circuit with engineered QS mechanism was tested with 300 nM of CdTe QDs as a model nanomaterial as used previously. Similar results were observed (Figure 2.14): Cells responded the toxic compound immediately in 15 min. However, QS mechanism increased the background signal because of the leaky nature of activation based systems. Thus, this circuit was also not suitable for a well-controlled toxicity sensor because of the high background at its uninduced form. As a conclusion, it might be more suitable to integrate a repressor in the circuits to provide tight control, to decrease the background, and to increase stressor signal.

2.6. Conclusion

Recent developments in nanotechnology accelerated nanomaterial applications in various fields. Their unique properties [119-121] such as small size, high surface-to-volume ratio, and catalytic activity make them potentially dangerous to living systems because they have ability to penetrate through tissues and cells easily [124-130, 132-134]. Thus, an early diagnostic toxicity assessment procedure is a necessity prior to NM application on living systems as well as on environment. Here we propose synthetic genetic circuits which are capable of sensing early stages of stress caused by NMs using an engineered HSR system [97]. In this

study, all stress responsive circuits were characterized by exposing the circuit harboring cells to elevated temperatures; later selected cells were used as the candidate sensors for NM exposure. Stress responsive circuits with mostly expressed native HSP promoters controlling a reporter output, GFP, were found to have a looser control on the expression and as a result high background signals were observed. Coupled with a set of synthetic riboregulators, engineered native HSP promoters were found to be more functional as sensing elements. Among the chosen native promoters, P_{ibpA} promoter also seemed to be the best performing promoter under stress conditions when coupled with a riboregulator system. The riboregulator we used prevented leaky protein expression as expected. Yet, they caused decrease in stressor signal as well. To overcome this issue, bacterial quorum sensing (QS) was integrated in a selected HSR circuit. Although results demonstrated an obvious increase in signal compared with any of other HSR circuits, the background also increased in parallel. Thus, more controllable mechanism is in demand to solve high background issue.

Whole cell sensors have a great potential for numerous future applications such as monitoring NM-triggered toxicity. In general, NM-triggered toxicity is a complex phenomenon. After the NPs enter to the blood stream or interact with the cells, many molecular mechanisms are triggered. However, to track these changes at genome and proteome level is labor intensive and costly process. Hence, we believe that our quick reporter systems will provide crucial initial data to make judgments about the level of toxicity. However, one should notice that our proposed circuit design is not tissue or organism specific but gives a general idea if the NM of interest triggers any toxicity. To be more specific about the reasons

for the toxicity, specific biomarkers should be identified using genome, transcriptome, or proteome level analysis for each type of NP available with varying surface properties. Such an attempt may have a potential to develop whole cell sensor with complex circuit designs including logic-based operations.

CHAPTER 3

Repression-based Control of Toxicity Sensing

This work is partially described in the following publication [74]:

Behide Saltepe,[†,‡] Eray Ulaş Bozkurt,[†,‡] Nedim Hacıosmanoğlu,[†,‡] Urartu Özgür Şafak Şeker*[†,‡]

† UNAM−Institute of Materials Science and Nanotechnology, National Nanotechnology Research Center, Bilkent University, 06800 Ankara, Turkey

‡ Institute of Materials Science and Nanotechnology, Bilkent University, 06800 Ankara, Turkey

* Corresponding author

E-mail address: urartu@bilkent.edu.tr

Reprinted (adapted) with permission from *ACS Synth. Biol*. 2019, 8, 10, 2404-2417. Copyright 2019 American Chemical Society.

3.1. Objective of the Study

Biocompatibility assessment of nanomaterials has been of great interest due to their potential toxicity. However, conventional biocompatibility tests fall short of providing a fast toxicity report. We developed a whole cell based biosensor to track biocompatibility of nanomaterials with the aim of providing fast feedback to engineer them with lower toxicity levels. In previous chapter we showed that heat shock response (HSR) protein promoters were not suitable to form such kind of sensor because of they are already very active in cells at normal growth conditions. On the other hand, althoug introducing riboregulators to native promoters eliminated unwanted background signals almost entirely, they caused a decrease in stressor signal. Besides, engineering of these circuits with quorum sensing (QS) mechanism increased both bakcgound and stressor signal dramatcially. Thus, instead of using an activator based genetic circuits which caused high background, a repression based genetic circuit, inspired by the HSR mechanism of *Mycobacterium tuberculosis*, was constructed. These genetic circuits could report the toxicity of quantum dot nanoparticles immediately after exposure. Our designed nanoparticle toxicity sensors can provide quick reports, which can lower the demand for additional experiments with more complex organisms.

3.2. Introduction

Although heat shock response (HSR) mechanism is highly conserved, it varies among prokaryotes. Some bacteria utilize positive regulation which orchestrates

sigma factors to selected promoters, while others use negative regulation with the help of special transcriptional repressors. Even in some microorganisms, both mechanisms co-exist [37]. As described previously (Chapter 1), HSR mechanism in *E. coli* is based on positive regulation. At stress conditions, σ^{32} factor interacts with RNAP initiating HSP expression [35]. On the other hand, negative regulation consists of two necessary components: a repressor and its recognition sequences on promoters. The HSR repressor controls expression of its operon blocking the promoter recognition at normal conditions while dissociating from the promoter allowing RNAP to initiate gene expression. This mechanism is utilized by *Bacillus subtilis* (has HrcA and CtsR repressors), *Streptomyces* genus (has HspR repressor), *Streptomyces albus* (has HrcA, HspR, and RheA repressors), *Campylobacter jejuni* (has HspR repressor), *Mycobacterium tuberculosis* (has HspR repressor), and *Deinococcus radiodurans* (has HspR repressor). Although discovered transcriptional repressors varies in species, they share a common base since they recognize very specific DNA sequences reside on the HSP promoters [37].

Unlike HSR mechanism in *E. coli*, *M. tuberculosis* regulates its HSR mechanism with a special repressor, HspR, synthesized from dnaKJE-hspR operon via a self-controlled feedback mechanism. HspR recognizes specific sequences found in promoter region called HspR-associated inverted repeats (HAIR) with the assistance of DnaK chaperone and blocks its own operon under normal growth conditions. However, upon stress, HspR and DnaK dissociates from promoter initiating the gene expression [152]. Additionally, it has been shown that HspR does not require DnaK assistance during HAIR recognition; in particular, DnaK

improves binding of HspR on promoter [153]. Native HSR system of *E. coli* has transcription factor working as an activator in the pathway, which may cause high background signal in circuits since these transcription factors are already active in cells at basal level. We proposed that a repression-based sensor design might be a solution to suppress high background signal. This hypothesis led us to design circuits with HSR systems from *M. tuberculosis*.

3.3. Materials and Methods

3.3.1.Media and Strains

E. coli DH5α (New England Biolabs, Inc.) was grown in LB medium (1% (w/v) tryptone, 0.5% (w/v) yeast extract, 0.5% (w/v) NaCl) with proper antibiotics at 37°C and 180 rpm shake in Erlenmeyer flasks. Overnight cultures were prepared from frozen glycerol stocks and incubated for 16 h with the same culturing conditions mentioned previously. 1% of inoculums from overnight cultures were used to start experimental cultures and monitored via spectrophotometer (GENESYS 10 Bio, Thermo Scientific) until OD_{600} reached 0.4-to-0.6 before induction steps were applied.

3.3.2.Plasmid Construction

M. tuberculosis dnaK promoter was amplified from *Mycobacterium bovis* genomic DNA, which has the same promoter sequence with *M. tuberculosis*, by primers shown in Table B1. Codon optimized *M. tuberculosis* HspR repressor was synthesized by GENEWIZ Company. Q5 Hot Start High-Fidelity DNA Polymerase (New England Biolabs, Inc.) was used for all PCR reactions

(Reaction conditions were described in Appendix E). To construct the stress sensor plasmid backbone, pZa-tetO-eGFP vector was digested with XhoI-KpnI restriction enzymes (New England Biolabs, Inc.) and pET-22b(+) was digested with SalI-SpeI restriction enzymes (New England Biolabs, Inc.) for repressor plasmid backbone construction (pET22b-mProD-HspR) (Reaction conditions were described in Appendix E). NucleoSpin Gel and PCR Clean-up kit (Macherey-Nagel) was used according to the manufacturer's instructors to purify digested DNA samples or PCR products from 1 to 1.8% Agarose gels stained with SYBR Safe DNA Gel Stain (Thermo Fisher Scientific). Plasmid construction was made via ligation with DNA T4 ligase (New England Biolabs, Inc.) or via Gibson Assembly method described by Gibson *et al.* [137] (Both reaction conditions were described in Appendix E). Expression vector for HspR (T7-HspR-pET22b) was constructed via Gibson Assembly method. First, backbone was digested with XbaI-XhoI enzymes, and HspR was amplified at two round PCR with specified primers in Table B1. After all assembly methods, mixes were directly transformed into chemical competent *E. coli* DH5α cells. Colonies were screened by plasmid digestion. Constructed genetic circuits were sequence verified by Sanger Sequencing (GENEWIZ). All genetic part sequences used this chapter was introduced in Table A1, and all constructed vector maps were indicated in Appendix C with verified sequencing results in Appendix D.

3.3.3. Chemical Competent Cell Preparation and Transformation of DNA in Cells

Overnight cultures of *E. coli* DH5α were prepared from frozen glycerol stocks and incubated for 16 h with the same culturing conditions mentioned previously. 1% of inoculums from overnight cultures were used to start fresh culture for competent cell preparation. Culture was incubated at 37°C and 180 rpm shake in Erlenmeyer flasks until OD_{600} reached 0.2-to-0.5. Following, culture was cooled in ice for 10 min and cells were collected by centrifugation at 1000 ×g for 10 min at +4°C. After centrifugation, supernatant was discarded and cell pellet was resuspended in 10% (v/v) of TSS Buffer (10% (w/v) PEG-8000, 5% (v/v) DMSO, 50 mM $MgCl_2$ pH 6.5 in LB). For each aliquot, 100 µl of cultures were placed in each microcentrifuge tubes and stored at -80°C.

Chemical competent cells were thawed on ice for 30 min before transformation. For transformation, whole ligation product, Gibson Assembly reaction product, or 100 ng of intact plasmid DNA was introduced to thawed cells and incubated on ice for 20-30 min. Following, cells were shocked by heat treatment at 42°C for 30 sec. After the heat shock, cells were cold shocked for 2 min on ice. Then, 250-1000 µl of LB was added onto the cells and incubated at 37°C and 180 rpm shake for 45-60 min. At the end of the incubation, cells were collected at 1000 ×g for 10 min and the supernatant was discarded. The collected cells were resuspended in 50 µl of LB and spread onto LB-agar supplemented with proper antibiotics.

3.3.4.Sequencing Alignments with Geneious Software

All plasmid maps were constructed on an online vector tool; Benchling. Following, all plasmid maps were exported as .gb files and imported in Geneious software together with the sequencing results of plasmid maps as .abi files. In order to align plasmid map and its sequencing data, both sequences were selected and pairwise alignment performed. The sequencing results for all vectors were indicated in Appendix D.

3.3.5.Heat Shock Experiments and Toxicity Assay

After OD_{600} of experimental cultures reached 0.4-to-0.6, Erlenmeyer flasks corresponding to heat shock treatment were immersed in 55°C water bath for 30 min as describe by Rodrigues *et al.* [82], while Erlenmeyer flasks corresponding to toxicity assay were treated with water-soluble thiol-capped CdTe QDs with varying concentrations. QDs were prepared using the method as explained in a previous work by Seker *et al.* [139]. For tert-Butyl hydroperoxide (TBHP) induction, 200 μM of TBHP was applied on cells and incubated at 37°C for 30 min. Control flasks were kept as untreated at 37°C. Three independent biological replicas were prepared for each group.

3.3.6.Fluorescence Measurement and Data Analysis

All fluorescence measurement studies were conducted via microplate reader (SpectraMax M5, Molecular Devices). Excitation and emission wavelengths for eGFP were set as 485 and 538 nm, respectively. Each measurement was

conducted in Corning 96-well clear flat bottom polystyrene plates with 250 μL of culture sample resuspended in 1×PBS (137 mM NaCl, 2.7 mM KCl, 4.3 mM Na_2HPO_4, 1.47 mM KH_2PO_4, pH 7.4). For signal normalization, raw fluorescence intensity was divided by OD_{600} values of each sample. For each treatment (corresponding temperature or concentration), its control group (cells with mock vector) was subtracted from sensor data. Only dose response curve (Figure 3.10) was drawn with two sets of groups (control and sensor) without mock subtraction. For 0-to-1 normalization, each value was subtracted from minimum value and divided by difference between maximum and minimum values in related groups. The data for the initial expression level was recorded as the 15th min to eliminate errors caused by delays in early protein expression.

3.3.7.HspR Expression and Western Blot Analysis

E. coli BL21 (DE3) cells (New England Biolabs, Inc.) carrying HspR expression vector (T7-HspR-pET22b) was grown in LB medium with proper antibiotics at 37 °C and 180 rpm in Erlenmeyer flasks. 1% of inoculums from overnight cultures were used to start expression cultures and monitored until OD_{600} reaches 0.4-to-0.6 before induction steps were applied. A control culture was kept as uninduced and other culture was induced with 1 mM of isopropylthio-galactoside (IPTG) for 3 h. Afterward, cells were collected, resuspended in 10 mM of imidazole buffer (pH 7.4) supplemented with 1 mM of phenyl methyl sulfonyl fluoride (PMSF) (AMRESCO Inc.), and proteins were extracted via freeze−thaw method. Protein concentrations were determined with BCA Assay (Thermo Fisher Scientific) and diluted to final concentration of 740 μg/ml. Proteins were denatured and resolved

on 15% SDS-PAGE gel prepared with BioRad SDS Gel casting system. 20 µL from protein samples were run on gel by using 6×Loading Dye (375 mM Tris-HCl (pH 6.8), 9% (w/v) SDS, 50% (v/v) Glycerol, 0.03% (v/v) Bromophenol blue). All samples were boiled at 95°C for 5 min prior to run on gel. 1×SDS Running Buffer (25 mM Tris-HCl, 200 mM Glycine, 0.1% (w/v) SDS) was used during the run. Further, gel was transferred to polyvinylidene difluoride (PVDF) membranes (Thermo Fisher Scientific). Membrane was blocked with 5% freeze-dried nonfat milk in TBS-T for 1 h at room temperature, and then incubated at +4°C overnight with primary antibody (His-Tag mouse McAb) (Proteintech Europe) diluted at 1:10000 in blocking solution. Afterward, membrane was washed with TBS-T and incubated with HRP conjugated goat antimouse secondary antibody (abcam) diluted at 1:10000 in blocking solution for 1 h and visualized by enhanced chemiluminescence (Bio-Rad) according to the manufacturer's protocol on ChemiDoc Imaging System with Image Lab Software − BioRad.

3.3.8.Electron Mobility Shift Assay (EMSA)

The following promoters used in electrophoretic mobility shift assay were amplified by PCR with stated primers in Table B1: mtPdnaK, PdnaK, PdnaK-IR2, PdnaK-IR2-IR2, PdnaK-IR3 and PdnaK-IR3-IR3 from plasmids mtPdnaK GFP pZa, PdnaK GFP pZa, PdnaK-IR2 GFP pZa, PdnaK-IR2-IR2 GFP pZa, PdnaK-IR3 GFP pZa, and PdnaK-IR3-IR3 GFP pZa, respectively. HspR protein was produced as stated above and purified from total protein by using HisTrap HP affinity columns (GE Healthcare Life Sciences) according to the manufacturer's

protocol. After purification, protein buffer was exchanged to HspR Buffer (20 mM Tris-HCl (pH 7.5), 10 mM NaCl, 1 mM DTT, 20% (v/v) glycerol, 1 mM $CaCl_2$, 0.1 mM EDTA, and 1 mM PMSF) via protein concentrators (Thermo Fisher Scientific). EMSA binding reactions were performed according to Bucca *et al.* [154]. Briefly, 20 µL of EMSA binding reaction (20 mM Tris-HCl (pH 7.5), 10 mM NaCl, 1 mM DTT, 5 mM $MgCl_2$, 1 mM $CaCl_2$, 30−40 ng DNA, and 40 µg HspR) was prepared and incubated at 25°C for 30 min. Before loading the samples on prerun 4% TBE-PAGE gel, Orange DNA Loading Dye (Thermo Fisher Scientific) was added, and samples were run at 10 V/cm at +4°C. Finally, the gel was stained with SYBR Safe (Thermo Fisher Scientific in 0.5×TBE buffer for visualization. Gel was visualized by ChemiDoc Imaging System with Image Lab Software − BioRad, according to the manufacturer's protocol.

3.3.9.RNA Purification and cDNA Synthesis

NucleoSpin RNA kit (New England Biolabs, Inc.) was used according to the manufacturer's instructors to isolate total RNA from each sample. Three independent biological replicas were prepared for each group. RNA concentration was quantified with NanoDrop 2000 spectrophotometer (Thermo Fisher Scientific). Samples were stored at −80°C until cDNA synthesis. Reverse transcribed RNA concentration were set to 500 ng in 20 µL of reaction volume for each sample. iScript cDNA Synthesis Kits (Bio-Rad) were used to convert RNAs into cDNAs according to the manufacturer's instructions (Reaction conditions were described in Appendix E).

3.3.10. qPCR and Data Analysis

After cDNA preparation, qPCR experiment was performed with 1 µL of cDNA for each sample via SsoAdvanced Universal SYBR Green Supermix (Bio-Rad) for *egfp*, *sodA*, and a housekeeping gene (*hcaT*) according to the manufacturer's instructions. Primers were specified in Table B1. Three technical replicas were prepared for each independent biological replica. PCR cycles were proceeded as follows: initial denaturation for 3 min at 95°C, denaturation for 10 sec at 95°C, annealing for 15 sec at 60°C, extension for 10 sec at 72°C for 39 cycles, 10 sec at 95°C (Reaction conditions were described in Appendix E). Product specificity was confirmed by a melting curve analysis (65−95 °C). Comparative Ct method (ΔΔCt) was used to analyze the results.

3.3.11. Microscopy

Samples were prepared together with each fluorescence measurement assays with specified time points in each figure. All imaging was conducted with LSM 510 Confocal Microscope (Zeiss). Samples were excited with Argon 488 nm for reporter imaging and emission was collected with LP 505 filter for eGFP, while QD samples were excited with HeNe 543 nm laser, and emission was collected with LP 585 filter. For dose−response curve analysis, bright field imagings of samples were also conducted, which were merged with corresponding fluorescence images afterward. All microscopy images of the sensors were provided in Appendix F.

3.3.12. Statistical Analysis

All data were expressed as mean ± standard error mean. Depending on the groups of interest, either one-way analysis of variance (ANOVA) or two-way ANOVA with Dunnett's/Tukey's/Sidak's multiple comparison tests (GraphPad Prism v6) were used to compare groups.

3.4. Results

3.4.1.Cloning of Repression-based Circuits

For cloning of PdnaK-IR2-GFP-pZa, PdnaK-IR2-IR2-GFP-pZa, and PdnaK-IR3-GFP-pZa vectors, PdnaK-GFP-pZa vector was used as template. All repeats were added with PCR primers in Table B.1 and linear vectors with HAIR repeats were obtained. All PCR products were run on 1% Agarose gel and isolated using MN-gel extraction kit according to manufacturer's instructions (Figure 3.1). Isolated PCR fragments were assembled with Gibson Assembly reaction (Appendix E), and selected colonies were verified by sequencing (Appendix D).

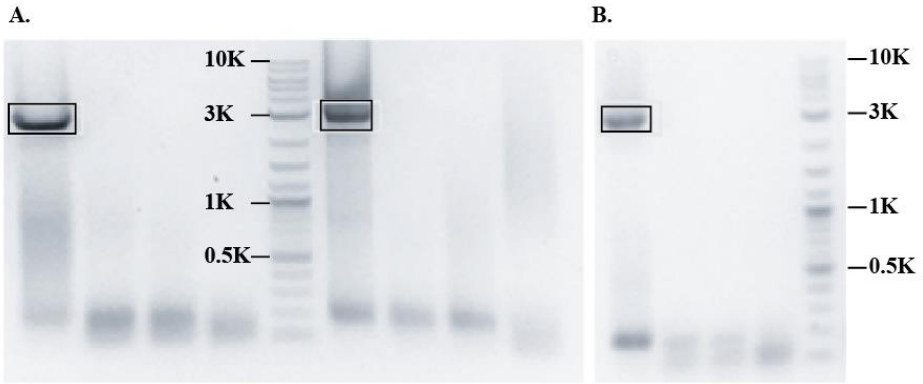

Figure 3.1: Construction of PdnaK-IR2-GFP-pZa, PdnaK-IR2-IR2-GFP-pZa, and PdnaK-IR3-GFP-pZa vectors. A. Single IR2 (left) and double IR2 (right) added

linear PdnaK-GFP-pZa vector were observed at 2900 bp. B. Single IR3 added linear PdnaK-GFP-pZa vector was observed at 2900 bp. 1 kb+ DNA Ladder (NEB) was used as DNA marker.

For cloning of PdnaK-IR3-IR3-GFP-pZa vector, an IR3 repeat was added to the downstream of PdnaK and an IR3 repeat was added to the upstream of eGFP via PCR primers in Table B.1. For backbone, PdnaK-GFP-pZa vector was digested with AatII-HindIII enzyme pairs. Both PCR and digestion products were run on 1% Agarose gel and isolated using MN-gel extraction kit according to manufacturer's instructions (Figure 3.2). Isolated fragments were assembled with Gibson Assembly reaction (Appendix E), and selected colonies were verified by sequencing (Appendix D).

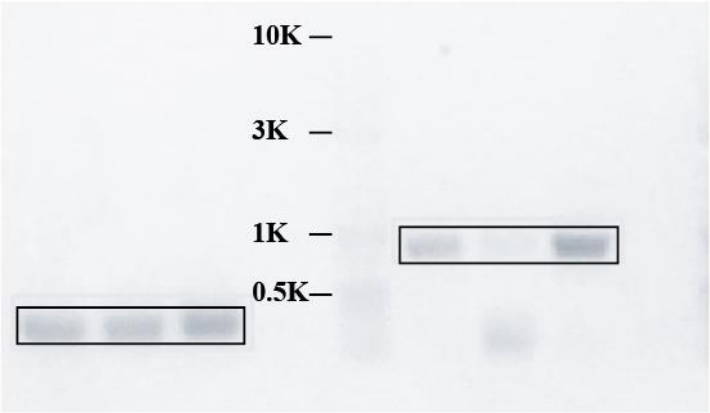

Figure 3.2: Construction of PdnaK-IR3-IR3-GFP-pZa vector. IR3 added PdnaK (left) and GFP (right) were observed at 270 bp and 800 bp, respectively. 1 kb+ DNA Ladder (NEB) was used as DNA marker.

For cloning of mtPdnaK-GFP-pZa vector, DnaK promoter of *M. tuberculosis* (mtPdnaK) was isolated from *M. bovis* genome (Figure 3.3A), sharing the same sequence, utilizing Gibson Assembly primers in Table B.1. For backbone, PdnaK-GFP-pZa vector was used and PCR was performed to exclude PdnaK promoter on the vector (Figure 3.3B). All PCR products were run on 1% Agarose gel and isolated using MN-gel extraction kit according to manufacturer's instructions (Figure 3.3). Isolated fragments were assembled with Gibson Assembly reaction (Appendix E), and selected colonies were verified by sequencing (Appendix D).

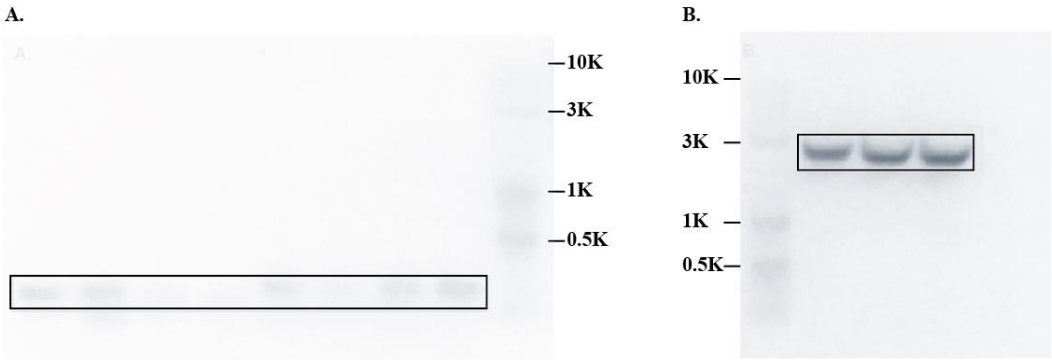

Figure 3.3: Construction of mtPdnaK-GFP-pZa vector. A. PCR products of mtPdnaK promoter were observed at 200 bp. B. PCR products of linear GFP-pZa vector were observed at 2600 bp. 1 kb+ DNA Ladder (NEB) was used as DNA marker.

For cloning of mProD-HspR-pET22b vector, formerly constructed PdnaK-HspR-pET22b vector was amplified with Gibson Assembly PCR primers (Table B.1) to exclude PdnaK promoter and to add mProD, instead. PCR products were run on 1% Agarose gel and isolated using MN-gel extraction kit according to manufacturer's instructions (Figure 3.4). Isolated fragments were assembled with

Gibson Assembly reaction (Appendix E), and selected colonies were verified by sequencing (Appendix D).

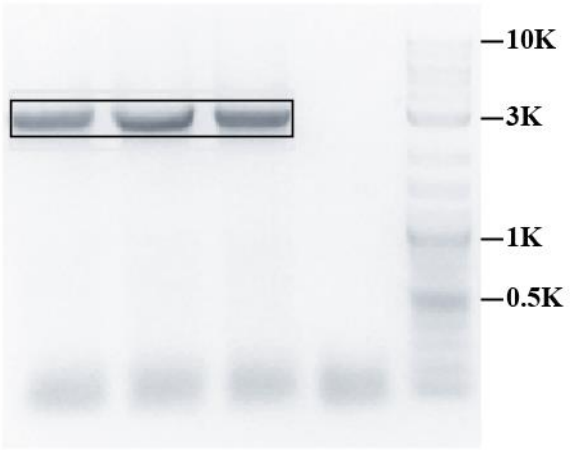

Figure 3.4: Construction of mProD-HspR-pET22b vector. PCR products of linear vector were observed at 3000 bp. 1 kb+ DNA Ladder (NEB) was used as DNA marker.

For cloning of T7-HspR-pET22b vector, pET22b-6H-ALP vector, constructed by our lab member Recep Erdem Ahan, was digested with SalI-SpeI restriction enzyme pair and run on 1% Agarose gel and isolated using MN-gel extraction kit according to manufacturer's instructions (Figure 3.5A). For HspR, formerly constructed mProD-HspR-pET22b vector was used template and HspR was amplified with primers in Table B.1. PCR product was run on 1% Agarose gel and isolated using MN-gel extraction kit according to manufacturer's instructions (Figure 3.5B). From the isolated HspR fragment, another PCR cycle was run to add Gibson Assembly homolog regions using primers in Table B.1. PCR products of HspR were run on 1% Agarose gel and isolated using MN-gel extraction kit

according to manufacturer's instructions (Figure 3.5C). Isolated backbone and HspR from the second PCR cycle were assembled with Gibson Assembly reaction (Appendix E), and selected colonies were verified by sequencing (Appendix D).

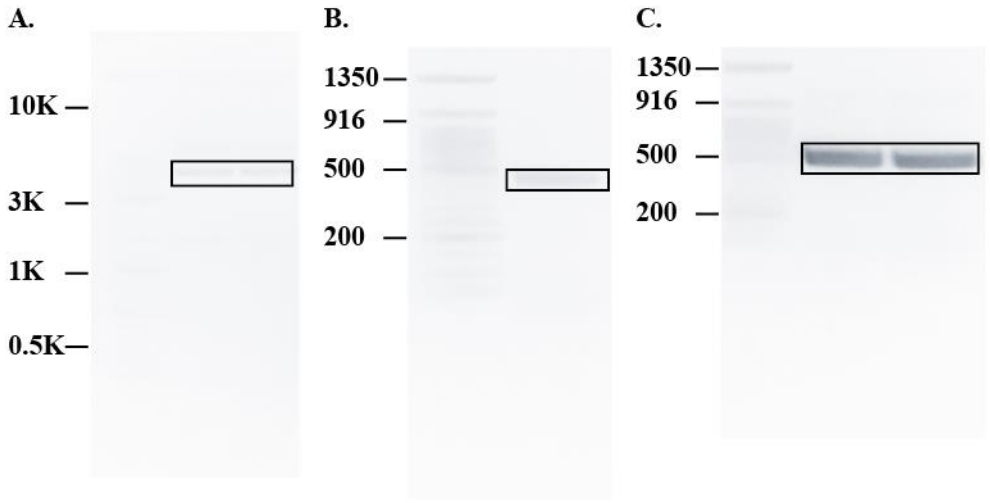

Figure 3.5: Construction of T7-HspR-pET22b vector. A. Digested linear vector was observed at 5500 bp. B. PCR product of HspR from the first cycle was observed at 465 bp. C. PCR product of HspR from the second cycle was observed at 480 bp. 1 kb+ DNA Ladder (NEB) and 50 bp DNA Ladder were used as DNA markers for large and small fragments, respectively.

3.4.2.Expression of HspR in *E. coli*

HspR expression vector (T7-HspR-pET22b) was transformed in *E. coli* BL21 (DE3) cells (New England Biolabs, Inc.) and induced with 1 mM of IPTG for 3 h. Expressed HspR was run on 15% SDS-PAGE and transferred to PVDF membrane for Western Blotting. His-tagged HspR was observed at 14 kDa upon induction (Figure 3.6, 2nd well). Also slight HspR expression was observed in uninduced cells (Figure 3.6, 1st well).

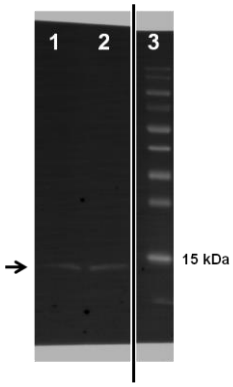

Figure 3.6: Western Blot results for recombinant HspR expression in *E. coli*. HspR expression from uninduced (1) and induced (2) *E. coli* BL21 (DE3) cells carrying T7-HspR-pET22B expression vector were shown at ~14 kDa. PageRuler Prestained Protein Ladder (3) (Thermo Fisher Scientific) was used as reference. Image generated by Chemidoc (BioRad) Imaging System.

3.4.3.Binding of HspR to Engineered HSP Promoters

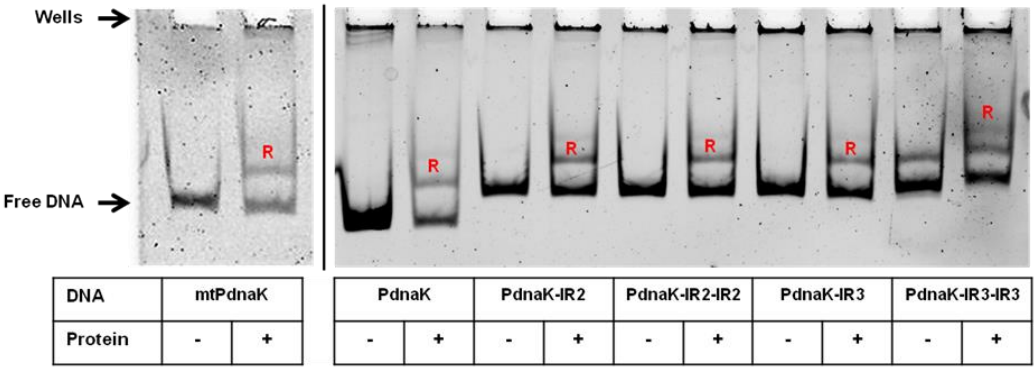

Figure 3.7: Gel retardation assay of HspR binding on engineered HSP promoter regions. PCR products of mtPdnaK, PdnaK, PdnaK-IR2, PdnaK-IR2-IR2, PdnaK-IR3, and PdnaK-IR3-IR3 were incubated without and with HspR, respectively. “R” represents retarded DNA fragment after HspR binding. The bottom fragment in each well indicates unbound free DNA.

To show DNA-protein iteraction between engineered HSP promoters and HspR repressor, an electron mobility shift assay (EMSA) was performed (Figure 3.7). Promoters incubated with HspR showed an extra band corresponding to retardation of the DNA fragments (Indicated with “R” on the gel) because of bound protein.

3.4.4.Characterization of Repression-based HSR Circuits with Heat Shock

For heat shock experiments, each group was subjected to either 37°C or 55°C heat treatment for 30 min. HSR circuits with engineered HSP promoters (mtPdnaK, PdnaK, PdnaK-IR2, PdnaK-IR2-IR2, PdnaK-IR3, and PdnaK-IR3-IR3) co-expressed with HspR repressor showed significant response upon exposure to elevated heat in 60 min (Figure 3.8), except circuits with mtPdnaK and PdnaK-IR3 (Figure 3.8A and Figure 3.8D, respectively). Among the characterized circuits, HspR-mediated PdnaK-IR3-IR3 circuit showed the most significant background reduction as well as stress signal increase in 60 min upon heat treatment at 55°C for 30 min (Figure 3.8F).

3.4.5.Sensing the Nanomaterial-triggered Toxicity through Repression-based HSR Circuits

For QD experiments, each group was either subjected to 300 nM of QDs or kept as untreated control (Figure 3.9). Results showed that, except mtPdnaK (Figure 3.9A), both PdnaK-IR2-IR2 (Figure 3.9B) and PdnaK-IR3-IR3 (Figure 3.9C)

responded to QD treatment immediately. To relate QD mechanism with ROS formation, selected PdnaK-IR3-IR3 sensor was treated with 200 µM of *tert*-Butyl hydroperoxide (TBHP), a well-known ROS forming agent, for 30 min (Figure 3.9D). Result showed that sensor reacted to the stressor immediately.

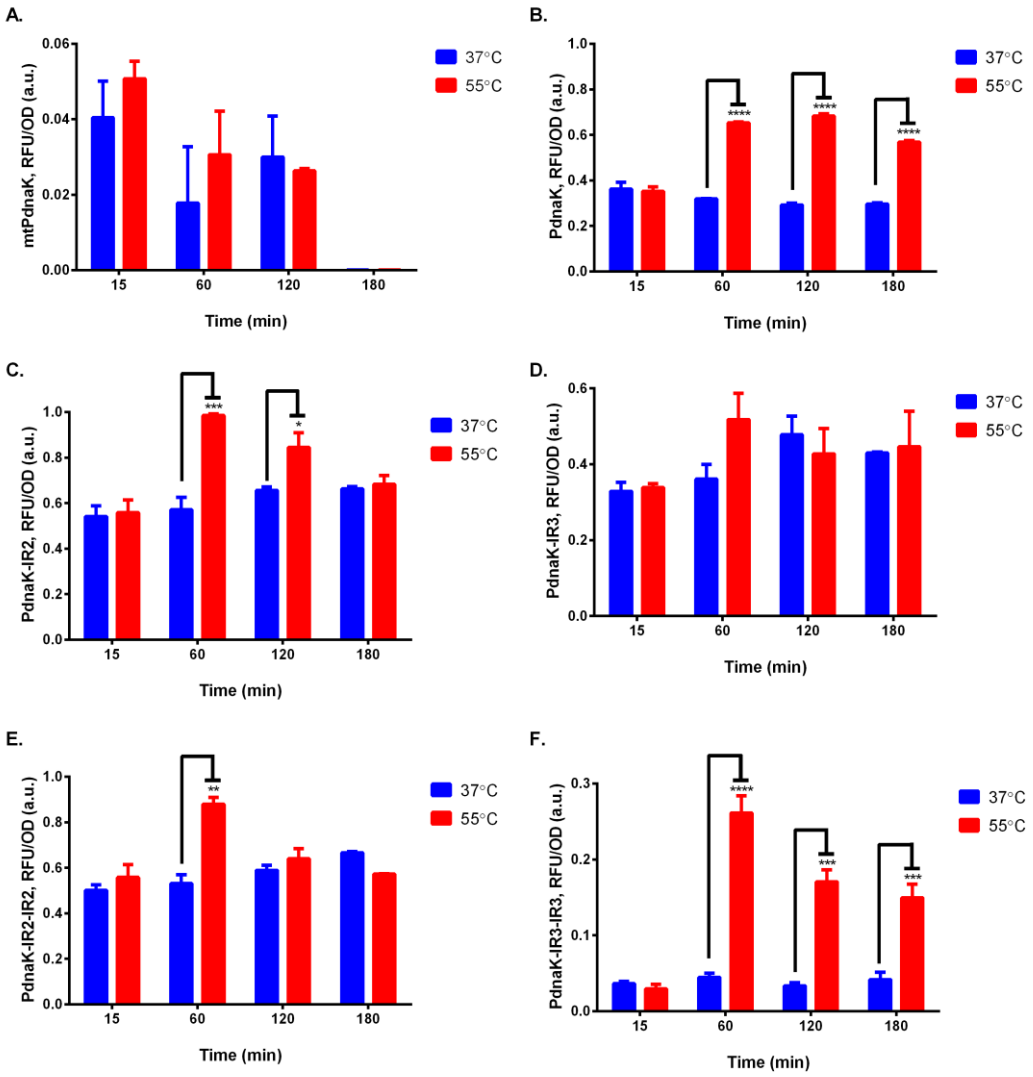

Figure 3.8: Fluorescent signal results of heat treated repressor-mediated toxicity sensors with mtPdnaK (A.), PdnaK (B.), PdnaK-IR2 (C.), PdnaK-IR3 (D.), PdnaK-IR2-IR2 (E.), and PdnaK-IR3-IR3 (F.). Experiments were performed as three biological replicates in different days. Heat shock was applied at 55°C water

bath for 30 min, and control samples were kept at 37°C. Fluorescence intensity of each group was compared with each other and normalized according to formula stated in Materials and Methods section. $p \leq 0.05$, $p \leq 0.01$, $p \leq 0.001$, and $p \leq 0.0001$ was represented with one, two, three, and four stars, respectively. Statistically non-significant results had no stars.

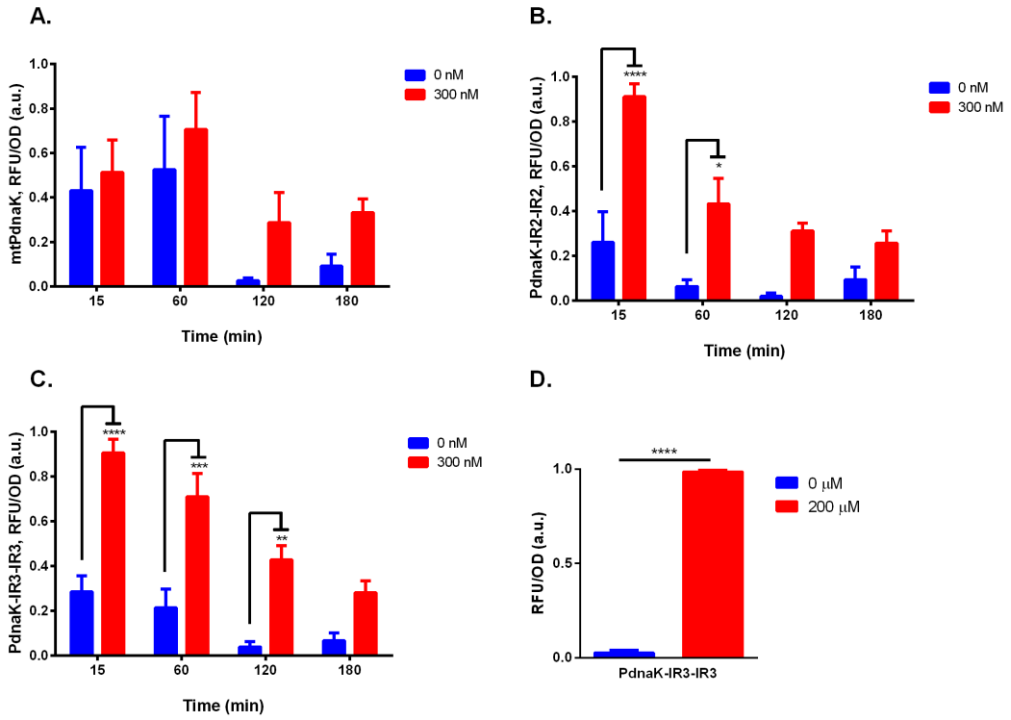

Figure 3.9: Fluorescent signal results of CdTe QD treated repressor-mediated toxicity sensors with mtPdnaK (A.), PdnaK-IR2-IR2 (B.), and PdnaK-IR3-IR3 (C.). Experiments were performed in three biological replicates on different days. 300 nM of QD was applied as stress agent. All data were normalized according to formula stated in Materials and Methods section. $p \leq 0.05$, $p \leq 0.01$, $p \leq 0.001$, and $p \leq 0.0001$ were represented with one, two, three, and four stars, respectively. Statistically non-significant results had no stars. D. Fluorescent signal of HspR-

mediated PdnaK-IR3-IR3 sensor treated with 200 µM of TBHP. Experiments were performed in three biological replicates on different days. All data were normalized according to formula stated in Materials and Methods section. $p \leq 0.0001$ was represented with four stars.

To demonstrate response curve of selected PdnaK-IR3-IR3 circuit as model stress sensing sensor, induction concentrations were selected from 0-to-250 nM of QDs. Results indicated that toxicity sensor could detect the presence of QDs even at lower concentrations (i.e. 2 nM) showing that detection limit of the sensor was very low (Figure 3.10).

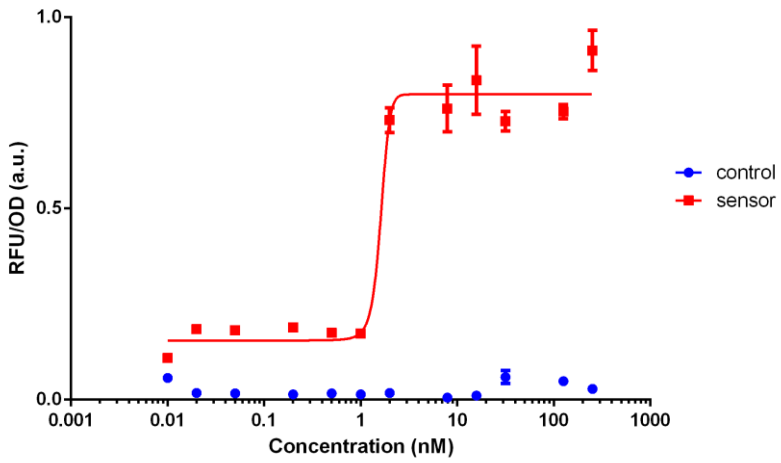

Figure 3.10: Dynamic range analysis of selected HspR mediated PdnaK-IR3-IR3 sensor treated with CdTe QDs. Experiments were performed as three biological replicates in different days. Measurements were taken at 60th min after QD treatment. All data were normalized according to formula stated in Materials and Methods section.

3.4.6.RT-qPCR of Repression-based HSR Circuits

To analyze response of toxicity circuits at mRNA level, PdnaK-IR3-IR3 circuit was chosen as model and treated with heat (55°C, 30 min), QD (300 nM), and TBHP (200 μM) for RNA isolation. Isolated RNAs after 60th min of heat treatment were run for *gfp* detection and results indicated that after heat treatment, reporter expression increases up to ~20-fold (Figure 3.11A). For 60 min after QD treatment, *gfp* expression was observed up to ~6-fold (Figure 3.11B), while *sodA*, a ROS indicating gene, expression was up to 3-fold (Figure 3.11D). As positive control, TBHP treatment showed up to12-fold of *sodA* expression (Figure 3.11C).

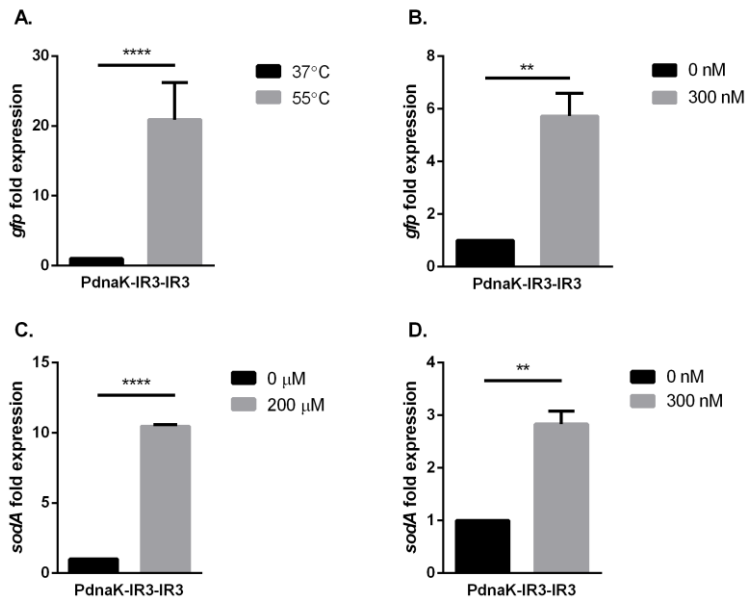

Figure 3.11: RT-qPCR analysis of HspR mediated PdnaK-IR3-IR3 sensor induced with heat, and CdTe QDs, and TBHP. A. *gfp* expression after 55°C, 30 min heat treatment of the sensor. Experiments were performed as three biological replicates in different days. Samples were collected for RNA isolation at 60th min after stress treatment. All data was normalized to un-treated control sample. $p \leq 0.0001$ was

represented with four stars. B. *gfp* expression after 300 nM of CdTe QD treatment of the sensor. Experiments were performed as three biological replicates in different days. Samples were collected for RNA isolation at 60th min after stress treatment. All data was normalized to un-treated control sample. $p \leq 0.01$ was represented with two stars. C. *sodA* expression after 200 μM of TBHP treatment of the sensor. Experiments were performed as three biological replicates in different days. Samples were collected for RNA isolation at 30th min after stress treatment. All data was normalized to un-treated control sample. $p \leq 0.0001$ was represented with four stars. D. *sodA* expression after 300 nM of CdTe QD treatment of the sensor. Experiments were performed as three biological replicates in different days. Samples were collected for RNA isolation at 60th min after stress treatment. All data was normalized to un-treated control sample. $p \leq 0.01$ was represented with two stars.

3.5. Discussion

In repression-based circuits, we employed a transcription repressor, HspR, found in HSR pathway of *M. tuberculosis* [155] to build a hybrid sensor system. We engineered natural *E. coli* dnaK promoter (PdnaK) with inverted repeat motifs (IR2 and IR3 sequences) of HAIR sequences [156] from natural *M. tuberculosis* dnaK promoter (mtPdnaK) to construct toxicity sensor circuits. Downstream of PdnaK was engineered with single and double repeats of IR motifs in one plasmid while HspR was cloned under a constitutive promoter, mProD, and cloned onto another plasmid. Proposed mechanism is to block reporter expression via constitutively expressed HspR under normal growth conditions (Figure 3.12A) as

HspR dissociates from the promoter driving reporter expression upon stress (Figure 3.12B). The recombinant HspR expression in *E. coli* was demonstrated in Western Blot analysis (Figure 3.6). Western blotting showed that, even though HspR was not a native protein to *E. coli*, it could be expressed successfully after codon optimization.

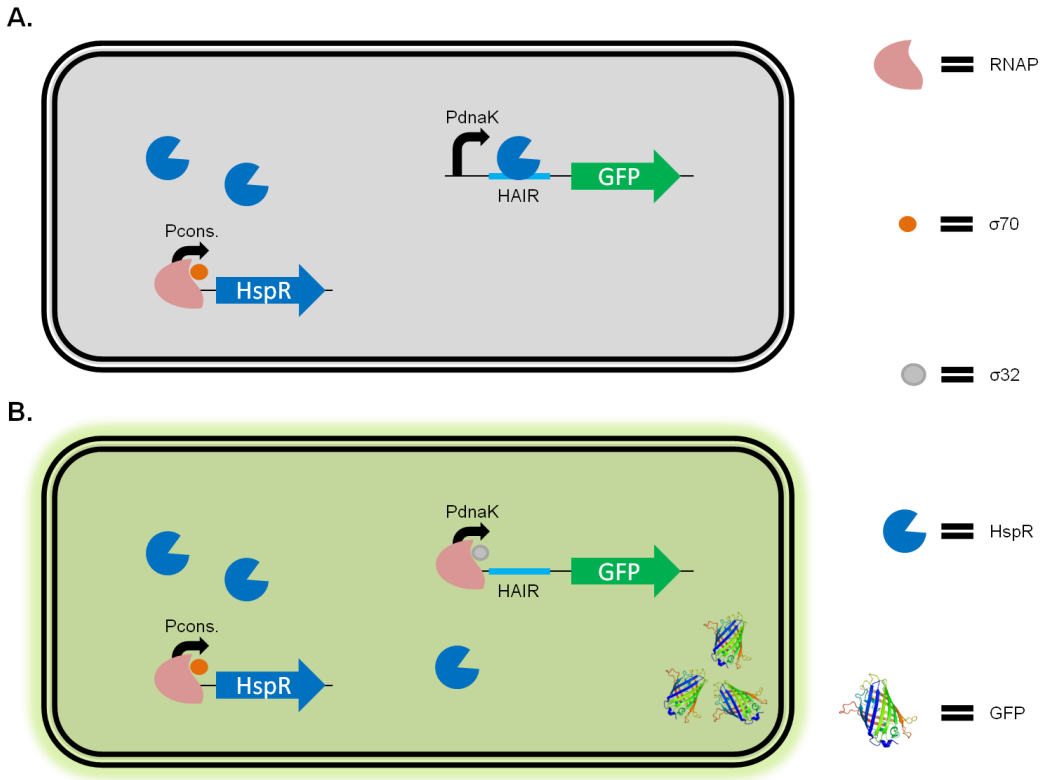

Figure 3.12 Working principle of HspR based stress circuits. A. At normal growth conditions, constitutively expressed HspR recognizes specific sequences (HAIR; IR2 or IR3) on promoter region blocking the gene expression. B. Upon stress, HspR is released from the promoter initiating gene expression.

HspR association with promoter regions has been shown with a gel retardation assay (Figure 3.7) to confirm that HspR could associate all engineered promoters.

First, HspR binding on its native promoter (mtPdnaK) was characterized as Bucca *et al.* described before [154]. Further, HspR binding on *E. coli* DnaK promoter and its modifications with HAIR sequences was shown with native polyacrylamide gel electrophoresis (PAGE). Each promoter regions were isolated by PCR and incubated with and without HspR protein. Results indicated that HspR addition caused retardation of PCR fragment showing an additional retarded fragment (represented by "R" on the figure) on the gel. Thus, background signal reduction due to HspR repression was verified by showing promoter-repressor interaction with the conducted gel retardation assay.

A comparison on the repression strengths of HspR on native mtPdnaK circuits and native PdnaK circuits have been shown in Figure 3.8A and Figure 3.8B, respectively. Reporter expression results confirmed that HspR favorably bound to mtPdnaK promoter region and repressed the gene expression. Yet, unlike our expectation, heat treatment was not enough to turn on the gene expression completely (Figure 3.8A). On the other hand, HspR repressed native *E. coli* P_{dnaK} less favorably compared to its native promoter, mtPdnak. It is proposed that HspR dissociated from promoter upon heat treatment which led to a two-fold increase after 60 min (Figure 3.8B). Comparing the engineered PdnaK sensors with HAIR motifs, single IR motifs showed no or little significant difference in terms of gene expression upon stress exposure (Figure 3.8C for IR2 and Figure 3.8D for IR3). These results confirmed that HspR favorably repressed the gene expression in the presence of IR2 and IR3 sequences in the circuits. Meantime, these sequences might trigger a lower degree of dissociation of HspR from promoter so that gene expression could not begin through stress promoters even though there was a

stress as an input. Also, double IR2 repeat indicated the same gene expression pattern with single IR repeats upon heat treatment (Figure 3.8E). On the other hand, double IR3 repeat significantly enhanced HspR repression of PdnaK blocking the gene expression under normal growth conditions. Data showed the highest HspR repression with the lowest background signal between HspR-mediated sensors (Figure 3.8F). Also, upon heat treatment, we observed a three-fold increase in GFP expression which was the highest reporter expression-fold compared with other modifications. The data was supported by representative fluorescent microscopy images in Appendix F.

After characterization of constructed circuits with heat, selected HSR circuits with engineered HSP promoters (mtPdnaK, PdnaK-IR2-IR2, and PdnaK-IR3-IR3) co-expressed with HspR repressor were screened by employing red emitting CdTe QDs to analyze NM-triggered toxicity as the main motivation was to detect toxicity of NMs. CdTe QDs were selected as representative NMs used for many applications (i.e., fluorescent labeling or drug delivery) in medicine. Selected HspR-mediated stress sensors were treated with CdTe QDs, and they showed quick response to QDs. On the other hand, sensor with mtPdnaK (Figure 3.9A) showed no response, indicating strong repression by HspR that inhibited transcription initiation of the reporter. On the other hand, sensor with PdnaK-IR2-IR2 (Figure 3.9B) and sensor with PdnaK-IR3-IR3 (Figure 3.9C) showed dramatic fluorescence increase upon QD treatment. Besides, overall signal upon induction was higher than the riboregulator-mediated sensors making them good candidates to determine nanotoxicity (See Chapter 2). Our observations from

fluorescent measurement are supported by representative fluorescent microscopy images in Appendix F.

Following QD characterization with selected sensors, we chose HspR-mediated PdnaK-IR3-IR3 sensor as potentially to be the best nanomaterial-toxicity determinant. Further, we analyzed dynamic range of this sensor via CdTe QD treatment (Figure 3.10) to determine sensor characteristics of analyte detection (i.e., detection limit). Induction concentrations were selected from 0-to-250 nM of QDs. Results indicated that toxicity sensor could detect the presence of QDs even at lower concentrations showing that detection limit of the sensor was very low. Also, as shown by previous studies, QD toxicity is concentration dependent [136, 157]; thus, higher concentrations of QDs in the media can cause higher cellular uptake or ROS generation. This can trigger higher and faster stress response compared to lower concentrations.

Further, we selected a representative HspR-mediated sensor to analyze gene expression at transcription level with heat and QD treatment. The sensor showed the highest expression level after heat treatment (Figure 3.11A) while QD treatment indicated lower expression (~6-fold) compared to heat treatment (~20-fold) (Figure 3.11B). Yet, sensor response upon QD exposure was notable and significant making it a good candidate to evaluate nanomaterial-triggered toxicity in biocompatibility tests of nanomaterials. Next, we expanded the toxicity evaluation of QDs through ROS mechanism since QD exposure activates not only HSR but also other stress related mechanisms such as oxidative stress pathways. *E. coli* has two oxidative-stress mechanisms: SoxR and OxyR. Former is related with superoxide and nitric oxide sensing and regulation of the related genes

(s*odA*, *acnA*, *nfo* etc.) while the latter is activated by hydrogen- and alkyl hydroperoxide and regulates *oxyS*, *katG*, *ahpCF*, *grxA*, and *gorA* expression [158]. Thus, HspR-mediated PdnaK-IR3-IR3 sensor, as the best nanotoxicity sensor candidate, was selected to evaluate ROS formation upon QD treatment (Figure 3.11D) and *superoxide dismutase* (*sodA*) gene expression was quantified via RT-qPCR after one hour upon QD treatment. Results indicated that *sodA* expression increased with QD treatment showing CdTe QDs caused ROS formation in cells. Since SodA is responsible from superoxide deactivation, results proposed that CdTe QDs led to superoxide radicals in cells which activated s*odA* expression up to 3-fold. Furthermore, stress and ROS formation in cells was verified by 200 μM of *tert*-Butyl hydroperoxide (TBHP), a well-known positive control agent for ROS formation, treatment of cells for 30 min. Sensors with PdnaK-IR3-IR3 showed both fluorescence increase indicating HSR activation (Figure 3.9C), and 12-fold of *sodA* expression indicating ROS formation (Figure 3.11C) upon treatment. As a conclusion, HspR-mediated PdnaK-IR3-IR3 sensor was characterized in terms of HSR and ROS pathway activation upon QD treatment.

3.6. Conclusion

As a conclusion, HspR binding on all promoters has been shown blocking the reporter expression at normal growth conditions, where as it has been turned on upon heat treatment. However, all engineered promoters showed different characteristics which might be caused by different interaction dynamics with the repressor. Besides, not only they can be repressed equally by the HspR, but also

their dissociation behavior differs. Among utilized promoters, it can be concluded that double IR3 sequence plays a strong role in HspR recruitment and turning the promoters ON/OFF. Data supports that the HAIR motifs are good candidates to be used in design of genetic circuits to monitor stress level. HspR toxicity sensors have a lower background signal under normal growth conditions while gene expression might dramatically increase upon stress.

Toxicity response to NMs is highly depending on cell type and chemical composition. Membrane structure and composition affects nanomaterial uptake through cells. For instance, even Gram negative and Gram positive bacteria do not respond similarly to the same NM since they have different membrane composition. Besides, thinner peptidoglycan layer makes Gram negative cells more vulnerable against nanotoxicity [145]. Here we demonstrate that our engineered bacterial NM-triggered stress sensors are able to sense and respond accordingly to the stress conditions. Considering that HSR mechanism is common in each cell type, we expect to transfer and modify this bacterial system to other cell types. Still, cell type response might require some further optimization to tune gene expression based on NM concentration and type. However, in general, we propose a whole cell sensor that can produce quick information about the toxicity of the NMs of interest from a global perspective. On the other hand, the proposed sensor does not provide detailed information about the NM-triggered toxicity including its action mechanism at the downstream of pathways of interests.

CHAPTER 4

A Living Sensor to Report the Source of Toxicity

4.1. Objective of the Study

Biocompatibility assessment of nanomaterials before field application is crucial becase they might be toxic to cells and may cause severe health conditions. In previous chapter we characterized a bacterial whole cell biosensor utilizing endineered heat shock response (HSR) mechanism to track biocompatibility of nanomaterials in 1 hour. Yet, the sensor is classified as semi-specific biosensor which indicates whether the compound cause stress on cells or not. Hence, our aim is to make a complex circuit with specific regulatory elements that can sense certain compounds such as heavy metals. We have begun with gold and cadmium detecting circuits to make circuits reporting the source of stressor. We showed that both gold and cadmium could be specifically detecting by engineered sensors and introducing a recombinase to the circuits provided tight control decreasing background signal. Additionally, this system can be expanded various analyte detection at the same time utilizing different reporters. This opens a room for researchers to identify which part of the engineered nanoparticle is toxic requiring more engineering to decrease its toxicity. Yet, further optimization is required to merge the system to make an all-in-one type of living sensor.

4.2. Introduction

Bacterial whole-cell biosensors have been commonly utilized to monitor microbial environment. These sensors provide bioavailability of various compounds which they have been exposed [159]. Hence, bacterial whole-cell biosensors have been useful tools to monitor toxicity of environmental samples which are also commercialized [160, 161]. Whole-cell biosensors that are used for toxicity monitoring are divided in three major gours: non-specific biosensors, semi-specific biosensors, and specific biosensors. The non-specific biosensor principle is based on the constitutive reporter expression in the sensor bacteria. When this sensor encounters any toxic compound, the reporter expression decreases indicating the decrease in metabolic activity (Figure 4.1A) [162]. On the other hand, the semi-specific biosensor principle is based on a stress responsive promoter encoding a reporter (Figure 4.1B). In this type of biosensor, cells respond only a certain compounds causing certain types of stress (i.e., SOS response controlled by DNA damage pathway, or protein damage response controlled by heat shock response pathway) [73]. Lastly, the specific biosensor principle is based on the interaction of a certain compound with a cognitive regulatory element (i.e., transctiprion factor) which controls the expression of a reporter through a specific promoter (Figure 4.1C) [73, 163, 164].

Specific bacterial sensors use cellular signaling and regulatory pathways by which are controlled compounds of interest. Coupling the operator-promoter pairs of DNA controls a measurable output such as luciferase, β-galactosidase, or reporter proteins. After internalization of the compound by a cell, the compound interacts

with its regulator which would be a transctiptional activator or repressor. This interaction leads an increase in the reporter which is detected with certain equipment easily. Most of the promoter-transctiption factor couples discovered so far is natural which have been isolated from various organisms. For instance, sensors constructed for organic compound detection is based on the relevant promoters of microorganisms which play role in degradation of the target compound, while heavy metal or antibiotic detecting sensors utilize resistance operons of microorganisms against these targets [164].

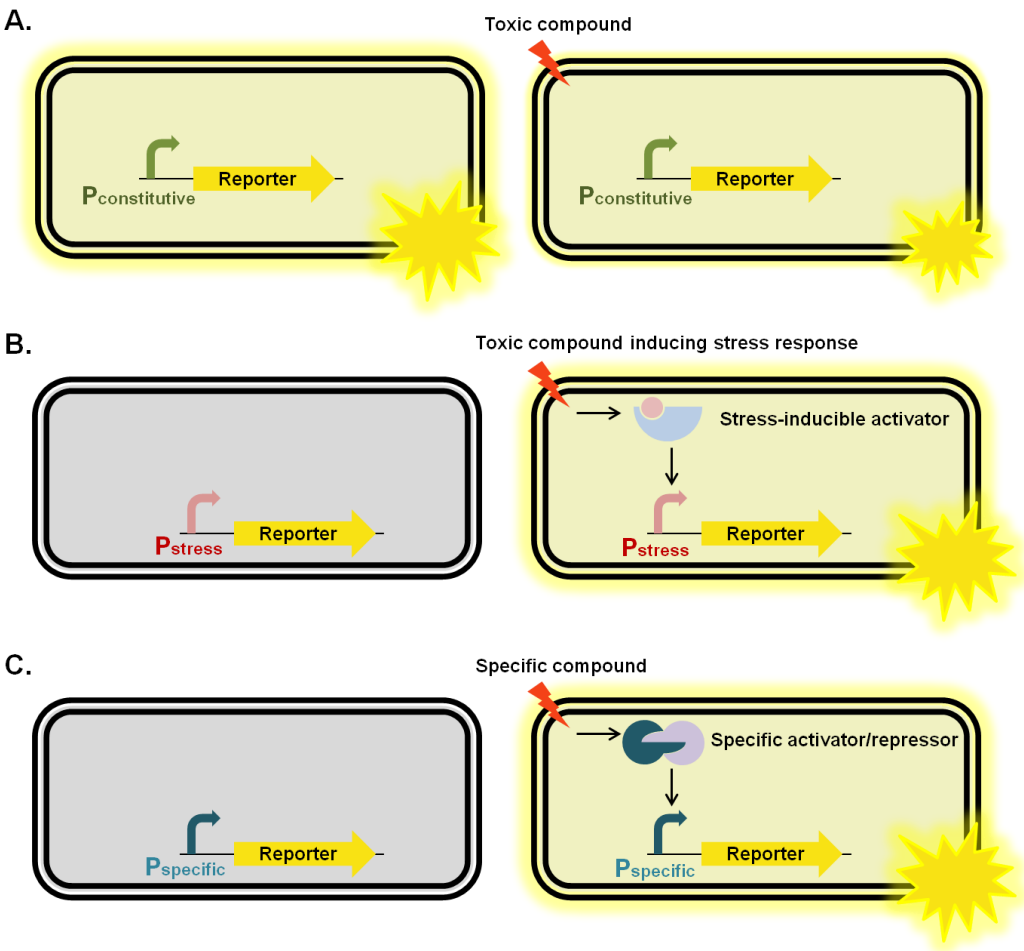

Figure 4.1: Working principles of bacterial biosensors developed for environmental monitoring. A. Non-specific biosensors express a reporter

constitutively (left). Exposing to a toxic compound decreases the reporter signal (right). B. Semi-specific biosensors express a reporter under the control of a stress promoter (left). Exposing to a toxic compound, which causes stress in cells, activates the reporter expression through the stress promoter (right). C. Specific biosensors express a reporter under the control of a specific promoter (left). Exposing to a certain compound activates the reporter expression through its cognitive promoter (right). Reprinted with permission from ref [73]. Copyright 2006 Elsevier.

Most of the transcription factors regonizing compounds are composed of a DNA-binding domain (DBD) and an effector-binding domain (EBD). Former one is responsible from the recognition and binding on the operator region of DNA sequence while the letter one is responsible for the oligomerization of the transcription factor and signal transmission through the DBD. Transctiprional activators recognize the operator sequences on DNA in the presence of analyte of interest and either recruit RNA polymerase to the promoter, or induce transcriptionally active RNA polymerase-promoter open complex formation (Figure 4.2A). Transctiprional repressors block recognition of the promoter by RNA polymerase via binding on the operator sites when their target analyte is absent; whereas, the binding of the analyte of interest to the repressors causes dissociation of the repressor from the operator allowing recognition of the promoter by RNA polymerase initiating the gene expression (Figure 4.2B). Additionally, a variation of this system is based on the presence of the analyte and

repression works only when both the analyte and the transcription factor (aporepressor) are found in the cell at the same time (Figure 4.2C) [165].

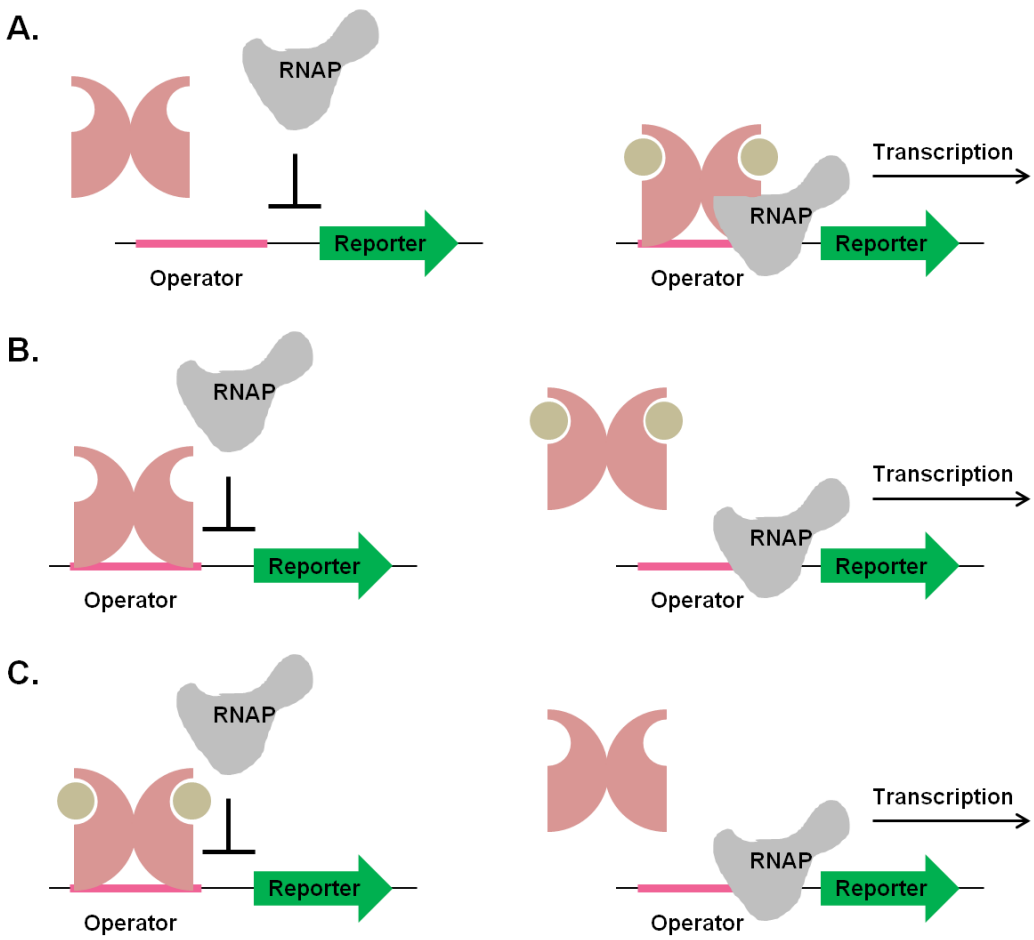

Figure 4.2: Working principles of activator and repressor based transcription factors in whole cell biosensors. A. Transctiprional activators recognize the operator sequences on DNA in the presence of analyte of interest and either recruit RNA polymerase to the promoter, or induce transcriptionally active RNA polymerase-promoter open complex formation. B. Transctiprional repressors block recognition of the promoter by RNA polymerase via binding on the operator sites when their target analyte is absent; whereas, the binding of the analyte of interest to the repressors causes dissociation of the repressor from the operator

allowing recognition of the promoter by RNA polymerase initiating the gene expression. C. Aporepressors block the gene expression in the presence of the analyte. Reprinted with permission from ref [165]. Copyright 2015 Frontiers Research Foundation.

Table 4.1: Examples of metal ion dependent transcriptional regulators.

Regulator	**Inducer**	**Regulated System**	**References**
MerR Family			
MerR	Hg (II)	Mercury resistance	[166]
CueR	Cu (I), Ag (I), Au (I)	Copper resistance	[167]
ZntR	Zn (II), Cd (II), Pb (II)	Zinc resistance	[167]
CadR	Cd (II)	Cadmium resistance	[168]
GolS	Au (I)	Gold resistance	[169]
ArsR Family			
ArsR	As (III)	Arsenic resistance	[170]
CadC	Cd (II), Pb(II), Zn(II)	Cadmium resistance	[171]
DtxR Family			
DtxR	Fe (II), Ni (II)	Diphteria toxin regulation	[172]
FurR Family			
Fur	Fe (II)	Iron uptake	[173]
Zur	Zn (II)	Zinc uptake	[174]
NikR Family			
NikR	Ni (II)	Nickel transporter	[175]

Some metals (i.e., Cu, Fe, K, Mg, or Mn) are essential nutrients for cells, while others (i.e., Ag, Al, Cd, Au, Pb, or Hg) have no biological function. Yet, most of the metals are toxic to cells at high concentrations [176]. Many bacterial whole-cell biosensors have been constructed so far to detect toxicity of metal ions especially to monitor environmental samples [177-180]. The most important characteristics of these biosensors is their specificity; defined as the metals that can be detected with the transciption factor, and their sensitivity; the detection limit of the sensor. Five major metal binding transcription factor families have been discovered so far which have been responsible for a certain metal detection [165]. Nevertheless, it has been shown that most of these transcription factors could interact with more than one metal ion (Table 4.1). One of the well-characterized families is MerR family which is composed of mercury responsive transcription factors. MerR protein is a transcription activator requiring mercury ions to recruit RNA polymerase to the operator initiating the expression of mercury resistance genes [166]. Although MerR is specific to mercury, not all MerR family transcription factors share the same characteristics. For instance, ZntR, a member of the MerR family, has been discovered as zinc responsive, further studies showed that it also interacts with cadmium and lead [181]. Similarly, another MerR family member, CueR, mainly responds to copper together with to silver and gold [166, 182]. Yet, sensitivity of transcription factors varies among different metals [166].

4.3. Materials and Methods

4.3.1.Media and Strains

E. coli DH5α (New England Biolabs, Inc.) was grown in LB medium (1% (w/v) tryptone, 0.5% (w/v) yeast extract, 0.5% (w/v) NaCl) with proper antibiotics at 37°C and 180 rpm shake in Erlenmeyer flasks. Overnight cultures were prepared from frozen glycerol stocks and incubated for 16 h with the same culturing conditions mentioned previously. 1% of inoculums from overnight cultures were used to start experimental cultures and their growth was monitored via spectrophotometer (GENESYS 10 Bio, Thermo Scientific). In metal induction experiments, MOPS minimal media (0.1 M potassium morpholinopropane sulfonate (MOPS), pH 7.4; 0.1 M Tricine, pH 7.4; 0.001 M $FeSO_4$; 0.19 M NH_4Cl; 0.0276 M K_2SO_4; 0.002 $CaCl_2$; 0.25 M $MgCl_2$; 0.5 M NaCl; micronutrients [3×10^{-2} M $(NH_4)_6Mo_7O_{24}$; 4×10^{-5} M H_3BO_3; 3×10^{-6} M $CoCl_2$; 10^{-6} M $CuS0_4$; 8×10^{-6} M $MnCl_2$; 10^{-6} M $ZnSO_4$]; 0.132 M K_2HPO_4; 1 mg/ml thiamine; 0.2% (v/v) glucose) defined by ref. [183] or heavy metal mops (HMM) media (40 mM MOPS, pH 7.2; 50 mM KCl; 10 mM NH_4Cl; 0.5 mM $MgSO_4$; 1 mM glycerol-2-phosphate (BGP); 1 μM $FeCl_3$; 0.4% (v/v) glucose) defined by ref. [184] were used, unless otherwise stated.

4.3.2.Plasmid Construction

To construct mProD HspR PgolB (inverted) GFP pET22b vector, Bxb1 recognition sites were amplified using “pET22b sfGFP logic” and GFP-rrnBT1 part using “PdnaK GFP pZa” templates constructed before with the primers in

Table B.1 For backbone, formerly constructed mProD HspR pET22b vector was linearized with SpeI (New England Biolabs, Inc.) restriction enzyme digestion. To construct PdnaK-IR3-IR3 Bxb1 GolS pZa vector, Bxb1 integrase part was amplified using "pZa-native TetO bxb1 pBad tp901" and GolS part using "YFP-Gold sensor" templates constructed before with the primers in Table B.1. For backbone, formerly constructed "PdnaK-IR3-IR3 GFP pZa" vector was digested with MluI (New England Biolabs, Inc.) restriction enzyme digestion to exclude GFP part. To construct mProD HspR PcadA (inverted) GFP pET22b vector, formerly constructed "mProD HspR PgolB (inverted) GFP pET22b" vector was used as template and amplified to exclude PgolB while adding PcadA regions via Gibson Assembly primers in Table B.1. To construct PdnaK-IR3-IR3 Bxb1 CadR pZa vector, Bxb1 integrase part was amplified using "pZa-native TetO bxb1 pBad tp901" and CadR part using "YFP-Cadmium sensor" templates constructed before with the primers in Table B.1. For backbone, formerly constructed "PdnaK-IR3-IR3 GFP pZa" vector was digested with MluI (New England Biolabs, Inc.) restriction enzyme digestion to exclude GFP part. To construct PcadA GFP pET22b vector, formerly constructed "PdnaK GFP pET22b" vector was used as template and amplified to exclude PdnaK while adding PcadA region with RBS via Gibson Assembly primers in Table B.1. To construct mProD MerR(mutated) pZs vector, first, MerR(mutated) was synthesized as gene fragments from GENEWIZ Company and Gibson Assembly homology regions were added with primers in Table B.1. For backbone, formerly constructed "mProD te-F-HspR-His pZs" vector was digested with KpnI-HindIII (New England Biolabs, Inc.) enzyme pair to exclude HspR part. Q5 Hot Start High-Fidelity DNA Polymerase (New

England Biolabs, Inc.) was used for all PCR reactions (Reaction conditions were described in Appendix E). NucleoSpin Gel and PCR Clean-up kit (Macherey-Nagel) was used according to the manufacturer's instructors to purify digested DNA samples or PCR products from 1 or 1.8% Agarose gels stained with SYBR Safe DNA Gel Stain (Thermo Fisher Scientific). Plasmid construction was made via Gibson Assembly method described by Gibson *et al.* [137] (Reaction conditions were described in Appendix E). After assembly, mixes were directly transformed into chemical competent *E. coli* DH5α cells. Constructed genetic circuits were sequence verified by Sanger Sequencing (GENEWIZ). All genetic part sequences used this chapter was introduced in Table A.1, and all constructed vector maps were indicated in Appendix C with their sequencing verification results in Appendix D.

4.3.3. Chemical Competent Cell Preparation and Transformation of DNA in Cells

Overnight cultures of *E. coli* DH5α were prepared from frozen glycerol stocks and incubated for 16 h with the same culturing conditions mentioned previously. 1% of inoculums from overnight cultures were used to start fresh culture for competent cell preparation. Culture was incubated at 37°C and 180 rpm shake in Erlenmeyer flasks until OD_{600} reached 0.2-to-0.5. Following, culture was cooled in ice for 10 min and cells were collected by centrifugation at 1000 ×g for 10 min at +4°C. After centrifugation, supernatant was discarded and cell pellet was resuspended in 10% (v/v) of TSS Buffer (10% (w/v) PEG-8000, 5% (v/v) DMSO,

50 mM $MgCl_2$ pH 6.5 in LB). For each aliquot, 100 µl of cultures were placed in each microcentrifuge tubes and stored at -80°C.

Chemical competent cells were thawed on ice for 30 min before transformation. For transformation, whole ligation product, Gibson Assembly reaction product, or 100 ng of intact plasmid DNA was introduced to thawed cells and incubated on ice for 20-30 min. Following, cells were shocked by heat treatment at 42°C for 30 sec. After the heat shock, cells were cold shocked for 2 min on ice. Then, 250-1000 µl of LB was added onto the cells and incubated at 37°C and 180 rpm shake for 45-60 min. At the end of the incubation, cells were collected at 1000 ×g for 10 min and the supernatant was discarded. The collected cells were resuspended in 50 µl of LB and spread onto LB-agar supplemented with proper antibiotics.

4.3.4.Sequencing Alignments with Geneious Software

All plasmid maps were constructed on an online vector tool; Benchling. Following, all plasmid maps were exported as .gb files and imported in Geneious software together with the sequencing results of plasmid maps as .abi files. In order to align plasmid map and its sequencing data, both sequences were selected and pairwise alignment performed. The sequencing results for all vectors were indicated in Appendix D.

4.3.5.Source Detection Assays

For all experiments, overnight cultures were prepared in LB media and incubated for 16 h at 37°C, 180 rpm. For recombinase-based gold and cadmium detection circuits, 0.4% of inoculums from overnight cultures were used to start

experimental cultures in fresh LB or MOPS media, and induced directly with ions indicated in related figures in varying concentrations. Cultures were incubated at 30°C, for 18 h before measurements, unless otherwise stated. At least three independent biological replicas were prepared for each group in each experiment.

For MerR-based cadmium circuit, 1% of inoculums from overnight cultures were used to start experimental cultures in fresh LB media, and grown at 37°C, 180 rpm until OD_{600} of cultures reached to 1.0-1.2. Following, cultures were collected at 3000 ×g for 10 min, supernatants were discarded, and cell pellets were re-suspended in fresh MOPS or HMM media. Cultures were induced with ions indicated in related figures in varying concentrations, and incubated at 37°C for 22 h before measurements, unless otherwise stated. At least three independent biological replicas were prepared for each group in each experiment.

4.3.6.Fluorescence Measurement and Data Analysis

All fluorescence measurement studies were conducted via microplate reader (SpectraMax M5, Molecular Devices). Excitation and emission wavelengths for eGFP were set as 485 and 538 nm, respectively. Each measurement was conducted in Corning 96-well clear flat bottom polystyrene plates with 250 μL of samples from each culture. For signal normalization, raw fluorescence intensity was divided by OD_{600} values of each sample and the control group (empty cells) was subtracted from sensor data. For 0-to-1 normalization, each value was subtracted from minimum value and divided by difference between maximum and minimum values in related groups.

4.3.7.Statistical Analysis

All data were expressed as mean ± standard error mean. Depending on the groups of interest, either one-way analysis of variance (ANOVA) or two-way ANOVA with Dunnett's/Tukey's/Sidak's multiple comparison tests (GraphPad Prism v6) were used to compare groups.

4.4. Results

4.4.1.Cloning of Source Detection Circuits

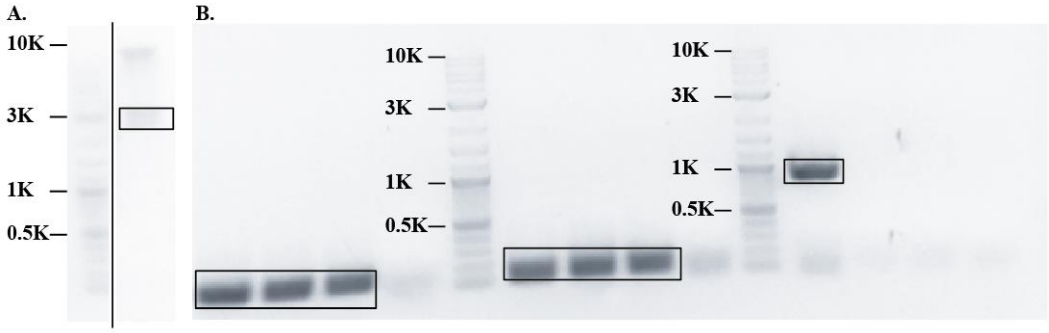

Figure 4.3: Construction of mProD HspR PgolB (inverted) GFP pET22b vector. A. Linearized backbone was observed at 3000 bp. B. PCR products of Bxb1-attP (left), Bxb1-attB (middle), and GFP-rrnBT1 (right) were observed at 168 bp, 141 bp, and 915 bp, respectively. 1 kb+ DNA Ladder (NEB) was used as DNA marker.

For cloning of mProD HspR PgolB (inverted) GFP pET22b vector, "mProD HspR pET22b" vector was linearized with SpeI restriction enzyme digestion. The digested product was run on 1% Agarose gel and isolated using MN-gel extraction

kit according to manufacturer's instructions (Figure 4.3A). To obtain other DNA pieces of the vector, Bxb1 recognition sites were amplified via PCR primers stated in Table B.1 using "pET22b sfGFP logic" vector as template, and GFP-rrnBT1 part was amplified via PCR primers stated in Table B.1 using "PdnaK GFP pZa" vector as template. Both PCR products were run on 1% Agarose gel and isolated using MN-gel extraction kit according to manufacturer's instructions (Figure 4.3B). Isolated fragments were assembled with Gibson Assembly reaction (Appendix E), and selected colonies were verified by sequencing (Appendix D).

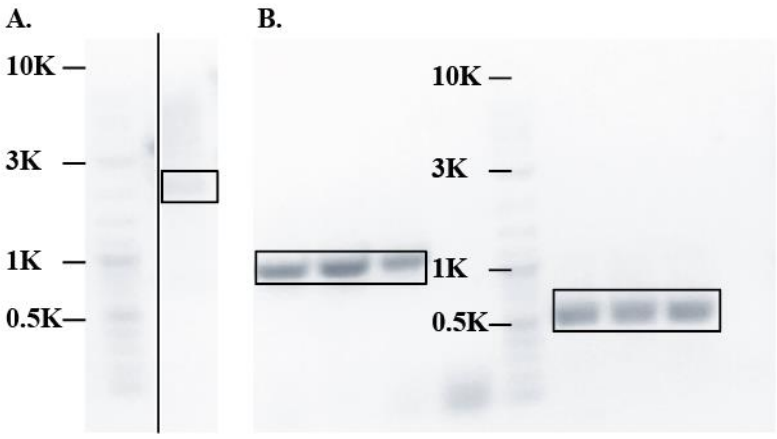

Figure 4.4: Construction of PdnaK-IR3-IR3 Bxb1 GolS pZa vector. A. Linearized backbone and extracted GFP were observed at 2100 bp and 700 bp, respectively. B. PCR products of Bxb1 recombinase (left), and GolS (right) were observed at 1199 bp, and 537 bp, respectively. 1 kb+ DNA Ladder (NEB) was used as DNA marker.

For cloning of PdnaK-IR3-IR3 Bxb1 GolS pZa vector, "PdnaK-IR3-IR3 GFP pZa" vector was digested with MluI enzyme to exclude GFP part. The digested product was run on 1% Agarose gel and isolated using MN-gel extraction kit

according to manufacturer's instructions (Figure 4.4A). To obtain other DNA pieces of the vector, Bxb1 recombinase was amplified via PCR primers stated in Table B.1 using "pZa-native TetO bxb1 pBad tp901" vector as template, and GolS was amplified via PCR primers stated in Table B.1 using "YFP-Gold sensor" vector as template. Both PCR products were run on 1% Agarose gel and isolated using MN-gel extraction kit according to manufacturer's instructions (Figure 4.4B). Isolated fragments were assembled with Gibson Assembly reaction (Appendix E), and selected colonies were verified by sequencing (Appendix D).

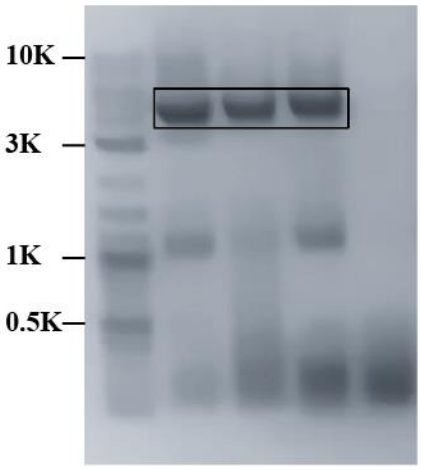

Figure 4.5: Construction of mProD HspR PcadA (inverted) GFP pET22b vector. Linearized backbone was observed at 4000 bp. 1 kb+ DNA Ladder (NEB) was used as DNA marker.

For cloning of mProD HspR PcadA (inverted) GFP pET22b vector, "mProD HspR PgolB (inverted) GFP pET22b" was amplified via PCR primers stated in Table B.1 to exclude PgolB while adding PcadA regions to be assembled in Gibson Assembly reaction. PCR products were run on 1% Agarose gel and

isolated using MN-gel extraction kit according to manufacturer's instructions (Figure 4.5). Isolated fragment was assembled with Gibson Assembly reaction (Appendix E), and selected colonies were verified by sequencing (Appendix D).

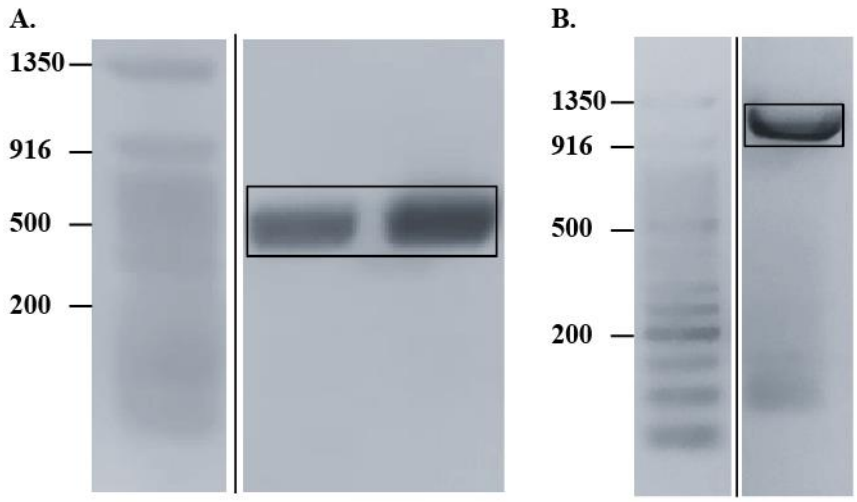

Figure 4.6: Construction of PdnaK-IR3-IR3 Bxb1 CadR pZa vector. A. PCR products of CadR were observed at 500 bp. B. PCR product of Bxb1 recombinase was observed at 1199 bp. 50 bp DNA Ladder (NEB) was used as DNA marker.

For cloning of PdnaK-IR3-IR3 Bxb1 CadR pZa vector, "PdnaK-IR3-IR3 GFP pZa" vector was digested with MluI enzyme to exclude GFP part. The digested product was run on 1% Agarose gel and isolated using MN-gel extraction kit according to manufacturer's instructions (Figure 4.4A). To obtain other DNA pieces of the vector, Bxb1 recombinase was amplified via PCR primers stated in Table B.1 using "pZa-native TetO bxb1 pBad tp901" vector as template, and CadR was amplified via PCR primers stated in Table B.1 using "YFP-Cadmium sensor" vector as template. Both PCR products were run on 1% Agarose gel and isolated using MN-gel extraction kit according to manufacturer's instructions

(Figure 4.6). Isolated fragments were assembled with Gibson Assembly reaction (Appendix E), and selected colonies were verified by sequencing (Appendix D).

For cloning of PcadA GFP pET22b vector, “PdnaK GFP pET22b” vector was amplified via PCR primers stated in Table B.1 to exclude PdnaK while adding PcadA region with RBS to be assembled in Gibson Assembly reaction. PCR products were run on 1% Agarose gel and isolated using MN-gel extraction kit according to manufacturer’s instructions (Figure 4.7). Isolated fragment was assembled with Gibson Assembly reaction (Appendix E), and selected colonies were verified by sequencing (Appendix D).

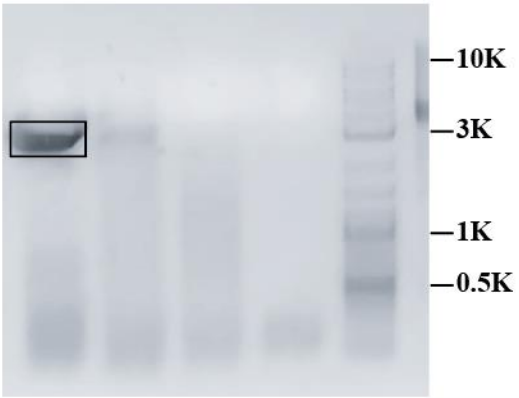

Figure 4.7: Construction of PcadA GFP pET22b vector. Linearized backbone was observed at 3350 bp. 1 kb+ DNA Ladder (NEB) was used as DNA marker.

For cloning of mProD MerR (mutated) pZs, “mProD te-F-HspR-His pZs” vector was digested with KpnI-HindIII enzyme pair. The digested product was run on 1% Agarose gel and isolated using MN-gel extraction kit according to manufacturer’s instructions (Figure 4.8A). MerR (mutated) part was synthesized as gene fragments from GENEWIZ Company. To add homology regions of the

backbone for Gibson Assembly reaction, the synthesized MerR (mutated) was amplified via PCR primers stated in Table B.1. PCR products were run on 1% Agarose gel and isolated using MN-gel extraction kit according to manufacturer's instructions (Figure 4.8B). Isolated fragments were assembled with Gibson Assembly reaction (Appendix E), and selected colonies were verified by sequencing (Appendix D).

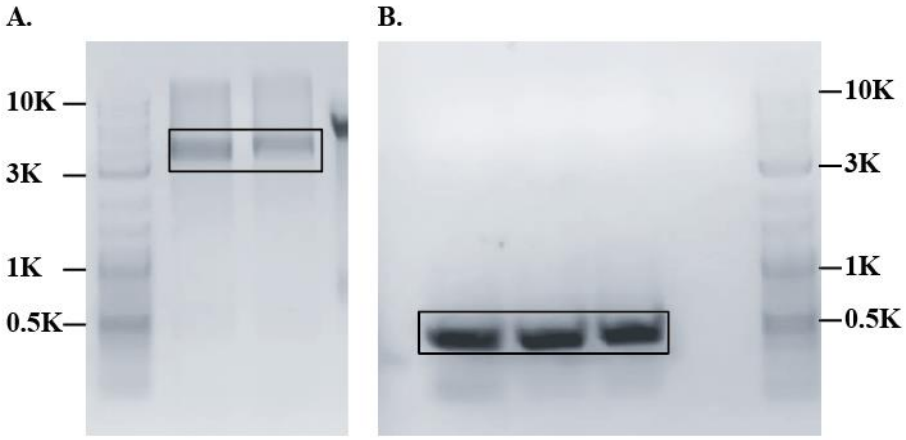

Figure 4.8: Construction of mProD MerR (mutated) pZs vector. A. Linearized backbone and HspR were observed at 3500 bp and 460 bp, respectively. B. PCR products of MerR (mutated) were observed at 490 bp. 1 kb+ DNA Ladder (NEB) was used as DNA marker.

4.4.2.Characterization of Gold Detecting Circuit

To determine optimum concentration to work with, recombinase-based gold sensor induced with 0-to-250 μM of gold ions for 18 h. Results showed that sensor response increased with increasing ion concentration (Figure 4.9).

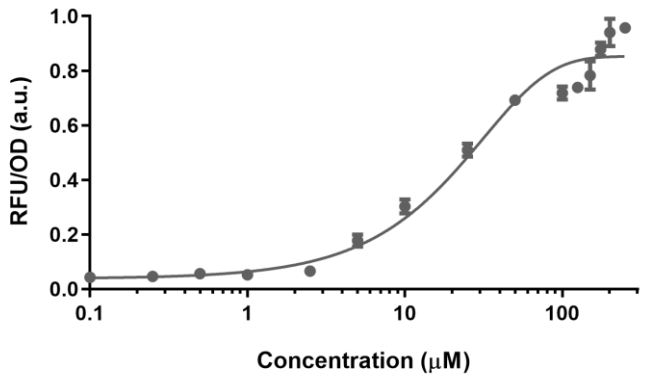

Figure 4.9: Dynamic range analysis of recombinase-based gold sensor in LB media. Cells were induced with varying gold concentrations for 18 h at 30°C before measurement. Experiments were performed as three biological replicates. All data were normalized according to formula stated in Materials and Methods section.

To show specificity of the recombinase-based gold sensor, cells were induced with 50 μM of metal ions for 18 h, and it has been shown that the sensor was responsive only to gold (Figure 4.10).

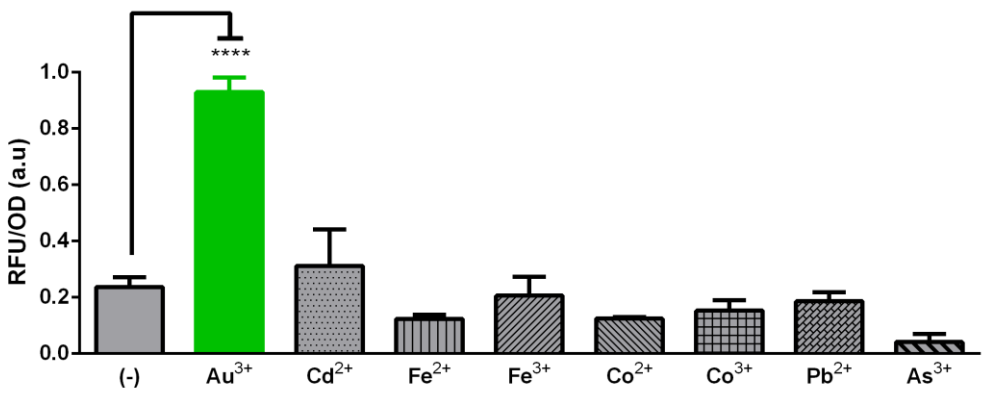

Figure 4.10: Cross-reactivity analysis of recombinase-based gold sensor in LB media. Cells were induced with 50 μM of metal ions for 18 h at 30°C before

measurement. Experiments were performed as three biological replicates. All data were normalized according to formula stated in Materials and Methods section.

To show robustness of the recombinase-based gold sensor, cells were incubated in MOPS minimal media, and induced with gold ions. Results showed that sensor also worked in minial media (Figure 4.11).

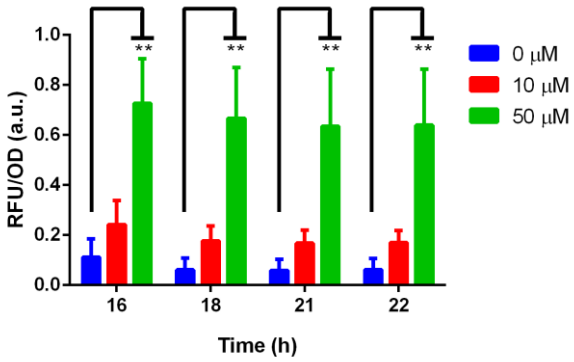

Figure 4.11: Response-time analysis of recombinase-based gold sensor in MOPS minimal media. Cells were induced with 0, 10, and 50 μM of gold concentrations at 30°C. Experiments were performed as three biological replicates. All data were normalized according to formula stated in Materials and Methods section.

4.4.3.Characterization of Cadmium Detecting Circuit

To determine optimum concentration to work with, recombinase-based cadmium sensor induced with 0-to-300 μM of cadmium ions for 18 h. Results showed maximum response (~3-fold signal increase) at 50 μM and decreasing afterward because of cadmium toxicity to cells (Figure 4.12).

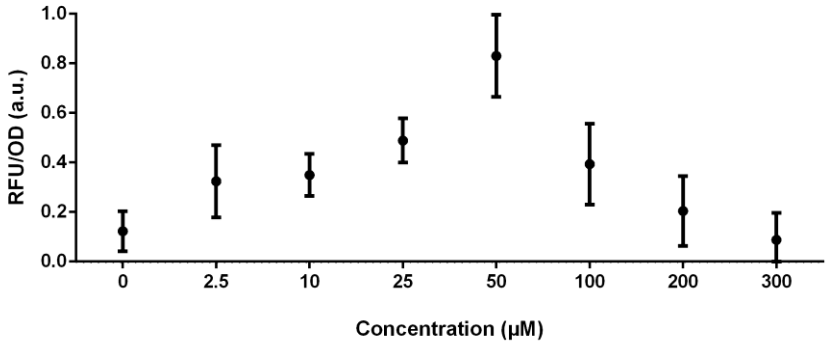

Figure 4.12: Dynamic range analysis of recombinase-based cadmium sensor in LB media. Cells were induced with varying cadmium concentrations for 18 h at 30°C before measurement. Experiments were performed as three biological replicates. All data were normalized according to formula stated in Materials and Methods section.

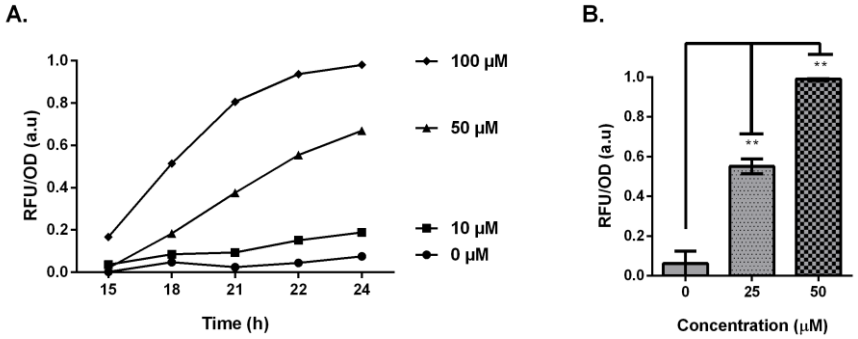

Figure 4.13: Characterization of MerR-based cadmium sensor in diffirent media. A. Response-time analysis of MerR-based cadmium detection sensor in MOPS minimal media. Cells were induced with 0, 10, 50, and 100 μM of cadmium at 37°C. Experiments were performed as three biological replicates. All data were normalized according to formula stated in Materials and Methods section. B. Induction of MerR-based cadmium detection sensor with 0, 25, and 50 μM of cadmium in HMM minimal media for 14 h at 37°C. Experiments were performed

as three biological replicates. All data were normalized according to formula stated in Materials and Methods section.

To determine optimum concentration and measurement time of MerR-based cadmium sensor, cells were induced with 0-to-100 μM of cadmium ions. Results showed increased response in time with increasing cadmium concentration (Figure 4.13A). Next, to show robustness of the MerR-based cadmium sensor, cells were induced in HMM minimal media for 14 h, and similar results were observed (Figure 4.13B).

4.5. Discussion

Bacterial whole-cell biosensors are useful tools to detect various compounds (i.e., toxic compounds or disease biomarkers) in environmental as well as biomedical samples [165]. Especially for environmental monitoring studies, several types of biosensor strategies have been developed. These biosensors are mainly categorized as non-specific [162], semi-specific [73], and specific biosensors [73, 163, 164]. In this study, we have made further engineering on our previously constructed semi-specific biosensor based on heat shock response (HSR) which is able to detect toxicity of nanomaterials in a very short time (see Chapter 3 for details), and have combined gold and cadmium specific transcription factors to investigate the source of the reported toxicity. Both gold and cadmium are investigated to be used in biomedical applications such as drug delivery or molecular imaging using nanoparticles. Hence, any release from surface of

nanoparticles may cause toxicity to cells which should be detecting and reported accordingly [59].

Microorganisms have developed well-controlled machinery against non-specific heavy metal intake so that they can pump out the toxic levels of ions [165]. Gold resistance in *Salmonella* is controlled by *gol* locus and it is very specific to gold. A functional GolS transcription factor is required for gold resistance which activates the gene expression in *gol* locus; a transporter (GolT), a metal-binding polypeptide (GolB), and GolS itself [169]. Because of its specificity to gold, we have chosen GolS and its cognitive promoter PgolB to construct a gold detecting circuit. Additionally, to make the circuit well-controlled, we integrated a DNA-arraging serine recombinase, Bxb1, to the sensor. Serine recombinases are utilized by bacteriophages to incorporate their genomic DNA into the host genome using specific attachment sites on bacteria (attB) and phage (attP) [185]. Mimicking this natural event, several studies have demonstrated that recombinases are useful tools in synthetic biology to make complex computation on DNA such as memory circuits or state machines [186, 187].

The working principle of recombinase-based gold detection circuit has been summarized in Figure 4.14: In the absence of gold, HspR constantly represses the stress promoter, PdnaK-IR3-IR3 so that neither Bxb1 nor GolS are expressed which control reporter expression (Figure 4.14A). However, presence of gold creates stress activating HSR, and HspR releases from the promoter so that Bxb1 and GolS expression are initiated. At first step, Bxb1 recombines the inverted gold sensitive promoter, PgolB. Secondly, GolS-gold complex comes in play to initiate the reporter expression (Figure 4.14B).

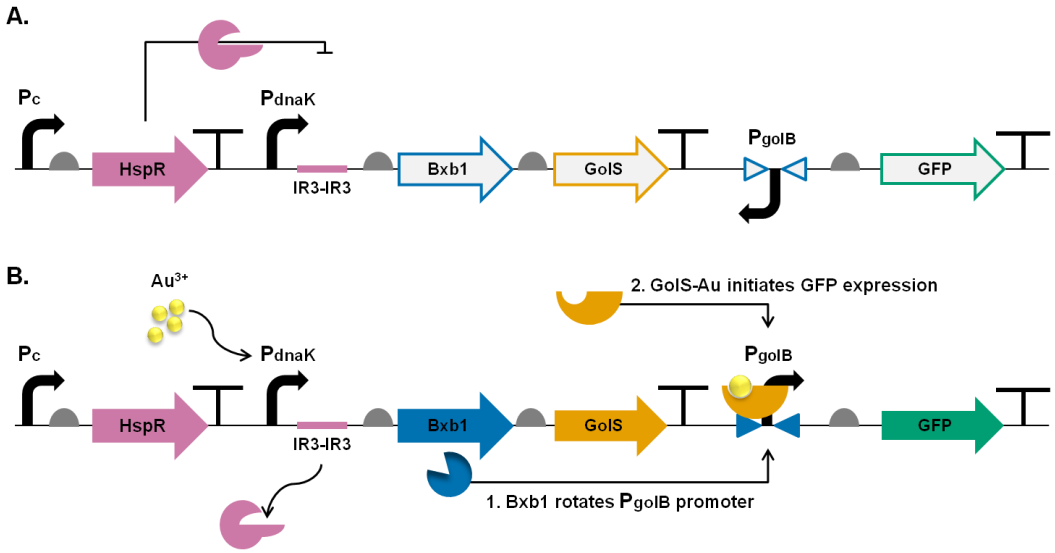

Figure 4.14: Working principle of recombinase-based gold detection circuit. A. At normal growth conditions, constitutively expressed HspR recognizes IR3-IR3 sequences on promoter blocking the gene expression. B. Upon gold treatment, HspR is released from the stress promoter initiating Bxb1 and GolS expression. First, Bxb1 converts gold-specific promoter; then, GolS-gold complex activates reporter expression.

To test the recombinase-based gold detection circuit, we diluted overnight cell cultures in fresh LB media supplemented with proper antibiotics and gold ions at varying concentrations. After 18 hours of incubation at 30°C, we measured the GFP response (Figure 4.9). Results showed that limit of detection (LOD) of the sensor was quite low (5 µM) and the reponse increased gradually with the increased gold concentration. We decided to use 50 µM of gold, which gave high signal (~6-fold) and was not detrimental to cells, for further assays. Next, we tested the specificity of the sensor with 50 µM of different heavy metals (Figure

4.10). Similarly, we diluted overnight cell cultures in fresh LB media supplemented with proper antibiotics and 50 μM of heavy metal ions. After 18 hours of incubation at 30°C, we measured the GFP response of each metal. As we expected, sensor showed response only to gold but not to others. Although GolS belongs to MerR family, group of heavy metal transcription factors, and shows similarity to copper responsive transcription factor of *E. coli* (CueR) which responses other metals such as silver and gold besides copper, GolS is very specific to gold [169, 188, 189]. Finally, we have characterized the sensor in different media to show the robustness of the sensor and utilized MOPS minimal media used in bacterial whole cell biosensor studies. We both controlled the expression time and responsive gold concentration, and induced the sensor with lower and higher concentrations of gold ions (10 and 50 μM, respectively). Results showed the same characteristics with studies in LB and could detect gold at lower concentrations and indicated higher response to high concentrations of gold (Figure 4.11). This result promises that we would be able to detect the presence of gold ions in various samples from rich to low medium composition.

Next step was to expand heavy metal sensors to detect other ions. Hence, we have chosen cadmium as the second heavy metal. Cadmium is one of the most toxic compounds to microorganisms; thereby, they have developed resistance to cadmium in order to pump out ions in cells. Among various microorganisms, *Pseudomonas putida* resists to cadmium with an efflux pump and a transcription factor; CadA and CadR, respectively [190]. Several biosensors have been developed using cadmium specific transcription factors from various microorganisms and adaped to *E. coli* [191, 192]. In our recombinase-based

cadmium detection circuit, we followed the same approach that we developed for gold detection; instead, we used CadR as transcription factor and its cognitive promoter, PcadA. Similar to the recombinase-based gold detecting circuit, HspR constantly represses the stress promoter, PdnaK-IR3-IR3, in the absence of cadmium, so that neither Bxb1 nor CadR are expressed which control reporter expression (Figure 4.15A). However, presence of cadmium creates stress activating HSR, and HspR releases from the promoter so that Bxb1 and CadR expression are initiated. At first step, Bxb1 recombines the inverted cadmium sensitive promoter, PcadA. Secondly, CadR-cadmium complex comes in play to initiate the reporter expression (Figure 4.15B).

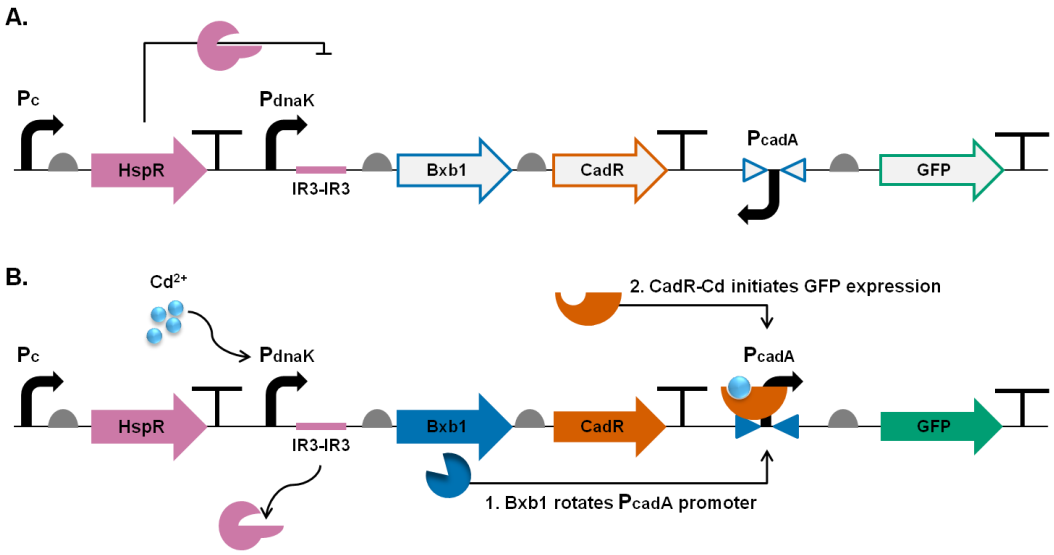

Figure 4.15: Working principle of recombinase-based cadmium detection circuit. A. At normal growth conditions, constitutively expressed HspR recognizes IR3-IR3 sequences on promoter blocking the gene expression. B. Upon cadmium treatment, HspR is released from the stress promoter initiating Bxb1 and CadR expression. First, Bxb1 converts cadmium-specific promoter; then, CadR-cadmium complex activates reporter expression.

To test the recombinase-based cadmium detection circuit, we diluted overnight cell cultures in fresh MOPS minimal media supplemented with proper antibiotics and cadmium ions at varying concentrations. After 18 hours of incubation at 30°C, we measured the GFP response (Figure 4.12). Results showed that although limit of detection (LOD) of the sensor was quite low (~10 μM) and the highest reponse to elevated cadmium concentration was lower compared to gold detection circuit (~6-fold for 50 μM of gold while ~3-fold for 50 μM of cadmium). Additionally, a decrease after 50 μM of cadmium was observed indicating toxic levels on cells. It could be concluded that cadmium is very toxic [193] cells causing cell death or growth inhibition at higher concentrations. When we consider all of these circumstances, another cadmium specific transcription factor would be useful to increase the dynamic range as well as specificity to gene circuit. Thus, we decided to use MerR-mutated transcription factor [168] and characterized its dynamics before integrating it to the HSR and recombinase-based circuits.

MerR is one of the first discovered metal-binding protein shows mercury resistance in *Pseudomonas aeruginosa* [194]. In the absence of mercury, MerR inactivates RNA polymerase while transcription is initiated in the presence of mercury. Although it is very specific to mercury, it shows low affinity to cadmium. Hakkila *et al.* applied a series of mutations on MerR and formed a library until they obtained a cadmium specific MerR mutant [168]. We utilized MerR (mutated) to check its activity first reproducing the same results that Hakkila *et al.* showed (Figure 4.16). In the constructed sensor, MerR (mutated) was constitutively expressed blocking the reporter expression from PcadA

promoter (Figure 4.16A). Upon cadmium treatment, MerR (mutated) released the promoter so that reporter expression started (Figure 4.16B). We first tested the sensor with varying concentrations of cadmium ions in MOPS minimal media (Figure 4.13A). Results indicated that sensor showed higher response to increased concentrations of cadmium (~4-fold). Finally, we have characterized the sensor in different minimal media (HMM media) defined for heavy metal detection studies to show the robustness of the sensor. We selected medium and high concentrations of cadmium (25 and 50 μM, respectively) to induce the sensor (Figure 4.13B). Similar results were observed.

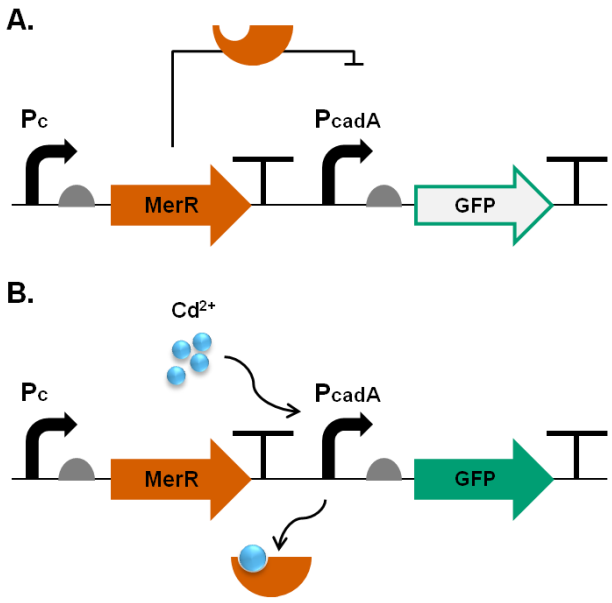

Figure 4.16: Working principle of MerR-based cadmium detection circuit. A. At normal growth conditions, constitutively expressed MerR blocks reporter expression. B. Upon cadmium treatment, MerR is released from the cadmium-specific promoter initiating reporter expression.

When we compared CadR and MerR (mutated) based sensing system, although they showed similar fold-induction with each other, MerR-based system is more promising because of its proposed specificity [168]. Thus, further optimizations and complex circuit designs will be constructed with MerR-based cadmium regulation.

4.6. Conclusion

As a concusion, previously characterized semi-specific [73] toxicity biosensor (Chapter 3) has been engineered with specific biosensor properties [73] to detect the source or stressor. To begin with, a well-characterized gold specific transcription factor, GolS [169], and two different cadmium specific transcription factors, CadR [190] and MerR (mutated) [168], have chosen since both gold NPs and cadmium-based QDs are very promising in nanotechnological applications in biomedicine [122]. Hence, early detection of the toxic part, especially for complex NPs such as QDs, is very critical to minimize the damage which might be caused after human exposure to NPs.

Here we demonstrate that our engineered stress sensors are able to sense the stressor together with its source. Although circuits require some more characterization and only have been developed for gold and cadmium, a multiplex cellular consortium is possible which responds multiple heavy metal transcription factors, and each heavy metal could be reported with a certain reporter.

CHAPTER 5

A Eukaryotic Cell-Based Biosensor to Monitor Nanomaterial-triggered Toxicity

5.1. Objective of the Study

In the last decades, nanomaterials have been used in a wide range of consumer and medical products increasing the safety concerns on environment and human health. Although some whole-cell biosensors have been developed using microorganisms to evaluate toxicity of nanomaterials and heavy metals, still a very limited number of mammalian cells have been engineered as living sensors for nanomaterial toxicity detection. Here we followed three approaches to construct a living sensor based on HSR in cells: usage of (i) HSP70 promoter and (ii) small HSP (sHSP) promoter, and (iii) engineering of eukaryotic HSR with bacterial repression-based mechanism. In all cases, expression of a reporter gene (*egfp*) was controlled with the HSP promoters and response was monitored upon stress exposure.

5.2. Introduction

Nanomaterial exposure may cause multiple changes in cells (For details see Chapter 1). To investigate effects of nanomaterials, various *in vivo* and *in vitro* tests have been developed to understand cell faith. Developed assays seek changes

in cells over nanomaterial exposure and assess reactive oxygen species (ROS) generation, viability, stress level, morphological changes, and cellular uptake mechanisms. Besides, cell culture assays with nanomaterials mainly depend on cultured cells (commercially available genetically altered or tissue-harvested primary cells) incubated with different types at different concentrations of nanomaterials with varying exposing time. However, response of different cell lines to different nanomaterials also varies which make difficult to reach a general conclusion. Additionally, these tests are expensive, time-consuming, and require an expert to conduct the tests [146]. Hence, live cell-based biosensors are promising tools to report toxicity with sensitive and fast response at lower costs [195]. Similar to conventional sensor principles, whole cell biosensors are composed of three modules: an input module which could be a receptor in cell membrane or cytoplasm, a processing unit which is a genetically engineered circuit responding the incoming signal, and an output module which transfers the incoming signal to a measurable output [196]. To date, multiple prokaryotic and eukaryotic cells have been utilized to evaluate environmental hazard such as bacteria [197], yeast [198], or algae [199-201]. Additionally, mammalian cell-based sensors have been introduced to evaluate safety of chemicals [202-206]. Yet, only a few studies have included mammalian whole-cell based approaches to monitor toxicity of nanomaterials [195, 207, 208]. It has been shown that nanomaterials cause protein denaturation or aggregation in mammalian cells activating heat shock proteins (HSPs) [195], inflammation activating NF-κB pathway [208], activation of DNA damage response [195], or increase in reactive oxygen species (ROS) [202]. Cytotoxicity of stressors on mammalian cells can be

detected with increased HSP expression. Especially, multiple studies showed that HSP70 expression increases upon many cytotoxic stimuli [195] which may also cause oxidative stress in cells further activating HSR [202]. Also, utilizing promoters of HSP70 allow reporting the cytotoxicity with a suitable reporter [202, 209-211].

5.3. Materials and Methods

5.3.1.Media and Strains

E. coli DH5α (New England Biolabs, Inc.) was used for all cloning steps and grown in LB medium (1% (w/v) tryptone, 0.5% (w/v) yeast extract, 0.5% (w/v) NaCl) with proper antibiotics at 37°C and 180 rpm shake in Erlenmeyer flasks. Human embryonic kidney cell line (HEK293T, ATCC®) was used as a model living sensor and grown in Dulbecco's Modified Eagle's Medium (DMEM) (Lonza) supplemented with heat inactivated 10% fetal bovine serum (FBS, Gibco), 1 g/L glucose, 2mM L-glutamine, and antibiotics (5000 U/ml penicillin and 100 mg/ml streptomycin) in humidified incubator at 37°C with 5% CO_2 (Binder).

5.3.2.Plasmid Construction

To construct Phsp70-pcDNA3-GFP and ABC-pcDNA3-GFP vectors, HSP70 promoter (Phsp70) was isolated from the genomic DNA of HEK293T cell line using primers shown in Table B1 while αB-crystallin (ABC) promoter was synthesized by Twist Bioscience Company. For plasmid backbone, pcDNA3-GFP vector (Addgene #13031) was digested with BamHI-MluI restriction enzymes

(New England Biolabs, Inc.). Reaction conditions were described in Appendix E. Both parts were assembled with Gibson Assembly reaction described by Gibson *et al.* [137]. To construct CMV HspR-His pcDNA3 and CMV His-HspR-NLS pcDNA3 vectors, HspR was amplified by primers stated in Table B.1 and pcDNA3-GFP vector (Addgene #13031) was digested with BamHI-XbaI restriction enzymes (New England Biolabs, Inc.) for plasmid backbone. Parts of CMV HspR-His pcDNA3 vector were assembled with Gibson Assembly while CMV His-HspR-NLS pcDNA3 vector was constructed with T4 ligation after PCR product of HspR was digested with the same enzyme pair used for backbone digestion. To construct SV40 GFP MeCP2 vector, SV40-GFP-polyA part was amplified from formerly constructed SV40 GFP pGL3 vector by primers stated in Table B.1, and PCR product was digested with EcoRI-MluI enzyme pair for ligation. For backbone, dCas9-KRAB-MeCP2 (Addgene #110821) vector was digested with the same enzyme pair. Both parts were assembled with T4 ligation. To construct SV40-IR3 GFP MeCP2 vector, IR3 repeat was added to SV40 promoter with the primers stated in Table B.1 and GFP-polyA part was also amplified by PCR. For backbone, dCas9-KRAB-MeCP2 (Addgene #110821) vector was digested with EcoRI-SalI enzyme pair. All parts were assembled with Gibson Assembly reaction. To construct SV40-IR3-IR3 GFP MeCP2 vector, SV40-IR3 GFP MeCP2 vector was digested with EcoRI-SalI and EcoRI-XhoI enzyme pairs. From the digested parts, longer part from EcoRI-SalI digestion and shorter part from EcoRI-XhoI digestion was assembled with T4 ligation. Q5 Hot Start High-Fidelity DNA Polymerase (New England Biolabs, Inc.) was used for all PCR reactions (Reaction conditions were described in Appendix E).

NucleoSpin Gel and PCR Clean-up kit (Macherey-Nagel) was used according to the manufacturer's instructors to purify digested DNA samples or PCR products from 1 to 1.8% Agarose gels stained with SYBR Safe DNA Gel Stain (Thermo Fisher Scientific). Plasmid construction was made via ligation with DNA T4 ligase (New England Biolabs, Inc.) or via Gibson Assembly method (Both reaction conditions were described in Appendix E). Constructed genetic circuits were sequence verified by Sanger Sequencing (GENEWIZ). All genetic part sequences used this chapter was introduced in Table A1, and all constructed vector maps were indicated in Appendix C with verified sequencing results in Appendix D.

5.3.3.Chemical Competent Cell Preparation and Transformation of DNA in Cells

Overnight cultures of *E. coli* DH5α were prepared from frozen glycerol stocks and incubated for 16 h with the same culturing conditions mentioned previously. 1% of inoculums from overnight cultures were used to start fresh culture for competent cell preparation. Culture was incubated at 37°C and 180 rpm shake in Erlenmeyer flasks until OD_{600} reached 0.2-to-0.5. Following, culture was cooled in ice for 10 min and cells were collected by centrifugation at 1000 ×g for 10 min at +4°C. After centrifugation, supernatant was discarded and cell pellet was resuspended in 10% (v/v) of TSS Buffer (10% (w/v) PEG-8000, 5% (v/v) DMSO, 50 mM $MgCl_2$ pH 6.5 in LB). For each aliquot, 100 µl of cultures were placed in each microcentrifuge tubes and stored at -80°C.

Chemical competent cells were thawed on ice for 30 min before transformation. For transformation, whole ligation product, Gibson Assembly reaction product, or 100 ng of intact plasmid DNA was introduced to thawed cells and incubated on ice for 20-30 min. Following, cells were shocked by heat treatment at 42°C for 30 sec. After the heat shock, cells were cold shocked for 2 min on ice. Then, 250-1000 µl of LB was added onto the cells and incubated at 37°C and 180 rpm shake for 45-60 min. At the end of the incubation, cells were collected at 1000 ×g for 10 min and the supernatant was discarded. The collected cells were resuspended in 50 µl of LB and spread onto LB-agar supplemented with proper antibiotics.

5.3.4.Sequencing Alignments with Geneious Software

All plasmid maps were constructed on an online vector tool; Benchling. Following, all plasmid maps were exported as .gb files and imported in Geneious software together with the sequencing results of plasmid maps as .abi files. In order to align plasmid map and its sequencing data, both sequences were selected and pairwise alignment performed. The sequencing results for all vectors were indicated in Appendix D.

5.3.5.Transfection

24 h prior to transfection, HEK293T cells were seeded in 96-well or 24-well plates at concentrations of 2×10^4 cells/well and 5×10^4 cells/well, respectively. After 60-70% of confluency, cells were transfected with either polyetylenimine (PEI) (Polysciences) or lipofectamine 3000 (invitrogen). For PEI transfection protocol, 500 ng of plasmid DNA and 1500 ng PEI were mixed in 100 µl of

serum-free DMEM and mixed gently. After incubation at RT for 20 min, the mixture was applied on cells. For lipofectamine 3000 transfection, 100-500 ng of plasmid DNA and supplied lipofectamine reagents was incubated in serum-free DMEM media at RT for 10-15 min according to manufacturer's instruction. After incubation, the mixture was applied on cells. After transfection, cells were transferred in humidified incubator (37°C, 5% CO_2) for 24 hours.

5.3.6.Heat Shock Experiments and Toxicity Assay

After 24 hours of transfection, cells were transferred in humidified incubator at 42°C, 5% CO_2 for 1 or 2 h for heat shock experiments. At the end of the heat shock, cells were returned back to the initial incubator (37°C, 5% CO_2) for 6 hours of recovery. For toxicity experiments, after 24 hours of transfection, cadmium acetate solution (Concentrations were indicated in figures.) were added on cells and incubated for 6 hours in humidified incubator (37°C, 5% CO_2). For all cases, untreated control samples were used. At the end of the induction period, cells were analyzed with microplate reader (SpectraMax M5, Molecular Devices).

5.3.7.Fluorescence Measurement and Data Analysis

All fluorescence measurement studies were conducted via microplate reader (SpectraMax M5, Molecular Devices). Excitation and emission wavelengths for eGFP were set as 485 and 538 nm, respectively. Each measurement was conducted in Corning 24-well clear flat bottom polystyrene plates. Before measurement, cell culture media was discarded carefully and cells were washed with 1×PBS (137 mM NaCl, 2.7 mM KCl, 4.3 mM Na_2HPO_4, 1.47 mM KH_2PO_4,

pH 7.4). After washing, 1 mL of 1×PBS was added on each well. For 0-to-1 signal normalization, each value was subtracted from minimum value and divided by difference between maximum and minimum values in related groups.

5.3.8.HspR Expression and Western Blot Analysis

After 24 h of transfection of CMV HspR-His pcDNA3 vector in HEK293T cell line, cells were washed, resuspenden in 1×PBS (137 mM NaCl, 2.7 mM KCl, 4.3 mM Na_2HPO_4, 1.47 mM KH_2PO_4, pH 7.4), and collected (500×g, 5 min). Cells were lysed with 100 µL of Mammalian Protein Extraction Reagent (M-PER™, Thermo Fisher Scientific). After lysis, 20 µL from protein fraction was load on 15% SDS-PAGE gel prepared with BioRad SDS Gel casting system. 20 µL from protein samples were run on gel by using 6×Loading Dye (375 mM Tris-HCl (pH 6.8), 9% (w/v) SDS, 50% (v/v) Glycerol, 0.03% (v/v) Bromophenol blue). All samples were boiled at 95°C for 5 min prior to run on gel. 1×SDS Running Buffer (25 mM Tris-HCl, 200 mM Glycine, 0.1% (w/v) SDS) was used during the run. Further, gel was transferred to polyvinylidene difluoride (PVDF) membranes (Thermo Fisher Scientific). Membrane was blocked with 5% freeze-dried nonfat milk in TBS-T for 1 h at room temperature, and then incubated at +4°C overnight with primary antibody (His-Tag mouse McAb) (Proteintech Europe) diluted at 1:10000 in blocking solution. Afterward, membrane was washed with TBS-T and incubated with HRP conjugated goat antimouse secondary antibody (abcam) diluted at 1:10000 in blocking solution for 1 h and visualized by enhanced chemiluminescence (Bio-Rad) according to the manufacturer's protocol on ChemiDoc Imaging System with Image Lab Software − BioRad.

5.3.9.Microscopy

All imaging was conducted with Inverted Fluorescence Microscope (Zeiss) and representative images were provided in Appendix F.

5.3.10. Statistical Analysis

All data were expressed as mean ± standard error mean. Depending on the groups of interest, either one-way analysis of variance (ANOVA) or two-way ANOVA with Dunnett's/Tukey's/Sidak's multiple comparison tests (GraphPad Prism v6) were used to compare groups.

5.4. Results

5.4.1.Cloning of Eukaryotic Toxicity Sensors

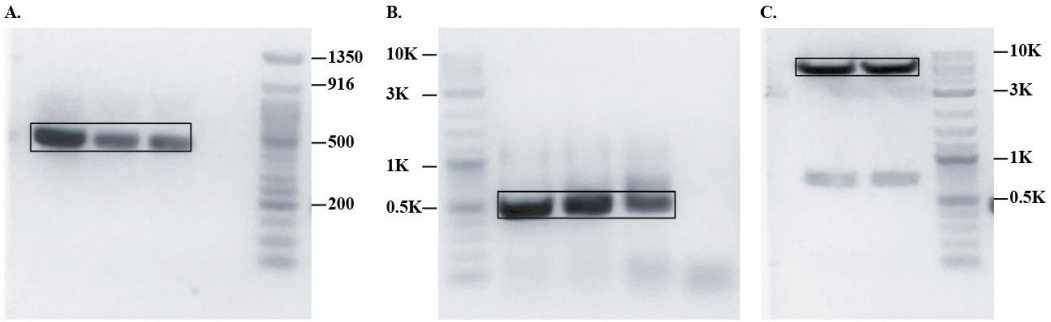

Figure 5.1: Construction of Phsp70-GFP-pcDNA3 vector. A. Phsp70 was isolated from HEK293T genome and observed at 430 bp on the gel. B. Homology sequences added on Phsp70 with Gibson Assembly primers and PCR products were observed at 492 bp on the gel. C. Digested pcDNA3-GFP vector with BamHI-MluI enzyme pairs. Linear vector and CMV promoter piece were observed at 5400 bp and 680 bp, respectively. 50 bp DNA Ladder (NEB) and 1

kb+ DNA Ladder (NEB) were used as DNA markers for small and large fragments, respectively.

For cloning of Phsp70-pcDNA3-GFP vector, HSP70 promoter (Phsp70) was isolated from the genomic DNA of HEK293T cell line using primers shown in Table B.1 PCR products were run on 1.8% Agarose gel (Figure 5.1A) and isolated using MN-gel extraction kit according to manufacturer's instructions. The isolated PCR product was amplified with Gibson Assembly primers (Table B.1) to add homology regions of backbone (Figure 5.1B). For backbone, pcDNA3-GFP vector was digested with BamHI-MluI restriction enzymes and run on 1% Agarose gel (Figure 5.1C). Obtained pieces were assembled with Gibson Assembly reaction. After Gibson Assembly, selected colonies were sent for sequencing (Appendix D).

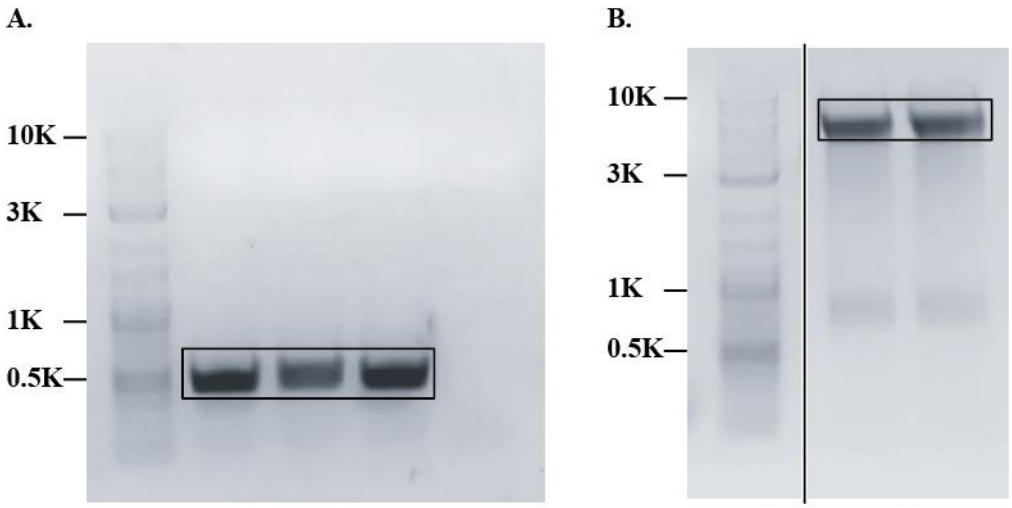

Figure 5.2: Construction of CMV HspR-His pcDNA3 vector. A. HspR was amplified with Gibson Assembly primers to add homology regions of backbone and observed at 468 bp on the gel. B. Digested pcDNA3-GFP vector with BamHI-

XbaI enzyme pairs. Linear vector and GFP were observed at 5370 bp and 730 bp, respectively. 1 kb+ DNA Ladder (NEB) was used as DNA marker.

For cloning of ABC-pcDNA3-GFP vector, synthesized fragment of αB-crystallin (ABC) promoter was assembled with BamHI-MluI digested pcDNA3-GFP backbone (Figure 5.1C). After Gibson Assembly, selected colonies were sent for sequencing (Appendix D).

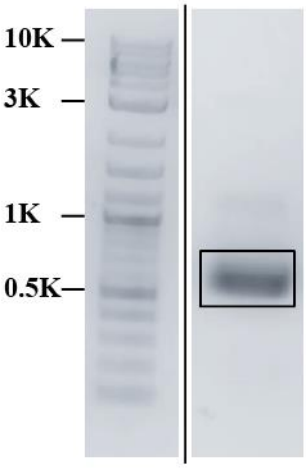

Figure 5.3: Construction of CMV His-HspR-NLS pcDNA3 vector. HspR was amplified with primers and observed at 484 bp on the gel. 1 kb+ DNA Ladder (NEB) was used as DNA marker.

For cloning of CMV HspR-His pcDNA3 vector, HspR was amplified by primers stated in Table B.1, run on 1% Agarose gel (Figure 5.2A), and isolated using MN-gel extraction kit according to manufacturer's instructions. For backbone, pcDNA3-GFP vector was digested with BamHI-XbaI restriction enzymes and run

on 1% Agarose gel (Figure 5.2B). Obtained pieces were assembled with Gibson Assembly reaction. After Gibson Assembly, selected colonies were sent for sequencing (Appendix D).

For cloning of CMV His-HspR-NLS pcDNA3 vector, HspR was amplified by primers stated in Table B.1, run on 1% Agarose gel (Figure 5.3), and isolated using MN-gel extraction kit according to manufacturer's instructions. After gel extraction, PCR product was digested with BamHI-XbaI enzyme pair similar to backbone (Figure 5.2B). Digested DNA fragments were assembled with T4 ligation reaction. After assembly, selected colonies were sent for sequencing (Appendix D).

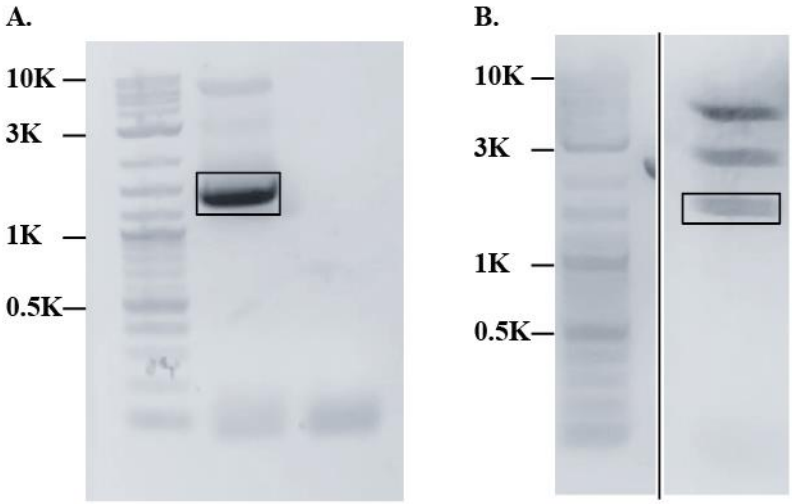

Figure 5.4: Construction of SV40 GFP MeCP2 vector. A. SV40-GFP-polyA fragment was amplified and observed at 1410 bp on the gel. B. Digested dCas9 KRAB MeCP2 vector with EcoRI-MluI enzyme pairs. Linear vector was observed at 1496 bp, and other DNA pieces were at 4527 bp and 2438 bp, respectively. 1 kb+ DNA Ladder (NEB) was used as DNA marker.

For cloning of SV40 GFP MeCP2 vector, SV40-GFP-polyA part was amplified from formerly constructed SV40 GFP pGL3 vector by primers stated in Table B.1, run on 1% Agarose gel (Figure 5.4A), and isolated using MN-gel extraction kit according to manufacturer's instructions. After gel extraction, PCR product was digested with EcoRI-MluI enzyme pair similar to backbone (Figure 5.4B). Digested DNA fragments were assembled with T4 ligation reaction. After assembly, selected colonies were sent for sequencing (Appendix D).

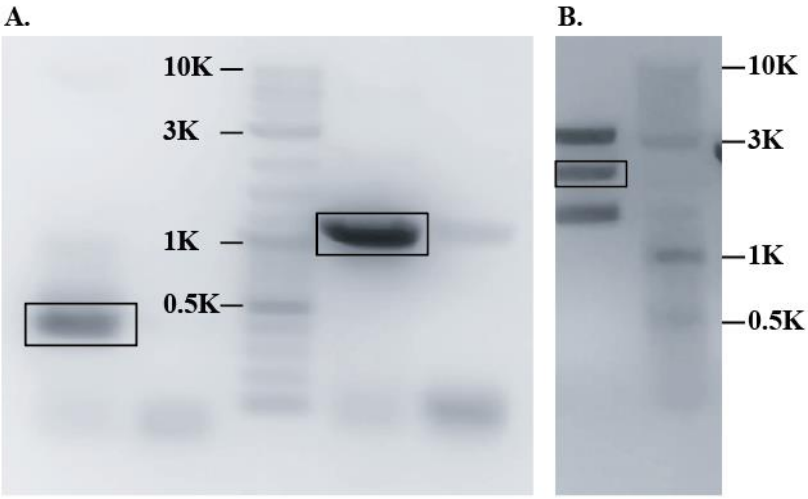

Figure 5.5: Construction of SV40-IR3 GFP MeCP2 vector. A. SV40-IR3 (left) and GFP-polyA (right) fragments were amplified and observed on the gel at 392 bp and 1089 bp, respectively. B. Digested dCas9 KRAB MeCP2 vector with EcoRI-SalI enzyme pairs. Linear vector was observed at 2200 bp, and other DNA pieces were at 3300 bp and 1500 bp, respectively. 1 kb+ DNA Ladder (NEB) was used as DNA marker.

For cloning of SV40-IR3 GFP MeCP2 vector, SV40-IR3 and GFP-polyA parts were amplified by primers stated in Table B.1, run on 1% Agarose gel (Figure

5.5A-left for SV40-IR3 fragment and Figure 5.5A-right for GFP-polyA fragment), and isolated using MN-gel extraction kit according to manufacturer's instructions. For backbone, dCas9-KRAB-MeCP2 vector was digested with EcoRI-SalI restriction enzymes and run on 1% Agarose gel (Figure 5.5B). Obtained pieces were assembled with Gibson Assembly reaction. After Gibson Assembly, selected colonies were sent for sequencing (Appendix D).

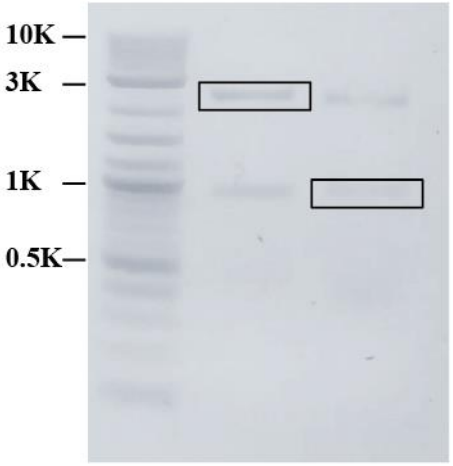

Figure 5.6: Construction of SV40-IR3-IR3 GFP MeCP2 vector. EcoRI-SalI digested SV40-IR3 GFP MeCP2 vector fragments were observed on the gel at 1019 bp and 2578 bp (2nd well), and EcoRI-XhoI digested SV40-IR3 GFP MeCP2 vector fragments were observed on the gel at 1052 bp and 2545 bp (3rd well). 1 kb+ DNA Ladder (NEB) was used as DNA marker.

For cloning of SV40-IR3-IR3 GFP MeCP2 vector, SV40-IR3 GFP MeCP2 vector was digested with EcoRI-SalI and EcoRI-XhoI enzyme pairs, run on 1% Agarose gel (Figure 5.6), and isolated using MN-gel extraction kit according to manufacturer's instructions. From the digested parts, longer part from EcoRI-SalI

digestion (2nd well of Figure 5.6), and shorter part from EcoRI-XhoI digestion (3rd well of Figure 5.6) was assembled with T4 ligation. After assembly, selected colonies were sent for sequencing (Appendix D).

5.4.2. Characterization of Eukaryotic Toxicity Sensors Constructed with Native HSP Promoters

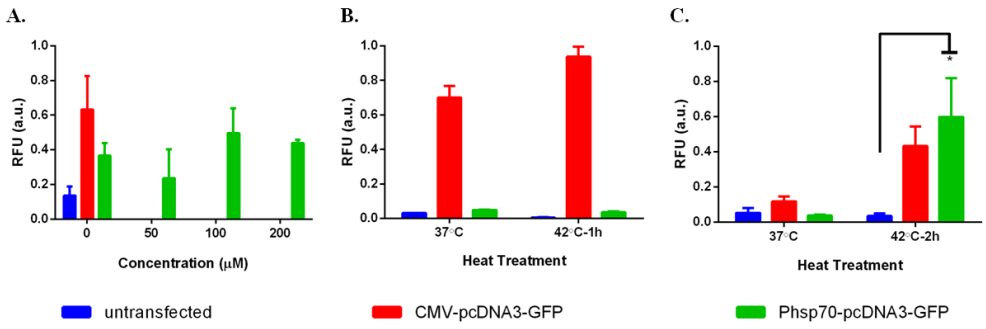

Figure 5.7: Fluorescent signal results of cadmium and heat treated eukaryotic Phsp70 pcDNA3-GFP sensor. A. The sensor was induced with varying concentrations of cadmium ions for 6 hours. B. The sensor was induced at 42°C for 1 hour following 6 hours of recovery at 37°C. C. The sensor was induced at 42°C for 2 hours following 6 hours of recovery at 37°C. Experiments were performed as three biological replicates. Fluorescence intensity of each group was compared with each other and normalized according to formula stated in Materials and Methods section. $p \leq 0.05$ was represented with one star. Statistically non-significant results had no stars.

First constructed eukaryotic HSR circuit, Phsp70 pcDNA3-GFP, was tested with cadmium ions and heat treatment. For cadmium ion induction, cells (transfected

and untransfected groups) were subjected to varying concentrations of cadmium ions for 6 hours. After induction, cell media was replaced with 1×PBS and measured with microplate reader. No significant signal was observed upon cadmium treatment (Figure 5.7A). For heat induction, cells were incubated at 42°C, 5% CO_2 for 1 and 2 h. At the end of the heat shock, cells were returned back to the initial incubator (37°C, 5% CO_2) for 6 hours of recovery. For 1 hours of induction did not show any significant signal increase (Figure 5.7B), while 2 hours of heat treatment showed a slight signal increase at the sensor (Figure 5.7C).

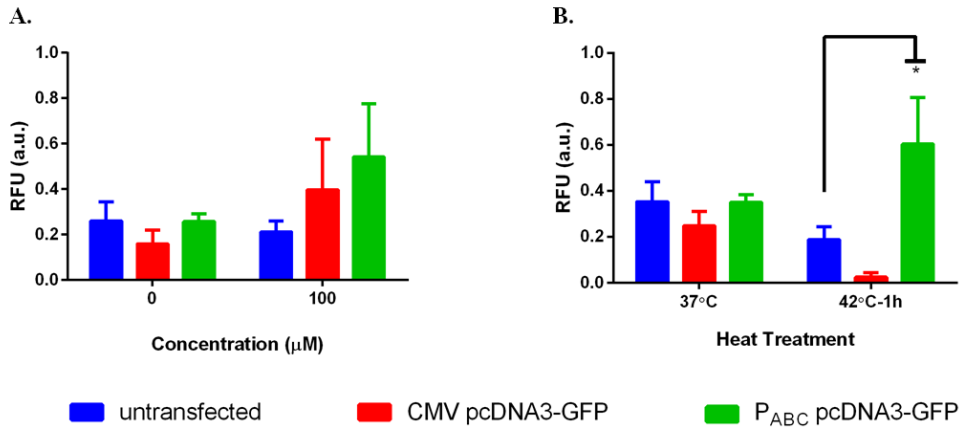

Figure 5.8: Fluorescent signal results of cadmium and heat treated eukaryotic P_{ABC} pcDNA3-GFP sensor. A. The sensor was induced with 100 μM of cadmium ions for 6 hours. B. The sensor was induced at 42°C for 1 hour following 6 hours of recovery at 37°C. Experiments were performed as three biological replicates. Fluorescence intensity of each group was compared with each other and normalized according to formula stated in Materials and Methods section. $p \leq 0.05$ was represented with one star. Statistically non-significant results had no stars.

Eukaryotic HSR circuit with sHSP promoter, P_{ABC} pcDNA3-GFP, was tested with cadmium ions and heat treatment. For cadmium ion induction, cells (transfected and untransfected groups) were subjected to 100 µM of cadmium ions for 6 hours. After induction, cell media was replaced with 1×PBS and measured with microplate reader. No significant signal was observed upon cadmium treatment (Figure 5.8A). For heat induction, cells were incubated at 42°C, 5% CO_2 for 1 h. At the end of the heat shock, cells were returned back to the initial incubator (37°C, 5% CO_2) for 6 hours of recovery. After heat treatment, the sensor cells showed increase in signal (Figure 5.8B).

5.4.3.Expression of HspR in Eukaryotes

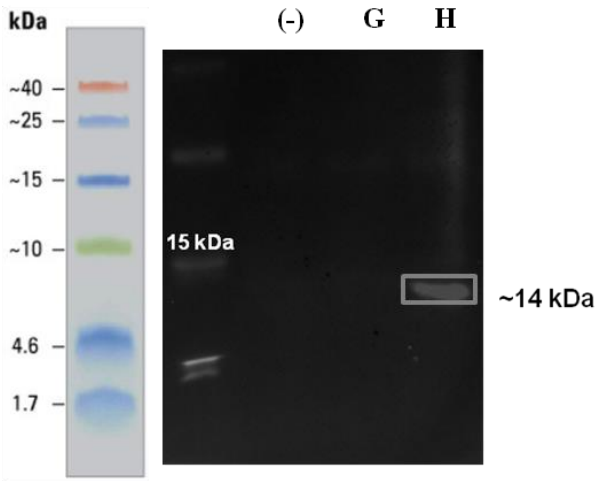

Figure 5.9: Western Blot results for recombinant HspR expression in HEK293T cell line. Untransfected cells (annotated as "(-)" on the gel), GFP expressing positive control vector (annotated as "(G)" on the gel), and HspR expressing vector (annotated as "(H)" on the gel) were run on the gel. HspR expression was observed at ~14 kDa. Spectra™ Multicolor Low Range Protein Ladder (Thermo

Fisher Scientific) was used as reference. Image generated by Chemidoc (BioRad) Imaging System.

Eukaryotic HspR expression vector (CMV HspR-His pcDNA3) was transfected in HEK293T cell line. After 24 hours of transfection, samples were collected and run on 15% SDS-PAGE and transferred to PVDF membrane for Western Blotting. His-tagged HspR was observed at 14 kDa in transfected cells while negative controls were clear on gel (Figure 5.9).

5.4.4.Characterization of Engineered Eukaryotic Toxicity Sensors with IR3 Motif

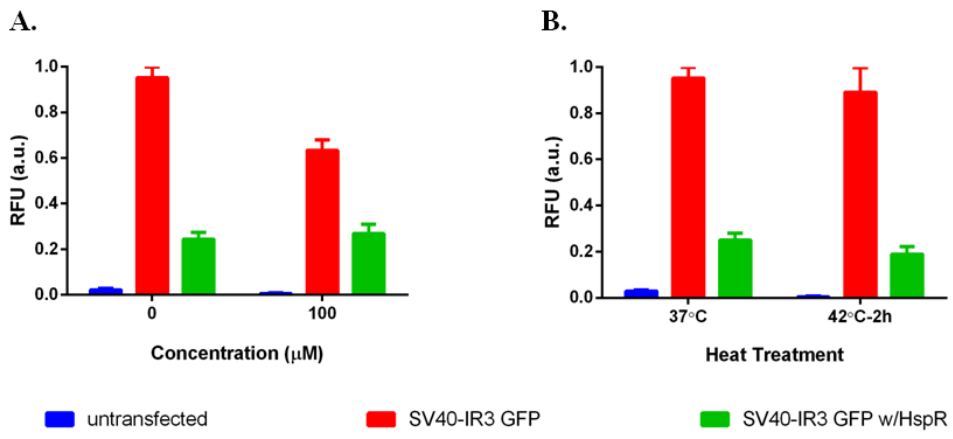

Figure 5.10: Fluorescent signal results of cadmium and heat treated eukaryotic SV40-IR3 GFP sensor co-transfected with HspR. A. The sensor was induced with 100 μM of cadmium ions for 6 hours. B. The sensor was induced at 42°C for 2 hour following 6 hours of recovery at 37°C. Experiments were performed as three biological replicates. Fluorescence intensity of each group was compared with

each other and normalized according to formula stated in Materials and Methods section. Statistically non-significant results had no stars.

After HspR expression was shown in eukaryotic cells, it co-transfected with IR3 motifs in cells. First, GFP expressing vector with single IR3 repeat was characterized with cadmium ion (100 µM, 6 h) and heat treatment (42°C, 2 h). At the end of the induction periods, cell media was replaced with 1×PBS and measured with microplate reader. Significant HspR repression was observed in co-transfected cells while no significant signal increase was noted upon stress exposure (Figure 5.10).

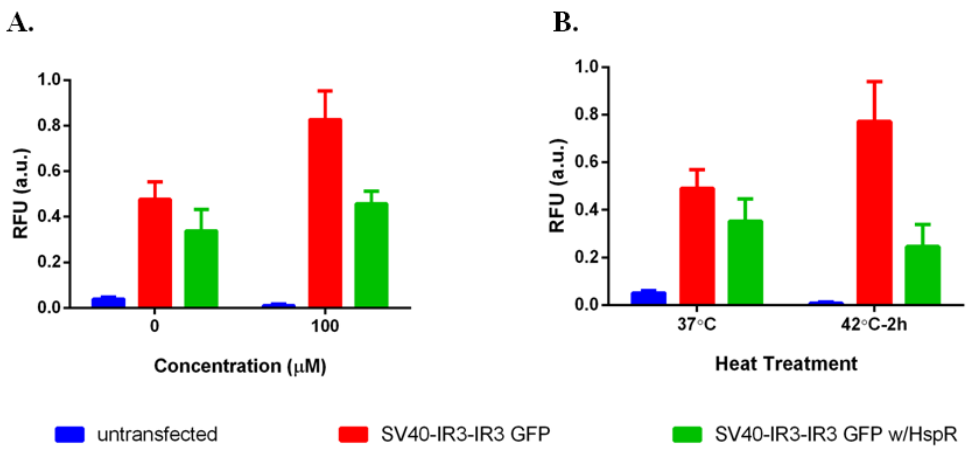

Figure 5.11: Fluorescent signal results of cadmium and heat treated eukaryotic SV40-IR3-IR3 GFP sensor co-transfected with HspR. A. The sensor was induced with 100 µM of cadmium ions for 6 hours. B. The sensor was induced at 42°C for 2 hour following 6 hours of recovery at 37°C. Experiments were performed as three biological replicates. Fluorescence intensity of each group was compared

with each other and normalized according to formula stated in Materials and Methods section. Statistically non-significant results had no stars.

Next, GFP expressing vector with double IR3 repeat was characterized with cadmium ion (100 μM, 6 h) and heat treatment (42°C, 2 h). At the end of the induction periods, cell media was replaced with 1×PBS and measured with microplate reader. Significant HspR repression was observed in co-transfected cells while no significant signal increase was noted upon stress exposure (Figure 5.11).

5.5. Discussion

Nanomaterials activate sets of genes and pathways in eukaryotic cells. Changes in HSP family are one of the pathways to monitor toxicity of nanomaterials. Living cells are efficient tools used as biosensors and nanomaterial-triggered toxicity detection is possible with a suitable engineered circuit integrated in cells [212]. Although several bacterial toxicity biosensors have been characterized so far, only a few studies have developed mammalian whole-cell biosensors for nanomaterial evaluation [195, 207, 208]. Among induced pathways upon nanomaterial exposure, we chose HSR response because of its universal characteristics compared to others. First, we built a circuit with a native Hsp70 promoter (Phsp70) controlling the expression of a reporter gene, *gfp*. Expression profile of Phsp70 has been characterized with multiple studies, previously [202, 209-211]. Thus, we tested the Phsp70-based stress sensor with cadmium ions as well as with elevated heat treatment (internal positive control of HSR). 24 h after HEK293T

cells were seeded on multi-well plates, cells were transfected either with the stress circuit or a constitutively active GFP vector, positive control for transfection. 24 h of post-transfection, cells were treated with various concentrations of cadmium ions and incubated for 6 h (Figure 5.7A). Results showed that Phsp70 promoter was already very active in cells and no significant signal increase was observed upon cadmium exposure. To check the mechanism with an internal control, sensor was treated with heat at 42°C for 1 h (Figure 5.7B) and for 2 h (Figure 5.7C). Results indicated that 1 h of induction did not trigger any reporter expression while 2 h of heat shock showed a slight increase upon induction.

To evaluate different types of promoters in HSP family, a sHSP protein promoter, αB-crystallin promoter (annotated as P_{ABC}), was chosen. Besides main chaperons in HSP family, sHSPs such as αB-crystallin also play role in stress conditions causing protein aggregation [213]. Multiple studies showed that αB-crystallin expression increases especially in certain cell types such as astrocytes upon heat shock as well as heavy metal exposure [214-216]. Hence, we constructed a stress circuit with P_{ABC}, and tested the circuit with cadmium ions and heat. Similar to the previous circuit, GFP expressing P_{ABC} circuit was transfected in HEK293T cells. 24 h of post-transfection, cells were treated with 100 μM of cadmium ions for 6 h (Figure 5.8A). However, although signal increase was observed upon induction, the increase was not as high as expected. Further, the circuit was subjected to heat shock as internal control and induced with 42°C, 1 h heat treatment following 6 h of recovery (Figure 5.8B). Results indicated that 1 h of heat treatment caused a slight increase in reporter expression.

Results showed that sensors with native HSP promoters were not enough for toxicity evaluation and further engineering was required to achieve more controllable circuit system in cells. Thus, we aimed to transfer previously engineered bacterial repression-based HSR mechanism (see Chapter 3 for details) into eukaryotes. To begin with, a recombinant HspR expression vector for eukaryotes was cloned that HspR was expressed through a strong constitutive promoter, CMV promoter. The eukaryotic HspR expression vector was transfected in HEK293T cell line and cells were collected after 24 h of transfection. The recombinant HspR expression in HEK293T cells was observed at 14 kDa in transfected cells (Figure 5.9).

Although several strategies have been developed to engineer eukaryotic promoters via synthetic biology approaches, one way is to select a minimal promoter and decorate up- and downstream of the selected promoter with series of operator sequences which express a reporter gene [212, 217]. Thus, we chose SV40 promoter to engineer with IR3 motifs controlling the GFP expression at the downstream. We integrated the first IR3 motif with PCR to the downstream of the SV40 promoter and co-transfected it with HspR expression vector. 24 h after transfection, cells were treated with cadmium ions (100 μM, 6 h) and heat (42°C, 2 h following 6 hours of recovery at 37°C). Results showed that HspR recognized IR3 motif showing a significant decline in GFP signal (Figure 5.10). Yet, no significant increase in signal was observed upon stress which may be a dissociation problem caused by HspR recognition. Further, SV40 promoter was engineered with double repeats of IR3 motif controlling the GFP expression. The engineered vector was co-transfected with HspR, and tested with cadmium ions

(100 μM, 6 h) and heat (42°C, 2 h following 6 hours of recovery at 37°C). Similar to single IR3 motif engineered circuit, a significant HspR repression was observed in co-transfected cells while no significant signal increase was noted upon stress exposure (Figure 5.11).

5.6. Conclusion

As a conclusion, as in the case of bacterial sensors with native HSP promoters, eukaryotic HSP promoters are not good candidates for sensors requiring tight control mechanism to tune the signal between OFF/ON states. On the other hand, it has been demonstrated that HspR-based system is a promising candidate for nanomaterial-triggered toxicity monitoring studies. Yet, further extensive studies should be required to optimize dissociation and association kinetics of HspR on IR3 motifs. It also should be noted that not every promoters respond the same way to every compounds. Thus, searching for the right response elements (promoters) is very crucial in biosensor design.

Although plenty of bacterial biosensors are developed for toxicity assessment of various compounds, only a few studies have been characterized using HSP70 promoters to track the cytotoxicity [202, 209-211]. Here we proposed a eukaryotic whole-cell biosensor for nanomaterial-triggered toxicity detection to expand the limited pool of mammalian cytotoxicity biosensors. Also, HSR mechanism is a common and conserved phenomenon between all domains of life which allow us to transfer one mechanism from one species to another. Hence, we were able to transfer bacterial HspR-based mechanism into eukaryotes. Still, the response might require some further optimization to tune the reporter expression based on

nanomaterial concentration and type. However, in general, here we propose a general toxicity indicator providing quick information about the fate of the nanomaterials before they applied to the field and on humans.

CHAPTER 6

Conclusion and Future Perspectives

In the past couple of decades, nanotechnology has dominated various fields such as food industry, cosmetics, electronics, and medicine. Thanks to their tunable unique properties (i.e., high surface-to-volume ratio, surface functionalization, small size), nanomaterials promise advantages in different application. Yet, same properties of nanomaterials have drived safety concerns [119-121]. Nanomaterials can penetrate easily through tissues and cell membranes because of their small sizes causing cellular dysfunction and stress [124-130, 132-134]. Although multiple methods for toxicity assessment have been developed, each method has its own drawbacks. In general, many of them require high expertise [68], expensive tools or consumables [68], longer times to report the toxicity [78, 84, 87], special model organisms [84-90]. Additionally, some of them use indirect measure of toxicity [85-88], or give false positive results [69]. Thus, an early detection of nanomaterial triggered toxicity is in demand so that toxic nanomaterials might be engineered with further modifications (i.e., surface functionalization with non-toxic compounds) to become less toxic.

Whole-cell biosensors have a great potential to detect any analyte of interest. To date, many types of whole-cell biosensors have been developed to monitore various types of stressors [70, 72, 107, 110, 112-115]. In this thesis, we proposed whole-cell biosensors to provide early detection of nanomaterial-triggered toxicity

using engineered genetic circuits constructed with synthetic biology tools. In our proposed toxicity circuits, we utilized heat shock response (HSR) which is the general stress indicatior of cells. Besides elevated temperature exposure, HSR mechanism is activated with various stressors such as osmotic shock, starvation, heavy metal exposure [97]. Using this information, we constructed circuits with a reporter, GFP, which is controlled by different heat shock protein (HSP) promoters. At the beginning, native HSP promoters controlling the reporter expression were tested with elevated temperature treatment. However, initial results showed that HSP promoters are already active in cells. Since HSR is cellular defence mechanism, cells need to be prepared in any drastic changes in their environment so that they can fight against stess and set back to their initial un-stressed state [97]. Next, we engineered circuits with native HSP promoters using riboregulator mechanism. As expected, riboregulators help eliminating any unwanted leakage signal [140]. However, we observed obvious lost in sensor signal upon stress treatment. Yet, sensors responded to QD treatment immediately. To gain the lost sensor signal back, a bacterial quorum sensing (QS) mechanism was introduced in the selected sensor. Moreover, an overall increase in signal was observed. Thus, a more tightly-controlled system is required to tune the sensor response.

Native HSR mechanism of *E. coli* is based on special sigma factor; σ^{32}, and it is assumed as activation based transcription control. Since the level of σ^{32} and HSPs are kept at a basal level in cells [35, 36, 101-106], high background signal of cells at normal growth conditions have been observed. To eliminate such scenario, a repression based transcription control mechanism is ideal. Contrary to *E. coli*, *M.*

tuberculosis controls its HSR machinery with a repressor; HspR [155]. HspR blocks its own operon at normal conditions by recognition inverted repeats (IR2 and IR3) called HAIR sequences [156]. We used single and double repeats of IR2 and IR3 sequences to decorate dnaK promoter of *E. coli* (PdnaK) to control reporter expression. At the same time, we constitutively expressed the repressor, HspR. All modifications showed decreased signal by repression at normal growth conditions, whereas signal increased upon heat treatment. However, results showed that not all modifications had the same repression characteristics. Besides, both the repression capability of each repeats and its dissociation behavior from sequences might be different. Nevertheless, IR3 sequence has a strong role in HspR recruitment and turning the promoters OFF/ON. Finally, PdnaK-IR3-IR3 sensor has the ability to report toxicity of nanomaterials with a tightly controlled mechanism eliminating false positive results.

To sum up, we demonstrated that HSR mechanism is a powerful candidate to manufacture ordered gene circuits to detect nanomaterial-triggered toxicity. Unlike recent reports utilizing HSR mechanism as stress indicating biosensors, we integrated promoter engineering strategies (i.e., modifications of HSP promoters with riboregulators, quorum sensing mechanism, and repressor binding sequences from HSR of *M. tuberculosis*) to obtain optimum signal upon stress. Hence, a fast-acting, easy-to-use, and cheap toxicity assessment test based on whole-cell biosensing has been developed. The initial toxicity detection response can be used as a feedback about nanomaterials of interest so that one can engineer them to make biocompatible before field application such as imaging on human.

After detecting the toxicity of nanomaterials, next step is to identify what is the toxic compound to cells. Especially for composite nanomaterials such as QDs which are composed of combinations of heavy metals, it is crucial to know which part of the composite needs modifications.

In nature, microorganisms have developed machinery to resist metal exposure [165]. Among them, we have chosen gold and cadmium based transcription factors from related species, and engineered our previously characterized HspR-based PdnaK-IR3-IR3 toxicity sensor for source detection purposes. For gold detection, we used GolS transcription factor from *Salmonella* [169], and CadR from *P. putida* for cadmium detection [190]. We integrated another circuit in sensor to make it tightly controlled using a serin recombinase; Bxb1 [185-187]. For both recombinase-based gold and cadmium sensors, expression of both Bxb1 and the metal specific transcription factor (either GolS or CadR) was controlled with PdnaK-IR3-IR3 promoter which is repressed by constitutively active HspR in normal conditions. Upon metal exposure, both Bxb1 and metal specific transcription factor expression start. Bxb1 converts cornitive promoter of gold (PgolB) or cadmium (PcadA), and transcription factors interact with metals initiating the reporter expression. Each source detection circuit showed that both ions created stress on cells removing HspR from the stress promoter PdnaK-IR3-IR3 and initiated actuating pieces of the living sensor. Especially gold detection sensor showed very delightful results showing the system is very specific to gold and not responded any other metals. Additionally, the sensor was very sensitive detecting gold ions at low concentrations. On the other hand, CadR did not respond to cadmium as high as recombinase-based gold detection circuit. Thus, an

additional cadmium specific transcription factor, MerR (mutated) has been utilized. MerR is one of the first discovered metal-binding protein shows mercury resistance in *P. aeruginosa* [194]. However, by introducing a series of mutations on MerR, a cadmium specific MerR transcription factor, named as MerR (mutated) in the thesis, has been obtained [168]. Before adapting the MerR (mutated) to the HSR-based sensor, we characterized its activity with its native form: a constitutively expressed MerR (mutated) blocks the PcadA promoter which controls the reporter expression. As expected, GFP signal increased upon cadmium treatment. Yet, the circuit requires further optimization such as specificity analysis using different metals.

In general perspective, here we demonstrate combination of a semi-specific [73] HSR-based whole cell biosensor and a specific [73, 163, 164] whole cell biosensor. These sensors report both the presence and its source when they used together. Although the constructed circuits report only gold and cadmium now, it is highly promising to form a multiplex cellular consortium to make large screens for multiple heavy metals creating stress and toxicity, and report them with different reporters so that they can be easily distinguished.

Plenty of bacterial biosensors have been developed for toxicity assessment of various compounds so far. However, still there is no such extended biosensors have been constructed using HSP70 promoters to track the cytotoxicity of nanomaterials [202, 209-211]. Thus, our aim was to extend whole-cell biosensor for nanotoxicity assessment to other cell types such as higher eukaryotes, and to expand the limited pool of mammalian cytotoxicity biosensors.

HSR mechanism is well-conserved phenomenon among all domains of life that aims prevention of possible damages caused by stress, and maintains cell survival. At first step, we began with the very basics of HSR mechanism as we did in bacterial sensors and chosen model HSP promoters. Similar to results obtained from bacterial toxicity sensors with native HSP promoters, eukaryotic HSPs indicated continuious activity causing background signal. Thus, we decided to integrate bacterial repression-based transcription control machinery to eukaryotes. We showed HspR expression in HEK293T cells, and signal decline indicating repression by HspR via interacting IR3 sequences at the downstream of minimal constitutive promoter. However, the sensor requires further modifications and optimizations to tune its repression/activation mechanism at normal conditions and upon stress. In general, here we proposed a cytotoxicity evaluation method using eukaryotic cells and HSR mechanism providing information about the fate of the nanomaterials before field application.

Toxicity of nanomaterials is very cell type and chemical composition dependent. Even cells with different types of membranes follow different uptake mechanism for nanomaterials. A well-known example of such case is the difference between Gram negative and Gram positive bacteria. Thinner peptidoglycan layer makes Gram negative cells more vulnerable than Gram positive cells against nanomaterials [145]. Additionally, nanomaterial-triggered toxicity is a complex phenomenon. After exposure to nanomaterials, they can be internalized by body through different routes such as inhalation or skin contact, and internalized nanomaterials can accumulate in organs and internalized by cells causing certain dysfunctioning. After exposure, many molecular mechanisms have been triggered.

Yet, tracking changes at genome and proteome level are cost expensive and labor intensive. At least, a quick test gives an idea about the level of toxicity, and helps narrowing down the targeted nanomaterials that should be criticized after exposing cells to check changes at omics level. In general, we proposed a test using a general stress indicator that can produce quick information about the toxicity of tested nanomaterials from a global perspective. Besides, this sensor principle does not provide any detailed information about the action mechanism of exposed nanomaterials at the downstream pathways. Since the proposed toxicity biosensor is not cell, tissue, or organism specific but gives a general idea about toxicity, specific biomarkers indicating the reason of toxicity may be useful. To make such living biosensors, genome, transcriptome, or proteome level of analysis is required after exposing certain types of cells to certain types of nanomaterials. Such studies have a great potential to engineer living biosensors with genetic circuits with complex logic operations.

BIBLIOGRAPHY

1. Milisav, I., *Cellular Stress Responses.* Advances in Regenerative Medicine, 2011: p. 215-232.
2. Buchberger, A., B. Bukau, and T. Sommer, *Protein Quality Control in the Cytosol and the Endoplasmic Reticulum: Brothers in Arms.* Molecular Cell, 2010. **40**(2): p. 238-252.
3. Spriggs, K.A., M. Bushell, and A.E. Willis, *Translational Regulation of Gene Expression during Conditions of Cell Stress.* Molecular Cell, 2010. **40**(2): p. 228-237.
4. Banic, B., et al., *DMSO modulates the pathway of apoptosis triggering.* Cellular & Molecular Biology Letters, 2011. **16**(2): p. 328-341.
5. Nipic, D., et al., *Preapoptotic Cell Stress Response of Primary Hepatocytes.* Hepatology, 2010. **51**(6): p. 2140-2151.
6. Kultz, D., *DNA damage signals facilitate osmotic stress adaptation.* American Journal of Physiology-Renal Physiology, 2005. **289**(3): p. F504-F505.
7. Pribenszky, C., et al., *Improving post-thaw survival of cryopreserved mouse blastocysts by hydrostatic pressure challenge.* Animal Reproduction Science, 2005. **87**(1-2): p. 143-150.
8. Pribenszky, C. and G. Vajta, *Cells under pressure: how sublethal hydrostatic pressure stress treatment increases gametes' and embryos' performance?* Reproduction Fertility and Development, 2011. **23**(1): p. 48-55.
9. Funderburk, S.F., Q.J. Wang, and Z.Y. Yue, *The Beclin 1-VPS34 complex - at the crossroads of autophagy and beyond.* Trends in Cell Biology, 2010. **20**(6): p. 355-362.
10. Zakeri, Z., et al., *Cell-Death - Programmed, Apoptosis, Necrosis, or Other.* Cell Death and Differentiation, 1995. **2**(2): p. 87-96.
11. Degterev, A., M. Boyce, and J.Y. Yuan, *A decade of caspases.* Oncogene, 2003. **22**(53): p. 8543-8567.
12. Zhu, C., et al., *The influence of age on apoptotic and other mechanisms of cell death after cerebral hypoxia-ischemia.* Cell Death and Differentiation, 2005. **12**(2): p. 162-176.
13. Ankarcrona, M., et al., *Glutamate-Induced Neuronal Death - a Succession of Necrosis or Apoptosis Depending on Mitochondrial-Function.* Neuron, 1995. **15**(4): p. 961-973.
14. Zong, W.X., et al., *Alkylating DNA damage stimulates a regulated form of necrotic cell death.* Genes & Development, 2004. **18**(11): p. 1272-1282.
15. Trachootham, D., et al., *Redox regulation of cell survival.* Antioxidants & Redox Signaling, 2008. **10**(8): p. 1343-1374.
16. Robertson, J.D., et al., *Biological reactive intermediates and mechanisms of cell death.* Biological Reactive Intermediates Vi, 2001. **500**: p. 1-10.
17. Genestra, M., *Oxyl radicals, redox-sensitive signalling cascades and antioxidants.* Cellular Signalling, 2007. **19**(9): p. 1807-1819.
18. Gorman, A.M., et al., *Antioxidant-mediated inhibition of the heat shock response leads to apoptosis.* Febs Letters, 1999. **445**(1): p. 98-102.

19. Gorman, A.M., et al., *Hsp27 inhibits 6-hydroxydopamine-induced cytochrome c release and apoptosis in PC12 cells.* Biochemical and Biophysical Research Communications, 2005. **327**(3): p. 801-810.
20. Swindell, W.R., M. Huebner, and A.P. Weber, *Transcriptional profiling of Arabidopsis heat shock proteins and transcription factors reveals extensive overlap between heat and non-heat stress response pathways.* Bmc Genomics, 2007. **8**.
21. Cullinan, S.B. and J.A. Diehl, *Coordination of ER and oxidative stress signaling: The PERK/Nrf2 signaling pathway.* International Journal of Biochemistry & Cell Biology, 2006. **38**(3): p. 317-332.
22. Roos, W.P. and B. Kaina, *DNA damage-induced cell death by apoptosis.* Trends in Molecular Medicine, 2006. **12**(9): p. 440-450.
23. Jackson, S.P., *Sensing and repairing DNA double-strand breaks - Commentary.* Carcinogenesis, 2002. **23**(5): p. 687-696.
24. Barnes, D.E. and T. Lindahl, *Repair and genetic consequences of endogenous DNA base damage in mammalian cells.* Annual Review of Genetics, 2004. **38**: p. 445-476.
25. Hoeijmakers, J.H.J., *Genome maintenance mechanisms for preventing cancer.* Nature, 2001. **411**(6835): p. 366-374.
26. Schroder, M. and R.J. Kaufman, *The mammalian unfolded protein response.* Annual Review of Biochemistry, 2005. **74**: p. 739-789.
27. Tamatani, M., et al., *ORP150 protects against hypoxia/ischemia-induced neuronal death.* Nature Medicine, 2001. **7**(3): p. 317-323.
28. Tanaka, S., T. Uehara, and Y. Nomura, *Up-regulation of protein-disulfide isomerase in response to hypoxia/brain ischemia and its protective effect against apoptotic cell death.* Journal of Biological Chemistry, 2000. **275**(14): p. 10388-10393.
29. Uehara, T., et al., *S-Nitrosylated protein-disulphide isomerase links protein misfolding to neurodegeneration.* Nature, 2006. **441**(7092): p. 513-517.
30. Kitao, Y., et al., *Pael receptor induces death of dopaminergic neurons in the substantia nigra via endoplasmic reticulum stress and dopamine toxicity, which is enhanced under condition of parkin inactivation.* Human Molecular Genetics, 2007. **16**(1): p. 50-60.
31. Hoshino, T., et al., *Endoplasmic reticulum chaperones inhibit the production of amyloid-beta peptides.* Biochemical Journal, 2007. **402**: p. 581-589.
32. Kitao, Y., et al., *Expression of the endoplasmic reticulum molecular chaperone (ORP150) rescues hippocampal neurons from glutamate toxicity.* Journal of Clinical Investigation, 2001. **108**(10): p. 1439-1450.
33. Nakagawa, T., et al., *Caspase-12 mediates endoplasmic-reticulum-specific apoptosis and cytotoxicity by amyloid-beta.* Nature, 2000. **403**(6765): p. 98-103.
34. Jaattela, M., *Heat shock proteins as cellular lifeguards.* Annals of Medicine, 1999. **31**(4): p. 261-271.
35. Arsene, F., T. Tomoyasu, and B. Bukau, *The heat shock response of Escherichia coli.* International Journal of Food Microbiology, 2000. **55**(1-3): p. 3-9.

36. Yura, T. and K. Nakahigashi, *Regulation of the heat-shock response.* Current Opinion in Microbiology, 1999. **2**(2): p. 153-158.
37. Roncarati, D. and V. Scarlato, *Regulation of heat-shock genes in bacteria: from signal sensing to gene expression output.* Fems Microbiology Reviews, 2017. **41**(4): p. 549-574.
38. Akerfelt, M., R.I. Morimoto, and L. Sistonen, *Heat shock factors: integrators of cell stress, development and lifespan.* Nature Reviews Molecular Cell Biology, 2010. **11**(8): p. 545-555.
39. Richter, K., M. Haslbeck, and J. Buchner, *The Heat Shock Response: Life on the Verge of Death.* Molecular Cell, 2010. **40**(2): p. 253-266.
40. Feynman, R.P., *There's Plenty of Room at the Bottom.* Engineering and Science, 1960. **23**(5): p. 22-36.
41. Moeinzadeh, S. and E. Jabbari, *Nanoparticles and Their Applications*, in *Springer Handbook of Nanotechnology*, B. Bhushan, Editor. 2017, Springer Berlin Heidelberg: Berlin, Heidelberg. p. 335-361.
42. Dhand, C., et al., *Methods and strategies for the synthesis of diverse nanoparticles and their applications: a comprehensive overview.* Rsc Advances, 2015. **5**(127): p. 105003-105037.
43. Buzea, C., I.I. Pacheco, and K. Robbie, *Nanomaterials and nanoparticles: Sources and toxicity.* Biointerphases, 2007. **2**(4): p. Mr17-Mr71.
44. Hafner, J.H., et al., *Structural and functional imaging with carbon nanotube AFM probes.* Progress in Biophysics & Molecular Biology, 2001. **77**(1): p. 73-110.
45. Li, Y., et al., *Antimicrobial effect of surgical masks coated with nanoparticles.* Journal of Hospital Infection, 2006. **62**(1): p. 58-63.
46. Harisinghani, M.G., et al., *Noninvasive detection of clinically occult lymph-node metastases in prostate cancer.* New England Journal of Medicine, 2003. **348**(25): p. 2491-U5.
47. He, F. and D.Y. Zhao, *Preparation and characterization of a new class of starch-stabilized bimetallic nanoparticles for degradation of chlorinated hydrocarbons in water.* Environmental Science & Technology, 2005. **39**(9): p. 3314-3320.
48. Ellis-Behnke, R.G., et al., *Nano neuro knitting: Peptide nanofiber scaffold for brain repair and axon regeneration with functional return of vision (vol 103, pg 5054, 2006).* Proceedings of the National Academy of Sciences of the United States of America, 2006. **103**(19): p. 7530-7530.
49. Uhrich, K.E., et al., *Polymeric systems for controlled drug release.* Chemical Reviews, 1999. **99**(11): p. 3181-3198.
50. Matsusaki, M., et al., *Nanosphere induced gene expression in human dendritic cells.* Nano Letters, 2005. **5**(11): p. 2168-2173.
51. Rosi, N.L. and C.A. Mirkin, *Nanostructures in biodiagnostics.* Chemical Reviews, 2005. **105**(4): p. 1547-1562.
52. Kumar, V., et al., *Evaluating the Toxicity of Selected Types of Nanochemicals*, in *Reviews of Environmental Contamination and Toxicology*, D.M. Whitacre, Editor. 2012, Springer New York: New York, NY. p. 39-121.

53. Oberdorster, G., E. Oberdorster, and J. Oberdorster, *Nanotoxicology: An emerging discipline evolving from studies of ultrafine particles.* Environmental Health Perspectives, 2005. **113**(7): p. 823-839.
54. Brown, D.M., et al., *Calcium and ROS-mediated activation of transcription factors and TNF-alpha cytokine gene expression in macrophages exposed to ultrafine particles.* American Journal of Physiology-Lung Cellular and Molecular Physiology, 2004. **286**(2): p. L344-L353.
55. Brown, D.M., K. Donaldson, and V. Stone, *Effects of PM10 in human peripheral blood monocytes and J774 macrophages.* Respiratory Research, 2004. **5**(29).
56. Long, H.Y., et al., *ROS-mediated TNF-alpha and MIP-2 gene expression in alveolar macrophages exposed to pine dust.* Particle and Fibre Toxicology, 2004. **1**(1).
57. Risom, L., P. Moller, and S. Loft, *Oxidative stress-induced DNA damage by particulate air pollution.* Mutation Research-Fundamental and Molecular Mechanisms of Mutagenesis, 2005. **592**(1-2): p. 119-137.
58. Peters, A., et al., *Translocation and potential neurological effects of fine and ultrafine particles a critical update.* Particle and Fibre Toxicology, 2006. **3**(1).
59. Djurisic, A.B., et al., *Toxicity of Metal Oxide Nanoparticles: Mechanisms, Characterization, and Avoiding Experimental Artefacts.* Small, 2015. **11**(1): p. 26-44.
60. Gou, N., A. Onnis-Hayden, and A.Z. Gu, *Mechanistic Toxicity Assessment of Nanomaterials by Whole-Cell-Array Stress Genes Expression Analysis.* Environmental Science & Technology, 2010. **44**(15): p. 5964-5970.
61. Monras, J.P., et al., *Microarray analysis of the Escherichia coli response to CdTe-GSH Quantum Dots: understanding the bacterial toxicity of semiconductor nanoparticles.* Bmc Genomics, 2014. **15**.
62. Garcia-Garcia, E., et al., *A methodology to study intracellular distribution of nanoparticles in brain endothelial cells.* International Journal of Pharmaceutics, 2005. **298**(2): p. 310-314.
63. Xia, T., et al., *Comparison of the abilities of ambient and manufactured nanoparticles to induce cellular toxicity according to an oxidative stress paradigm.* Nano Letters, 2006. **6**(8): p. 1794-1807.
64. Penn, A., et al., *Combustion-derived ultrafine particles transport organic toxicants to target respiratory cells.* Environmental Health Perspectives, 2005. **113**(8): p. 956-963.
65. Castillo, J., et al., *Biosensors for life quality - Design, development and applications.* Sensors and Actuators B-Chemical, 2004. **102**(2): p. 179-194.
66. Daunert, S., et al., *Genetically engineered whale-cell sensing systems: Coupling biological recognition with reporter genes.* Chemical Reviews, 2000. **100**(7): p. 2705-2738.
67. Saltepe, B., et al., *Cellular Biosensors with Engineered Genetic Circuits.* Acs Sensors, 2018. **3**(1): p. 13-26.

68. Collins, A.R., et al., *High throughput toxicity screening and intracellular detection of nanomaterials.* Wiley Interdisciplinary Reviews-Nanomedicine and Nanobiotechnology, 2017. **9**(1).
69. Ma, X.Y.Y., et al., *Bioassay based luminescent bacteria: Interferences, improvements, and applications.* Science of the Total Environment, 2014. **468**: p. 1-11.
70. Cha, H.J., et al., *Green fluorescent protein as a noninvasive stress probe in resting Escherichia coli cells.* Applied and Environmental Microbiology, 1999. **65**(2): p. 409-414.
71. Seo, J.H., D.G. Kang, and H.J. Cha, *Comparison of cellular stress levels and green-fluorescent-protein expression in several Escherichia coli strains.* Biotechnology and Applied Biochemistry, 2003. **37**: p. 103-107.
72. Nemecek, S., et al., *Design of transcriptional fusions of stress sensitive promoters and GFP to monitor the overburden of Escherichia coli hosts during recombinant protein production.* Bioprocess and Biosystems Engineering, 2008. **31**(1): p. 47-53.
73. Sorensen, S.J., M. Burmolle, and L.H. Hansen, *Making bio-sense of toxicity: new developments in whole-cell biosensors.* Current Opinion in Biotechnology, 2006. **17**(1): p. 11-16.
74. Saltepe, B., et al., *Genetic Circuits To Detect Nanomaterial Triggered Toxicity through Engineered Heat Shock Response Mechanism.* Acs Synthetic Biology, 2019. **8**(10): p. 2404-2417.
75. Li, W.J., J. Zhou, and Y.Y. Xu, *Study of the in vitro cytotoxicity testing of medical devices.* Biomedical Reports, 2015. **3**(5): p. 617-620.
76. Wang, X.F., et al., *Evaluation of MTT assay for measurement of emodin-induced cytotoxicity.* Assay and Drug Development Technologies, 2006. **4**(2): p. 203-207.
77. Jo, H.Y., et al., *The Unreliability of MTT Assay in the Cytotoxic Test of Primary Cultured Glioblastoma Cells.* Experimental Neurobiology, 2015. **24**(3): p. 235-245.
78. van Meerloo, J., G.J.L. Kaspers, and J. Cloos, *Cell Sensitivity Assays: The MTT Assay*, in *Cancer Cell Culture: Methods and Protocols*, I.A. Cree, Editor. 2011, Humana Press: Totowa, NJ. p. 237-245.
79. Kirkpatrick, C.J., et al., *Current trends in biocompatibility testing.* Proceedings of the Institution of Mechanical Engineers Part H-Journal of Engineering in Medicine, 1998. **212**(H2): p. 75-84.
80. Poynton, H.C., et al., *Toxicity and Transcriptomic Analysis in Hyalella azteca Suggests Increased Exposure and Susceptibility of Epibenthic Organisms to Zinc Oxide Nanoparticles.* Environmental Science & Technology, 2013. **47**(16): p. 9453-9460.
81. Simon, D.F., et al., *Transcriptome Sequencing (RNA-seq) Analysis of the Effects of Metal Nanoparticle Exposure on the Transcriptome of Chlamydomonas reinhardtii.* Applied and Environmental Microbiology, 2013. **79**(16): p. 4774-4785.
82. Rodrigues, J.L., et al., *Selection of Escherichia coli heat shock promoters toward their application as stress probes.* Journal of Biotechnology, 2014. **188**: p. 61-71.

83. Guadagnini, R., et al., *Toxicity screenings of nanomaterials: challenges due to interference with assay processes and components of classic in vitro tests.* Nanotoxicology, 2015. **9**: p. 13-24.
84. Lovern, S.B. and R. Klaper, *Daphnia magna mortality when exposed to titanium dioxide and fullerene (C-60) nanoparticles.* Environmental Toxicology and Chemistry, 2006. **25**(4): p. 1132-1137.
85. Hund-Rinke, K. and M. Simon, *Ecotoxic effect of photocatalytic active nanoparticles TiO2 on algae and daphnids.* Environmental Science and Pollution Research, 2006. **13**(4): p. 225-232.
86. Lee, K.J., et al., *In vivo imaging of transport and biocompatibility of single silver nanoparticles in early development of zebrafish embryos.* Acs Nano, 2007. **1**(2): p. 133-143.
87. King-Heiden, T.C., et al., *Quantum Dot Nanotoxicity Assessment Using the Zebrafish Embryo.* Environmental Science & Technology, 2009. **43**(5): p. 1605-1611.
88. Zhang, W., et al., *Toxicity assessment of zebrafish following exposure to CdTe QDs.* Journal of Hazardous Materials, 2012. **213**: p. 413-420.
89. Chong, Y., et al., *The in vitro and in vivo toxicity of graphene quantum dots.* Biomaterials, 2014. **35**(19): p. 5041-5048.
90. Liu, J.W., et al., *Assessing Clinical Prospects of Silicon Quantum Dots: Studies in Mice and Monkeys.* Acs Nano, 2013. **7**(8): p. 7303-7310.
91. Gutierrez, J.C., F. Amaro, and A. Martin-Gonzalez, *Heavy metal whole-cell biosensors using eukaryotic microorganisms: an updated critical review.* Frontiers in Microbiology, 2015. **6**.
92. Hietakangas, V. and L. Sistonen, *Regulation of the heat shock response by heat shock transcription factors*, in *Chaperones: 16*, I. Braakman, Editor. 2006, Springer Berlin Heidelberg: Berlin, Heidelberg. p. 1-34.
93. Ahamed, M., et al., *Silver nanoparticles induced heat shock protein 70, oxidative stress and apoptosis in Drosophila melanogaster.* Toxicology and Applied Pharmacology, 2010. **242**(3): p. 263-269.
94. Voicu, S.N.P., et al., *Silica Nanoparticles Induce Oxidative Stress and Autophagy but Not Apoptosis in the MRC-5 Cell Line.* International Journal of Molecular Sciences, 2015. **16**(12): p. 29398-29416.
95. Migita, S., et al., *Quantum dots induce heat shock-related cytotoxicity at intracellular environment.* In Vitro Cell Dev Biol Anim, 2014. **50**(4): p. 367-72.
96. Cicchetti, R., et al., *Effects of single-wall carbon nanotubes in human cells of the oral cavity: Geno-cytotoxic risk.* Toxicology in Vitro, 2011. **25**(8): p. 1811-1819.
97. Lindquist, S. and E.A. Craig, *The Heat-Shock Proteins.* Annual Review of Genetics, 1988. **22**: p. 631-677.
98. Verghese, J., et al., *Biology of the Heat Shock Response and Protein Chaperones: Budding Yeast (Saccharomyces cerevisiae) as a Model System.* Microbiology and Molecular Biology Reviews, 2012. **76**(2): p. 115-158.
99. Parsell, D.A., et al., *Protein Disaggregation Mediated by Heat-Shock Protein Hsp104.* Nature, 1994. **372**(6505): p. 475-478.

100. Laskowska, E., et al., *Degradation by proteases Lon, Clp and HtrA, of Escherichia coli proteins aggregated in vivo by heat shock; HtrA protease action in vivo and in vitro.* Molecular Microbiology, 1996. **22**(3): p. 555-571.
101. Grossman, A.D., J.W. Erickson, and C.A. Gross, *The Htpr Gene-Product of Escherichia-Coli Is a Sigma-Factor for Heat-Shock Promoters.* Cell, 1984. **38**(2): p. 383-390.
102. Straus, D.B., W.A. Walter, and C.A. Gross, *The Heat-Shock Response of Escherichia-Coli Is Regulated by Changes in the Concentration of Sigma-32.* Nature, 1987. **329**(6137): p. 348-351.
103. Nakahigashi, K., H. Yanagi, and T. Yura, *Isolation and Sequence-Analysis of Rpoh Genes Encoding Sigma(32) Homologs from Gram-Negative Bacteria - Conserved Messenger-Rna and Protein Segments for Heat-Shock Regulation.* Nucleic Acids Research, 1995. **23**(21): p. 4383-4390.
104. Tilly, K., et al., *The Dnak Protein Modulates the Heat-Shock Response of Escherichia-Coli.* Cell, 1983. **34**(2): p. 641-646.
105. Tomoyasu, T., et al., *Levels of DnaK and DnaJ provide tight control of heat shock gene expression and protein repair in Escherichia coli.* Molecular Microbiology, 1998. **30**(3): p. 567-581.
106. Tatsuta, T., et al., *Heat shock regulation in the ftsH null mutant of Escherichia coli: dissection of stability and activity control mechanisms of sigma(32) in vivo.* Molecular Microbiology, 1998. **30**(3): p. 583-593.
107. Paton, G.I., et al., *Assessment of Bioavailability of Heavy-Metals Using Lux Modified Constructs of Pseudomonas-Fluorescens.* Letters in Applied Microbiology, 1995. **20**(1): p. 52-56.
108. Chaudri, A.M., et al., *Determination of acute Zn toxicity in pore water from soils previously treated with sewage sludge using bioluminescence assays.* Environmental Science & Technology, 1999. **33**(11): p. 1880-1885.
109. Sato, T. and Y. Kobayashi, *The ars operon in the skin element of Bacillus subtilis confers resistance to arsenate and arsenite.* Journal of Bacteriology, 1998. **180**(7): p. 1655-1661.
110. Lee, S., et al., *A Novel Microbial Sensor Using Luminous Bacteria.* Biosensors & Bioelectronics, 1992. **7**(4): p. 273-277.
111. Gill, R.T., et al., *Generating controlled reducing environments in aerobic recombinant Escherichia coli fermentations: Effects on cell growth, oxygen uptake, heat shock protein expression, and in vivo CAT activity.* Biotechnology and Bioengineering, 1998. **59**(2): p. 248-259.
112. Sagi, E., et al., *Fluorescence and bioluminescence reporter functions in genetically modified bacterial sensor strains.* Sensors and Actuators B-Chemical, 2003. **90**(1-3): p. 2-8.
113. Aertsen, A., et al., *Heat shock protein-mediated resistance to high hydrostatic pressure in Escherichia coli.* Applied and Environmental Microbiology, 2004. **70**(5): p. 2660-2666.
114. Vandyk, T.K., et al., *Rapid and Sensitive Pollutant Detection by Induction of Heat-Shock Gene-Bioluminescence Gene Fusions.* Applied and Environmental Microbiology, 1994. **60**(5): p. 1414-1420.

115. Ben-Israel, O., H. Ben-Israel, and S. Ulitzur, *Identification and quantification of toxic chemicals by use of Escherichia coli carrying lux genes fused to stress promoters.* Applied and Environmental Microbiology, 1998. **64**(11): p. 4346-4352.
116. Padilla-Martinez, F., et al., *Cell damage detection using Escherichia coli reporter plasmids: fluorescent and colorimetric assays.* Archives of Microbiology, 2015. **197**(6): p. 815-821.
117. Goers, L., et al., *Engineering Microbial Biosensors.* Microbial Synthetic Biology, 2013. **40**: p. 119-156.
118. Park, M., S.L. Tsai, and W. Chen, *Microbial Biosensors: Engineered Microorganisms as the Sensing Machinery.* Sensors, 2013. **13**(5): p. 5777-5795.
119. Alivisatos, A.P., *Semiconductor clusters, nanocrystals, and quantum dots.* Science, 1996. **271**(5251): p. 933-937.
120. Weller, H., *Quantum size colloids: from size-dependent properties of discrete particles to self-organized superstructures.* Current Opinion in Colloid & Interface Science, 1998. **3**(2): p. 194-199.
121. Nel, A., et al., *Toxic potential of materials at the nanolevel.* Science, 2006. **311**(5761): p. 622-627.
122. Li, Y., Y. Zhang, and B. Yan, *Nanotoxicity Overview: Nano-Threat to Susceptible Populations.* International Journal of Molecular Sciences, 2014. **15**(3): p. 3671-3697.
123. Ray, P.C., H.T. Yu, and P.P. Fu, *Toxicity and Environmental Risks of Nanomaterials: Challenges and Future Needs.* Journal of Environmental Science and Health Part C-Environmental Carcinogenesis & Ecotoxicology Reviews, 2009. **27**(1): p. 1-35.
124. Saptarshi, S.R., A. Duschl, and A.L. Lopata, *Interaction of nanoparticles with proteins: relation to bio-reactivity of the nanoparticle.* Journal of Nanobiotechnology, 2013. **11**.
125. Singh, N., et al., *NanoGenotoxicology: The DNA damaging potential of engineered nanomaterials.* Biomaterials, 2009. **30**(23-24): p. 3891-3914.
126. Lindberg, H.K., et al., *Genotoxicity of nanomaterials: DNA damage and micronuclei induced by carbon nanotubes and graphite nanofibres in human bronchial epithelial cells in vitro.* Toxicology Letters, 2009. **186**(3): p. 166-173.
127. Ahmad, J., et al., *Apoptosis induction by silica nanoparticles mediated through reactive oxygen species in human liver cell line HepG2.* Toxicology and Applied Pharmacology, 2012. **259**(2): p. 160-168.
128. Dumas, E.M., et al., *Toxicity of CdTe Quantum Dots in Bacterial Strains.* Ieee Transactions on Nanobioscience, 2009. **8**(1): p. 58-64.
129. Lyon, D.Y., et al., *Antibacterial activity of fullerene water suspensions (nC(60)) is not due to ROS-mediated damage.* Nano Letters, 2008. **8**(5): p. 1539-1543.
130. Sharma, V., et al., *Zinc Oxide Nanoparticle Induced Genotoxicity in Primary Human Epidermal Keratinocytes.* Journal of Nanoscience and Nanotechnology, 2011. **11**(5): p. 3782-3788.
131. Slavin, Y.N., et al., *Metal nanoparticles: understanding the mechanisms behind antibacterial activity.* Journal of Nanobiotechnology, 2017. **15**.

132. Hussain, S., J.A.J. Vanoirbeek, and P.H.M. Hoet, *Interactions of nanomaterials with the immune system.* Wiley Interdisciplinary Reviews-Nanomedicine and Nanobiotechnology, 2012. **4**(2): p. 169-183.
133. Truong, L., et al., *Surface functionalities of gold nanoparticles impact embryonic gene expression responses.* Nanotoxicology, 2013. **7**(2): p. 192-201.
134. Tkach, A.V., et al., *Direct Effects of Carbon Nanotubes on Dendritic Cells Induce Immune Suppression Upon Pulmonary Exposure.* Acs Nano, 2011. **5**(7): p. 5755-5762.
135. Wang, A.Y. and D.E. Crowley, *Global gene expression responses to cadmium toxicity in Escherichia coli.* Journal of Bacteriology, 2005. **187**(9): p. 3259-3266.
136. Fang, T.T., et al., *Toxicity evaluation of CdTe quantum dots with different size on Escherichia coli.* Toxicology in Vitro, 2012. **26**(7): p. 1233-1239.
137. Gibson, D.G., et al., *Enzymatic assembly of DNA molecules up to several hundred kilobases.* Nature Methods, 2009. **6**(5): p. 343-U41.
138. Weber, E., et al., *A Modular Cloning System for Standardized Assembly of Multigene Constructs.* Plos One, 2011. **6**(2).
139. Seker, U.O.S., T. Ozel, and H.V. Demir, *Peptide-Mediated Constructs of Quantum Dot Nanocomposites for Enzymatic Control of Nonradiative Energy Transfer.* Nano Letters, 2011. **11**(4): p. 1530-1539.
140. Isaacs, F.J., et al., *Engineered riboregulators enable post-transcriptional control of gene expression.* Nature Biotechnology, 2004. **22**(7): p. 841-847.
141. Mogk, A., et al., *Identification of thermolabile Escherichia coli proteins: prevention and reversion of aggregation by DnaK and ClpB.* Embo Journal, 1999. **18**(24): p. 6934-6949.
142. Caspeta, L., et al., *The Effect of Heating Rate on Escherichia coli Metabolism, Physiological Stress, Transcriptional Response, and Production of Temperature-induced Recombinant Protein: A Scale-Down Study.* Biotechnology and Bioengineering, 2009. **102**(2): p. 468-482.
143. Zolkiewski, M., *ClpB cooperates with DnaK, DnaJ, and GrpE in suppressing protein aggregation - A novel multi-chaperone system from Escherichia coli.* Journal of Biological Chemistry, 1999. **274**(40): p. 28083-28086.
144. LeThanh, H., P. Neubauer, and F. Hoffmann, *The small heat-shock proteins IbpA and IbpB reduce the stress load of recombinant Escherichia coli and delay degradation of inclusion bodies.* Microbial Cell Factories, 2005. **4**.
145. Gomes, S.A.O., et al., *CdTe and CdSe Quantum Dots Cytotoxicity: A Comparative Study on Microorganisms.* Sensors, 2011. **11**(12): p. 11664-11678.
146. Jones, C.F. and D.W. Grainger, *In vitro assessments of nanomaterial toxicity.* Advanced Drug Delivery Reviews, 2009. **61**(6): p. 438-456.
147. Vanbogelen, R.A., P.M. Kelley, and F.C. Neidhardt, *Differential Induction of Heat-Shock, Sos, and Oxidation Stress Regulons and Accumulation of Nucleotides in Escherichia-Coli.* Journal of Bacteriology, 1987. **169**(1): p. 26-32.

148. Goeser, L., et al., *Small Heat-Shock Proteins, IbpAB, Protect Non-Pathogenic Escherichia coli from Killing by Macrophage-Derived Reactive Oxygen Species.* Plos One, 2015. **10**(3).
149. Matuszewska, E., et al., *Escherichia coli heat-shock proteins IbpA/B are involved in resistance to oxidative stress induced by copper.* Microbiology-Sgm, 2008. **154**: p. 1739-1747.
150. Rutherford, S.T. and B.L. Bassler, *Bacterial Quorum Sensing: Its Role in Virulence and Possibilities for Its Control.* Cold Spring Harbor Perspectives in Medicine, 2012. **2**(11).
151. Hastings, J.W. and E.P. Greenberg, *Quorum sensing: the explanation of a curious phenomenon reveals a common characteristic of bacteria.* Journal of Bacteriology, 1999. **181**(9): p. 2667-2668.
152. Bucca, G., et al., *The HspR regulon of Streptomyces coelicolor: a role for the DnaK chaperone as a transcriptional co-repressor.* Molecular Microbiology, 2000. **38**(5): p. 1093-1103.
153. Bandyopadhyay, B., et al., *DnaK Dependence of the Mycobacterial Stress-Responsive Regulator HspR Is Mediated through Its Hydrophobic C-Terminal Tail.* Journal of Bacteriology, 2012. **194**(17): p. 4688-4697.
154. Bucca, G., et al., *The Dnak Operon of Streptomyces-Coelicolor Encodes a Novel Heat-Shock Protein Which Binds to the Promoter Region of the Operon.* Molecular Microbiology, 1995. **17**(4): p. 663-674.
155. Stewart, G.R., et al., *Dissection of the heat-shock response in Myobacterium tuberculosis using mutants and microarrays.* Microbiology-Sgm, 2002. **148**: p. 3129-3138.
156. Grandvalet, C., V. de Crecy-Lagard, and P. Mazodier, *The clpB ATPase of Streptomyces albus G belongs to the HspR heat shock regulon.* Molecular Microbiology, 1999. **31**(2): p. 521-532.
157. Lai, L., et al., *Adhesion of quantum dots-induced membrane damage of Escherichia coli.* Journal of Colloid and Interface Science, 2013. **389**: p. 61-70.
158. Park, H.J., et al., *Silver-ion-mediated reactive oxygen species generation affecting bactericidal activity.* Water Research, 2009. **43**(4): p. 1027-1032.
159. Hansen, L.H. and S.J. Sorensen, *The use of whole-cell biosensors to detect and quantify compounds or conditions affecting biological systems.* Microbial Ecology, 2001. **42**(4): p. 483-494.
160. Bulich, A.A. and D.L. Isenberg, *Use of the Luminescent Bacterial System for the Rapid Assessment of Aquatic Toxicity.* Isa Transactions, 1981. **20**(1): p. 29-33.
161. Jennings, V.L.K., M.H. Rayner-Brandes, and D.J. Bird, *Assessing chemical toxicity with the bioluminescent photobacterium (Vibrio fischeri): A comparison of three commercial systems.* Water Research, 2001. **35**(14): p. 3448-3456.
162. Vollmer, A.C. and T.K. Van Dyk, *Stress responsive bacteria: Biosensors as environmental monitors.* Advances in Microbial Physiology, Vol. 49, 2004. **49**: p. 131-174.
163. D'Souza, S.F., *Microbial biosensors.* Biosensors & Bioelectronics, 2001. **16**(6): p. 337-353.

164. van der Meer, J.R., D. Tropel, and M. Jaspers, *Illuminating the detection chain of bacterial bioreporters.* Environmental Microbiology, 2004. **6**(10): p. 1005-1020.
165. Fernandez-Lopez, R., et al., *Transcription factor-based biosensors enlightened by the analyte.* Frontiers in Microbiology, 2015. **6**.
166. Brown, N.L., et al., *The MerR family of transcriptional regulators.* Fems Microbiology Reviews, 2003. **27**(2-3): p. 145-163.
167. Changela, A., et al., *Molecular basis of metal-ion selectivity and zeptomolar sensitivity by CueR.* Science, 2003. **301**(5638): p. 1383-1387.
168. Hakkila, K.M., et al., *Cd-Specific Mutants of Mercury-Sensing Regulatory Protein MerR, Generated by Directed Evolution.* Applied and Environmental Microbiology, 2011. **77**(17): p. 6215-6224.
169. Checa, S.K., et al., *Bacterial sensing of and resistance to gold salts.* Molecular Microbiology, 2007. **63**(5): p. 1307-1318.
170. Busenlehner, L.S., M.A. Pennella, and D.P. Giedroc, *The SmtB/ArsR family of metalloregulatory transcriptional repressors: structural insights into prokaryotic metal resistance.* Fems Microbiology Reviews, 2003. **27**(2-3): p. 131-143.
171. Ye, J., et al., *Crystal structure of the Staphylococcus aureus pI258 CadC Cd(II)/Pb(II)/Zn(II)-responsive repressor.* Journal of Bacteriology, 2005. **187**(12): p. 4214-4221.
172. White, A., et al., *Structure of the metal-ion-activated diphtheria toxin repressor tox operator complex.* Nature, 1998. **394**(6692): p. 502-506.
173. Sheikh, M.A. and G.L. Taylor, *Crystal structure of the Vibrio cholerae ferric uptake regulator (Fur) reveals insights into metal co-ordination.* Molecular Microbiology, 2009. **72**(5): p. 1208-1220.
174. Gilston, B.A., et al., *Structural and Mechanistic Basis of Zinc Regulation Across the E. coli Zur Regulon.* Plos Biology, 2014. **12**(11).
175. Schreiter, E.R., et al., *NikR-operator complex structure and the mechanism of repressor activation by metal ions.* Proceedings of the National Academy of Sciences of the United States of America, 2006. **103**(37): p. 13676-13681.
176. Bruins, M.R., S. Kapil, and F.W. Oehme, *Microbial resistance to metals in the environment.* Ecotoxicology and Environmental Safety, 2000. **45**(3): p. 198-207.
177. Bontidean, L., et al., *Biosensors for detection of mercury in contaminated soils.* Environmental Pollution, 2004. **131**(2): p. 255-262.
178. Amaro, F., et al., *Functional GFP-metallothionein fusion protein from Tetrahymena thermophila: a potential whole-cell biosensor for monitoring heavy metal pollution and a cell model to study metallothionein overproduction effects.* Biometals, 2014. **27**(1): p. 195-205.
179. Priyadarshi, H., et al., *A GFP-based bacterial biosensor with chromosomally integrated sensing cassette for quantitative detection of Hg(II) in environment.* Journal of Environmental Sciences, 2012. **24**(5): p. 963-968.
180. Wang, B.J., M. Barahona, and M. Buck, *A modular cell-based biosensor using engineered genetic logic circuits to detect and integrate multiple*

environmental signals. Biosensors & Bioelectronics, 2013. **40**(1): p. 368-376.
181. Binet, M.R.B. and R.K. Poole, *Cd(II), Pb(II) and Zn(II) ions regulate expression of the metal-transporting P-type ATPase ZntA in Escherichia coli.* Febs Letters, 2000. **473**(1): p. 67-70.
182. Stoyanov, J.V. and N.L. Brown, *The Escherichia coli copper-responsive copA promoter is activated by gold.* Journal of Biological Chemistry, 2003. **278**(3): p. 1407-1410.
183. Neidhardt, F.C., P.L. Bloch, and D.F. Smith, *Culture medium for enterobacteria.* Journal of Bacteriology, 1974. **119**(3): p. 736-47.
184. LaRossa, R.A., D.R. Smulski, and T.K. Van Dyk, *Interaction of lead nitrate and cadmium chloride with Escherichia coli K-12 and Salmonella typhimurium global regulatory mutants.* J Ind Microbiol, 1995. **14**(3-4): p. 252-8.
185. Ghosh, P., N.R. Pannunzio, and G.F. Hatfull, *Synapsis in phage Bxb1 integration: Selection mechanism for the correct pair of recombination sites.* Journal of Molecular Biology, 2005. **349**(2): p. 331-348.
186. Roquet, N., et al., *Synthetic recombinase-based state machines in living cells.* Science, 2016. **353**(6297): p. 363-+.
187. Siuti, P., J. Yazbek, and T.K. Lu, *Synthetic circuits integrating logic and memory in living cells.* Nature Biotechnology, 2013. **31**(5): p. 448-+.
188. Audero, M.E.P., et al., *Target transcription binding sites differentiate two groups of MerR-monovalent metal ion sensors.* Molecular Microbiology, 2010. **78**(4): p. 853-865.
189. Ibanez, M.M., et al., *Dissecting the Metal Selectivity of MerR Monovalent Metal Ion Sensors in Salmonella.* Journal of Bacteriology, 2013. **195**(13): p. 3084-3092.
190. Lee, S.W., E. Glickmann, and D.A. Cooksey, *Chromosomal locus for cadmium resistance in Pseudomonas putida consisting of a cadmium-transporting ATPase and a MerR family response regulator.* Applied and Environmental Microbiology, 2001. **67**(4): p. 1437-1444.
191. Bereza-Malcolm, L., et al., *Functional characterization of Gram-negative bacteria from different genera as multiplex cadmium biosensors.* Biosensors & Bioelectronics, 2017. **94**: p. 380-387.
192. Tao, H.C., et al., *Optimizing cadmium and mercury specificity of CadR-based E-coli biosensors by redesign of CadR.* Biotechnology Letters, 2013. **35**(8): p. 1253-1258.
193. Nies, D.H., *Microbial heavy-metal resistance.* Applied Microbiology and Biotechnology, 1999. **51**(6): p. 730-750.
194. Brown, N.L., et al., *Nucleotide-Sequence of a Gene from the Pseudomonas Transposon-Tn501 Encoding Mercuric Reductase.* Biochemistry, 1983. **22**(17): p. 4089-4095.
195. Taniguchi, A., *Live cell-based sensor cells.* Biomaterials, 2010. **31**(23): p. 5911-5915.
196. Wang, B.J. and M. Buck, *Customizing cell signaling using engineered genetic logic circuits.* Trends in Microbiology, 2012. **20**(8): p. 376-384.

197. Shing, W.L., L.Y. Heng, and S. Surif, *Performance of a Cyanobacteria Whole Cell-Based Fluorescence Biosensor for Heavy Metal and Pesticide Detection.* Sensors, 2013. **13**(5): p. 6394-6404.
198. Vopalenska, I., L. Vachova, and Z. Palkova, *New biosensor for detection of copper ions in water based on immobilized genetically modified yeast cells.* Biosensors & Bioelectronics, 2015. **72**: p. 160-167.
199. Chouteau, C., et al., *Development of novel conductometric biosensors based on immobilised whole cell Chlorella vulgaris microalgae.* Biosensors & Bioelectronics, 2004. **19**(9): p. 1089-1096.
200. Singh, J. and S.K. Mittal, *Chlorella sp based biosensor for selective determination of mercury in presence of silver ions.* Sensors and Actuators B-Chemical, 2012. **165**(1): p. 48-52.
201. Chouteau, C., et al., *A bi-enzymatic whole cell conductometric biosensor for heavy metal ions and pesticides detection in water samples.* Biosensors & Bioelectronics, 2005. **21**(2): p. 273-281.
202. Hofmann, U., et al., *A Sensitive Sensor Cell Line for the Detection of Oxidative Stress Responses in Cultured Human Keratinocytes.* Sensors, 2014. **14**(7): p. 11293-11307.
203. Liu, F., et al., *A lab-on-chip cell-based biosensor for label-free sensing of water toxicants.* Lab on a Chip, 2014. **14**(7): p. 1270-1280.
204. Xing, J.Z., et al., *Microelectronic cell sensor assay for detection of cytotoxicity and prediction of acute toxicity.* Toxicology in Vitro, 2006. **20**(6): p. 995-1004.
205. Banerjee, P. and A.K. Bhunia, *Mammalian cell-based biosensors for pathogens and toxins.* Trends in Biotechnology, 2009. **27**(3): p. 179-188.
206. Wang, T.H., G.H. Hui, and S.P. Deng, *A novel sweet taste cell-based sensor.* Biosensors & Bioelectronics, 2010. **26**(2): p. 929-934.
207. Chen, P., et al., *Detection of cellular response to titanium dioxide nanoparticle agglomerates by sensor cells using heat shock protein promoter.* Biotechnology and Bioengineering, 2012. **109**(12): p. 3112-3118.
208. Dubiak-Szepietowska, M., et al., *A cell-based biosensor for nanomaterials cytotoxicity assessment in three dimensional cell culture.* Toxicology, 2016. **370**: p. 60-69.
209. Wada, K.I., et al., *Rapid and highly sensitive detection of cadmium chloride induced cytotoxicity using the HSP70B ' promoter in live cells.* Biotechnology and Bioengineering, 2005. **92**(4): p. 410-415.
210. Wada, K.I., A. Taniguchi, and T. Okano, *Highly sensitive detection of cytotoxicity using a modified HSP70B' promoter.* Biotechnology and Bioengineering, 2007. **97**(4): p. 871-876.
211. Koizumi, S., K. Suzuki, and S. Yamaguchi, *Heavy metal response of the heat shock protein 70 gene is mediated by duplicated heat shock elements and heat shock factor 1.* Gene, 2013. **522**(2): p. 184-191.
212. Haynes, K.A. and P.A. Silver, *Eukaryotic systems broaden the scope of synthetic biology.* Journal of Cell Biology, 2009. **187**(5): p. 589-596.
213. Head, M.W., L. Hurwitz, and J.E. Goldman, *Transcriptional regulation of alpha B-crystallin in astrocytes: Analysis of HSF and AP1 activation by*

different types of physiological stress. Journal of Cell Science, 1996. **109**: p. 1029-1039.

214. Klemenz, R., et al., *Alpha-B-Crystallin Is a Small Heat-Shock Protein.* Proceedings of the National Academy of Sciences of the United States of America, 1991. **88**(9): p. 3652-3656.
215. Kato, K., et al., *Coinduction of 2 Low-Molecular-Weight Stress Proteins, Alpha-B-Crystallin and Hsp28, by Heat or Arsenite Stress in Human Glioma-Cells.* Journal of Biochemistry, 1993. **114**(5): p. 640-647.
216. Iwaki, T., et al., *Alpha-B-Crystallin and 27-Kd Heat-Shock Protein Are Regulated by Stress Conditions in the Central-Nervous-System and Accumulate in Rosenthal Fibers.* American Journal of Pathology, 1993. **143**(2): p. 487-495.
217. Saxena, P., D. Bojar, and M. Fussenegger, *Design of Synthetic Promoters for Gene Circuits in Mammalian Cells.* Mammalian Synthetic Promoters, 2017. **1651**: p. 263-273.
218. Zhou, K., et al., *Novel reference genes for quantifying transcriptional responses of Escherichia coli to protein overexpression by quantitative PCR.* Bmc Molecular Biology, 2011. **12**.
219. Lu, Z.S., et al., *Mechanism of antimicrobial activity of CdTe quantum dots.* Langmuir, 2008. **24**(10): p. 5445-5452.

APPENDIX A

DNA sequences of constructs used in this study

Table A.1: Promoter and coding sequences used in this study

Name	Type	Sequence 5'-to-3'
PdnaK	Promoter	AAAAGCACAAAAAATTTTTGCATCTCCCCCT TGATGACGTGGTTTACGACCCCATTTAGTAG TCAACCGCAGTGAGTGAGTCTGCAAAAAAAT GAAATTGGGCAGTTGAAACCAGACGTTTCGC CCCTATTACAGACTCACAACCACATGATGAC CGAATATATAGTGGAGACGTTTAGATG
PdnaK-IR2	Promoter	AAAAGCACAAAAAATTTTTGCATCTCCCCCT TGATGACGTGGTTTACGACCCCATTTAGTAG TCAACCGCAGTGAGTGAGTCTGCAAAAAAAT GAAATTGGGCAGTTGAAACCAGACGTTTCGC CCCTATTACAGACTCACAACCACATGATGAC CGAATATATAGTGGAGACGTTTAGATGAGTA AGTTGAGTGCATCAGGCTCAG
PdnaK-IR2-IR2	Promoter	AAAAGCACAAAAAATTTTTGCATCTCCCCCT TGATGACGTGGTTTACGACCCCATTTAGTAG TCAACCGCAGTGAGTGAGTCTGCAAAAAAAT GAAATTGGGCAGTTGAAACCAGACGTTTCGC CCCTATTACAGACTCACAACCACATGATGAC CGAATATATAGTGGAGACGTTTAGATGAGTA AGTTGAGTGCATCAGGCTCAGAGTAAGTTGA GTGCATCAGGCTCAG
PdnaK-IR3	Promoter	AAAAGCACAAAAAATTTTTGCATCTCCCCCT TGATGACGTGGTTTACGACCCCATTTAGTAG TCAACCGCAGTGAGTGAGTCTGCAAAAAAAT GAAATTGGGCAGTTGAAACCAGACGTTTCGC CCCTATTACAGACTCACAACCACATGATGAC CGAATATATAGTGGAGACGTTTAGATGGCAA GCTTGAGCGGGGTGCACTCATCA
PdnaK-IR3-IR3	Promoter	AAAAGCACAAAAAATTTTTGCATCTCCCCCT TGATGACGTGGTTTACGACCCCATTTAGTAG TCAACCGCAGTGAGTGAGTCTGCAAAAAAAT GAAATTGGGCAGTTGAAACCAGACGTTTCGC CCCTATTACAGACTCACAACCACATGATGAC CGAATATATAGTGGAGACGTTTAGATGGCAA

		GCTTGAGCGGGGTGCACTCATCAGCAAGCTT GAGCGGGGTGCACTCATCA
PclpB	Promoter	CTTGAATAATTGAGGGATGACCTCATTTAAT CTCC
PibpA	Promoter	GAGCTCAAAATAACATCATCATTACGTCGCA CTGTGGCGGCTATCGCACTTTAACGTTTCGTG CTGCCCCCTCAGTCTATGCAATAGACCATAA ACTGCAAAAAAAAGTCCGCTGATAAGGCTTG AAAAGTTCATTTCCAGACCCATTTTTACATCG
PibpA*	Engineered Promoter with RBS sequence	GAGCTCAAAATAACATCATCATTACGTCGCA CTGTGGCGGCTATCGCACTTTAACGTTTCGTG CTGCCCCCTCAGTCTATGCAATAGACCATAA ACTGCAAAAAAAAGTCCGCTGATAAGGCTTG AAAAGTTCATTTCCAGACCCATTTTTACATCG GTCCATAAACGGAATTAGGG
PfxsA	Promoter	GAGCTCGAGGATTTCTACCGTAATCTGGATC ACTTTAAGTGTCGGTTTTTACCCCTTAATTAT TAATTTGTGAAATAGATCACCGCTTTGGGAT TACTACCAAAAATAGTTGCGCAAACATCTTG AAATTTTGCTAATGACCACAATATAAGCTAA A
PfxsA*	Engineered Promoter with RBS sequence	GAGCTCGAGGATTTCTACCGTAATCTGGATC ACTTTAAGTGTCGGTTTTTACCCCTTAATTAT TAATTTGTGAAATAGATCACCGCTTTGGGAT TACTACCAAAAATAGTTGCGCAAACATCTTG AAATTTTGCTAATGACCACAATATAAGCTAA AGAAAGCACGACGGATCGGGA
mProD	Promoter	TCTAGATTTACAGCTAGCTCAGTCCTAGGTA TAATGCTAGCTACTAGAG
ProD	Promoter	CACAGCTAACACCACGTCGTCCCTATCTGCT GCCCTAGGTCTATGAGTGGTTGCTGGATAAC TTTACGGGCATGCATAAGGCTCGTATAATAT ATTCAGGGAGACCAAATAATTTTGTTTAACT TT
T7	Promoter	TAATACGACTCACTATAGGG
J23119	Promoter	TTGACAGCTAGCTCAGTCCTAGGTATAATGC TAGC
Plux	Promoter	ACCTGTAGGATCGTACAGGTTTACGCAAGAA AATGGTTTGTTATAGTCGAATAAA
PcadA	Promoter	TTGACTCTGTAGTTGCTACAGGGTGTGCAAT
PgolB	Promoter	CTTGACCTTCCAACACTGGCAAGGTCCAGAC TGGCAACA
mtPdnaK	Promoter	GAATTCCGACCCGCACGACCAGCGTTAGCAT GCTCAGTAAGTTGAGTGCATCAGGCTCAGCT CTGAATTGACAGCACACCGCCGTCGAGGCAA GCTTGAGCGGGGTGCACTCATCATAGTGCAG GAAAGAAGCTCTACATATTCAGGAGGATTCA CC
PαBc (from -537 to +21)	Promoter	TGCTGACATGTTGACCATCACTGCTCTCTTCC AAGGACTCACAAAGAGTTAATGTCCCTGGGG CTCAGCCTAGGAAGATTCCAGTCCCTGCCCA GGCCCAAGATAGTTGCTGGCCTGATTCCCCT

		GGCATTCAGGACTGGAAAGGAGGAGGAGGG GCACACTACGCCGGCTCCCATCCCTCCCCCC ACCCCGCGTGCCTGCTTGGGATTCCTGACTCT GTACCAGCTTCAGAGAACAGGGGTGGGGGT GGGTGCCATTGGGTGTGGACAGAAAGCTAGT GAAACAAGACCATGACAAGTCACTGGCCGG CTCAGACGTGTTTGTGTCTCTCTTTTCTTAGC TCAGTGAGTACTGGGTATGTGTCACATTGCC AAATCCCGGATCACAAGTCTCCATGAACTGC TGGTGAGCTAGGATAATAAAACCCCTGACAT CACCATTCCAGAAGCTTCACAAGACTGCATA TATAAGGGGCTGGCTGTAGCTGCAGCTGAAG GAGCTGACCAGCCAGCTGACCCCTCACACTC ACCTAGCCACCATGGACATCGCCATCCACCA C
Phsp70 (from -270 to +156)	Promoter	ATGGAGACCAACACCCTTCCCACCGCCACTC CCCCTTCCTCTCAGGGTCCCTGTCCCCTCCAG TGAATCCCAGAAGACTCTGGAGAGTTCTGAG CAGGGGGCGGCACTCTGGCCTCTGATTGGTC CAAGGAAGGCTGGGGGGCAGGACGGGAGGC GAAACCCCTGGAATATTCCCGACCTGGCAGC CTCATCGAGCTCGGTGATTGGCTCAGAAGGG AAAAGGCGGGTCTCCGTGACGACTTATAAAA GCCCAGGGGCAAGCGGTCCGGATAACGGCT AGCCTGAGGAGCTGCTGCGACAGTCCACTAC CTTTTTCGAGAGTGACTCCCGTTGTCCCAAG GCTTCCCAGAGCGAACCTGTGCGGCTGCAGG CACCGGCGCGTCGAGTTTCCGGCGTCCGGAA GGACCGAGCTCTTCTCGCGGATCC
SV40 with Enhancer	Promoter	GTGTGTCAGTTAGGGTGTGGAAAGTCCCCAG GCTCCCCAGGCAGGCAGAAGTATGCAAAGC ATGCATCTCAATTAGTCAGCAACCAGGTGTG GAAAGTCCCCAGGCTCCCCAGCAGGCAGAA GTATGCAAAGCATGCATCTCAATTAGTCAGC AACCATAGTCCCGCCCCTAACTCCGCCCATC CCGCCCCTAACTCCGCCCAGTTCCGCCCATTC TCCGCCCCATGGCTGACTAATTTTTTTTATTT ATGCAGAGGCCGAGGCCGCCTCTGCCTCTGA GCTATTCCAGAAGTAGTGAGGAGGCTTTTTT GGAGGCCTAGGCTTTTGCAAA
CMV with Enhancer	Promoter	GACATTGATTATTGACTAGTTATTAATAGTA ATCAATTACGGGGTCATTAGTTCATAGCCCA TATATGGAGTTCCGCGTTACATAACTTACGG TAAATGGCCCGCCTGGCTGACCGCCCAACGA CCCCCGCCCATTGACGTCAATAATGACGTAT GTTCCCATAGTAACGCCAATAGGGACTTTCC ATTGACGTCAATGGGTGGACTATTTACGGTA AACTGCCCACTTGGCAGTACATCAAGTGTAT CATATGCCAAGTACGCCCCCTATTGACGTCA ATGACGGTAAATGGCCCGCCTGGCATTATGC CCAGTACATGACCTTATGGGACTTTCCTACTT GGCAGTACATCTACGTATTAGTCATCGCTAT

		TACCATGGTGATGCGGTTTTGGCAGTACATC AATGGGCGTGGATAGCGGTTTGACTCACGGG GATTTCCAAGTCTCCACCCCATTGACGTCAA TGGGAGTTTGTTTTGGCACCAAAATCAACGG GACTTTCCAAAATGTCGTAACAACTCCGCCC CATTGACGCAAATGGGCGGTAGGCGTGTACG GTGGGAGGTCTATATAAGCAGAGCT
taRNA	Regulatory RNA	ACCCAAATCCAGGAGGTGATTGGTAGTGGTG GTTAATGAAAATTAACTTACTACTACCATAT ATC
crRNA-RBS	Regulatory RNA	TACCATTCACCTCTTGGATTTGGGTATTAAAG AGGAGAAA
Nuclear Localization Signal	Regulatory	CCAAAGAAGAAACGGAAGGTG
Kozak	Regulatory	GCCGCCATG
eGFP	CDS	ATGCGTAAAGGAGAAGAACTTTTCACTGGAG TTGTCCCAATTCTTGTTGAATTAGATGGTGAT GTTAATGGGCACAAATTTTCTGTCAGTGGAG AGGGTGAAGGTGATGCAACATACGGAAAAC TTACCCTTAAATTTATTTGCACTACTGGAAAA CTACCTGTTCCATGGCCAACACTTGTCACTAC TTTCGGTTATGGTGTTCAATGCTTTGCGAGAT ACCCAGATCATATGAAACAGCATGACTTTTT CAAGAGTGCCATGCCCGAAGGTTATGTACAG GAAAGAACTATATTTTTCAAAGATGACGGGA ACTACAAGACACGTGCTGAAGTCAAGTTTGA AGGTGATACCCTTGTTAATAGAATCGAGTTA AAAGGTATTGATTTTAAAGAAGATGGAAACA TTCTTGGACACAAATTGGAATACAACTATAA CTCACACAATGTATACATCATGGCAGACAAA CAAAAGAATGGAATCAAAGTTAACTTCAAA ATTAGACACAACATTGAAGATGGAAGCGTTC AACTAGCAGACCATTATCAACAAAATACTCC AATTGGCGATGGCCCTGTCCTTTTACCAGAC AACCATTACCTGTCCACACAATCTGCCCTTTC GAAAGATCCCAACGAAAAGAGAGACCACAT GGTCCTTCTTGAGTTTGTAACAGCTGCTGGG ATTACACATGGCATGGATGAACTATACAAAT AA
mEGFP	CDS	GTGAGCAAGGGCGAGGAGCTGTTCACCGGG GTGGTGCCCATCCTGGTCGAGCTGGACGGCG ACGTAAACGGCCACAAGTTCAGCGTGCGCGG CGAGGGCGAGGGCGATGCCACCAACGGCAA GCTGACCCTGAAGTTCATCTGCACCACCGGC AAGCTGCCCGTGCCCTGGCCCACCCTCGTGA CCACCCTGACCTACGGCGTGCAGTGCTTCAG CCGCTACCCCGACCACATGAAGCAGCACGAC TTCTTCAAGTCCGCCATGCCCGAAGGCTACG TCCAGGAGCGCACCATCTCCTTCAAGGACGA CGGCACCTACAAGACCCGCGCCGAGGTGAA GTTCGAGGGCGACACCCTGGTGAACCGCATC

		GAGCTGAAGGGCATCGACTTCAAGGAGGAC GGCAACATCCTGGGGCACAAGCTGGAGTAC AACTTCAACAGCCACAACGTCTATATCACGG CCGACAAGCAGAAGAACGGCATCAAGGCGA ACTTCAAGATCCGCCACAACGTCGAGGACGG CAGCGTGCAGCTCGCCGACCACTACCAGCAG AACACCCCCATCGGCGACGGCCCCGTGCTGC TGCCCGACAACCACTACCTGAGCACCCAGTC CAAGCTGAGCAAAGACCCCAACGAGAAGCG CGATCACATGGTCCTGCTGGAGTTCGTGACC GCCGCCGGGATCACTCTCGGCATGGACGAGC TGTACAAGTAG
HspR	CDS	ATGGCCAAAAATCCGAAAGATGGCGAAAGC CGCACCTTCCTGATTAGCGTGGCCGCCGAAC TGGCCGGTATGCATGCCCAGACCCTGCGCAC CTATGATCGTCTGGGTCTGGTGAGCCCGCGT CGTACCAGTGGTGGTGGTCGTCGTTATAGCC TGCATGATGTGGAGCTGCTGCGCCAGGTTCA GCATCTGAGCCAGGATGAAGGCGTGAATCTG GCCGGCATCAAACGCATCATTGAACTGACCA GCCAGGTGGAAGCACTGCAGAGCCGCCTGC AGGAAATGGCCGAAGAACTGGCCGTGCTGC GCGCCAATCAGCGTCGTGAAGTGGCCGTGGT GCCGAAAAGCACCGCCCTGGTGGTGTGGAA ACCGCGTCGTTAA
LuxR	CDS	ATGAAAAACATAAATGCCGACGACACATAC AGAATAATTAATAAAATTAAAGCTTGTAGAA GCAATAATGATATTAATCAATGCTTATCTGA TATGACTAAAATGGTACATTGTGAATATTAT TTACTCGCGATCATTTATCCTCATTCTATGGT TAAATCTGATATTTCAATCCTAGATAATTACC CTAAAAAATGGAGGCAATATTATGATGACGC TAATTTAATAAAATATGATCCTATAGTAGAT TATTCTAACTCCAATCATTCACCAATTAATTG GAATATATTTGAAAACAATGCTGTAAATAAA AAATCTCCAAATGTAATTAAAGAAGCGAAA ACATCAGGTCTTATCACTGGGTTTAGTTTCCC TATTCATACGGCTAACAATGGCTTCGGAATG CTTAGTTTTGCACATTCAGAAAAAGACAACT ATATAGATAGTTTATTTTTACATGCGTGTATG AACATACCATTAATTGTTCCTTCTCTAGTTGA TAATTATCGAAAAATAAATATAGCAAATAAT AAATCAAACAACGATTTAACCAAAAGAGAA AAAGAATGTTTAGCGTGGGCATGCGAAGGA AAAAGCTCTTGGGATATTTCAAAAATATTAG GTTGCAGTGAGCGTACTGTCACTTTCCATTTA ACCAATGCGCAAATGAAACTCAATACAACA AACCGCTGCCAAAGTATTTCTAAAGCAATTT TAACAGGAGCAATTGATTGCCCATACTTTAA AAATTAA
LuxI	CDS	ATGACTATAATGATAAAAAAATCGGATTTTT TGGCAATTCCATCGGAGGAGTATAAAGGTAT

		TCTAAGTCTTCGTTATCAAGTGTTTAAGCAA AGACTTGAGTGGGACTTAGTTGTAGAAAATA ACCTTGAATCAGATGAGTATGATAACTCAAA TGCAGAATATATTTATGCTTGTGATGATACT GAAAATGTAAGTGGATGCTGGCGTTTATTAC CTACAACAGGTGATTATATGCTGAAAAGTGT TTTTCCTGAATTGCTTGGTCAACAGAGTGCTC CCAAAGATCCTAATATAGTCGAATTAAGTCG TTTTGCTGTAGGTAAAAATAGCTCAAAGATA AATAACTCTGCTAGTGAAATTACAATGAAAC TATTTGAAGCTATATATAAACACGCTGTTAG TCAAGGTATTACAGAATATGTAACAGTAACA TCAACAGCAATAGAGCGATTTTTAAAGCGTA TTAAAGTTCCTTGTCATCGTATTGGAGACAA AGAAATTCATGTATTAGGTGATACTAAATCG GTTGTATTGTCTATGCCTATTAATGAACAGTT TAAAAAAGCAGTCTTAAATGCTGCAAACGAC GAAAACTACGCTTTAGTAGCTTAA
CadR	CDS	ATGAAGATCGGAGAACTGGCCAAAGCCACC GACTGCGCCGTGGAAACCATCCGCTACTACG AGCGTGAACAGCTGCTGCCGGAGCCGGCAC GCAGCGACGGCAACTACCGGCTGTACACCCA GGCCCACGTCGAGCGGCTTACCTTCATCCGC AACTGCCGCACCCTGGACATGACCCTGGATG AAATCCGCAGCCTGCTACGCCTGCGCGACAG CCCCGATGATTCGTGCGGCAGCGTCAATGCG CTGATCGACGAGCATATCGAGCATGTGCAGG CACGGATCGATGGTCTGGTGGCGTTGCAGGA ACAGCTGGTGGAGCTGCGGCGGCGCTGCAAT GCACAAGGGGCGGAGTGTGCGATCTTGCAGC AACTGGAGACGAACGGGGCGGTATCGGTGC CGGAAACCGAGCATTCGCATGTAGGGCGAA GCCACGGGCATTAA
MerR(mut)	CDS	ATGGAGAACAATCTGGAGAACCTGACCATTG GCGTGTTTGCCAAAGCCGCCGGTGTGAACGT GGAAACCATCCGCTTCTATCAGCGCAAAGGT CTGCTGCGCGAACCGGATAAACCGTATGGCA GCATTCGCCGCTATGGTGAAGCCGATGTGGT GCGCGTGAAATTCGTGAAAAGCGCCCAGCGT CTGGGCTTTAGCCTGGACGAGATTGCCGACT TTCTGCGCATTGACGAAGGCACCGGTTGTGT GGGTCATGACGCCCTGGCCGAACATAAACTG AAGGATGTGCGCGAGAAAATGGCCGACCTG GCCCGCATGGAAACCGTGCTGAGCGAGCTGA CCGGTATGTGTAATCTGCCGCCGGGCAATGT GAGCTGTCCGCTGATTGAAAGCTTACAAGGT GAAGCAGGTCTGGCCCGTAGCGCAATGCCGT AA
GolS	CDS	ATGAACATCGGTAAAGCAGCTAAAGCATCG AAAGTCTCGGCCAAAATGATTCGCTACTATG AACAGATTGGTCTGATTCCCGCGGCAAGTCG GACGGATTCCGGCTATCGGGCCTATACCCAG

		GCTGATGTTAATCAATTGCATTTTATACGCCG CGCGCGCGACCTCGGTTTTTCAGTTGCTGAA ATCAGCGACTTACTGAATCTTTGGAATAACC AGTCGCGGCAAAGCGCTGACGTCAAACGCCT GGCGCAGACGCACATTGATGAACTGGACAG ACGTATCCAGAACATGCAGCACATGGCGCAA ACCCTCAAAGCGCTGATTCACTGCTGCGCCG GCGACGCGCTGCCAGATTGCCCCATTCTGCA TACGCTTGGACAACCTGACGATAGCGAGCCG GAGGCGCGTACCGGAGCGGTATTGCGACGTC CTCGTCGCCACGGACTGGCAAAGCGTCTGTA A
Bxb1	CDS	ATGGGAACGGTGGCGCAGATGGAATTAGAA GCGATCAAAGAGCGGAACCGTTCGGCTGCGC ATTTCAATATCCGCGCCGGGAAATACCGAGG ATCCCTGCCGCCGTGGGGATACCTGCCTACG CGCGTGGACGGGGAGTGGCGGCTGGTGCCG GACCCTGTGCAGCGAGAGCGCATCCTCGAGG TGTATCACCGCGTCGTCGACAACCACGAGCC GCTGCATCTGGTGGCCCACGACCTGAACCGG CGTGGTGTCCTGTCGCCGAAGGACTACTTCG CGCAGCTGCAAGGCCGCGAGCCGCAGGGCC GGGAGTGGTCGGCTACCGCGCTGAAGCGATC GATGATCTCCGAGGCGATGCTCGGGTACGCG ACTCTGAACGGTAAGACCGTCCGAGACGACG ACGGAGCCCCGCTGGTGCGGGCTGAGCCGAT CCTGACCCGTGAGCAGCTGGAGGCGCTGCGC GCCGAGCTCGTGAAGACCTCCCGGGCGAAGC CCGCGGTGTCTACCCCGTCGCTGCTGCTGCG GGTGTTGTTCTGCGCGGTGTGCGGGGAGCCC GCGTACAAGTTCGCCGGGGGAGGACGTAAG CACCCGCGCTACCGCTGCCGCTCGATGGGGT TCCCGAAGCACTGCGGGAACGGCACGGTGG CGATGGCCGAGTGGGACGCGTTCTGCGAGGA GCAGGTACTGGATCTGCTCGGGGACGCGGAG CGTCTGGAGAAAGTCTGGGTAGCGGGCTCGG ACTCCGCGGTCGAACTCGCGGAGGTGAACGC GGAGCTGGTGGACCTGACGTCGCTGATCGGC TCCCCGGCCTACCGGGCGGGCTCTCCGCAGC GAGAAGCACTGGATGCCCGTATTGCGGCGCT GGCCGCGCGGCAAGAGGAGCTGGAGGGCCT GGAGGCTCGCCCGTCTGGCTGGGAGTGGCGC GAGACCGGGCAGCGGTTCGGGGACTGGTGG CGGGAGCAGGACACCGCGGCAAAGAACACC TGGCTTCGGTCGATGAACGTTCGGCTGACGT TCGACGTCCGCGGCGGGCTGACTCGCACGAT CGACTTCGGGGATCTTCAGGAGTACGAGCAG CATCTCAGGCTCGGCAGCGTGGTCGAACGGC TACACACCGGGATGTCGTAA

* Engineered PibpA and PfxsA sequences were obtained from [82].

APPENDIX B

List of primers used in this study

Table B.1: Primer list used in this study

Primer	Sequence 5'-to-3'	Purpose
pBS1	CTCGAGAAAAGCACAAAAAATTTTTGCATCTCCCC	PdnaK GFP pZa construction
pBS2	ACGCGTTTTCTCCTCTTTCATCTAAACGTCTCCACTATATATTCG	
pBS3	GGGATGACCTCATTTAATCTCCAAAGAGGAGAAAGGTACCATGCGTAAAGGAGAAGAACT	PclpB GFP pZa construction
pBS4	CTCCTCTTTGGAGATTAAATGAGGTCATCCCTCAATTATTCAAGCTCGAGGACGTCGATATCTGG	
pBS5	GACGTCCTCGAGGAGCTCGAGGATTTCTACCGT	PfxsA GFP pZa construction
pBS6	GGTACCTCCCGATCCGTCGTGCTTTCTTTAGCTTATATTGTGGTCATTAGCAA	
pBS7	CTCGAGGAGCTCAAAATAACATCATCATT	PibpA GFP pZa construction
pBS8	GGTACCCCCTAATTCCGTTTATGGACCGATGTAAAAATGGGTCTGGA	
pBS9	ACGTCTCATTTTCGCCACTGCAGAAAAGCACAAAAAATTTTTGCA	Primers for PdnaK-taRNA extension to construct PdnaK riboswitch sensor plasmid
pBS10	TCATTAACCACCACTACCAATCACCTCCTGGATTTGGGTGTCGACCATCTAAACGTCTCCACTATATA	
pBS11	TGGTAGTGGTGGTTAATGAAAATTAACTTACTACTACCATATATCAAGCTTGGCATCAAATAAAACGAAAGGCTCAGTCG	Primers for taRNA-terminator extension to construct PdnaK riboswitch sensor plasmid
pBS12	TGCAAAAATTTTTTGTGCTTTTCTCGAGTCTAGGGCGGCGGATTTGTCCT	
pBS13	GTAGGACAAATCCGCCGCCCTAGACTCGAGAAAAGCACAAAAAATTTTTGCATCTCC	Primers for PdnaK-crRNA extension to construct PdnaK riboswitch sensor plasmid
pBS14	TAATACCCAAATCCAAGAGGTGAATGGTAGGATCCCATCTAAACGTCTCCACTATATATTCGGTC	
pBS15	TTCACCTCTTGGATTTGGGTATTAAAGAGGAGA	Primers for

	AAGGTACCATGCGTAAAGGAGA	crRNA-GFP extension to construct PdnaK riboswitch sensor plasmid
pBS16	AGCCTTTCGTTTTATTTGATGCCCTTAAGTTATTTGTATAGTTCATCCATGCCAT	
pBS17	TGCCGATCAACGTCTCATTTTCGCCACTGCAGGAGCTCGAGGATTTCTACC	Primers for PfxsA-taRNA extension to construct PfxsA riboswitch sensor plasmid
pBS18	CCACTACCAATCACCTCCTGGATTTGGGTGTCGACTTTAGCTTATATTGTGGTCATTAGCA	
pBS19	GTAGGACAAATCCGCCGCCCTAGACTCGAGGAGCTCGAGGATTTCTACC	Primers for PfxsA-crRNA extension to construct PfxsA riboswitch sensor plasmid
pBS20	TAATACCCAAATCCAAGAGGTGAATGGTAGGATCCTTTAGCTTATATTGTGGTCATTAGCA	
pBS21	CTGCAGTGGCGAAAATGAGACGTTGAT	REV primer for backbone extension to construct PibpA riboswitch sensor plasmid (coupled with pBS7)
pBS22	ACGTGCCGATCAACGTCTCATTTTCGCCACTGCAGGAGCTCAAAATAACATCATCATTAC	Primers for PibpA-taRNA fragment gene extension to construct PibpA riboswitch sensor plasmid
pBS23	GCGACGTAATGATGATGTTATTTTGAGCTCCTCGAGTCTAGGGCGGCG	
pBS24	TCATTTTCGCCAGATATCGACGTCCTCGAGGAATTCCGACCCGCACGA	Primers for mtPdnaK extension from gDNA
pBS25	ACGCATGGTACCACGCGTTTTCTCCTCTTTGGTGAATCCTCCTGAATATGTAGAG	
pBS26	AGATGAGTAAGTTGAGTGCATCAGGCTCAGAAAGAGGAGAAAACGCGT	Primers for to add IR2 to PdnaK-GFP-pZa
pBS27	TCTTTCTGAGCCTGATGCACTCAACTTACTCATCTAAACGTCTCCACTATA	
pBS28	CTCAGAGTAAGTTGAGTGCATCAGGCTCAGAAAGAGGAGAAAACGCGT	Primers for to add IR2-IR2 to PdnaK-GFP-pZa
pBS29	CCTGATGCACTCAACTTACTCTGAGCCTGATGCACTCAACTTACTCATCTAAACGTCTCCACTATA	
pBS30	ATGGCAAGCTTGAGCGGGGTGCACTCATCAAAAGAGGAGAAAACGCGT	Primers for to add IR3 to PdnaK-GFP-
pBS31	TTTTGATGAGTGCACCCCGCTCAAGCTTGCCATC	

	TAAACGTCTCCACTATA	pZa
pBS32	ACTCATCAGCAAGCTTGAGCGGGGTGCACTCATCAAAAGAGGAGAAAACGCGT	Primers for to add IR3-IR3 to PdnaK-GFP-pZa
pBS33	CACCCCGCTCAAGCTTGCTGATGAGTGCACCCCGCTCAAGCTTGCCATCTAAACGTCTCCACTATA	
pBS34	GTTTAACTTTTACTAGAGAAAGAGGAGAAAGGTACCATGGCCAAAAATCCG	Primers for HspR expression vector cloning
pBS35	CTCGAGTTAGTGGTGGTGGTGGTGGTGGCTACCGCCACGACGCGGTTTCCACA	
pBS36	TAGCAGCCGGATCTCAGTGGTGGTGGTGGTGGTGCTCGAGACCGCTACCGCCACGA	Gibson Assembly primers for HspR expression vector cloning
pBS37	CTATAGGGGAATTGTGAGCGGATAACAATTCCCCTCTAGAAAAGAGGAGAAAGGTACCATGGC	
pBS38	CCATGGCCAACACTTGTCAC	qPCR primers for *egfp*
pBS39	GGGCATGGCACTCTTGAAAA	
pBS40	GCTGCTCGGCTTTCTCATCC	qPCR primers for *hcaT* **
pBS41	CCAACCACGCTGACCAACC	
pBS42	AGCTGATCACCAAACTGGACC	qPCR primers for *sodA** **
pBS43	CGCTTTTTCAAATTCTGC	
pBS44	GCCGATCAACGTCTCATTTTC	Promoter extension primers for EMSA
pBS45	GGTACCACGCGTTTTCTCCT	
pBS46	AAAATGGTTTGTTATAGTCGAATAAAAAAGAGGAGAAAGGTACCACGCGTGGCATCAAATAAAAC	Primers for pZa linear vector extension to construct quorum sensing plasmid
pBS47	TTTCTCCTCTTTGCTAGCATTATACCTAGGACTGAGCTAGCTGTCAAGACGTCGATATCTGGCGAAAA	
pBS48	CTGCAGCAAATAAAACGAAAGGCTCAGT	Primers for rrnBT1-Plux extension to construct quorum sensing plasmid
pBS49	CTTGCGTAAACCTGTACGATCCTACAGGTGTCGACATTTGTCCTACTCAGGAGAGC	
pBS50	ACCCATCGGTCTCGAAGGATCCATGAAAAACATAAAT	Primers for luxR-BsaI extension to construct quorum sensing plasmid
pBS51	ACCCATCGGTCTCGGCTCGAGTTAATTTTTAAAGTATGG	
pBS52	ACCCATCGGTCTCGGCATGACTATAATGATAAAAAAATCGG	Primers for luxI-BsaI

pBS53	ACCCATCGGTCTCGAGTTAAGCTACTAAAGCGTAGT	extension to construct quorum sensing plasmid
pBS54	ACCCATCGGTCTCCCTAAAAGCACAAAAAATTTTTGCATCTCCCC	Primers for PdnaK-BsaI extension to construct quorum sensing plasmid
pBS55	ACCCATCGGTCTCCATGCGGCCGCTTTCTCCTCT	
pBS56	ACCCATCGGTCTCGGAGCAAATAAAACGAAAGGCTC	Primers for rrnBT1-BsaI extension to construct quorum sensing plasmid
pBS57	ACCCATCGGTCTCGTTAGATCTATTTGTCCTACTCAG	
pBS58	ACCCATCGGTCTCGAACTGCAGCAAATAAAACGA	Primers for rrnBT1-Plux-BsaI extension to construct quorum sensing plasmid
pBS59	ACCCATCGGTCTCGTTCTTGCGTAAACCTGTACG	
pBS60	ACCCATCGGTCTCCAGAAAATGGTTTGTTATAGTCGA	Primers for pZa-BsaI linear vector extension to construct quorum sensing plasmid
pBS61	ACCCATCGGTCTCCCCTTTCTCCTCTTTGCTAGC	
pBS62	AACGCTCTCCTGAGTAGGACAAATGTCGACAAAAGCACAAAAAATTTTTGC	Primers for PdnaK extension to construct quorum sensing plasmid
pBS63	ATTTTTTTATCATTATAGTCATGCGGCCGCTTTCTCCTCTTTCATCTAAAC	
pBS64	CGTTTAGATGAAAGAGGAGAAAGCGGCCGCATGACTATAATGATAAAAAAATCGG	Primers for luxI extension to construct quorum sensing plasmid
pBS65	CGACTGAGCCTTTCGTTTTATTTGCTGCAGTTAAGCTACTAAAGCGTAGTT	
pBS66	GAAAACTACGCTTTAGTAGCTTAACTGCAGCAAATAAAACGAAAGGCTCAGTC	Primers for rrnBT1 extension to construct quorum
pBS67	GTAAACCTGTACGATCCTACAGGTAGATCTATTTGTCCTACTCAGGAGAGC	

		sensing plasmid
pBS68	ACGCGTATGGAGACCAACACCCTTCC	Primers for Phsp70 to isolate from the HEK293T genome
pBS69	GGATCCGCGAGAAGAGCT	
pBS70	GCGCTGCTTCGCGATGTACGGGCCAGATATACGCGTATGGAGACCAACA	Primers for Phsp70 to construct eukaryotic Phsp70 GFP pcDNA3 vector
pBS71	CCCGGTGAACAGCTCCTCGCCCTTGCTCACGGATCCGCGAGAAGAGCT	
pBS72	AGACCCAAGCTTGGTACCGAGCTCGGATCCATGGCCAAAAATCCGAAAGAT	Primers for HspR to construct eukaryotic CMV HspR-His pcDNA3 vector
pBS73	AGGTGACACTATAGAATAGGGCCCTCTAGATTAGTGGTGGTGGTGGT	
pBS74	CCAAGCTTGGTACCGAGCTCGGATCCATGCATCATCATCATCATCATGGCGGTAGCGGTGCCAAAAATCCGAAAGATGGC	Primers for HspR to construct eukaryotic CMV His-HspR-NLS pcDNA3 vector
pBS75	GACACTATAGAATAGGGCCCTCTAGATTACACCTTCCGTTTCTTCTTTGGACGACGCGGTTTCCACAC	
pBS76	TACTGCCATTTGTCTCGAGGTCGAGAATTCCCATAGAGCCCACCGCAT	Primers for SV40-GFP-polyA to construct eukaryotic SV40 GFP MeCP2 vector
pBS77	ATTAAGGTACGGGAGGTACTTGGAACGCGTGTGTGTCAGTTAGGGTGT	
pBS78	ATTTCCCCGAAAAGTGCCACCTGACACGCGTGTGTGTCAGTT	Primers for SV40-IR3 to construct eukaryotic SV40-IR3 GFP MeCP2 vector
pBS79	TGAGTGCACCCCGCTCAAGCTTGCCTCGAGTTTGCAAAAGCCTAGGCC	
pBS80	AGCTTGAGCGGGGTGCACTCATCAGTCGACGCCGCCATGGTGAGCAA	Primers for GFP-polyA to construct eukaryotic SV40-IR3 GFP MeCP2 vector
pBS81	AGCCTCCCCCGTTTAAACTCATTACTAACCGGTAGGGATCGAATTCCCATAGAGCCCACCG	
pBS82	CGCTCTCCTGAGTAGGACAAATCCACTAGTACTGGATTGCCATTCTCTC	Primers for Bxb1-attP to construct mProD HspR
pBS83	CCAACACTGGCAAGGTCCAGACTGGCAACAGTCGGGGTTTGTACCGT	

		PgolB GFP pET22b vector
pBS84	TGCCAGTCTGGACCTTGCCAGTGTTGGAAGGTCAAGGCCCGGATGATCCTGA	Primers for Bxb1-attB to construct mProD HspR PgolB GFP pET22b vector
pBS85	CCTTTACGCATGGTACCACGCGTTTTCTCCTCTTTCGGCCTCTAAAGTAGAGC	
pBS86	CGACAAGCCGGCCGACAGCTCTACTTTAGAGGCCGAAAGAGGAGAAAACGCG	Primers for GFP-rrnBT1 to construct mProD HspR PgolB GFP pET22b vector
pBS87	TTAGCAGCCGGATCTCAGTGGTGGTGGTGGTGGTGATTTGTCCTACTCAGGAGA	
pBS88	AGCGGGGTGCACTCATCAAAAGAGGAGAAAGGTACCATGGGAACGGTG	Primers for Bxb1 to construct PdnaK-IR3-IR3 Bxb1 GolS pZa
pBS89	GCTTTACCGATGTTCATTTTCTCCTCTTTACGCGTTTACGACATCCCGGTGTG	
pBS90	CGGCTACACACCGGGATGTCGTAAACGCGTAAAGAGGAGAAAATGAACATCGG	Primers for GolS to construct PdnaK-IR3-IR3 Bxb1 GolS pZa
pBS91	GAGCCTTTCGTTTTATTTGATGCCCTGCAGTTACAGACGCTTTGCCAGT	
pBS92	GAACGGCTACACACCGGGATGTCGTAAACGCGTATTAAAGAGGAGAAAGGTACCA	Primers for CadR to construct PdnaK-IR3-IR3 Bxb1 CadR pZa
pBS93	GAGCCTTTCGTTTTATTTGATGCCCTGCAGTTAATGCCCGTGGCTTC	
pBS94	AGCGGGGTGCACTCATCAAAAGAGGAGAAAGGTACCATGGGAACGGTG	Primers for Bxb1 to construct PdnaK-IR3-IR3 Bxb1 CadR pZa
pBS95	TCTTCATGGTACCTTTCTCCTCTTTAATACGCGTTTACGACATCCCGGTGTG	
pBS96	TGCCAAGTGAACACCCTGTAGCCACTATAGGGTCAAGCCGCCCGGATGATCCTGAC	Primers for backbone to construct mProD HspR PcadA GFP pET22b vector
pBS97	CTATAGTGGCTACAGGGTGTTCACTTGGCAACAGGCGTCGGGGTTTGTACCGT	
pBS98	CTGAGGCCTGCAGGGATCCAAGCTTTTACGGCATTGCGCTACG	Primers for MerR(mutated) to construct mProD MerR (mutated) pZs vector
pBS99	TAGCTACTAGAGAAAGAGGAGAAAGGTACCATGGAGAACAATCTGGAGAACC	
pBS100	GTTGCTACAGGGTGTGCAATGAAAGAGGGGACAAACTAGAGGTACCATGCGTAAAGGAGAA	Primers for backbone to

pBS101	CCCTCTTTCATTGCACACCCTGTAGCAACTACAG AGTCAAGTCGACTGAGCAAAAGGC	construct PcadA GFP pET22b vector

****** qPCR primers of *hcaT* were obtained from [218].

******* qPCR primers of *soda* were obtained from [219].

APPENDIX C

Plasmid maps used in this study

Plasmid maps used in Chapter 2:

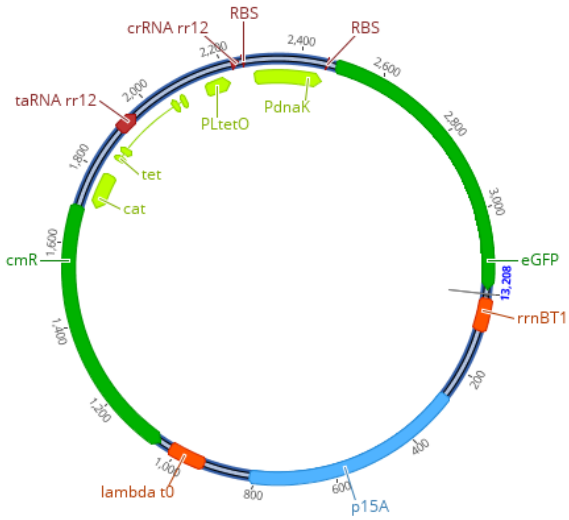

Figure C.1: Schematic representation of PdnaK GFP pZa-tet vector.

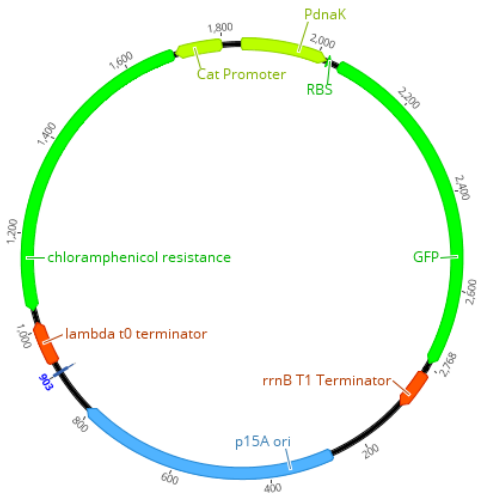

Figure C.2: Schematic representation of PdnaK GFP pZa vector.

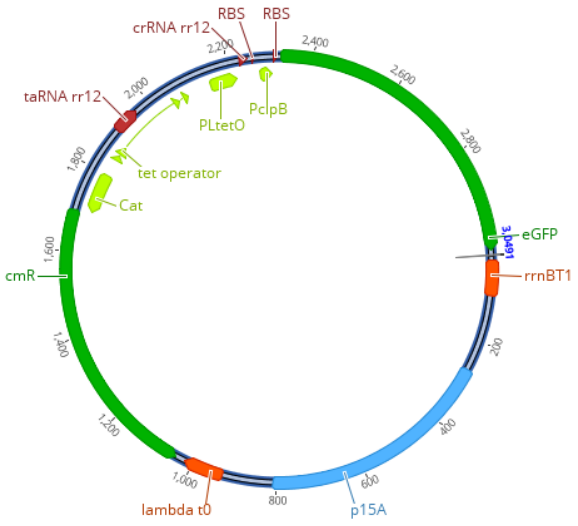

Figure C.3: Schematic representation of PclpB GFP pZa-tet vector.

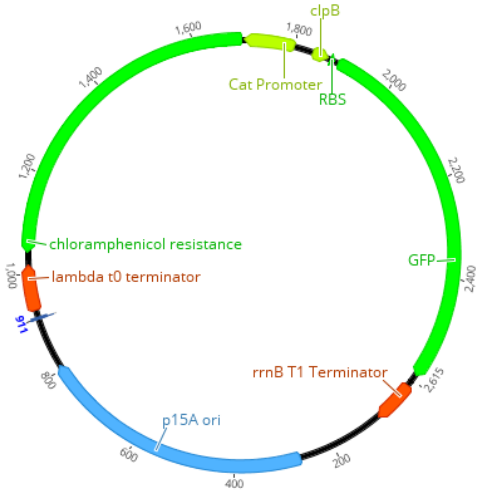

Figure C.4: Schematic representation of PclpB GFP pZa vector.

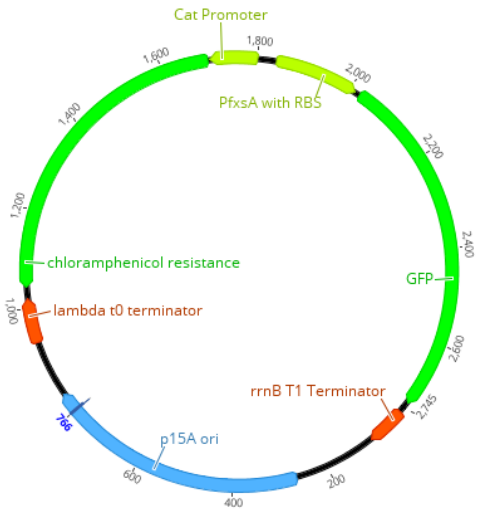

Figure C.5: Schematic representation of PfxsA GFP pZa vector.

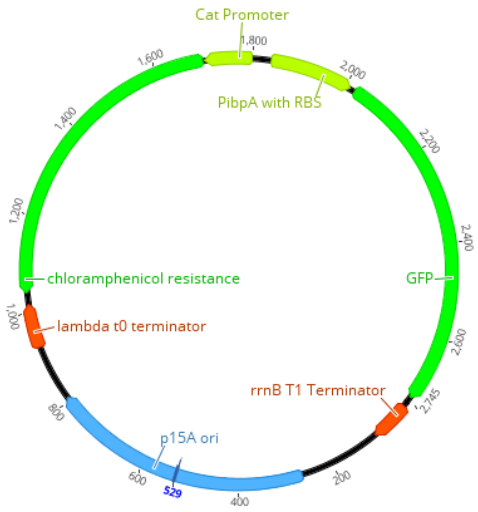

Figure C.6: Schematic representation of PibpA GFP pZa vector.

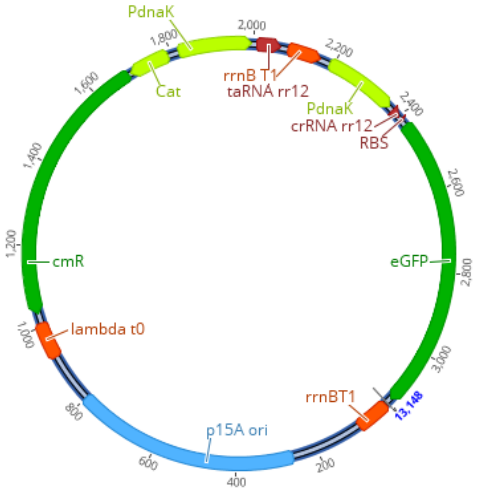

Figure C.7: Schematic representation of PdnaK riboswitch GFP pZa vector.

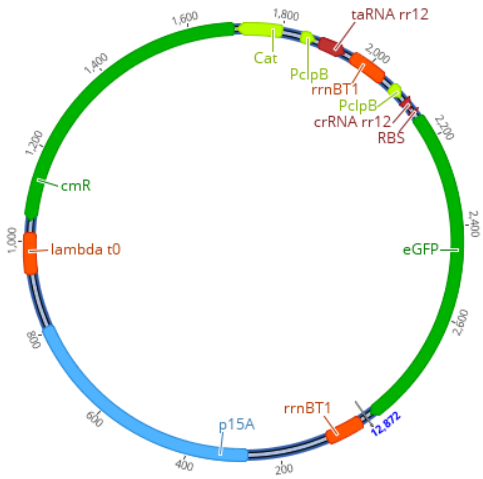

Figure C.8: Schematic representation of PclpB riboswitch GFP pZa vector.

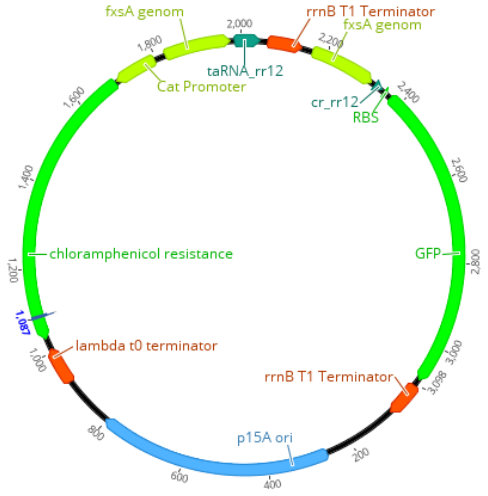

Figure C.9: Schematic representation of PfxsA riboswitch GFP pZa vector.

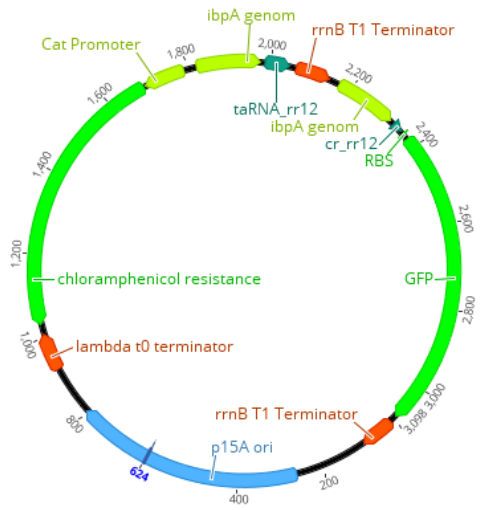

Figure C.10: Schematic representation of PibpA riboswitch GFP pZa vector.

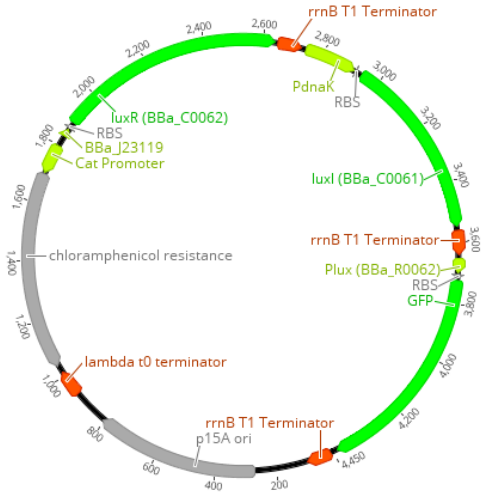

Figure C.11: Schematic representation of engineered quorum sensing vector.

Plasmid maps used in Chapter 3:

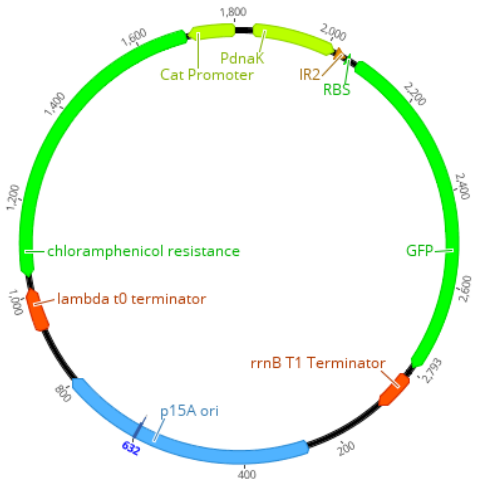

Figure C.12: Schematic representation of PdnaK-IR2 GFP pZa vector.

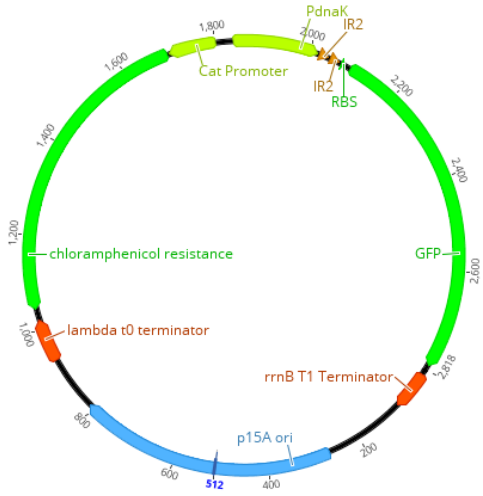

Figure C.13: Schematic representation of PdnaK-IR2-IR2 GFP pZa vector.

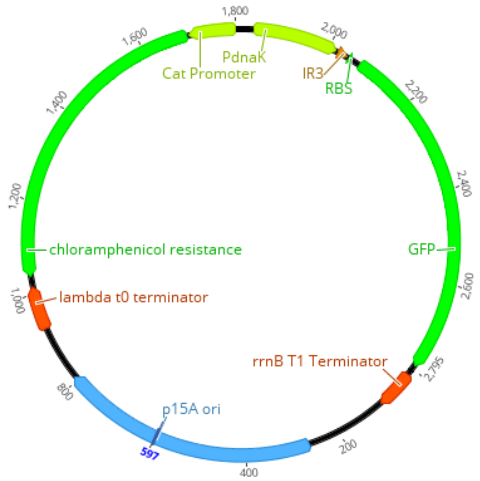

Figure C.14: Schematic representation of PdnaK-IR3 GFP pZa vector.

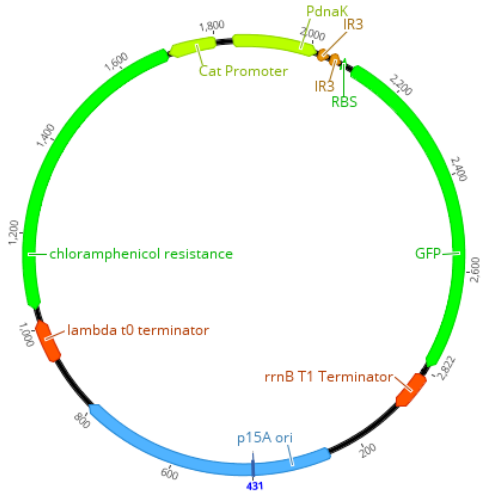

Figure C.15: Schematic representation of PdnaK-IR3-IR3 GFP pZa vector.

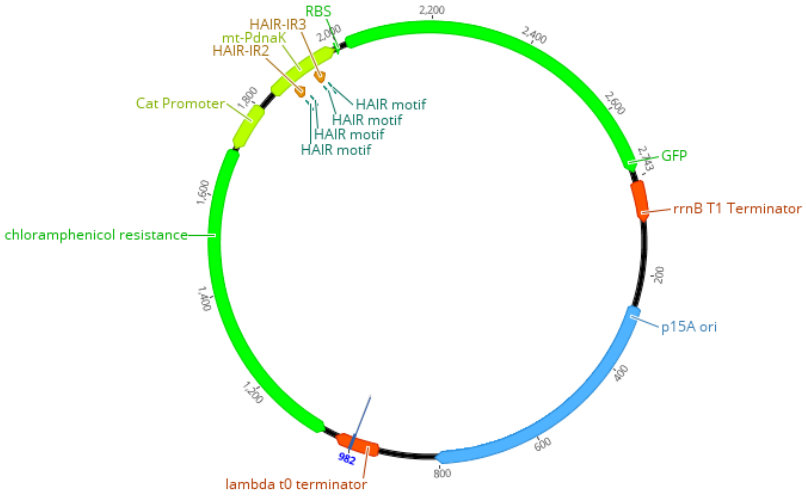

Figure C.16: Schematic representation of mtPdnaK GFP pZa vector.

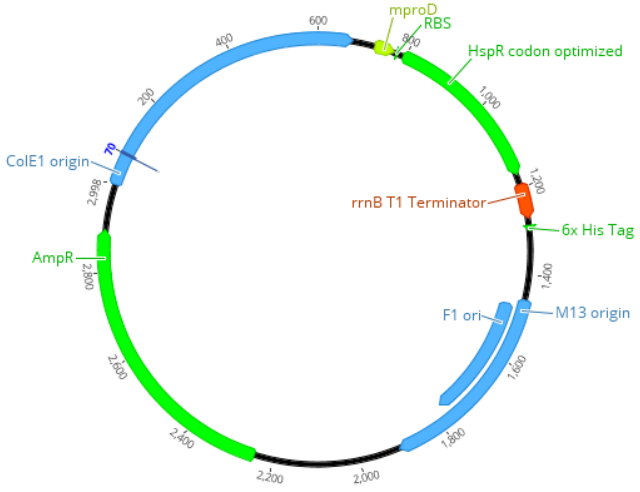

Figure C.17: Schematic representation of mProD HspR pET22b vector.

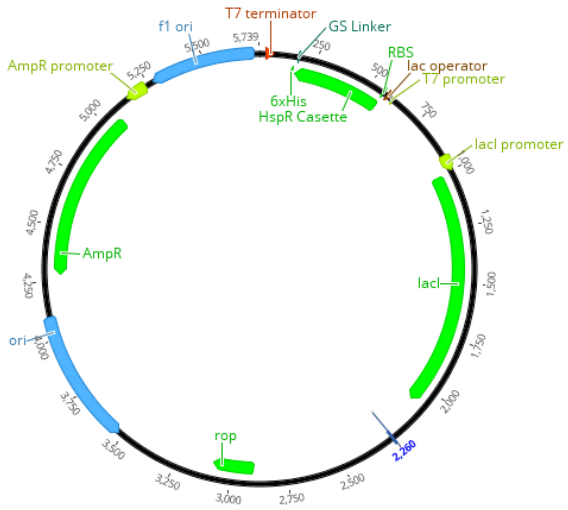

Figure C.18: Schematic representation of T7 HspR pET22b expression vector.

Plasmid maps used in Chapter 4:

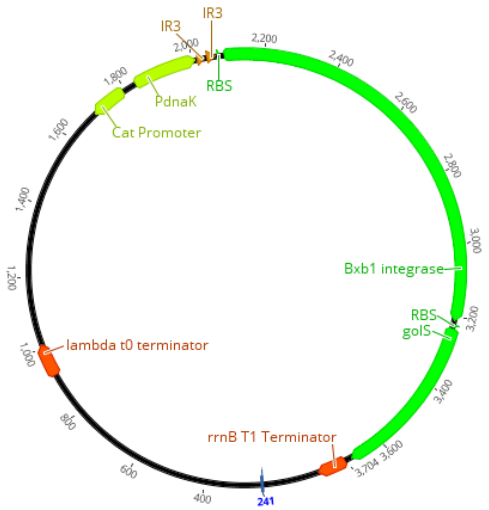

Figure C.19: Schematic representation of PdnaK-IR3-IR3 Bxb1 GolS pZa vector.

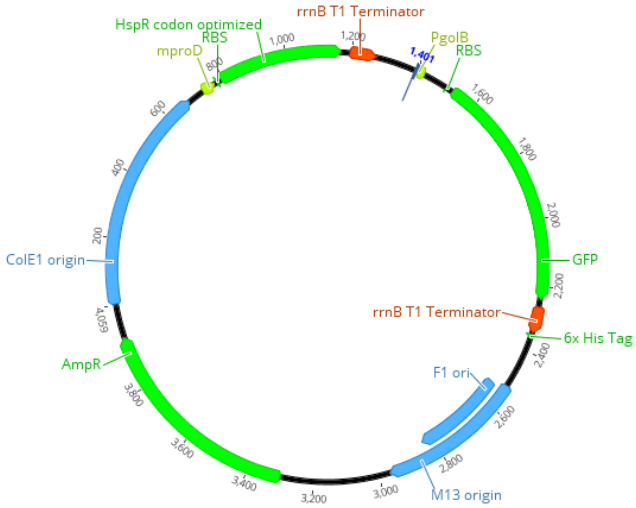

Figure C.20: Schematic representation of mProD HspR PgolB (inverted) GFP pET22b vector.

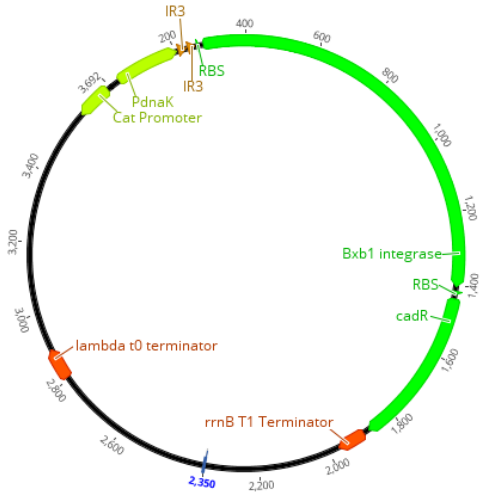

Figure C.21: Schematic representation of PdnaK-IR3-IR3 Bxb1 CadR pZa vector.

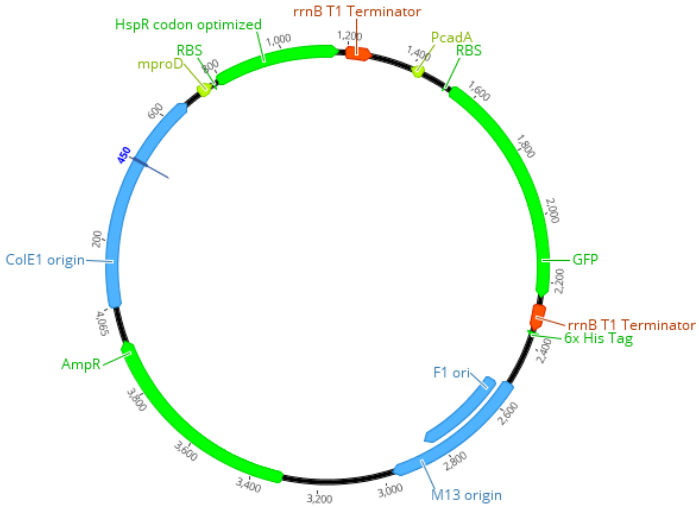

Figure C.22: Schematic representation of mProD HspR PcadA (inverted) GFP pET22b vector.

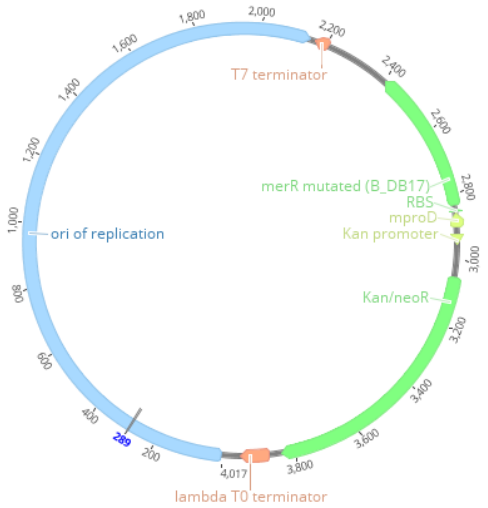

Figure C.23: Schematic representation of mProD MerR(mutated) pZs vector.

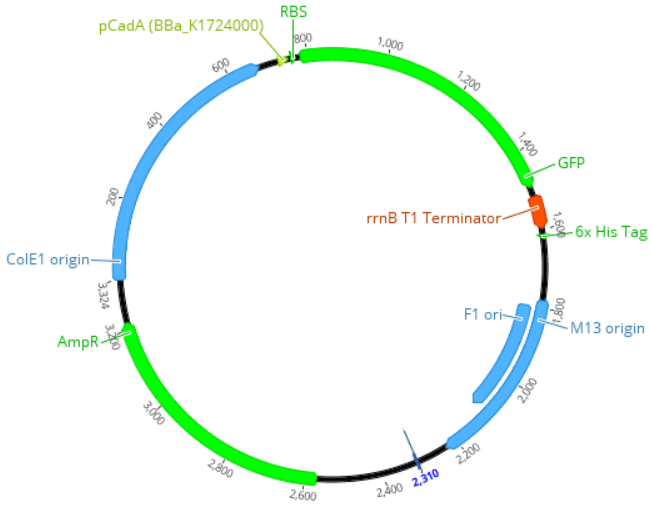

Figure C.24: Schematic representation of PcadA GFP pET22b vector.

Plasmid maps used in Chapter 5:

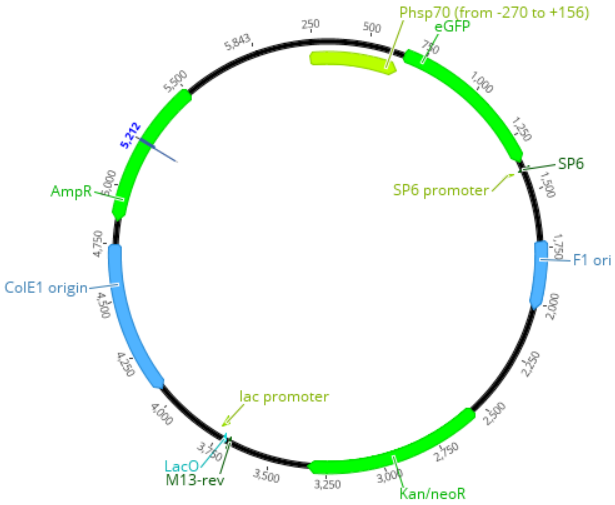

Figure C.25: Schematic representation of Phsp70 GFP pcDNA3 vector.

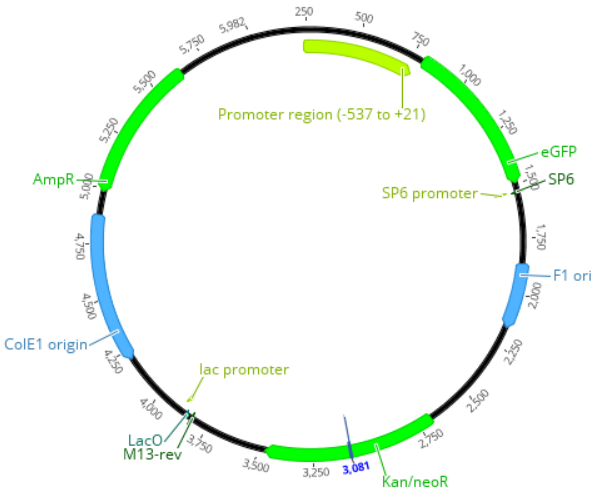

Figure C.26: Schematic representation of αB-crystallin (ABC) GFP pcDNA3 vector.

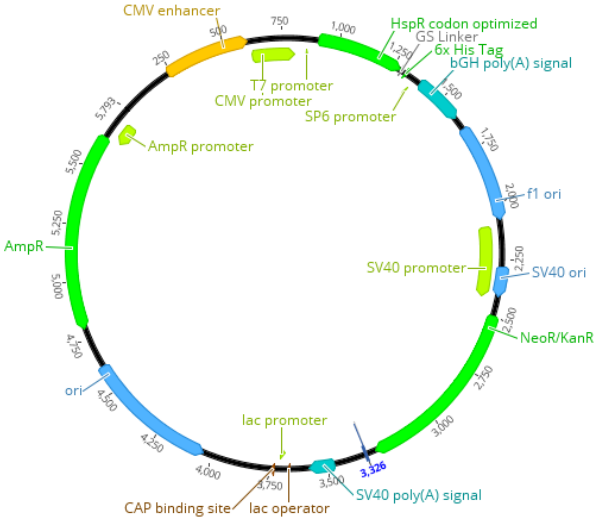

Figure C.27: Schematic representation of CMV HspR-6×His pcDNA3 vector.

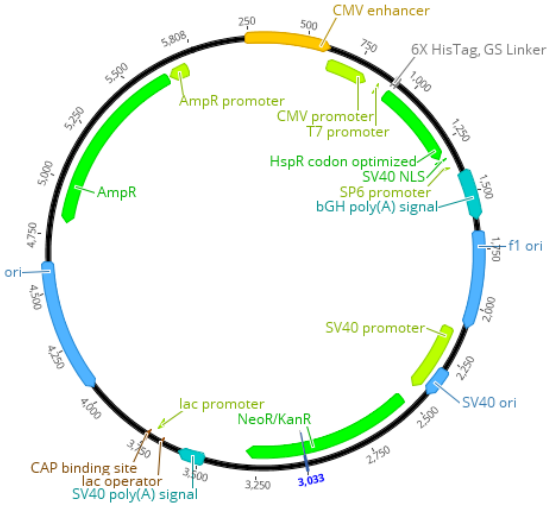

Figure C.28: Schematic representation of CMV 6×His-HspR-NLS pcDNA3 vector.

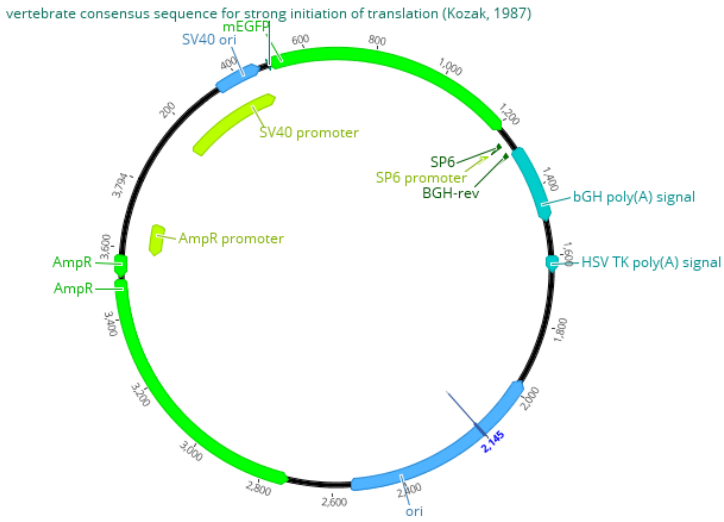

Figure C.29: Schematic representation of SV40 GFP MeCP2 vector.

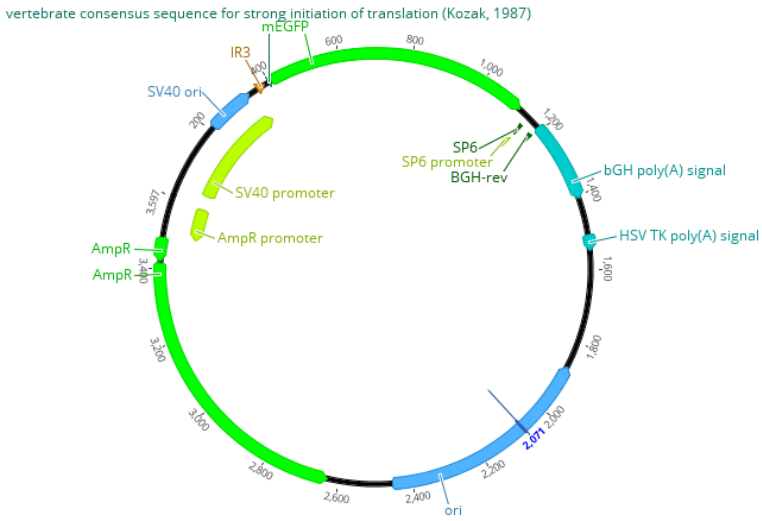

Figure C.30: Schematic representation of SV40-IR3 GFP MeCP2 vector.

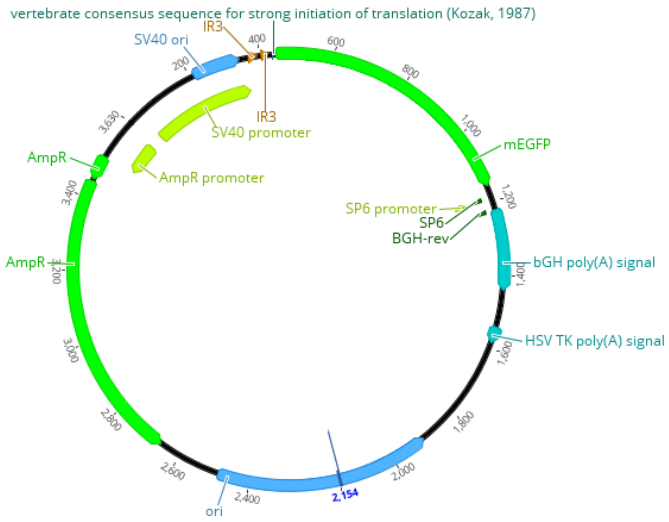

Figure C.31: Schematic representation of SV40-IR3-IR3 GFP MeCP2 vector.

APPENDIX D

Sanger sequencing results of the plasmids in this thesis

Sanger sequencing results of vectors used in Chapter 2:

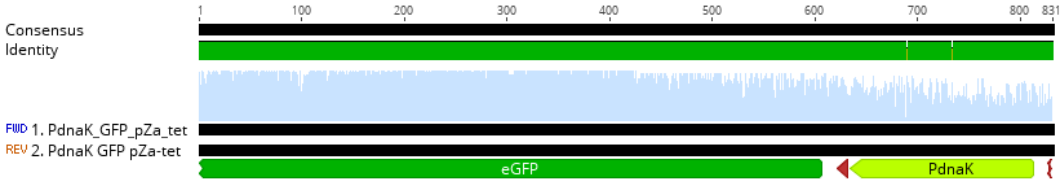

Figure D.1: Sanger sequencing results of PdnaK GFP pZa-tet vector.

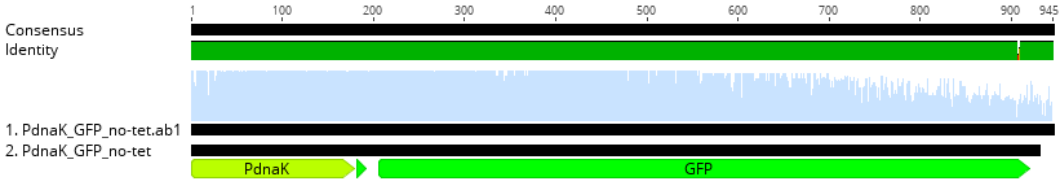

Figure D.2: Sanger sequencing results of PdnaK GFP pZa vector.

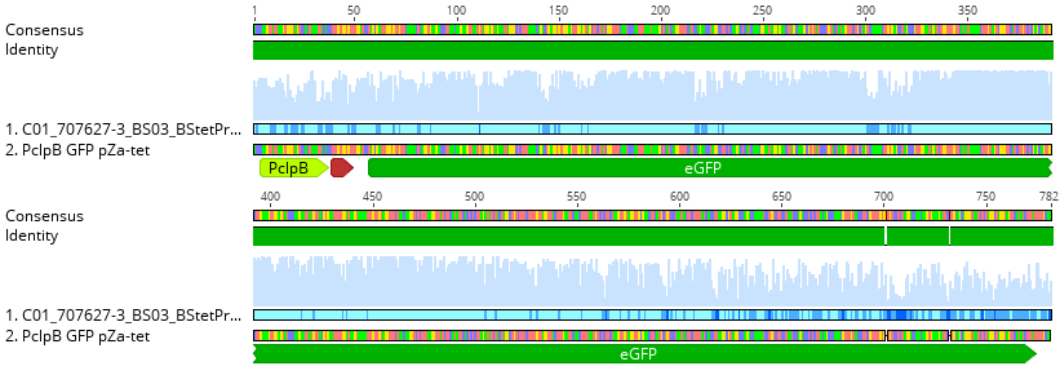

Figure D.3: Sanger sequencing results of PclpB GFP pZa-tet vector.

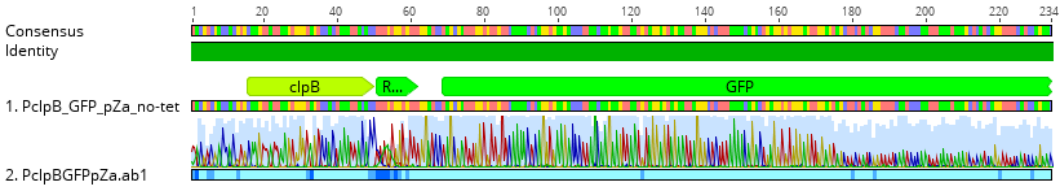

Figure D.4: Sanger sequencing results of PclpB GFP pZa vector.

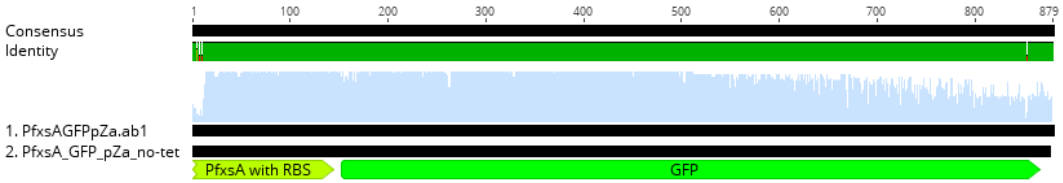

Figure D.5: Sanger sequencing results of PfxsA GFP pZa vector.

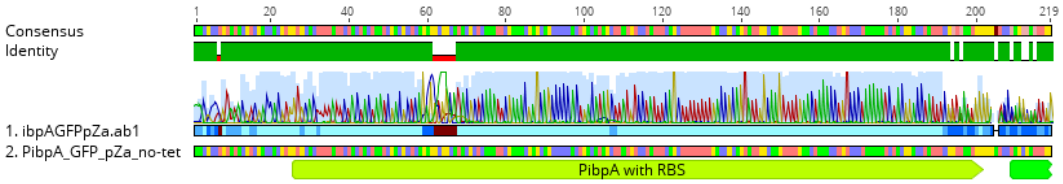

Figure D.6: Sanger sequencing results of PibpA GFP pZa vector.

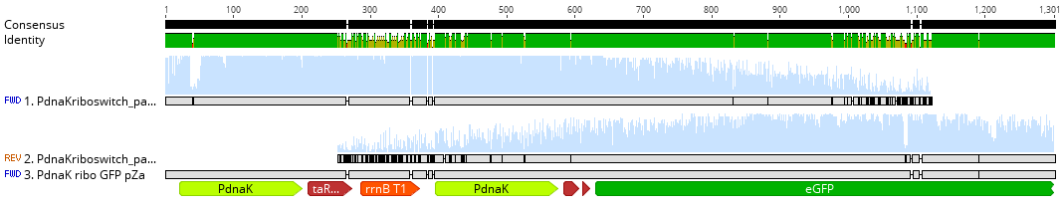

Figure D.7: Sanger sequencing results of PdnaK riboswitch GFP pZa vector.

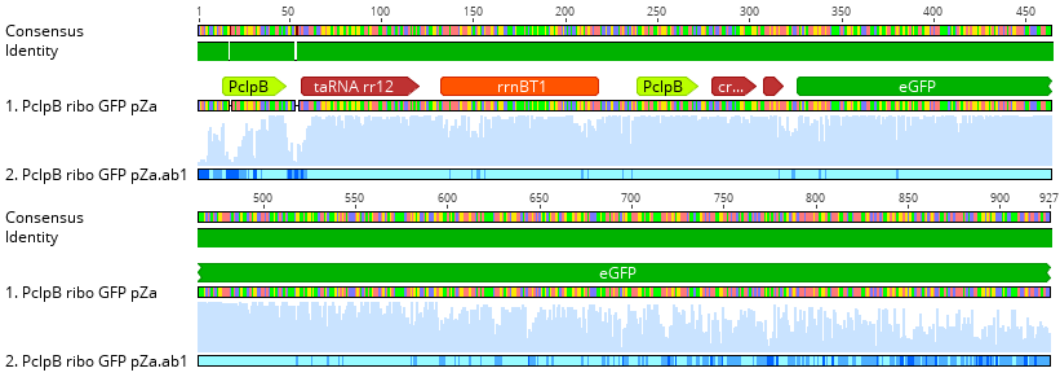

Figure D.8: Sanger sequencing results of PclpB riboswitch GFP pZa vector.

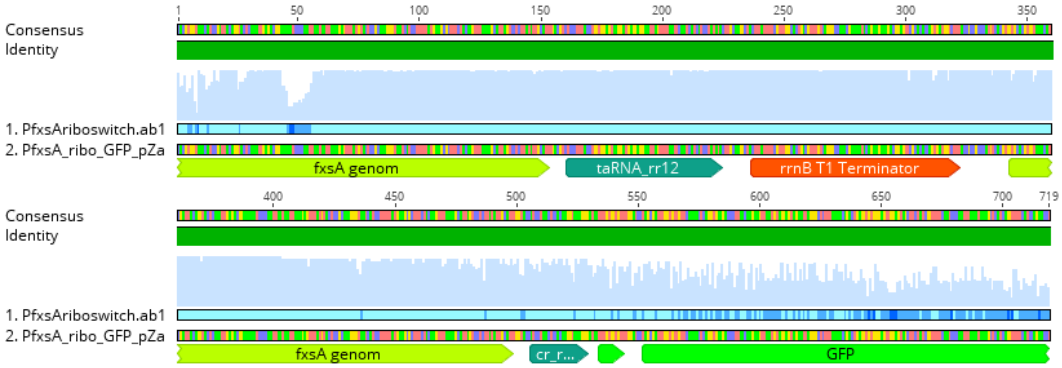

Figure D.9: Sanger sequencing results of PfxsA riboswitch GFP pZa vector.

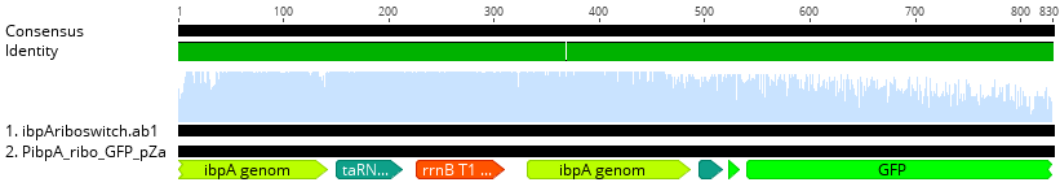

Figure D.10: Sanger sequencing results of PibpA riboswitch GFP pZa vector.

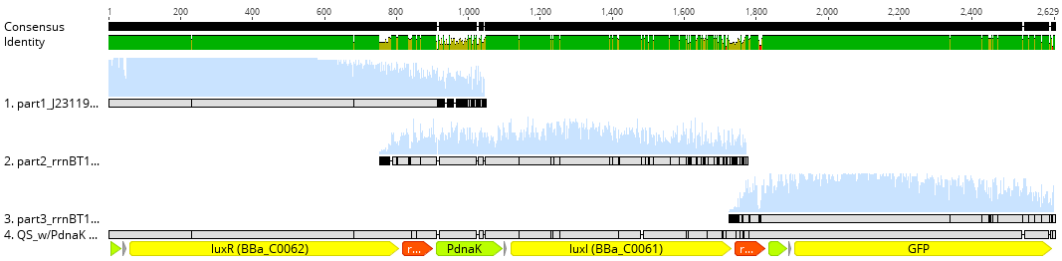

Figure D.11: Sanger sequencing results of engineered quorum sensing vector.

Sanger sequencing results of vectors used in Chapter 3:

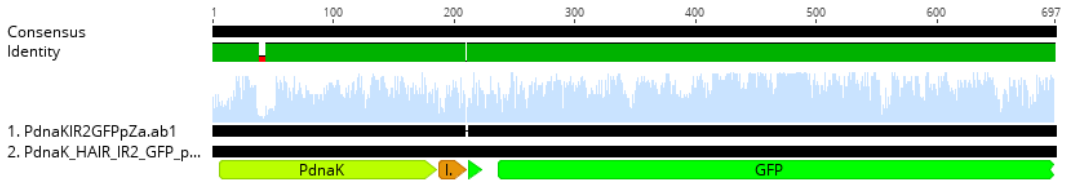

Figure D.12: Sanger sequencing results of PdnaK-IR2 GFP pZa vector.

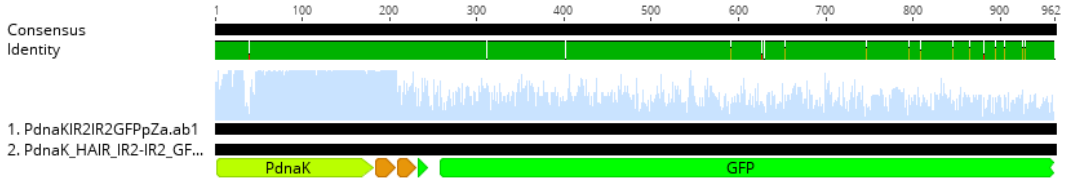

Figure D.13: Sanger sequencing results of PdnaK-IR2-IR2 GFP pZa vector.

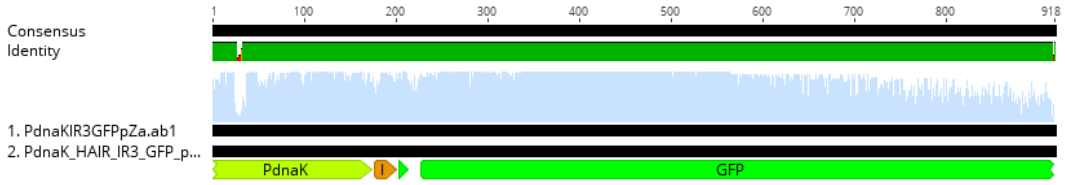

Figure D.14: Sanger sequencing results of PdnaK-IR3 GFP pZa vector.

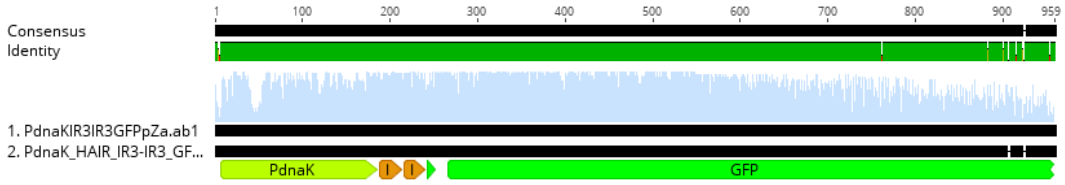

Figure D.15: Sanger sequencing results of PdnaK-IR3-IR3 GFP pZa vector.

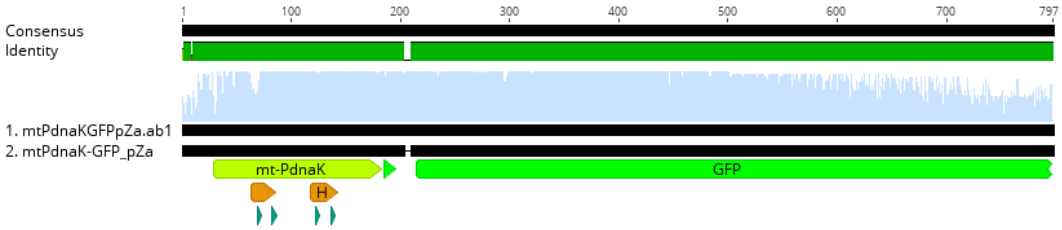

Figure D.16: Sanger sequencing results of mtPdnaK GFP pZa vector.

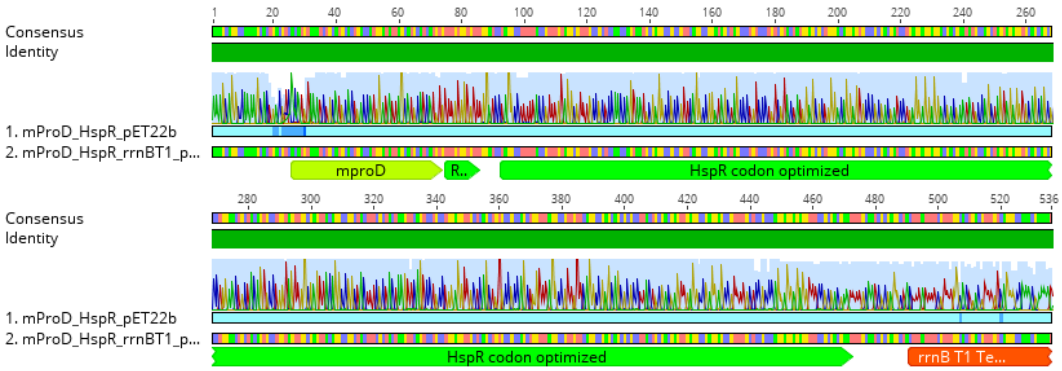

Figure D.17: Sanger sequencing results of mProD HspR pET22b vector.

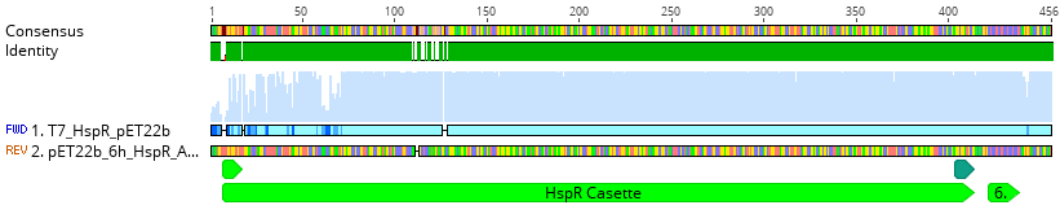

Figure D.18: Sanger sequencing results of T7 HspR pET22b expression vector.

Sanger sequencing results of vectors used in Chapter 4:

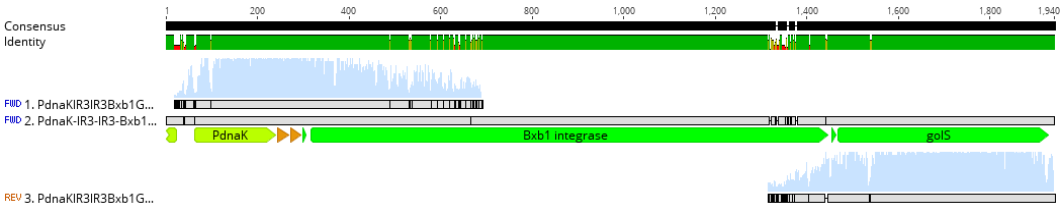

Figure D.19: Sanger sequencing results of PdnaK-IR3-IR3 Bxb1 GolS pZa vector.

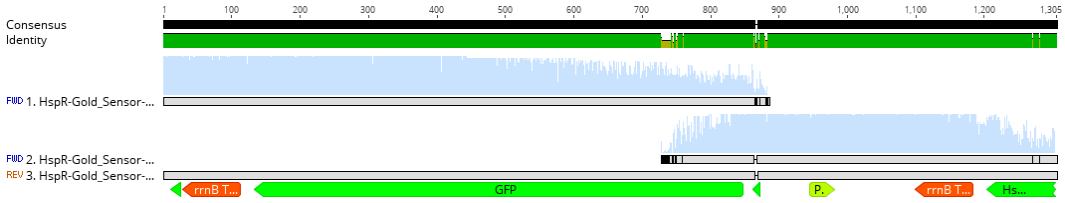

Figure D.20: Sanger sequencing results of mProD HspR PgolB GFP pET22b vector.

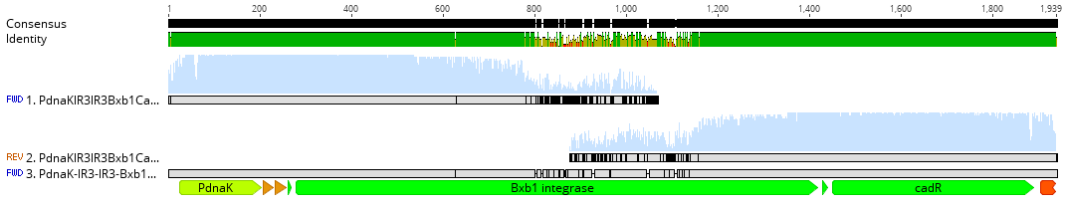

Figure D.21: Sanger sequencing results of PdnaK-IR3-IR3 Bxb1 CadR pZa vector.

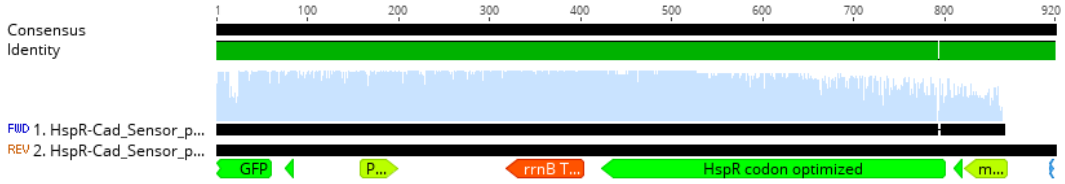

Figure D.22: Sanger sequencing results of mProD HspR PcadA GFP pET22b vector.

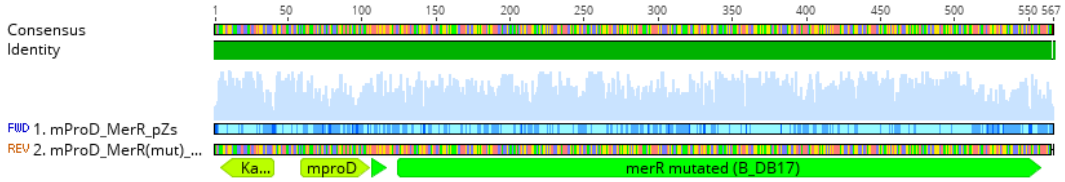

Figure D.23: Sanger sequencing results of mProD MerR(mutated) pZs vector.

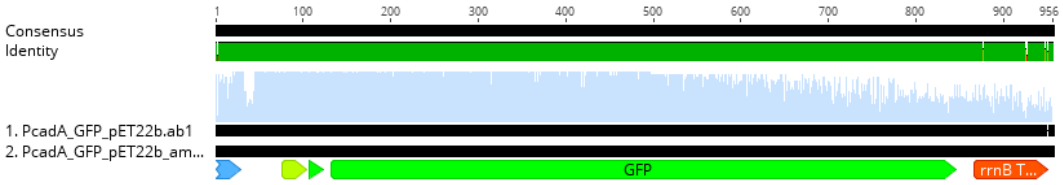

Figure D.24: Sanger sequencing results of PcadA GFP pET22b vector.

Sanger sequencing results of vectors used in Chapter 5:

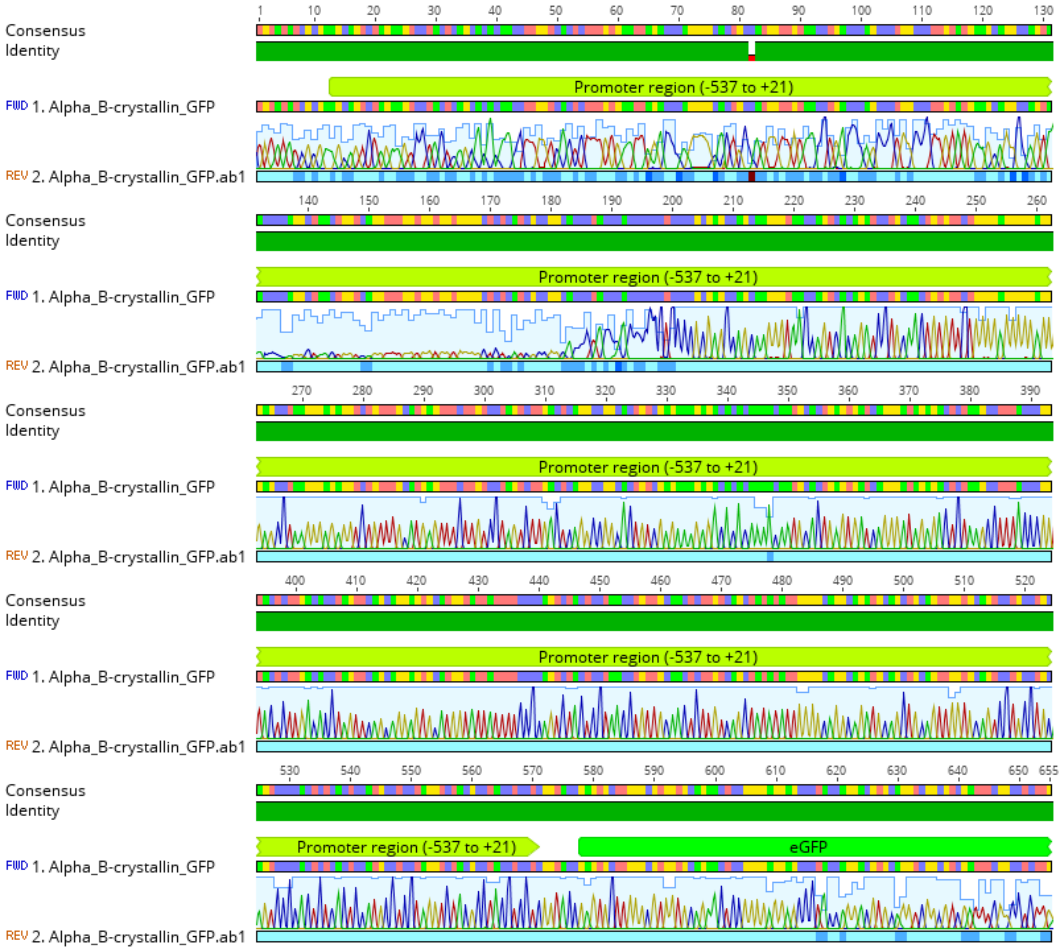

Figure D.25: Sanger sequencing results of ABC GFP pcDNA3 vector.

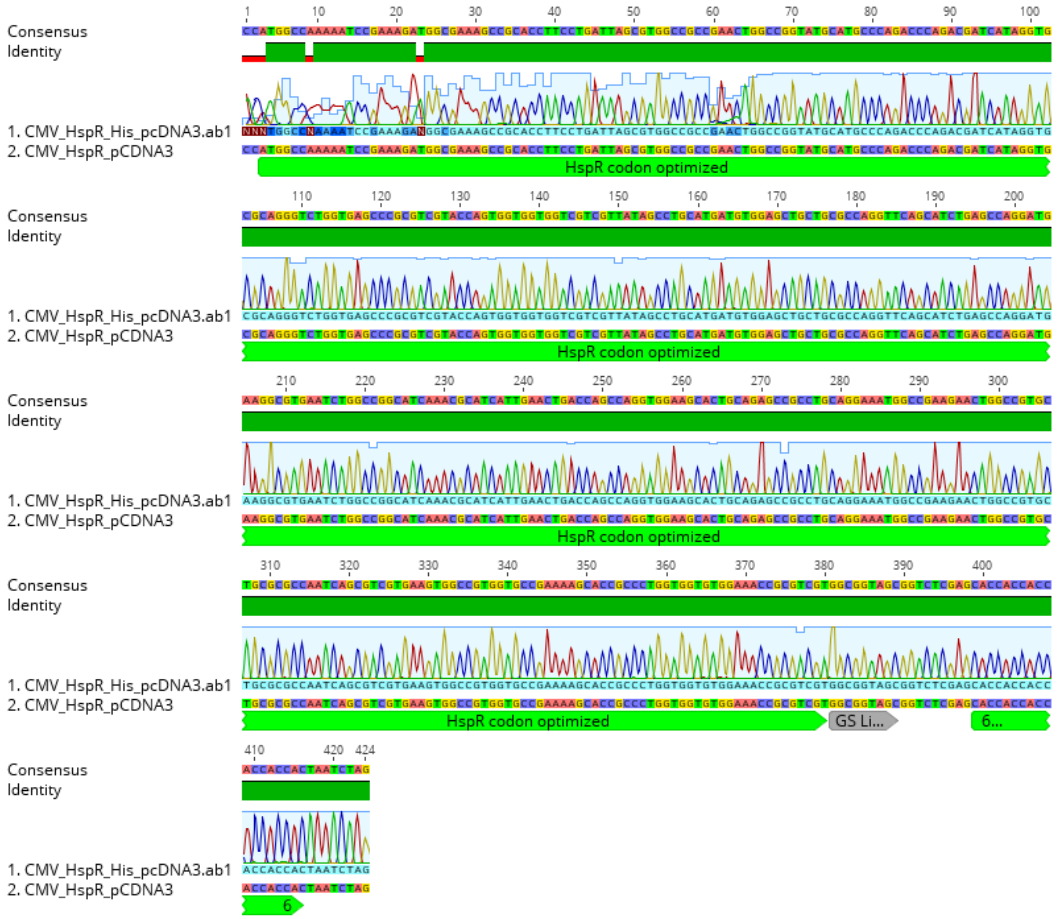

Figure D.26: Sanger sequencing results of CMV HspR-His pcDNA3 vector.

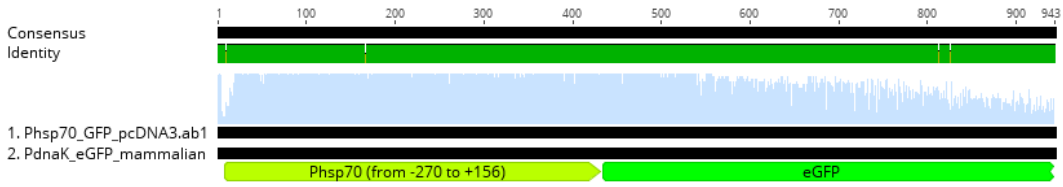

Figure D.27: Sanger sequencing results of Phsp70 GFP pcDNA3 vector.

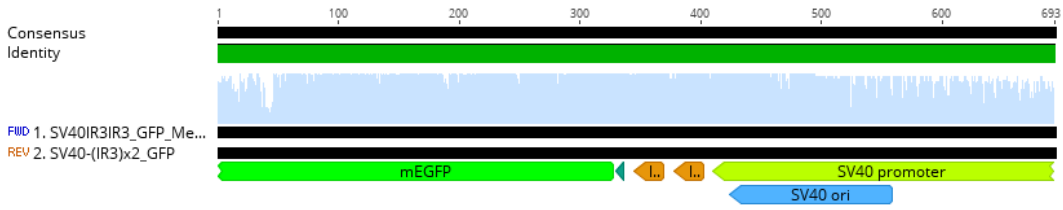

Figure D.28: Sanger sequencing results of SV40-IR3-IR3 GFP MeCP2 vector.

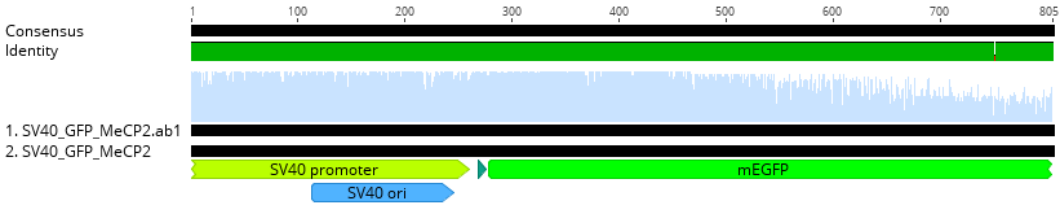

Figure D.29: Sanger sequencing results of SV40 GFP MeCP2 vector.

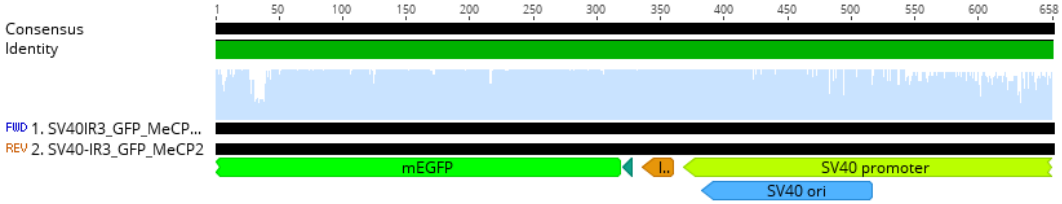

Figure D.30: Sanger sequencing results of SV40-IR3 GFP MeCP2 vector.

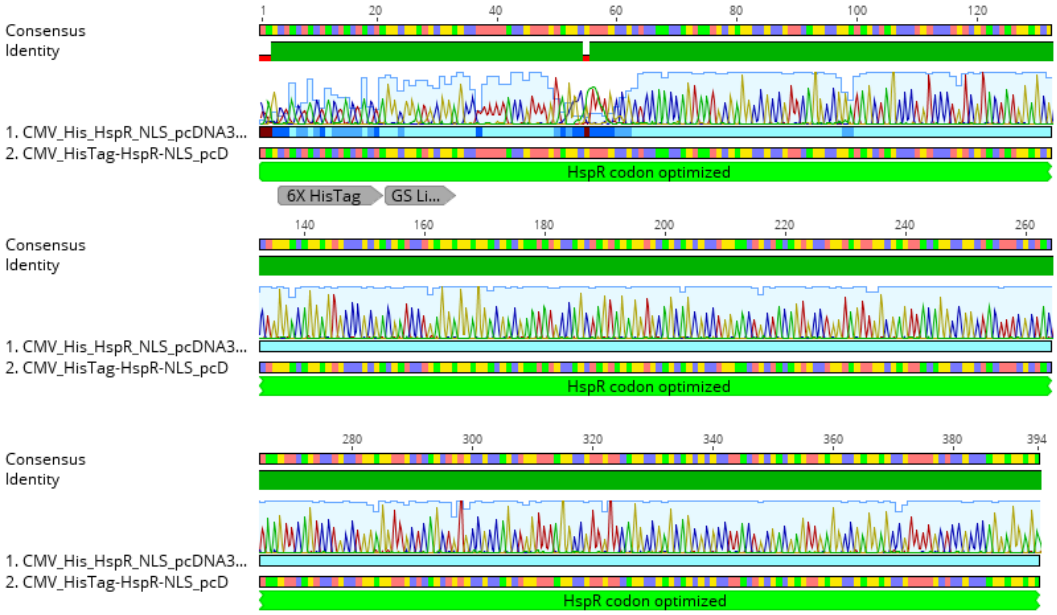

Figure D.31: Sanger sequencing results of CMV His-HspR-NLS pcDNA3 vector.

APPENDIX E

Detailed reaction recipes and methods

Table E.1: DNA digestion reaction recipe with restriction enzymes

Component	**20 µl Reaction**
10X Buffer	2 µl
DNA	1000 ng
Restriction Enzyme 1	0.4 µl
Restriction Enzyme 2	0.4 µl
Nuclease-free water	to 20 µl

Table E.2: T4 ligation reaction recipe

Component	**20 µl Reaction**
10X T4 DNA Ligase Buffer	2 µl
Vector DNA	50 ng
Insert DNA	3X molar to vector DNA
Nuclease-free water	to 20 µl
T4 DNA Ligase	1 µl

Table E.3: PCR reaction setup of Q5 DNA Polymerase

Component	**25 µl Reaction**	**Final Concentration**
5X Q5 Reaction Buffer	5 µl	1X
10 mM dNTPs	0.5 µl	200 µM
10 µM 5' Primer	1.25 µl	0.5 µM
10 µM 3' Primer	1.25 µl	0.5 µM
Template DNA	variable	<1000 ng
Q5 High-Fidelity DNA Polymerase	0.5 µl	0.02 U/µl
5X Q5 High GC Enhancer (optional)	5 µl	1X
Nuclease-Free Water	to 25 µl	

Table E.4: PCR conditions with Q5 DNA Polymerase

Step	**Temperature**	**Time**
Initial Denaturation	98°C	30 seconds
Extension	98°C	5–10 seconds
25–35 Cycles	50–72°C	10–30 seconds
	72°C	20–30 seconds/kb
Final Extension	72°C	2 minutes
Hold	4–10°C	

Table E.5: Reaction setup for Golden Gate Assembly

Component	**20 µl Reaction**
10X Golden Gate Reaction Buffer	2 µl
Golden Gate Assembly Mix	1 µl
Linear DNA vector	75 ng
Insert DNA PCR products	2X molar to vector DNA from each
Nuclease-Free Water	to 20 µl

Table E.6: Thermocycler conditions for Golden Gate Assembly

Step	**Time**	**Cycles**
37°C	5 minutes	30
16°C	10 minutes	
55°C	5 minutes	
Hold	12°C	

Table E.7: Gibson Assembly mix recipe (1.33x)

Substance	**Amount**
Taq DNA Ligase (40 U/ µl)	50 µl
5X Isothermal Reaction Buffer	100 µl
T5 Exonuclease (1 U/µl)	2 µl
Phusion DNA Polymerase (2 U/µl)	6.25 µl
Nuclease-Free Water	216.75 µl

Table E.8: 5x isothermal buffer recipe

Substance	**Amount**
PEG-8000	25%
Tris-HCl	500 mM, pH 7.5
$MgCl_2$	50 mM
DTT	50 mM
NAD	5 mM
dNTPs	1 mM each

Table E.9: cDNA synthesis reaction

Component	**20 µl Reaction**
5X iScript Reaction Mix	4 µl
iScript Reverse Transcriptase	1 µl
Template RNA	500 ng
Nuclease-free water	to 20 µl

Table E.10: Thermocycler conditions for cDNA synthesis

Step	**Time**
25°C	5 minutes
42°C	30 minutes
85°C	5 minutes
Hold	4°C

Table E.11: RT-qPCR reaction setup

Component	**20 µl Reaction**	**Final Concentration**
2X Enzyme/SYBR Mix	10 µl	1X
10 µM 5' Primer	0.6 µl	0.3 µM
10 µM 3' Primer	0.6 µl	0.3 µM
cDNA	2 µl	50 ng
Nuclease-Free Water	6.8 µl	

Table E.12: RT-qPCR conditions

Step	**Temperature**	**Time**
Initial Denaturation	95°C	3 minutes
Extension	95°C	10 seconds
39 Cycles	55–72°C	15 seconds
	72°C	10 seconds
Final Extension	72°C	2 minutes
Melting Curve	65–95°C	

APPENDIX F

Additional Results

Time-resolved fluorescence spectroscopy analysis for GFP-QD interaction

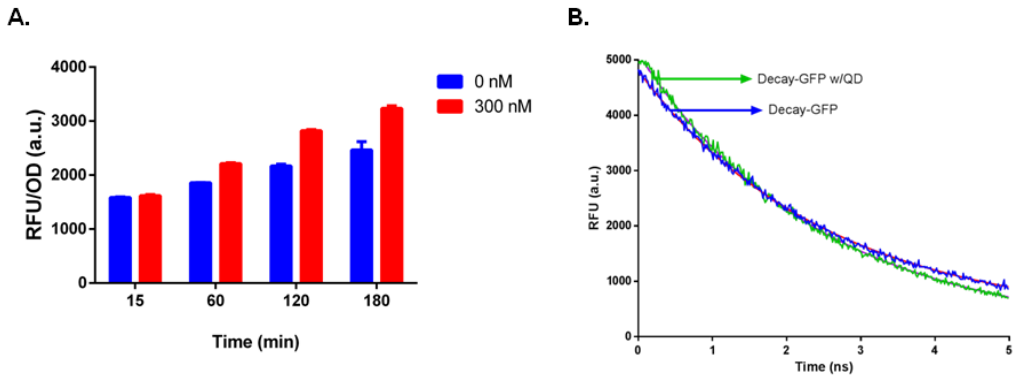

Figure F.1: Fluorescent signal effect analysis of QDs over GFP signal. A. Time dependent fluorescence signal results of constitutively expressed GFP plasmid carrying cells (positive control) treated with 300 nM CdTe QDs. B. Time resolved fluorescence spectroscopy analysis of positive control cells treated with CdTe QDs.

Growth curves (OD_{600}) of sensors treated with stressors

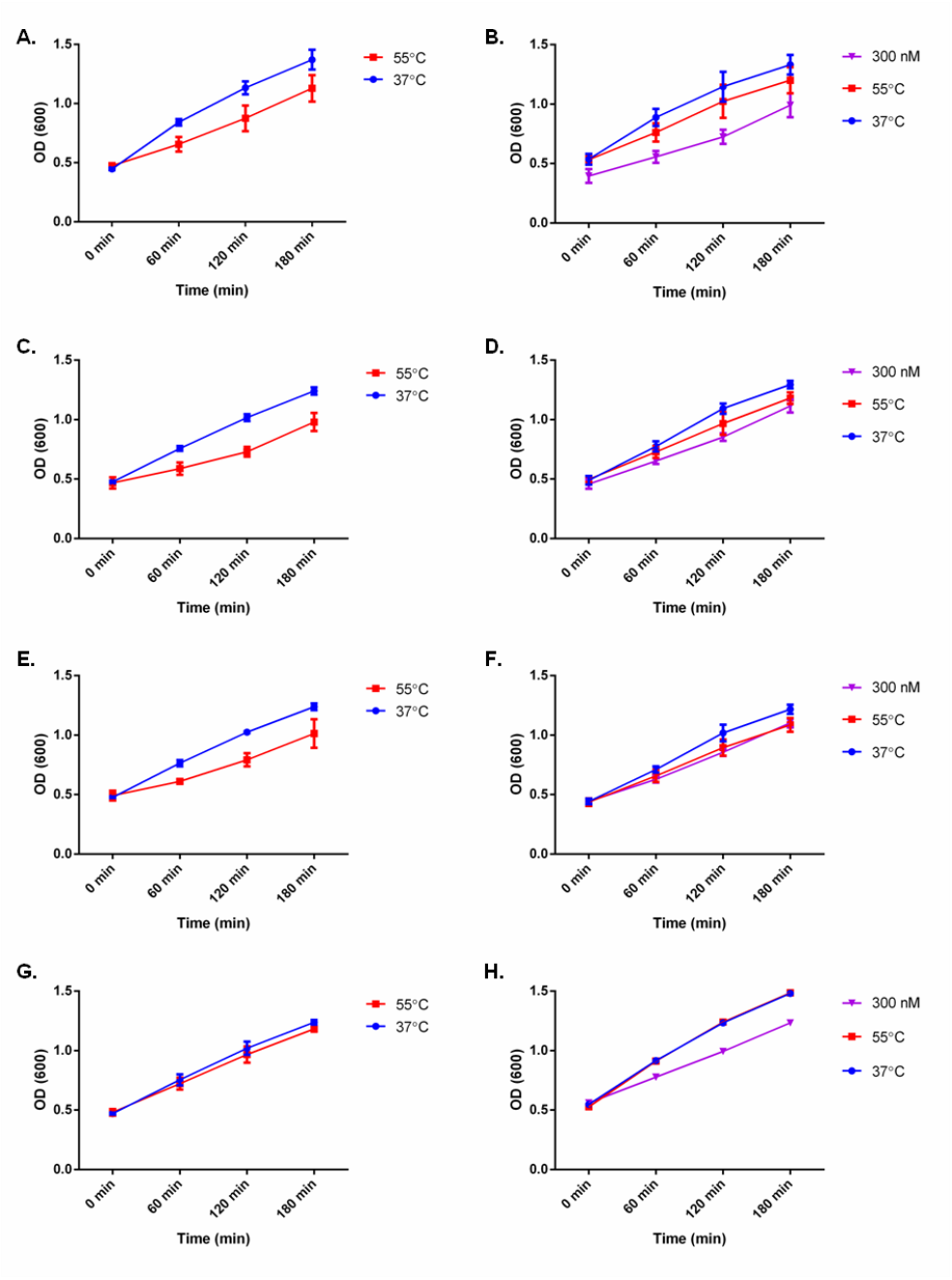

Figure F.2: Growth curves of nanotoxicity sensors at OD_{600}. A. Native PdnaK sensor treated with heat (37°C and 55°C). B. Riboregulator mediated PdnaK sensor treated with heat (37°C and 55°C) and CdTe QDs (300 nM). C. Native PclpB sensor treated with heat (37°C and 55°C). D. Riboregulator mediated PclpB

sensor treated with heat (37°C and 55°C) and CdTe QDs (300 nM). E. Native PfxsA sensor treated with heat (37°C and 55°C). F. Riboregulator mediated PfxsA sensor treated with heat (37°C and 55°C) and CdTe QDs (300 nM). G. Native PibpA sensor treated with heat (37°C and 55°C). H. Riboregulator mediated PibpA sensor treated with heat (37°C and 55°C) and CdTe QDs (300 nM).

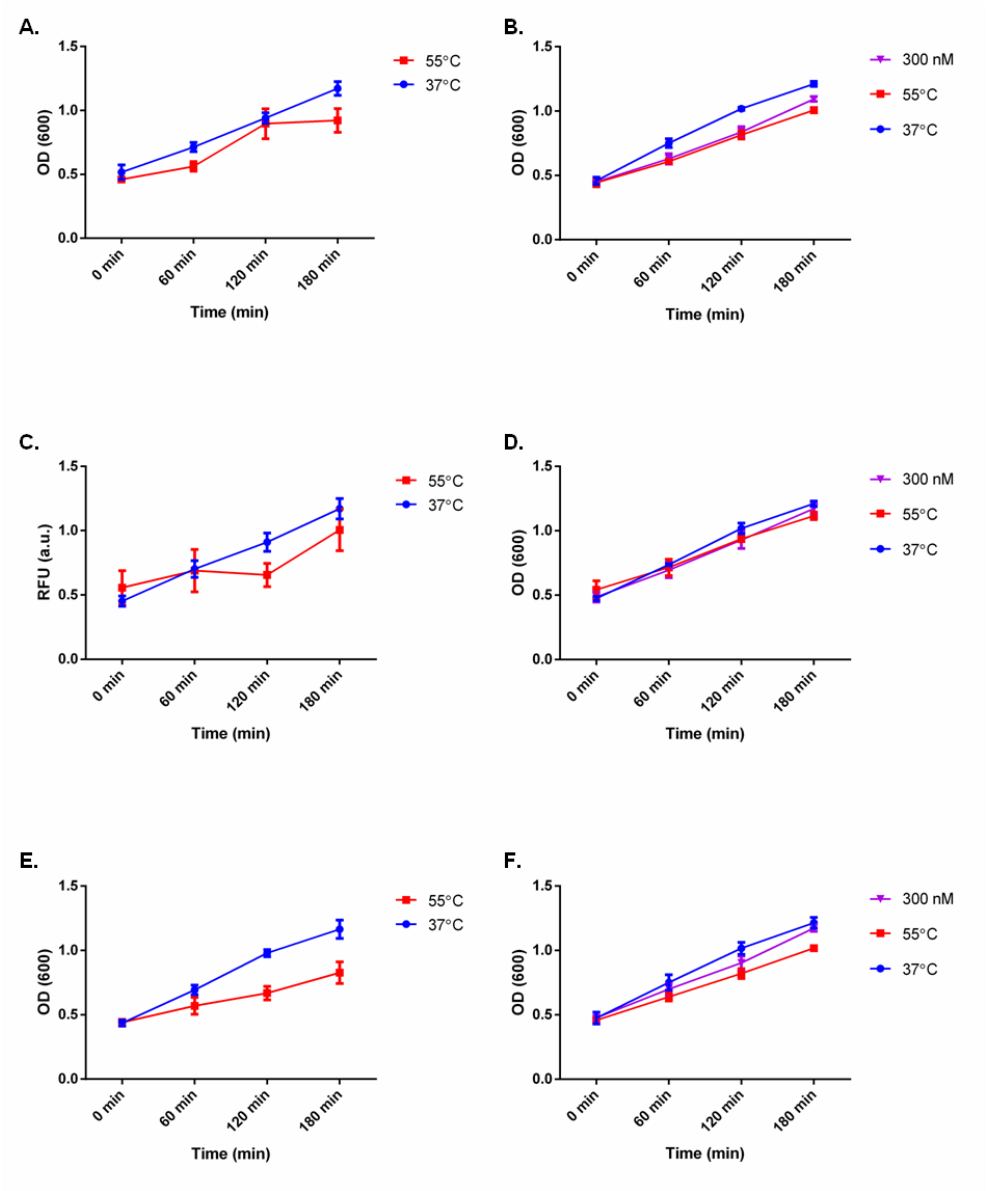

Figure F.3: Growth curves of HspR mediated nanotoxicity sensors at OD_{600}. A. HspR mediated PdnaK sensor treated with heat (37°C and 55°C). B. HspR

mediated mtPdnaK sensor treated with heat (37°C and 55°C) and CdTe QDs (300 nM). C. HspR mediated PdnaK-IR2 sensor treated with heat (37°C and 55°C). D. HspR mediated PdnaK-IR2-IR2 sensor treated with heat (37°C and 55°C) and CdTe QDs (300 nM). E. HspR-mediated PdnaK-IR3 sensor treated with heat (37°C and 55°C). F. HspR mediated PdnaK-IR3-IR3 sensor treated with heat (37°C and 55°C) and CdTe QDs (300 nM).

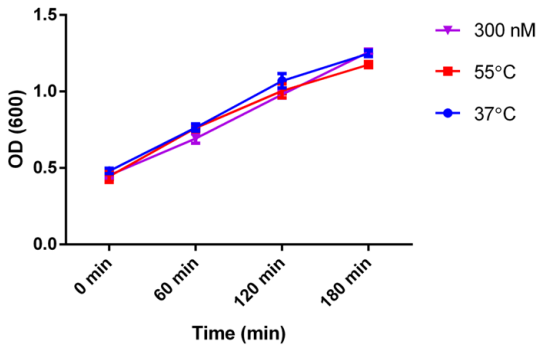

Figure F.4: Growth curve of negative control plasmid carrying cells treated with heat (37°C and 55°C) and CdTe QDs (300 nM) at OD_{600}.

Representative fluorescent microscopy images of sensors

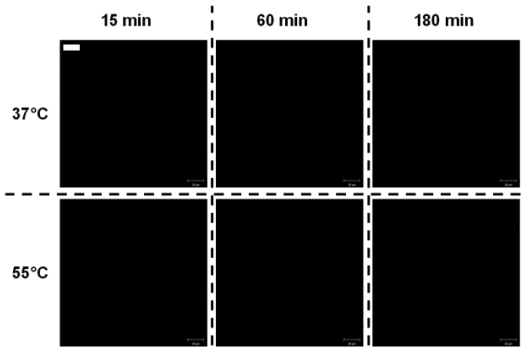

Figure F.5: Time dependent fluorescence microscopy images of control samples under heat shock treatment. The first row indicates samples treated with 37°C

while second row indicates heat shock treated samples (55°C). Heat shock was applied for 30 min. Scale bar indicates 20 μm.

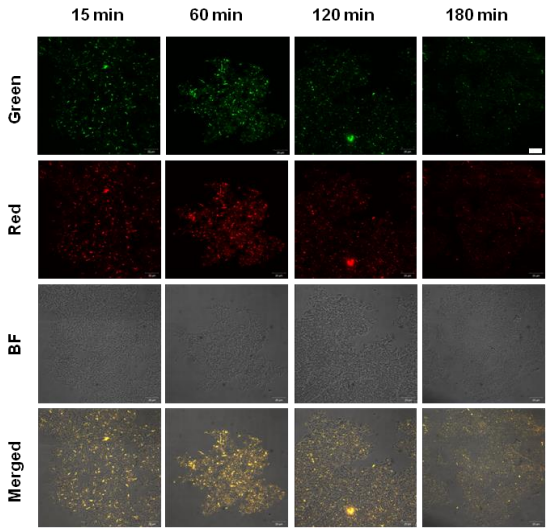

Figure F.6: Time dependent fluorescence microscopy images of control samples under QD treatment (300 nM). The first row was excited with Argon 488 nm laser and emission was collected with LP 505 filter while second row was excited with HeNe 543 nm laser and emission was collected with LP 585 filter. Fluorescence of QDs is shown on bright-field mode at third row. All three pictures were merged at fourth row. Scale bar indicates 20 μm.

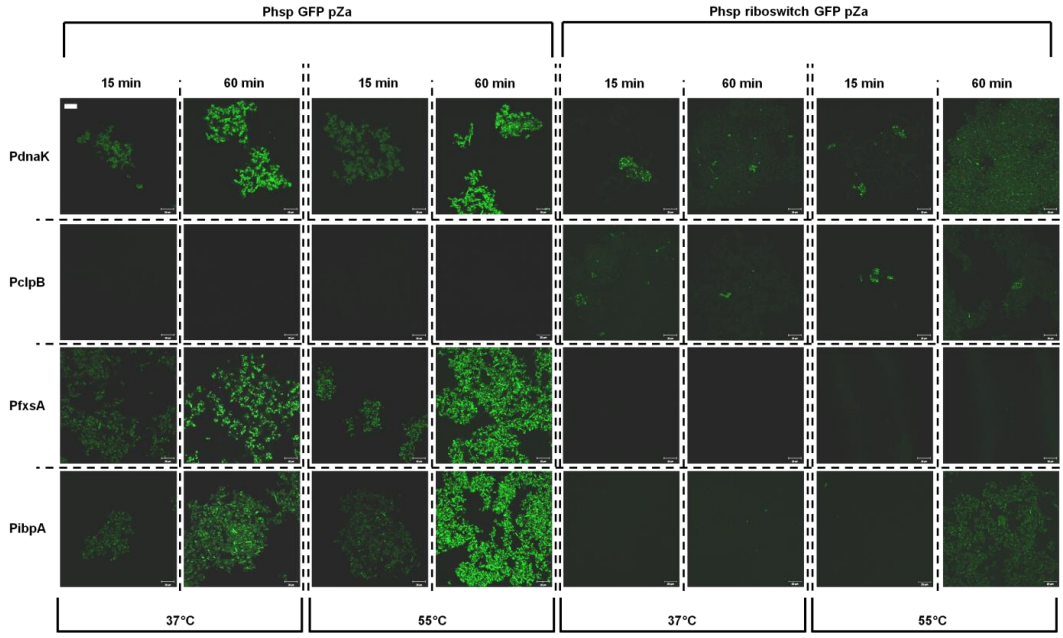

Figure F.7: Time dependent fluorescence microscopy images of heat shock treated initial toxicity sensors. Each row represents stress sensors with HSP promoter (left) and its riboregulator mediated sensors (right) (PdnaK, PclpB, PfxsA and PibpA, respectively). Each column indicates fluorescence of stress sensors upon heat treatment at 37°C and 55°C at 15th min and 60th min which are the first-time point and the highest signal point of stress sensors, respectively. Scale bar indicates 20 µm.

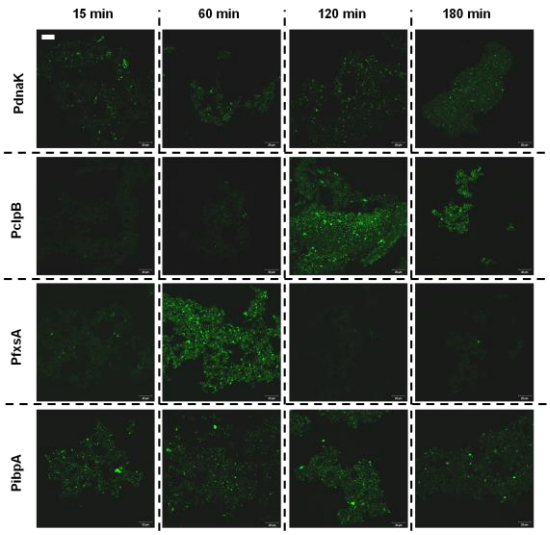

Figure F.8: Time dependent fluorescence microscopy images of QD treated riboregulator mediated sensors. Each row represents different promoters (PdnaK, PclpB, PfxsA and PibpA, respectively) and each column indicates time dependent fluorescent response caused by CdTe QDs (300 nM). Scale bar indicates 20 µm.

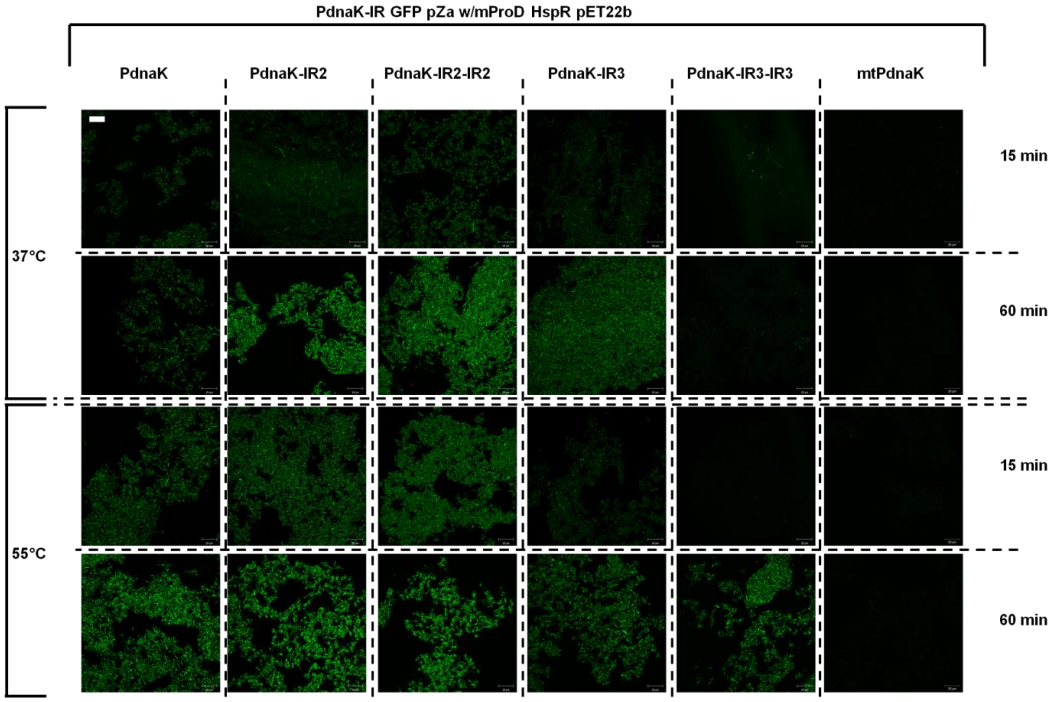

Figure F.9: Time dependent fluorescence microscopy images of HspR mediated sensors. Each column represents different modifications of promoters (PdnaK, PdnaK-IR2, PdnaK-IR2-IR2, PdnaK-IR3, PdnaK-IR3-IR3, and mtPdnaK, respectively.). Each row indicates fluorescence of stress sensors upon heat treatment either at 37°C (upper) or 55°C (lower) at 15th min and 60th min which are the first time point and the highest signal point of stress sensors, respectively. Scale bar indicates 20 µm.

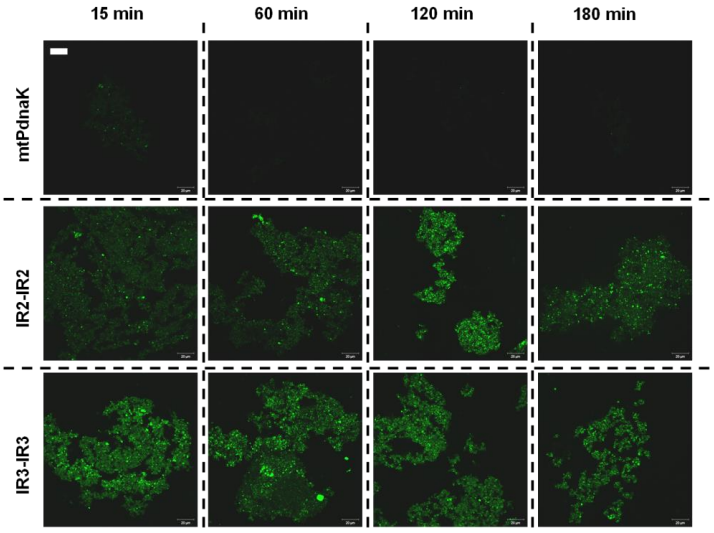

Figure F.10: Time dependent fluorescence microscopy images of QD treated HspR mediated sensors. Each row represents different promoters (mtPdnaK, PdnaK-IR2-IR2, and PdnaK-IR3-IR3, respectively.). Each column indicates time dependent fluorescent response caused by CdTe QDs (300 nM). Scale bar indicates 20 µm.

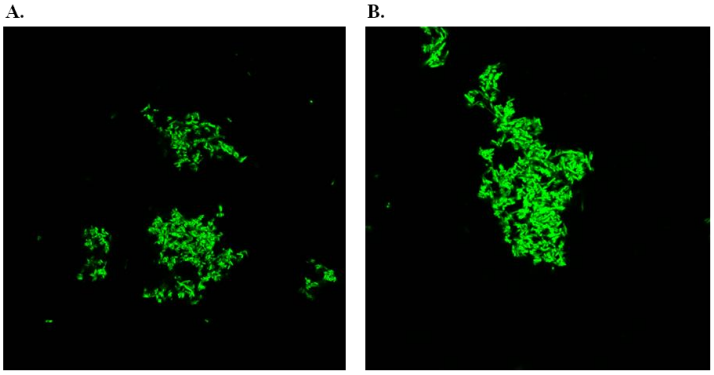

Figure F.11: Fluorescence microscopy images of QD treated engineered quorum sensing sensor with HSR. A. 0 nM CdTe QDs treatment. B. 300 nM CdTe QDs treatment.

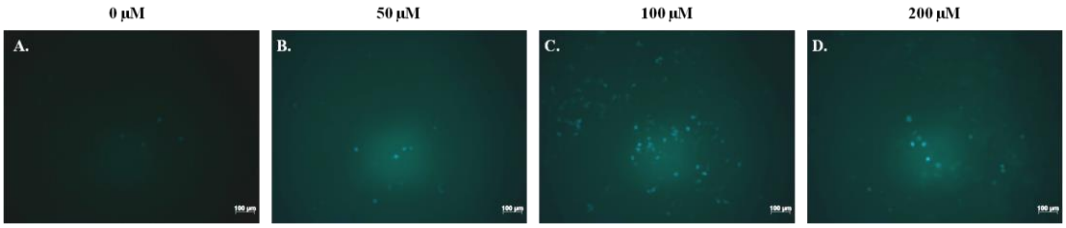

Figure F.12: Fluorescence microscopy images of eukaryotic Phsp70 pcDNA3-GFP sensor treated with cadmium ions for 6 h. A. 0 µM, B. 50 µM, C. 100 µM, and D. 200 µM. Scale bar indicates 100 µm.

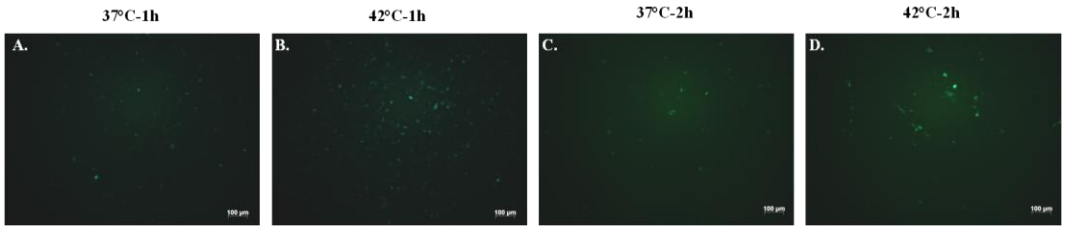

Figure F.13: Fluorescence microscopy images of eukaryotic Phsp70 pcDNA3-GFP sensor treated with heat. A. at 37°C for 1 h, B. at 42°C for 1 h, C. at 37°C for 2 h, and D. at 42°C for 2 h. Scale bar indicates 100 µm.

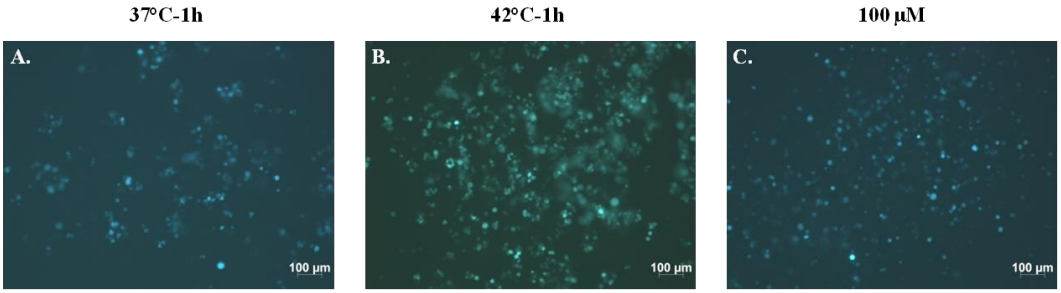

Figure F.14: Fluorescence microscopy images of eukaryotic P_{ABC} pcDNA3-GFP sensor treated with cadmium and heat. A. at 37°C for 1 h, B. at 42°C for 1 h, C. 100 µM cadmium for 6 h. Scale bar indicates 100 µm.

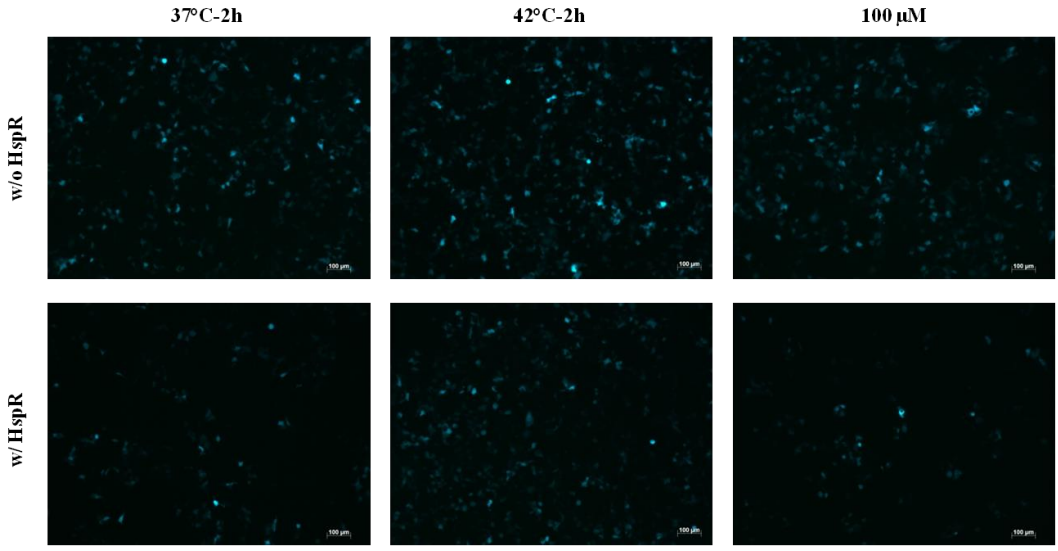

Figure F.15: Fluorescence microscopy images of eukaryotic SV40-IR3 GFP sensor treated with cadmium (100 µM cadmium for 6 h) and heat (37°C and 42°C for 2 h). Upper row indicates GFP sensor only and lower row indicates GFP vector co-expression with HspR. Scale bar indicates 100 µm.

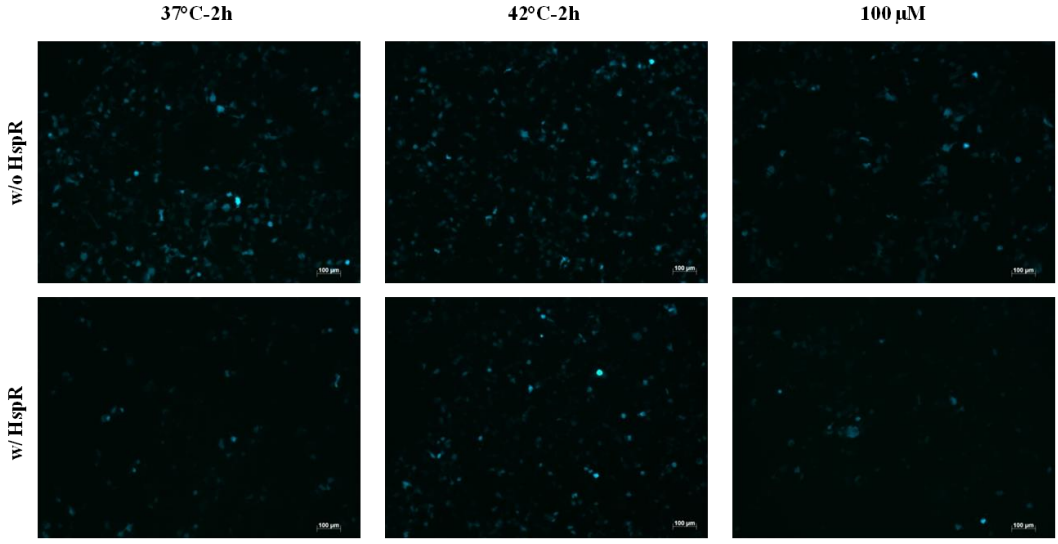

Figure F.16: Fluorescence microscopy images of eukaryotic SV40-IR3-IR3 GFP sensor treated with cadmium (100 µM cadmium for 6 h) and heat (37°C and 42°C for 2 h). Upper row indicates GFP sensor only and lower row indicates GFP vector co-expression with HspR. Scale bar indicates 100 µm.